



Guidelines for long ultrafine grained steel production and application to the automotive sector (LUNA)

EUROPEAN COMMISSION

Directorate-General for Research and Innovation
Directorate G — Industrial Technologies
Unit G.5 — Research Fund for Coal and Steel

E-mail: rtd-steel-coal@ec.europa.eu
RTD-PUBLICATIONS@ec.europa.eu

Contact: RFCS Publications

European Commission
B-1049 Brussels

European Commission

Research Fund for Coal and Steel

Guidelines for long ultrafine grained steel production and application to the automotive sector (LUNA)

I. Salvatori, C. Guarnaschelli, T. Coppola

Centro Sviluppo Materiali S.p.A. (CSM)

Via di Castel Romano 100, 00128 Roma, ITALY

G. Goldhan

Technische Universität Bergakademie Freiberg (TUBEF)

Akademiestrasse 6, 09599 Freiberg, GERMANY

Z. Idoyaga Olano, R. Elvira

Gerdau Investigaciones Desarrollo Europa Sa (GERDAU)

Barrio Ugarte s/n Apartado de Correos 152, 48970 Basauri, SPAIN

S. Betti

O.R.I. Martin (ORI MARTIN)

Via C. Canovetti 13, 25128 Brescia, ITALY

J. Aldazabal, I. Ocana, J. M. Martinez-Esnaola

Centro de Estudios e Investigaciones Tecnicas de Gipuzkoa (CEIT)

Po. de Manuel Lardizabal 15, Barrio de Ibaeta 20009 San Sebastian, SPAIN

S. Plano

Centro Ricerche FIAT (CRF)

Strada Torino 50, 10043 Orbassano, Torino, ITALY

Grant Agreement RFSR-CT-2009-00012

1 July 2009 to 31 December 2012

Final report

Directorate-General for Research and Innovation

LEGAL NOTICE

Neither the European Commission nor any person acting on behalf of the Commission is responsible for the use which might be made of the following information.

The views expressed in this publication are the sole responsibility of the authors and do not necessarily reflect the views of the European Commission.

***Europe Direct is a service to help you find answers
to your questions about the European Union***

**Freephone number (*):
00 800 6 7 8 9 10 11**

(*) Certain mobile telephone operators do not allow access to 00 800 numbers or these calls may be billed.

More information on the European Union is available on the Internet (<http://europa.eu>).

Cataloguing data can be found at the end of this publication.

Luxembourg: Publications Office of the European Union, 2013

ISBN 978-92-79-33089-6
doi:10.2777/42639

© European Union, 2013
Reproduction is authorised provided the source is acknowledged.

Printed in Luxembourg

PRINTED ON WHITE CHLORINE-FREE PAPER

TABLE OF CONTENTS

FINAL SUMMARY	5
1 SCIENTIFIC AND TECHNICAL DESCRIPTION OF THE RESULTS	13
Objectives of the project	13
2 DESCRIPTION OF ACTIVITIES AND DISCUSSION	15
2.1 WORK PACKAGE 1:	
SELECTION AND SUPPLY OF MATERIALS	15
Task 1.1: Material selection	15
Task 1.2: Manufacturing of starting material and its characterisation	16
Task 1.3: Identification of prototype components and definition of technical requirements	21
Task 1.4: Definition of test procedure	24
Summary	28
2.2 WORK PACKAGE 2:	
SIMULATION OF THERMOMECHANICAL CYCLES FOR UFG STEELS PRODUCTION	29
Task 2.1: Determination of DIFT parameters for different C steels	29
Task 2.2: Heavy γ deformation: determination of parameters for different steels	52
Task 2.3: Identification of the mechanisms to be exploited for producing UFG long product	80
2.3 WORK PACKAGE 3:	
EXPERIMENTAL PRODUCTION OF LONG UFG STEELS ON PILOT MILL AND INDUSTRIAL PLANT	81
Task 3.1: Definition of thermomechanical processes to be tested on pilot plant	81
Task 3.2: Experimental production of long UFG steels	88
Task 3.3: Parametric investigation of relationship between microstructural features and cold formability in the new UFG long steels	97
Task 3.4: Industrialization trials on pilot plants and/or industrial plants	114
Conclusions	119
2.4 WORK PACKAGE 4:	
EVALUATION OF UFG STEELS THROUGH MICROSTRUCTURAL AND MECHANICAL CHARACTERIZATION	121
Task 4.1: Static mechanical properties	121
Task 4.2: Response to fatigue	131
Task 4.3: Response to machining	144
Conclusions	146
2.5 WORK PACKAGE 5:	
MECHANICAL COMPONENTS REALIZATION AND FULL-SCALE ASSESSMENT	147
Task 5.1: Cold heading application of new UFG long steels and component qualification	147
Task 5.2: Fabrication and qualification of prototype automotive components in UFG steels	149
Task 5.3: Quantitative identification of criticalities and merits	154
2.6 WORK PACKAGE 6:	
GUIDELINES FOR UFG STEEL LONG PRODUCTS APPLICATION TO AUTOMOTIVE SECTOR	157
Task 6.1: Guidelines for UFG long steels application to automotive components and applications	157

3. CONCLUSIONS.....	159
4. EXPLOITATION AND IMPACT OF THE RESEARCH RESULTS.....	161
5. REFERENCES.....	163
LIST OF FIGURES.....	165
LIST OF TABLES.....	171
LIST OF ACRONYMS AND ABBREVIATIONS.....	173

FINAL REPORT SUMMARY

In order to meet the increasing needs from economic and social developments in future, the research on new generation steels with higher strength and longer duration, has become a worldwide issue. It is well known that various mechanisms to strengthen the steels exist, but grain refinement is the only method to improve both strength and toughness simultaneously.

A ferrite grain size in the range of 1÷4 µm and a steel microstructure characterised by a mixture of ferrite-pearlite and/or martensite, bainite microstructure, could give a very good combination of mechanical (strength, ductility, toughness, fatigue) and technological properties (machinability, cold/warm metal forming, etc.) for final application to automotive components.

Objectives of the project

The general aim of LUNA project is to define the guidelines for the production and best utilisation of ultrafine grained (UFG) carbon steel long products for mechanical applications, using existing productive plants, through the exploitation of advanced thermomechanical processes.

In particular the objectives of the project are:

- Definition of the most suitable thermomechanical process for long ultrafine grained (UFG) steel production.
- Identification of merits, in terms of microstructural and mechanical properties of UFG long steels in as-rolled conditions and after cold/warm forming.
- Production of components or component-like dummies in UFG long products and evaluation of their mechanical performances.
- To give guidelines for power train and automotive UFG long products applications.

WP1: Selection and supply of materials and identification of mechanical components for final applications

A number of different chemical compositions have been selected, with carbon content included in the range 0.15-0.60 %. The prototype components to be manufactured by UFG steels have been identified among the following two families: fasteners applications (e.g. screws, bolts) and automotive applications (powertrain components, springs).

The initial materials, to be used in the investigations of thermomechanical cycles and mechanisms of formation of UFG microstructures, have been manufactured by means of industrial process (Ori Martin, Gerdau) and laboratory scale equipment (CSM and Gerdau).

Fasteners application: screw (carbon range 0.15-0.30 %)

For fastener applications the range of carbon content 0.15-0.30 % has been investigated.

In particular, in order to study the effect of chemical composition on UFG production, two different C and Mn contents have been selected. Since in these applications the addition of chemical elements enhancing hardenability is required, boron addition has been also investigated. On this basis, the following grades have been selected: 30MnB4, 18MnB2, 30MnB7, 18MnB7, 18Mn7.

The expected advantages of UFG steel in this range of applications consist firstly of the chance to reduce or possibly avoid the annealing, which is usually made before cold forming and is very expensive in terms of energy and time. Such reduction is supposed to be possible as a finer microstructure promotes the development of a more globular pearlite [1-3], at the same time preventing the formation of hard phases (e.g. bainite) during the cooling on the Stelmor conveyor.

For similar reasons, a further possible advantage could be the reduction of scraps caused by forging bursts in screw heads occurring during cold forming process

The selected components are three screws of different shapes, sizes and final applications, produced by the company Agrati SpA. Their main features are summarised in Table S1.

Automotive – Powertrain component: gear shaft (carbon range 0.15-0.20 %)

With regard to automotive powertrain applications, steel grades for carburising have been taken into account, as 18CrMo4, 17CrV6, 17CrVNb6. The former has been chosen because it is a steel grade which is usually used for the manufacturing of some powertrain components, while the other steel grades have been selected with the aim to obtain more easily ultrafine grain size.

The main interests to ultrafine-grade steel for the automotive industry are related to the possibility to achieve:

- Higher fatigue and impact resistance properties in comparison to similar steel composition.
- Lower alloy content in particular to avoid the use of Ni alloyed steel
- Cost and weight saving.

Component	Size / class	Application	Steel (currently used)	Annealing	UFG objectives
Screw, bi-hexagonal flange head with hexagon socket	M7x1x42 / 10.9	Car steering system	30MnB4	YES	- Elimination of annealing - Reduction of scraps
Screw, bi-hexagonal socket head cap screw with flange	M14x1.5x70 / 10.9	Suspension system	30MnB4	YES	- Elimination of annealing - Reduction of scraps
Screw, hexa-lobular flange	M8x1.25x43 / 10.9	Power train	30MnB4	NO	- Reduction of scraps

Table S1: Selected components (fasteners).

The prototype component selected by CRF, jointly to FIAT Powertrain Technologies, is the gear shaft. The part is currently produced by 17NiCrMo4 steel for high stressed application. The aim is to find an UFG steel without Ni, like 18CrMo4, able to replace the original 17NiCrMo4 steel.

The gear shaft manufacturing process is divided in two main parts: the first part performed by TEKFORD (forging supplier), the second made in FIAT Powertrain Technology plant.

The main critical aspects of this manufacturing cycle are related to the points where the part must stay at a temperature higher than the austenitization point. The related phase transformation may reduce the advantages coming from UFG structure.

To evaluate the effect of UFG microstructure prior to carburizing treatment, it has been decided to address the experimental activity on simple fatigue test comparing two different grain sizes of 18CrMo4 carburized with the same heat treatment cycle and two different grain sizes of 17CrV6 proposed by Gerdau. In this steel a finer grain size could be achieved, in comparison to 18CrMo4, due to vanadium addition.

Automotive – Suspension component: spring (carbon range 0.40-0.60 %)

In the case of automotive spring applications, the proposed steel is 50SiMoVNb8, which is a steel grade used for helicoidal suspension springs, at present produced with standard grain size. The aim of grain refinement is to increase the fatigue performances of high stressed spring steel.

Two different manufacturing ways to achieve suspension spring are at present used in ARA: “Hot Route” and “Cold Route”.

“Cold route” process is convenient for UFG steel as the heat treatment of the wire is done by induction hardening. This process involves very short soaking time preventing grain growth.

The steel proposed by Gerdau is 50SiVMo8Nb which allows, even with the current rolling technology, to achieve a smaller grain size. The disadvantage is its high cost due to the expensive alloying system. After several contacts with the main suspension spring manufacturers held by CRF in order to assess their interest and commitment on this project and share the selection of the chemical steel composition, it was decided jointly to a suspension spring manufacturer ARA (ALLEVARD REJNA AUTOSUSPENSION), in spite of the cost, to proceed with this steel focusing the experimental activity on the assessment of the real improvement due to the grain refinement without changing the chemical steel composition.

WP2: Simulation of thermomechanical cycles for UFG steels production.

Determination of DIFT parameters for different C steels

Driving force for phase transformation depends on chemical composition and temperature.

The typical phase transformations in steels are austenite to ferrite, austenite to pearlite, austenite to bainite, austenite to martensite and precipitation of nitrides and carbides.

If an external load is applied to the system above the static transformation temperature, the free energy of the system will be certainly raised. If the load (e.g. deformation) is applied to the austenite above transformation temperature and the free energy of austenite is raised to the extent over the free energy of ferrite at the same temperature, the transformation from austenite to ferrite will occur, which could not be found to happen without deformation.

This kind of ferrite transformation induced by deformation has been called Deformation Induced Ferrite Transformation (DIFT).

It was assessed that it is a dynamic phase transformation occurring during deformation at temperature slightly higher than Ar_3 due to the strain energy accumulated in the austenite phase that induces an early γ - α phase transformation.

This mechanism has a critical strain to occur that depends on strain rate, deformation temperature, content of carbon, alloying elements, and prior austenite grain size.

The resulting ferritic grains are very fine and for this reason DIFT is considered one of the mechanisms which is proven to be an effective method for grain refinement in plain low carbon steels. The aim of this experimentation was to assess the hot deformation conditions in the austenite region for producing fine grain sizes through DIFT mechanism.

From the results it is evident that the processing parameters and initial microstructure can influence the occurrence of DIFT and the DIFT ferrite grain size and volume fraction.

(a) - Critical strain

As explained before, deformation accelerates the phase transformation kinetics. However if the imposed strain is too small the dynamic transformation is not activated. The critical strain for DIFT occurrence resulted to depend on C content, prior austenite grain size and deformation temperature.

Results showed that smaller prior austenite grain sizes shows the smaller critical strain value, while it decreases with the deformation temperature.

(b) - Strain

It can be confirmed that increasing strain, more DIFT grains can be obtained. When the strain is small, DIFT ferrite starts to form along the prior austenite grain boundaries. As the strain is increased, the interiors of austenite grains are activated as nucleation sites for DIFT ferrite, which are probably deformation bands or twin boundaries. About the grain size, it was noted that increasing the strain the ferrite grain size decreases.

(c) - Prior austenite grain size

Smaller prior austenitic grain size, the higher is the volume fraction of DIFT ferrite under a given deformation condition. This is mainly because the prior austenite grain boundary is a preferential nucleation site for DIFT ferrite. A smaller prior austenite grain size has the longer grain boundary area in a given volume of material, and this will result in the larger volume fraction of ferrite and consequently finer grain size.

(d) - Deformation Temperature

Deformation temperature influences the critical strain, and ferrite volume fraction. The lower the deformation temperature, the lower is the critical strain. If the critical strain for DIFT is reduced, a finer ferrite grain size and more volume fraction at given strain are observed.

The effect of low deformation temperature is important when the strain is relatively small, because decreasing the deformation temperature is very effective in increasing the amount of DIFT, but at relatively high strains decreasing the deformation temperature will affect only slightly the amount of DIFT.

(e) - Strain rate

The effect of strain rate on ferrite volume fraction seems to be not significant, at least in the analyzed range ($1-30 \text{ s}^{-1}$).

(f) – Chemical composition

Critical strain increases with C and Mn content. The Mn content increases the critical strain at the same C content. However it has a weaker effect if compared with the C content. The level of ferrite refinement increases slightly with the carbon content. The presence of B increases the critical strain.

Heavy γ deformation: Determination of parameters for different C steels

Another approach to obtain ultra fine grains in steels is to give severe plastic straining during hot rolling in order to have deformed austenite that transforms in ferrite during cooling.

Most of the ultra-fine ferrite comes from nucleation on grain boundaries and deformation bands in the deformed austenite.

Usually, in industrial production, the austenite is deformed at high Zener-Hollomon parameter to cause austenite refinement by dynamic recrystallization. Decreasing the rolling temperature the austenite is deformed in the no-recrystallization temperature region. This gives elongated austenite grains, helpful for ferrite grain refinement during cooling. In the temperature range between A_{e3} and A_{r3} , also DIFT can occur if the critical strain is achieved.

In this task the activity has been focused on the identification of the conditions to obtain grain refinement through transformation of heavily deformed austenite to ferrite during cooling.

Summarising, the results found proved that it is possible, by means of high deformations imposed in a temperature range where the dynamic recrystallization is inhibited and strain is accumulated in austenite structure, to obtain grain refinement. The microstructures obtained are characterised by fine ferrite grain size and high ferrite volume fractions, especially when the prior austenite grain size is held at sufficiently small values. However, at the same deformation conditions (strain and prior austenite grain size) DIFT showed a more refining power.

Identification of the mechanisms to be exploited for producing UFG long product

On the basis of the results reported in the previous sections, both DIFT and Heavy γ deformation mechanisms can be exploited to obtain UFG long product steels.

Very promising results in terms of grain size has been achieved both exploiting DIFT (deformation temperature between $A_{r3} +15^{\circ}\text{C}$ and $A_{r3} +40^{\circ}\text{C}$) and Heavy γ deformation mechanisms (deformation temperature at around $A_{r3} +70^{\circ}\text{C}$).

DIFT mechanism has a higher refining power, however it is difficult to fully exploit it using industrial configurations because of high deformation level required at low temperature.

So, for industrial production steel, the final microstructure will be a mix DIFT ferrite and Heavy γ deformation ferrite. For this reason it is necessary to optimize the thermomechanical cycle in order to maximize DIFT.

Main parameters that control the formation of ultrafine ferrite are the following:

- C content: DIFT occurs at $C < 0.35\%$. For higher C contents the critical strain becomes too high to be applied in a industrial mill.
- Mn content: a Low Mn content ($<1\%$) is favourable for DIFT.
- Small Prior Austenite grain size: it is the most important parameter that can be tuned in an industrial plant. Small prior austenite grain size is always beneficial for both DIFT and Heavy γ deformation mechanisms and should be held lower than $20\ \mu\text{m}$ (better around $10\ \mu\text{m}$) in order to achieve fine ferrite grains and high ferrite volume fraction.
- Deformation: High strain level in the last rolling pass (possibly higher than $\epsilon=0.35$) or high accumulated deformation in austenite at this stage are required to obtain UFG ferrite.

WP3: Experimental production of long UFG steels on pilot mill and industrial plant

Production of UFG steels at TUBAF pilot mill

Experimental production of long UFG steels was carried out on pilot rolling mill at TUBAF.

The rolling trials were divided in two groups:

- Rolling of steels 18CrMo4 and 50SiMoVNb8 on the continuous rolling mill whose aim was to study the influence of the rolling speed and finish rolling temperature on the microstructure and mechanical properties;

- Rolling of steels 18MnB2 and 30MnB4 on the roughing reversing mill of the continuous line whose aim was to study the influence of finish rolling temperature on the microstructure and mechanical properties.

For all the tested steels, it was possible to obtain ultrafine ferrite grains ranging from 2-4 μm .

The trend of 18CrMo4 steel average grain size is to decrease with the finishing rolling temperature and with increasing the rolling speed.

Regarding 30MnB4 and 18MnB2 same results as before can be assessed. In particular ferrite grain size is fine for all the hot rolling temperatures and decreases with the hot rolling temperature.

For 50SiMoVNB8 steels both hardness and average grain size have not a clear trend, both in terms of rolling speed and finish rolling temperature effect.

Industrial production of UFG steel

Industrial production of long UFG steel was carried out at ORI MARTIN industrial plants. The chosen chemical composition was 30MnB4.

The material was hot rolled to wire-rods of 8 and 14mm diameter as agreed with Agrati (fastener producer) for the production of prototype screws (as reported in WP5). The steel was hot rolled according to the process indications suggested from the results after hot rolling in TUBAF pilot mill and it consisted to lower the entrance temperature at the finishing mill in order both to obtain a small prior austenite grain size and to do finishing rolling in a DIFT temperature range. It could be done tuning the cooling devices before finishing mill in order to get at the entrance the requested temperature.

Results showed that the average grain size of final product industrially produced was 7 μm .

The corresponding conventional material grain size produced by ORI Martin is around 12 μm . It means that only decreasing the entrance temperature at finishing mill helps to almost halve the final grain size, even if it is not enough to arrive at ultrafine range ($< 4\mu\text{m}$). To furtherly decrease the grain size it is necessary to act on the deformation at finishing mill and to modify the cooling pattern.

Parametric investigation of relationship between microstructural features and cold formability in the new UFG long steels

Relationships between steel microstructure and plastic deformation behavior (cold formability) of the material was investigated by FEM modeling. The main feature that was considered was the ferrite grain size. In particular the study focused on the comparison between steel with conventional and ultrafine microstructure. Calibration of the model was carried out by analyzing the UFG steel produced in TUBAF pilot mill (grain size about 3-4 μm) and the conventional one produced by ORI MARTIN (grain size about 12 μm).

The results of the mechanical tests allowed to build the ductility curves (strain to failure vs. triaxiality) related to the different microstructures to be used to simulate cold forming taking into account the material damage.

By using the identified damage model, it was possible to evaluate the plastic damage accumulation during the head screw forming and in the compression tapered specimen.

It was noted that the conventional 30MnB4 steel accumulates more plastic damage respect to UFG 30MnB4 steel and that the compression tests, that have been used for building the ductility curves, are more severe than the screw forming process, leading to an higher damage in the critical points.

This means that any small deviation in geometry or any small local defect in the material may generate a crack initiation more likely in the conventional steel than in UFG steel. This is confirmed by the compression test results. In fact UFG steel didn't show any defect in any condition, while the conventional steel exhibited a surface crack in the barrelled region in one of the tests.

WP4: Evaluation of UFG steels through microstructural and mechanical characterization.

In this WP the steels produced according the new hot rolling practices defined in WP2 and applied in WP3 (UFG steels), from pilot mill and/or industrial plant, have been characterized in terms of mechanical and microstructural properties as well as, when it is required by the application, the response to fatigue and machining. The characterization has been carried out in comparison with the current material used for the same application.

Fasteners

The differences found in tensile properties between the steel hot rolled with low finishing temperature (UFG) and the reference product hot rolled with conventional cycle (STD) consist of a slight decrease of tensile strength and an increase of reduction of area, which is a measure of ductility. The microstructure of UFG material consists of ferrite and pearlite and the average ferrite grain size (7 μm) is significantly finer than that of standard product (10-12 μm).

The increase in reduction of area by UFG steels can be explained both by the finer grain size and by the complete absence of hard phases as bainite in the final microstructure. This is probably due to the initial austenite grain size, which is finer than in the conventional product, where a certain amount of hard phases may be present.

Automotive – gear shaft

After producing UFG steels by pilot mill as foreseen by the procedure reported in WP1 for fabrication of gear shaft some test samples of 18CrMo4 and 17CrV6 have been carburized.

After the carburizing treatment, the hardness profiles have been practically the same for the samples of standard grain size and of ultra fine grain size, and no clear difference has been found between the austenitic grain size of the standard samples and of the UFG samples.

No significant differences have been found in the tensile properties of 18CrMo4 after hardening and stress relief for the steel with standard grain size and with ultra-fine grain size. The values of impact energy, determined by Charpy test, are higher for the samples with ultra fine grain size than for the samples with standard grain size. The torsion tests don't show a clear difference between the 18CrMo4 with standard and with ultra fine grain size.

In terms of response to fatigue, the smaller grain size of UFG steel in comparison to STDG steel achieved after carburizing treatment has not lead to a significant improvement on the fatigue properties of steels 18CrMo4 and 17CrV6.

The machining tests performed with the UFG 18CrMo4 and the STD 18CrMo4, in as-rolled conditions, show a higher flank wear in the case of UFG steel, presumably due to its higher hardness.

Automotive – spring

UFG steel has the same fatigue limit than STDG steel. The Woehler curves are characterized by the same scatter band and the same slope. All the expected advantages related to the grain refinement could not be evaluated since before induction hardening STDG and UFG steels had almost the same grain size. The positive aspect is that induction hardening seems to have not a detrimental effect on grain size coarsening, so potentially could be used to treat this kind of steel.

WP5: Mechanical components realization and full-scale assessment.

The objectives of this Work Package were the realization of selected components with the developed UFG steel long wire rods and bars, and the process and component qualification according to Internal Quality procedures and the identification of merits and criticalities.

Fasteners (carbon range 0.15-0.30 %)

The expected advantages in using UFG wire rod for the manufacturing of screw components were identified in a reduced amount of the scrap after cold forging due to forging bursts and in the possible suppression of the annealing of hot rolled wire rod before cold forging.

The cold forging trials performed at Agrati, were related to two different diameters screws: M8 (8 mm diameter) and M14 (14 mm of diameter). In both cases, UFG wire rod produced by ORI MARTIN (ferrite grain size 7 μm) and STD wire rod (ferrite grain size 12 μm) were compared. In the specific case of M14 screw, whose process route includes annealing of wire rod, a lot was also produced without annealing.

The results of the cold forming trials did not show evident improvements ascribable to the use of UFG wire rod in terms of scrap amount. Moreover, when investigated (M14 screw) the suppression of annealing of wire rod produced a net increase of scrap amount.

The possible reasons identified for that behaviour, in contrast with the results of the damage model reported in WP3, are that (1) the experimented grain refinement (up to 7 μm) and the consequent

increase in ductility are not enough to produce a significant difference during the cold forming process and (2) the presence of some surface defect in the produced bars invalidated the results.

It must be noted that the parametric investigation of relationship between microstructural features and cold formability in WP3, which put in evidence significant improvement in the forming behaviour of UFG steel, refers to the steel produced in TUBAF whose grain size was 3-4 μm .

On the other hand, no important criticalities have been identified in the component quality, as the results of the product qualification show that the mechanical properties of the finished parts fall completely in the accepted ranges.

Automotive – spring (carbon range 0.40-0.60 %)

The expected advantages in using UFG wire rod for the manufacturing of spring components were identified in an improvement of fatigue resistance. Actually the results showed that the fatigue life of UFG steel springs was shorter than that of STDG steel springs (approximately 50%).

This result can be explained by the fact that the austenite grain size of STDG steel, after induction treatment, was finer than that of UFG steel. This means that the microstructure after the treatment is not affected by the hot rolled microstructure, so the use of UFG steel in this case doesn't bring any advantage.

WP6: Guidelines for UFG steel long products application to automotive sector

Automotive – gear shaft and spring

The prototype component selected for this steel grade (gear shaft) requires to be case hardened (carburized) in order to achieve the required surface hardness.

Metallurgical and fatigue test performed on 18CrMo4 and 17CrV6 UFG steels assessed that the grain refinement is completely lost during carburizing because the long permanence at the austenitization temperature produce phase transformation, so UFG and STD steels have final comparable grain size. The fatigue resistance properties are therefore very similar.

As consequence, the possibility to produce the gear shaft in carburizing UFG steel, doesn't bring any advantage.

Same is valid for spring application. In fact, even in this case microstructure after the treatment is not affected by the previous hot rolled microstructure, so the use of UFG steel in this case doesn't bring any advantage.

Fasteners

The results of the cold forming trials did not show evident improvements ascribable to the use of UFG wire rod in terms of scrap amount. The possible reason identified for that behaviour is that the experimented grain refinement of steels industrially produced by ORI MARTIN was about 7 μm while the conventional steel show about 12 μm and the consequent change of ductility is not enough to produce a significant effect during the cold forming process.

However, it has to be noted that the data of scrap amount, determined during the forging operations at Agrati, merely refer to the total scrap, as no selection of the defect type has been done.

Actually, it has been found that for a significant number of pieces the real cause of rejection was not due to *forging bursts*, but to surface defects which were pre-existing on the wire rod.

No criticalities have been identified in the component quality, as the results of the product qualification show that the mechanical properties of the finished parts fall completely in the accepted ranges.

In addition, the investigation of relationship between microstructural features and cold formability carried out using the steel produced on pilot mill with grain size around 3 μm , put in evidence significant improvement in the forming behaviour of UFG steel. It means that a further refinement of grain size should have produced a more evident effect in scrap reduction during the cold forming process. Moreover, results showed that any small deviation in geometry or any small local defect in the material may generate a crack initiation more likely in the conventional steel compared to the UFG steel, and, if it were necessary to increase the complexity of the design of a screw introducing a more severe forming pattern, the use of UFG steel could be helpful and should have an higher safety margin respect to the conventional one.

Conclusions

The use of UFG steel showed to be potentially able to allow the improvement of cold forming for fastener production. This evidence showed up when the UFG steel from pilot mill (grain size around 3 μm) and conventional steel (grain size around 12 μm) were compared, while the difference was not so evident between the industrially produced UFG (grain size around 7 μm) and conventional steel because it was not possible to produce industrially a finer grain size.

To furtherly decrease the grain size it is necessary to better tune the operating practices for hot rolling in terms of deformation passes at finishing mill and cooling pattern.

The selected components for powertrain application (gear shaft and spring) after their fabrication require a further heat treatment that destroy the memory of the previous microstructure, as consequence, the possibility to produce the gear shaft or suspension springs in UFG steel doesn't bring any advantage.

SCIENTIFIC AND TECHNICAL DESCRIPTION OF THE RESULTS

In order to meet the increasing needs from economic and social developments in future, the research on new generation steels, with higher strength and longer duration, has become a worldwide issue. It is well known that there exist various mechanisms to strengthen the steels, but grain refinement is the only method to improve both strength and toughness simultaneously.

A ferrite grain size in the range of 1÷4 µm and a steel microstructure characterised by a mixture of ferrite-pearlite and/or martensite, bainite, retained austenite microstructure, can give a very good combination of mechanical (strength, ductility, toughness, fatigue) and technological properties (machinability, cold/warm metal forming, etc.) for final application to automotive components.

Final application to full-scale automotive components will quantify improvements with respect to current materials and processes.

Objectives of the project

The general aim of LUNA project is to define the guidelines for the production and best utilisation of ultrafine grained (UFG) carbon steel long products for mechanical applications, using existing productive plants, through the exploitation of advanced thermomechanical processes.

In particular the objectives of the project are:

- Definition of the most suitable thermomechanical process for long ultrafine grained (UFG) steel production.
- Identification of merits, in terms of microstructural and mechanical properties of UFG long steels in as-rolled conditions and after cold/warm forming.
- Production of components or component-like dummies in UFG long products and evaluation of their mechanical performances.
- To give guidelines for power train and automotive UFG long products applications.

2. DESCRIPTION OF ACTIVITIES AND DISCUSSION

2.1 WORK PACKAGE 1: SELECTION AND SUPPLY OF MATERIALS AND IDENTIFICATION OF MECHANICAL COMPONENTS FOR FINAL APPLICATIONS

The objectives of this WP are:

- Selection of steel chemical compositions.
- Production and supply of starting materials.
- Identification of mechanical components for final applications.

Various chemical compositions have been chosen in a wide range of C contents (0.15-0.6%C) and the starting materials have been manufactured in laboratory and/or in industrial plant.

Identification of prototype components, definition of their technical requirements, and identification of the most adequate process route and possible variations to conventional productive procedures have been assessed. After choosing the prototype components, test procedures and plan for final characterization have been assessed.

Task 1.1: Material selection

A number of different chemical compositions, with carbon content included in the range 0.15-0.60 % have been selected. The prototype components have been identified among the following two families: fasteners (e.g. screws, bolts) and automotive applications (powertrain components, springs).

Fasteners (carbon range 0.15-0.30 %)

For fastener applications the range of carbon content 0.15-0.30 % has been investigated.

In particular, in order to study the effect of chemical composition on UFG production, two different C and Mn contents have been selected. Since in these applications – due to the production route which includes quenching – the addition of chemical elements enhancing hardenability is required, boron addition has been also investigated. On this basis, the following grades have been selected: 30MnB4, 18MnB2, 30MnB7, 18MnB7, 18Mn7.

The first two grades – 30MnB4 and 18MnB2 – are both C-boron-added steels, which are currently produced by Ori Martin. The grades designated as 30MnB7 and 18MnB7 are variants characterised by a higher manganese content (target 1.70 %), and the grade named 18Mn7 is a further high-Mn variant which does not contain boron addition.

An usual production route for fasteners is the following:

- hot rolling in a wire rod mill followed by controlled cooling (Stelmor cooling) with very low cooling rates (~ 0.1 K/s) to promote low tensile strength and avoid the formation of hard phases (e.g. bainite);
- spheroidizing annealing, or in alternative a shorter annealing cycle, depending on requirements, of wire rod (typical annealing cycles last 8-12 hours);
- cutting and fastener manufacturing (cold forming);
- quenching and tempering;
- surface treatment (e.g. galvanising) when required.

The expected advantages of UFG steel in this range of applications consist firstly in the chance to reduce or possibly avoid the annealing, which is usually made before cold forming and is very expensive in terms of energy and time. Such reduction is supposed to be possible as a finer microstructure promotes the development of a more globular pearlite [1-3], at the same time preventing the formation of hard phases (e.g. bainite) during Stelmor cooling. For similar reasons, a further possible advantage could be a reduction of scraps caused by forging bursts in screw heads occurring during cold forming process.

Automotive – powertrain (carbon range 0.15-0.20 %)

With regard to automotive powertrain applications, steel grades for carburising have been taken into account, as 18CrMo4, 17CrV6, 17CrVNb6. The former has been chosen because it is a steel grade which is usually used for the manufacturing of some powertrain components, while the other steel grades have been selected with the aim to obtain more easily ultrafine grain size.

The main interests to ultrafine-grade steel for the automotive industry are related to the possibility to achieve:

- Higher fatigue and impact resistance properties in comparison to similar steel composition.
- Lower alloy content in particular to avoid the use of Ni alloyed steel
- Cost and weight saving.

Automotive – spring (carbon range 0.40-0.60 %)

In the case of automotive spring applications, the proposed steel is 50SiMoVNb8, which is a steel grade used for helicoidal suspension springs, at present produced with standard grain size. The aim of grain refinement is to increase the fatigue performances of high stressed spring steel.

Task 1.2: Manufacturing of starting material and its characterisation

The initial materials, to be used in the investigations of thermomechanical cycles and mechanisms of formation of ultrafine (UFG) microstructures, have been manufactured by means of industrial process (Ori Martin, Gerdau) and laboratory scale equipment (CSM and Gerdau).

Fasteners (carbon range 0.15-0.30 %)

The materials, produced as industrial billets and experimental ingots are listed in Tables 1 and 2.

Grade/Heat	C	Mn	Si	S	P	Cr	Ni	Cu	Al	Ti	N	B
30MnB4 AE1055	0.30	0.82	0.08	0.013	0.013	0.14	0.05	0.12	0.023	0.050	60	27
18MnB2 AE4008	0.17	0.73	0.06	0.008	0.009	0.12	0.05	0.008	0.028	0.043	78	21

Table 1: Chemical compositions of Ori Martin industrial heats (% mass, N and B in ppm).

Grade/Heat	C	Mn	Si	S	P	Cr	Ni	Cu	Al	Ti	N	B
30MnB7/ VM2625	0.28	1.70	0.09	0.014	0.013	0.13	0.10	0.12	0.020	0.050	60	27
18MnB7/ VM2624	0.17	1.70	0.07	0.009	0.010	0.12	0.10	0.08	0.023	0.041	70	21
18Mn7/ VM2623	0.16	1.67	0.08	0.008	0.010	0.12	0.10	0.08	0.029	0.041	70	-

Table 2: Chemical compositions of CSM laboratory heats (% mass, N and B in ppm).

The industrial square billets (140 x 140 mm, length 12 m) have been produced and hot rolled to bars with diameter 50 mm at Ori Martin plant. Before hot rolling, the billets have been reheated in a walking-beam furnace, passing through the following three zones:

1. Preheating (T1);
2. Heating (T2);
3. Equalization (T3).

The main rolling parameters (temperatures and rolling speed) of the bars are reported in Table 3.

Grade/Heat	Reheating Furnace Temperatures (°C)			Rolling Temperatures (°C)		Rolling Speed (m/s)
	T1	T2	T3	Step 7	Step 15A	
30MnB4/ AE1055	943	1118	1164	1015	962	2.21
18MnB2/ AE4008	942	1126	1158	1019	966	2.21

Table 3: Rolling parameters for 50 mm diameter bars produced at Ori Martin.

Grade/ Heat	A _{c1}	A _{c3}	A _{r3}	A _{r1}	M _s
30MnB4/ AE1055	720	811	750	663	360
18MnB2/ AE4008	719	840	797	676	430
30MnB7/ VM2625	713	805	691	596	350
18MnB7/ VM2624	712	838	720	583	390
18Mn7/ VM2623	708	835	730	585	430

Table 4: Phase transition critical points of steels for fasteners (°C).

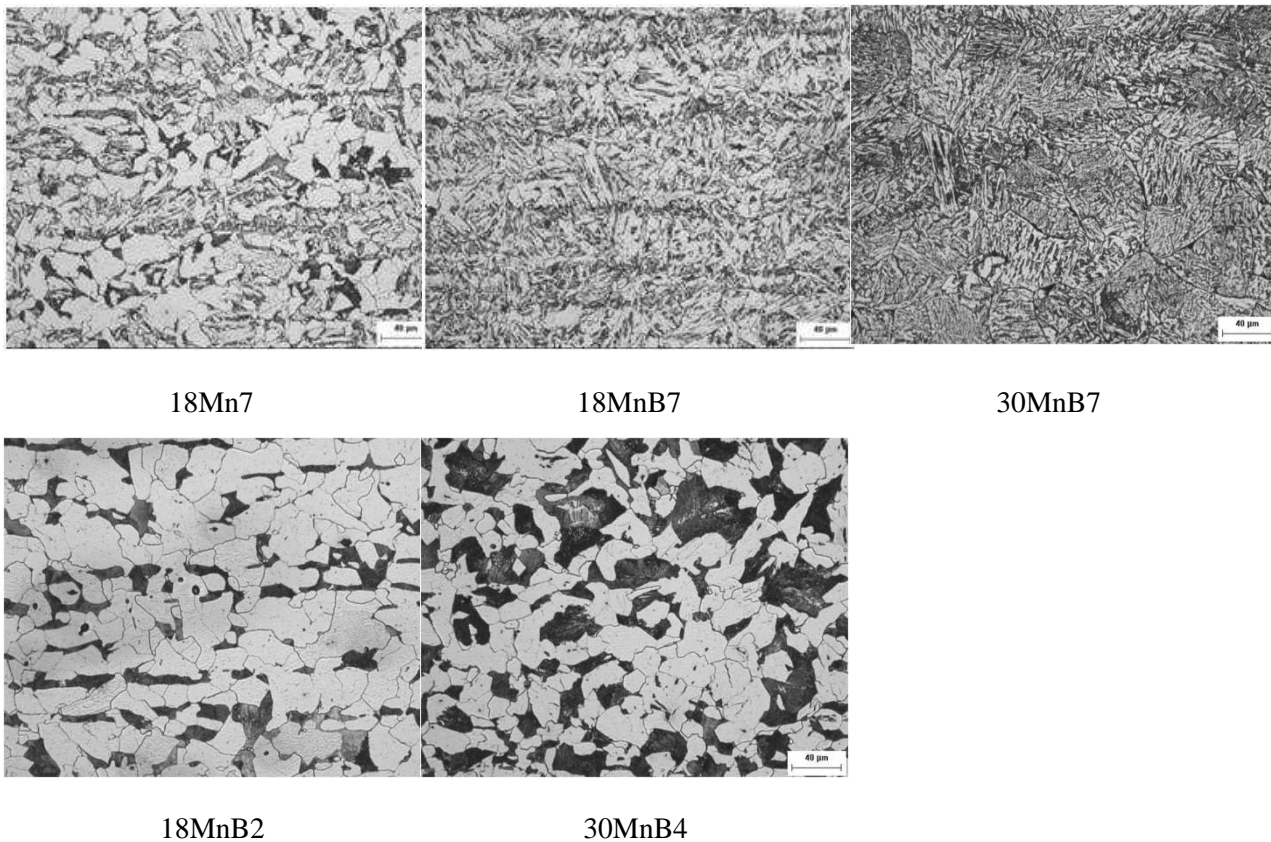


Figure 1: Initial microstructure of samples selected for fasteners applications.

The laboratory ingots (CSM) have been hot rolled to plates of thickness 14mm according to a rolling schedule with eight passes. The reheating temperature was 1270°C, the steel temperature during hot rolling (measured by a pyrometer) ranged from 1090 °C (1st pass) to 1020°C (9th pass). The applied forces increased with pass number due to work hardening, and ranged between 20 and 40 t. The phase transition critical points, determined by dilatometry tests through slow heating at 0.05 K/s up to 900 °C followed by slow cooling at 0.05 K/s, are reported in Table 4. M_s has been determined through quenching at 150 K/s (see CCT diagrams in Task 2.2).

Microstructures of the as-rolled samples are reported in Figure 1. The industrial bars (30MnB4 and 18MnB2) show ferrite-pearlite microstructure induced by the slow cooling used in ORI Martin bar process.

Automotive – powertrain (carbon range 0.15-0.20 %)

The materials industrially produced by Gerdau are listed in Table 5. The industrial 18CrMo4 has been rolled to bars of diameter 50 mm and then send to TU Freiberg for experimental hot rolling trials. Steel

17CrV6 has been rolled to bars of diameter 70 mm and heat treated with isothermal annealing. The critical points of the industrial heats have been calculated and the results are shown in Table 6. The mechanical and microstructural characterisations of the industrial 17CrV6 have been performed and are reported in Table 7 and Figure 2. The microstructure is 100% ferrite-pearlite with some bands in the core.

Grade/ Heat	C	Mn	Si	P	S	Cr	Ni	Mo	V	Cu	Al
18CrMo4	0.17	0.79	0.32	0.011	0.024	1.07	0.22	0.17	0.006	0.23	0.020
17CrV6	0.18	0.94	0.30	0.010	0.028	1.53	0.10	0.02	0.050	0.17	0.023

Table 5: Chemical compositions of Gerdau industrial heats (% mass).

Material	Ac ₁ (°C)	Ac ₃ (°C)	B _s (°C)	B _f (°C)	M _s (°C)	M _f (°C)
17CrV6	744	841	589	459	439	224
18CrMo4	737	848	609	479	442	227

Table 6: Critical points of industrial heats.

Rm (MPa)	Re (MPa)	Re/Rm	Z (%)	A(%)	Hardness (HB)
637	391	0.61	69	29	156

Table 7: Mechanical characteristics of 17CrV6 isothermally annealed.

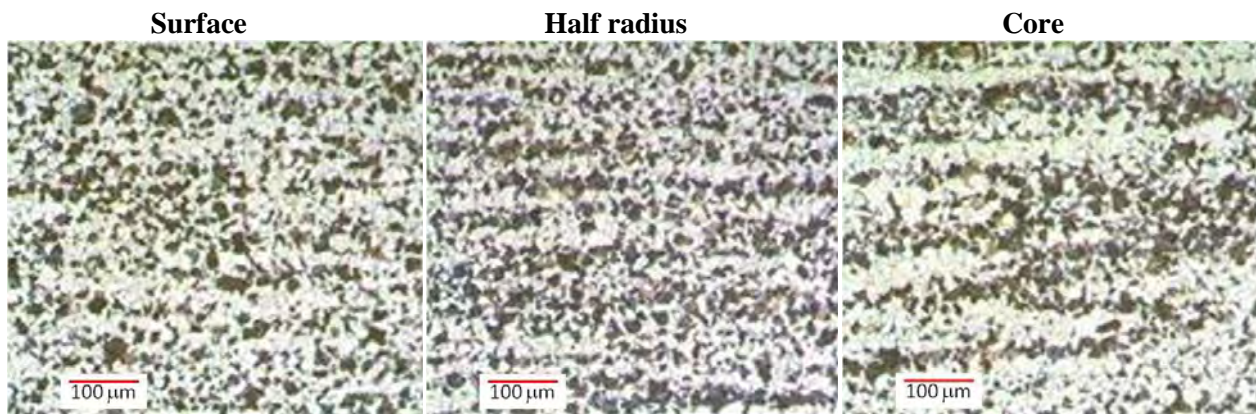


Figure 2: Microstructure of a sample of 17CrV6 with isothermal annealing.

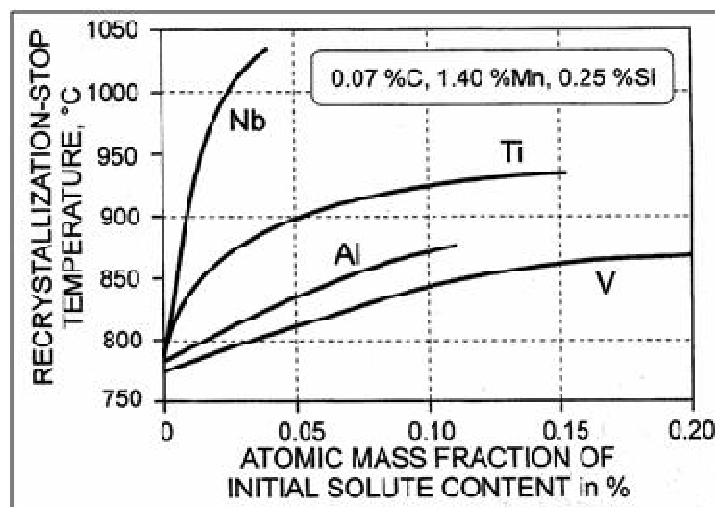


Figure 3: Influence of the different microalloying elements on the recrystallization-stop temperature.

As niobium is the most effective element to increase the non recrystallization temperature (Figure 3) it has been held interesting to manufacture some experimental heats of 17CrV6 containing a Nb addition, to favour the attainment of ultrafine grain size.

At low strain rates of 10^{-1} – 10^{-3} s⁻¹ dynamic precipitation of Nb(CN) occurs, which results in the retardation of dynamic recrystallization. Static recrystallization is markedly retarded by the Nb initially in solution. The majority of research results indicate that the retardation of recovery and recrystallization is caused by strain induced precipitation of Nb(CN) which exerts a pinning effect on the deformed substructures.

For the reasons above explained, three different experimental heats have been manufactured to do a comparison between the heat with addition of Nb and the two other steel grades which have been also manufactured as industrial heats.

Grade/ Heat	C	Mn	Si	P	S	Cr	Ni	Mo	V	Al	Nb
18CrMo4/	0.18	0.87	0.29	0.010	0.025	1.05	0.15	0.18	0.004	0.016	-
17CrV6/	0.18	0.93	0.27	0.012	0.019	1.49	0.10	$\frac{0.00}{3}$	0.050	0.019	-
17CrVNb6/	0.18	0.94	0.29	0.010	0.016	1.51	0.10	$\frac{0.00}{8}$	0.050	0.015	0.025

Table 8: Chemical compositions of Gerdau Experimental heats (% mass).

Material	Heat number	Ac ₁ (°C)	Ac ₃ (°C)	B _s (°C)	B _f (°C)	M _s (°C)	M _f (°C)
17CrV6	719	744	841	589	459	439	224
18CrMo4	720	737	848	609	479	442	227
17CrVNb6	721	745	841	586	456	438	223

Table 9: Critical points of experimental heats.

	UTS (MPa)	YS (MPa)	Hardness (HV)	Z(%)
17CrV6 (719)	657	478	192 - 212	71
17CrVNb6 (721)	753	517	206 - 224	50

Table 10: Mechanical properties of 17CrV6 and 17CrVNb6.

In Table 8 the chemical composition of the three experimental heats are shown. These three experimental heats have been manufactured in an induction furnace and afterwards have been forged to diameter 50mm. The calculated critical points are shown in Table 9. The mechanical properties and the microstructures are shown in Table 10 and Figure 4.

Automotive – spring (carbon range 0.40-0.60 %)

A billet of 50SiMoVNb8, with the chemical composition reported in Table 11, has been rolled to diameter 50 mm for the cold manufacturing of helicoidal suspension springs. The calculated critical points are shown in Table 12.

As illustrated in Figure 5, steel 50SiMoVNb8 is constituted of a ferritic–pearlitic microstructure. Some isolated bainitic and martensitic packets have been detected as well.

Grade/ Heat	C	Si	Mn	P	S	Ni	Cr	Mo	Cu	Al	Ti	V	Nb
50SiMoVNb8	0.52	2.08	0.72	0.012	0.010	0.05	0.31	0.28	0.08	0.004	0.003	0.17	0.036

Table 11: Chemical composition of Gerdau industrial heat (% mass).

Material	Heat number	Ac ₁ (°C)	Ac ₃ (°C)	B _s (°C)	B _f (°C)	M _s (°C)	M _f (°C)
50SiMoVNb8	48988	780	889	578	448	229	84

Table 12: Critical points of industrial heat.

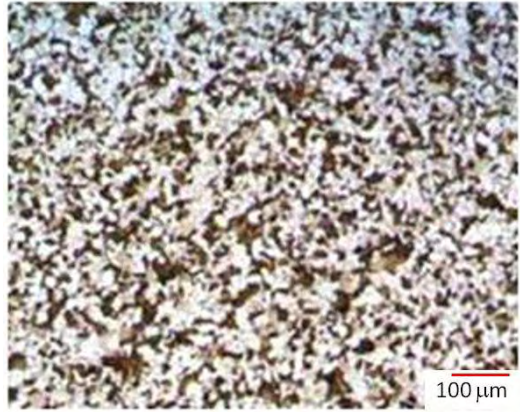
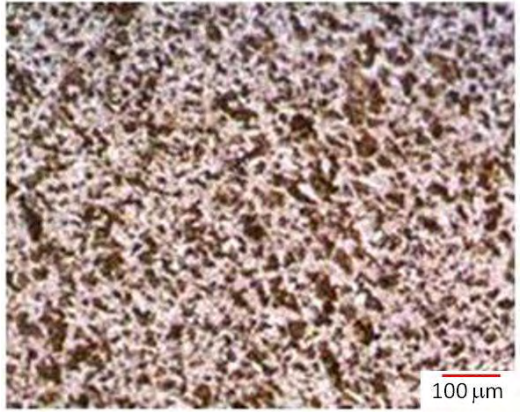
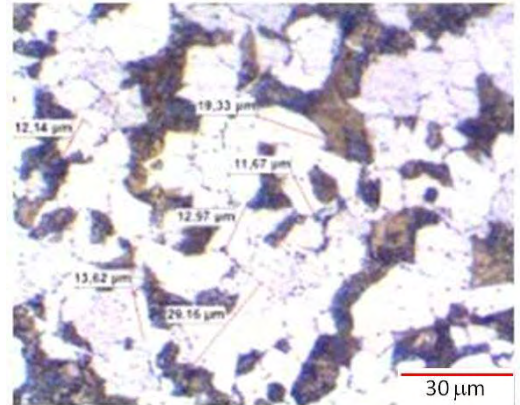
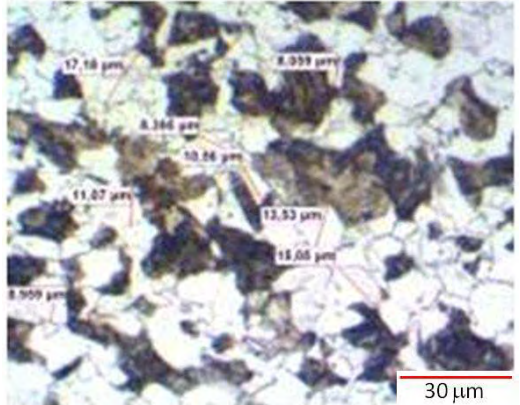
	17CrV6 (719) Experimental	17CrVNb6 (721) Experimental
		
Grain size: Between 8 and 30 μm		

Figure 4: Microstructures of laboratory heats.

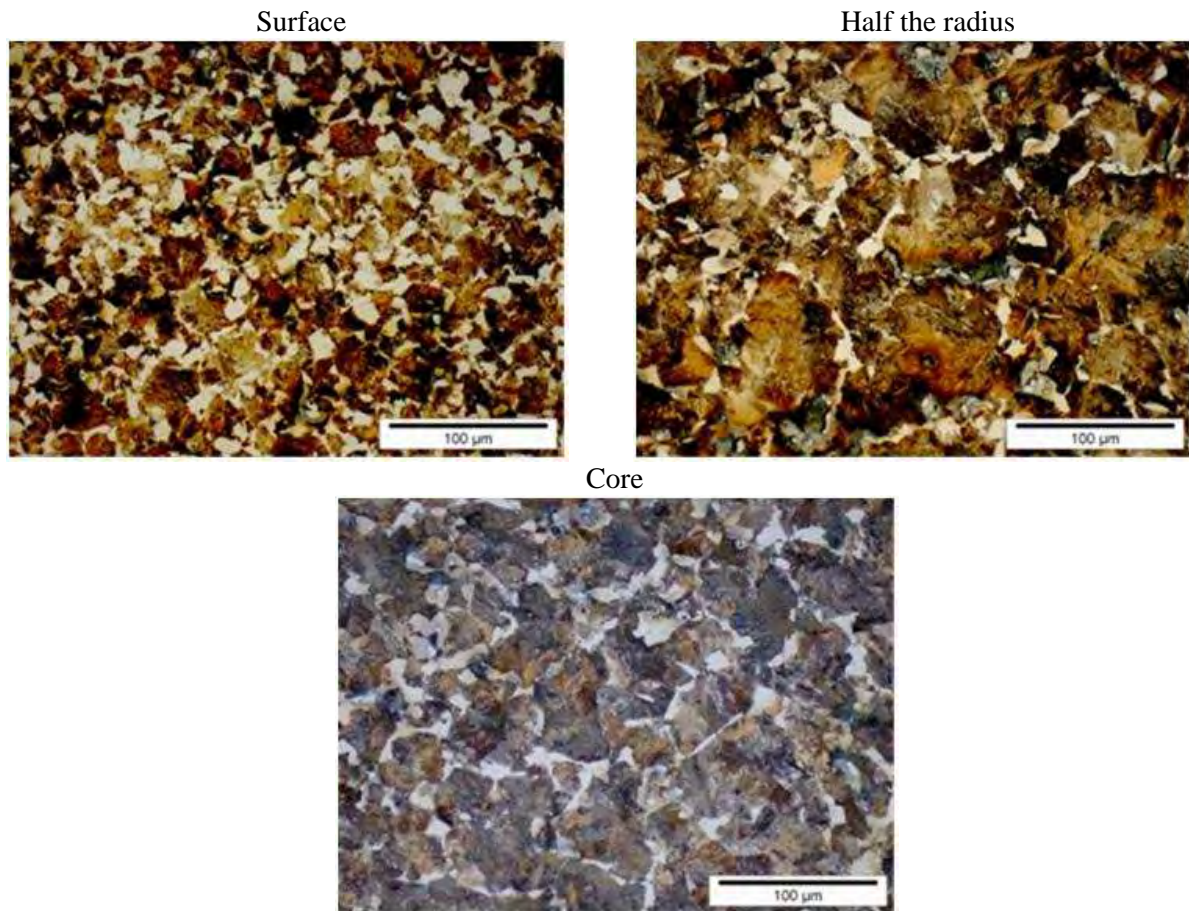


Figure 5: The ferritic-pearlitic microstructure of steel 50SiMoVNb8 (etched in Nital for 5-10 s).

Task 1.3: Identification of prototype components and definition of technical requirements

Fasteners (carbon range 0.15-0.30 %)

The selected components are three screws of different shapes, sizes and final applications, produced by the company Agrati SpA. Their main features are summarised in Table 13. All the components selected to investigate the possible benefits of ultrafine microstructure are currently manufactured in 30MnB4. Such steel is the most common and was considered the most interesting by the producer.

The manufacturing process route is the following:

- selection of wire incoming diameter, depending on the specific screw;
- annealing (no spheroidizing) when required (M7x1x42 and M14x1.5x70);
- cold drawing to diameter depending on the specific screw;
- cold forging and thread rolling;
- quenching and tempering;
- coating;

The three-dimensional drawings are shown in Figure 6.

The final aim of UFG steel for this application is to eliminate the annealing step (for the components where it is applied, i.e. M7 and M14 bi-hexagonal screws) and to reduce the scraps due to the forging bursts (Figure 7) in screw head, which can occur during cold forming (for all the components selected).

Component	Size / class	Application	Steel (currently used)	Annealing	UFG objectives
Screw, bi-hexagonal flange head with hexagon socket	M7x1x42 / 10.9	Car steering system	30MnB4	YES	- Elimination of annealing - Reduction of scraps
Screw, bi-hexagonal socket head cap screw with flange	M14x1.5x70 / 10.9	Suspension system	30MnB4	YES	- Elimination of annealing - Reduction of scraps
Screw, hexalobular flange	M8x1.25x43 / 10.9	Power train	30MnB4	NO	- Reduction of scraps

Table 13: Selected components (fasteners).



Figure 6: Overall views of the three screws selected.

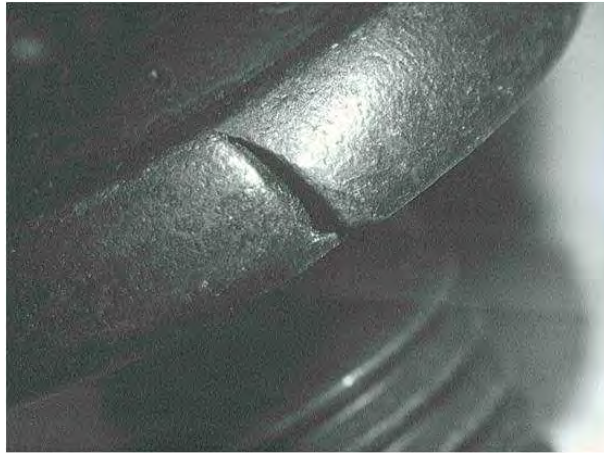


Figure 7: Example of forging burst.

Automotive – powertrain (carbon range 0.15-0.20 %)

The prototype component selected by CRF, jointly to FIAT Powertrain Technologies, is the 1st gear shaft belonging to the C514 gear (Figure 8). The part is currently produced with 17NiCrMo4 steel for high stressed application. The aim is to find an UFG steel without Ni, like 18CrMo4, able to replace the original 17NiCrMo4 steel.

The component is cold formed, the maximum hardness required is 180 HB. The steel bar diameter must be 32.5 mm. The gear shaft manufacturing process (Figure 9) is divided in two main parts: the first part performed by TEKFOR (forging supplier), the second made in FIAT Powertrain Technology plant.



Figure 8: 1st gear shaft. C514 gear.

TEKFOR	FIAT Powertrain
<ol style="list-style-type: none"> 1. Bar cutting (if hardness is 180HB) 2. Grid blasting 3. Phosphating and soaping 4. Cold forming 5. Heat treatment <ul style="list-style-type: none"> - isothermal annealing (FPT) total cycle time is about 11h. <ul style="list-style-type: none"> pre-heating at 950°C for 3h30min cooling down to 650°C in 6min30sec stabilization at 650°C for 7-8h until 180°C - Isothermal annealing (TEKFOR) total cycle time is about 9h. <ul style="list-style-type: none"> pre-heating @ 920° C for 1h30min cooling down to 500-550°C stabilization at 610°C for 6h 	<ol style="list-style-type: none"> 6. Centering 7. Complete turning 8. Hobbing (one or more operations depending on specific gear) 9. Rolling (spline generation by plastic deformation) 10. Teeth chamfering 11. Drilling and milling 12. Gear shaving 13. Heat treatment <ul style="list-style-type: none"> - gas carburizing with ENDOGAS + 3% Methane <ul style="list-style-type: none"> pre-heating at 800 – 900°C for 1h30min carburizing at 920°C for 3,5h diffusion at 820°C for 1h50min quenching at 120°C with hot oil washing: water 60°C - stress relief: 160°C for 2h 14. Straightening 15. Grinding of diameters, grooves and shim 16. Gear super-finishing or final shaving

Figure 9: TEKFOR and FPT manufacturing cycle.

The main critical aspects of this manufacturing cycle are related to the isothermal annealing, required to have good machinability after cold forming (point 5) and the carburizing treatment necessary to give the required hardness on the gear surface (point 13) since the parts must stay to a temperature higher than the austenitization point. The related grain coarsening could reduce the advantages coming from UFG structure.

To evaluate the effect of UFG microstructure prior to carburizing treatment, it has been decided to address the experimental activity on simple fatigue test comparing two different grain sizes of 18CrMo4 carburized with the same heat treatment cycle and two different grain sizes of 17CrV6 proposed by Gerdau. In this steel a finer grain size could be achieved, in comparison to 18CrMo4, due to vanadium addition.

Automotive – spring (carbon range 0.40-0.60 %)

CRF effort has been to finalize LUNA project outputs, regarding the grain refinement of spring steels, on a suspension spring component (Figure 10) through the involvement of a FIAT supplier.



Figure 10: Suspension spring.

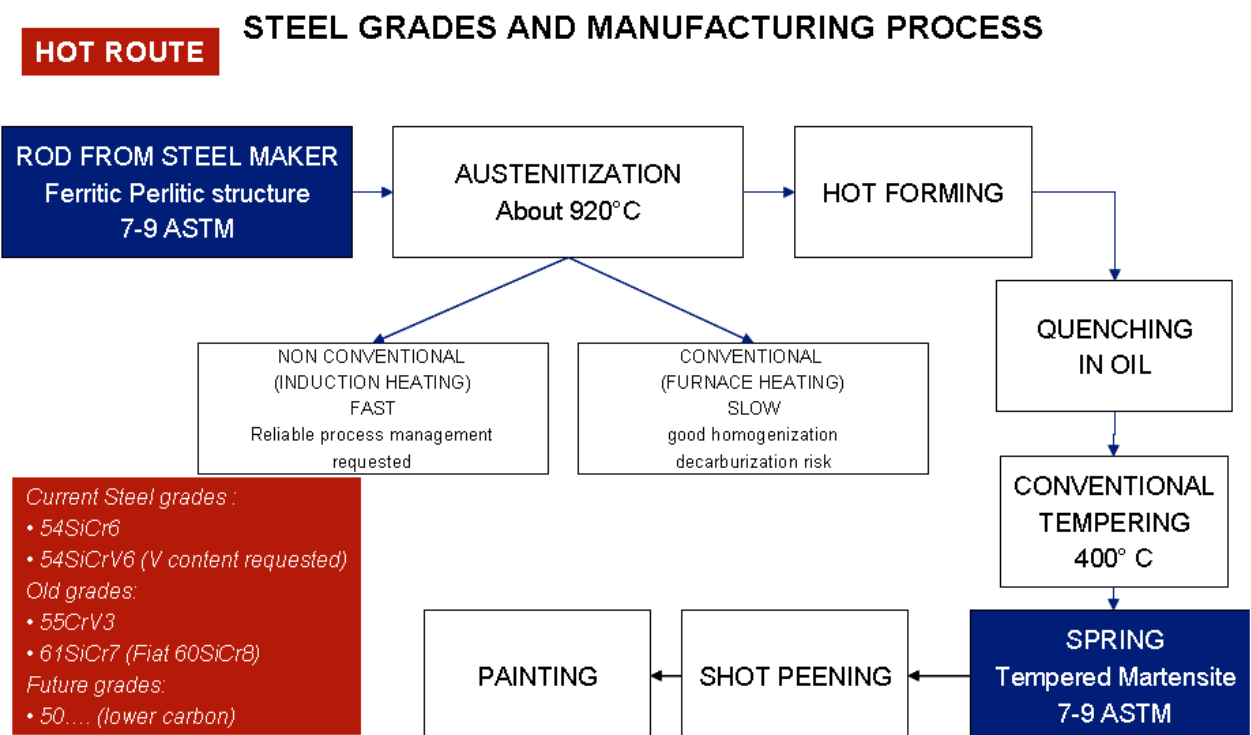


Figure 11: HOT ROUTE for helicoidally spring manufacturing.

Several contacts with the main suspension spring manufacturers (MUBEA and ALLEVARO REJNA AUTOSUSPENSION-ARA) were held by CRF in order to assess their interest and commitment on this project and share the selection of the chemical steel composition.

ARA showed its interest to grain refinement considered as a way to achieve better performances without cost increasing for the limited addition of expensive elements in the chemical steel composition. Two different manufacturing ways to achieve suspension spring are at present used in ARA: “Hot Route” (Figure 11) and “Cold Route” (Figure 12).

“Cold route” process is convenient for UFG steel as the heat treatment of the wire is done by induction hardening. This process involves very short soaking time preventing grain growth.

The steel grade at present used by ARA, with this manufacturing process, is 54SiCr6. This steel has the following advantages:

- V content not requested for cold route application
- Lower price for automotive market
- Austenitic grain size 9 ASTM (at the end of the hardening cycle)

The disadvantage is its high difficulty to reach a significant grain refinement with standard rolling equipment due to the complete absence of micro-alloyed elements.

STEEL GRADES AND MANUFACTURING PROCESS

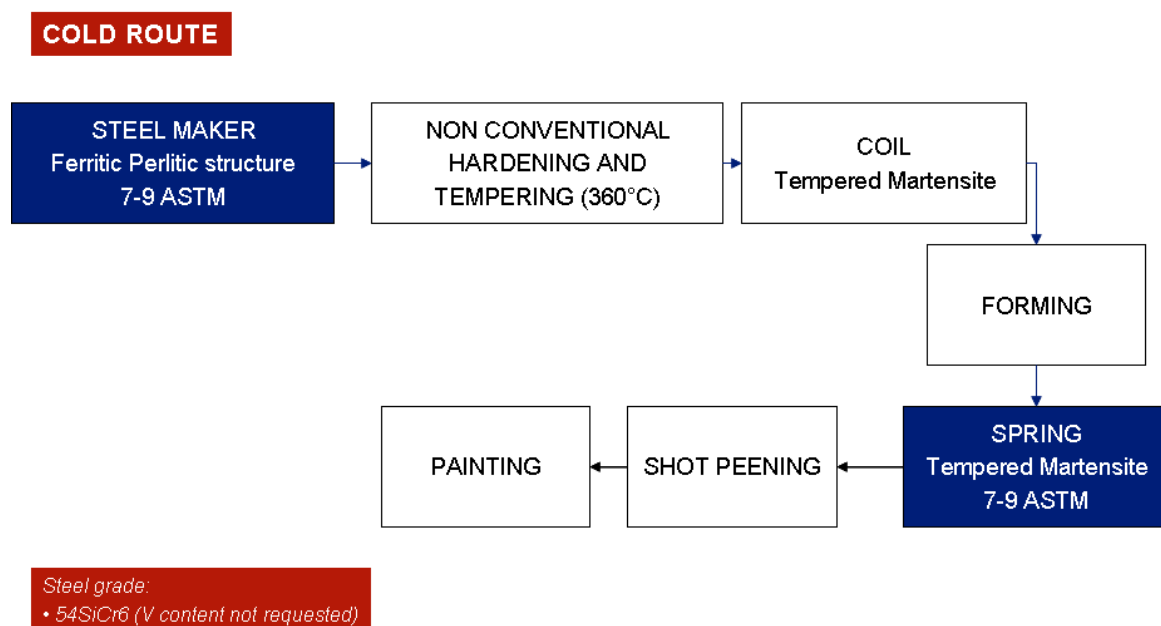


Figure 12: COLD ROUTE for helicoidally spring manufacturing.

The steel proposed by Gerdau is 50SiVMo8Nb. In comparison to 54SiCr6 it has:

- Best compromise between chemical composition (alloying and micro-alloying elements) and at present rolling technology to achieve the smaller grain size
- Austenitic grain size 13 ASTM already reached by Gerdau with a highly “stressed” rolling process.

The disadvantage is its high cost due to the expensive elements.

It was decided jointly to ARA, in spite of the cost, to proceed with the steel proposed by GERDAU focusing the experimental activity on the assessment of the real improvement due to the grain refinement without changing the chemical steel composition.

Task 1.4: Definition of tests procedure

Fasteners (carbon range 0.15-0.30 %)

For fasteners application two groups of tests have been identified: the first group includes the tests to be performed on wire rod before the forming operations, the second group includes the tests to be run on final products (finished screws).

Tests to be performed on wire rod:

- tensile test rod (before and after annealing) to obtain yield strength (YS) and elongation (EI);

- ferrite grain size evaluation;

Test to be performed on end product (finished screw):

- evaluation of compliance with the mechanical features provided for the respective classes of resistance;
- evaluation of percentage of scrap due to cracks and layering defects (failures, skin defects);
- evaluation of accidents / tool wear (tentative).

Even for these tests the results obtained with UFG steels will be compared to historical data when available and by direct comparison, by parallel processing of one batch of UFG steel and one batch of conventional steel. Tool wear on limited production batches is difficult to measure and its evaluation has to be considered tentative.

Automotive – powertrain (carbon range 0.15-0.20 %)

To compare the mechanical properties of the carburizing steel with two different grain sizes it has been decided to proceed as per the following way (Figure 13):

- Steel supply: CRF was supplied by Gerdau with 50mm diameter bars with standard grain size (STDG), while UFG bars (15mm) were supplied by Freiberg University.
- Preliminary test: CRF test procedure started with simple rotate bending fatigue test. The same procedure was followed with 17CrV6 steel (Figure 14).
- Test on component mock-up: By positive results of preliminary tests, that is significant improvement on the fatigue behaviour, the characterisation would have been carried on comparing 18CrMo4 UFG with 17NiCrMo4 STDG by rotate bending fatigue and further detailed investigation (eg. Three Point Bending Fatigue test, Impact test, etc.).

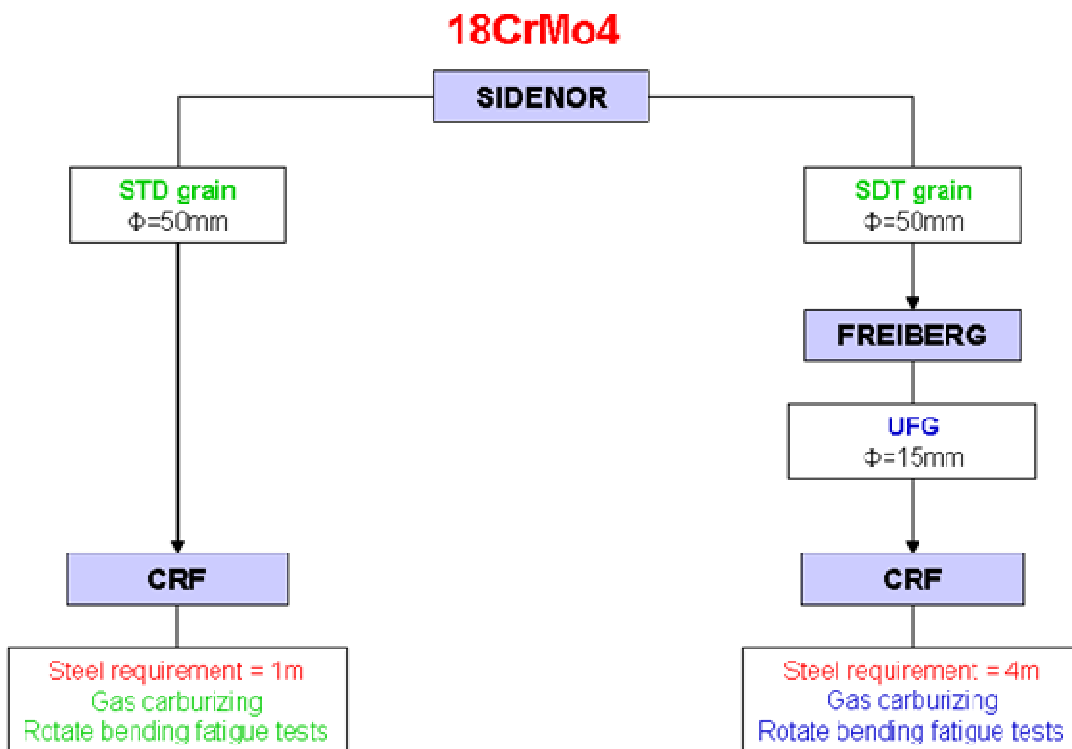


Figure 13: 18CrMo4 gear steel flow.

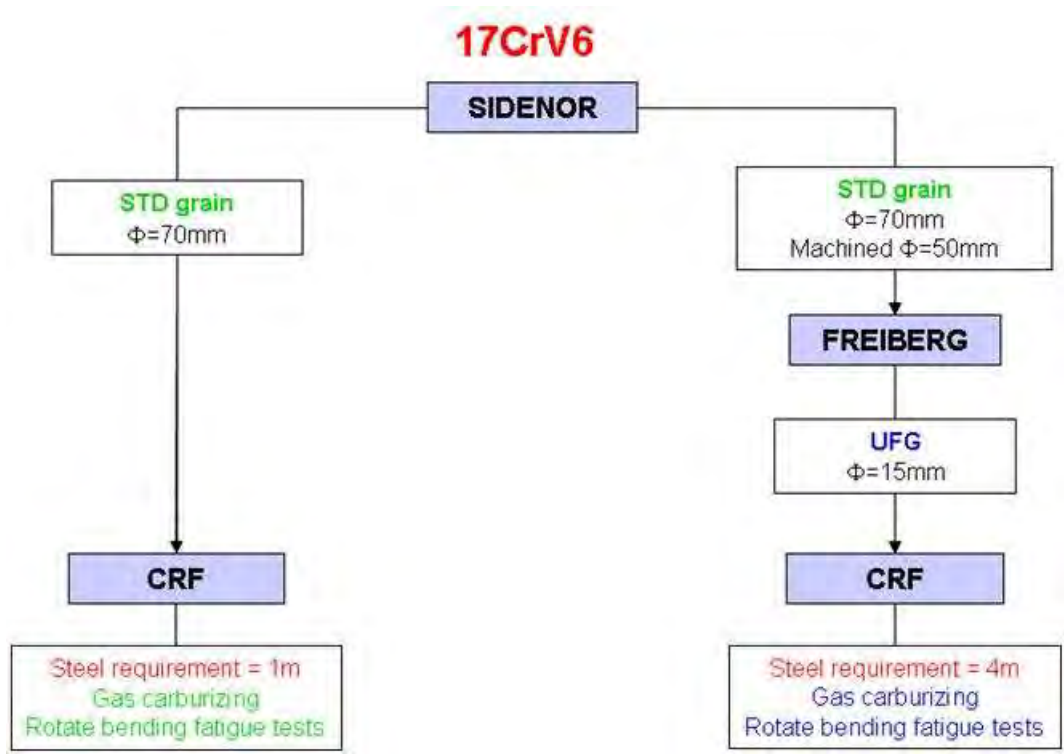


Figure 14: 17CrV6 carburizing steel flow.

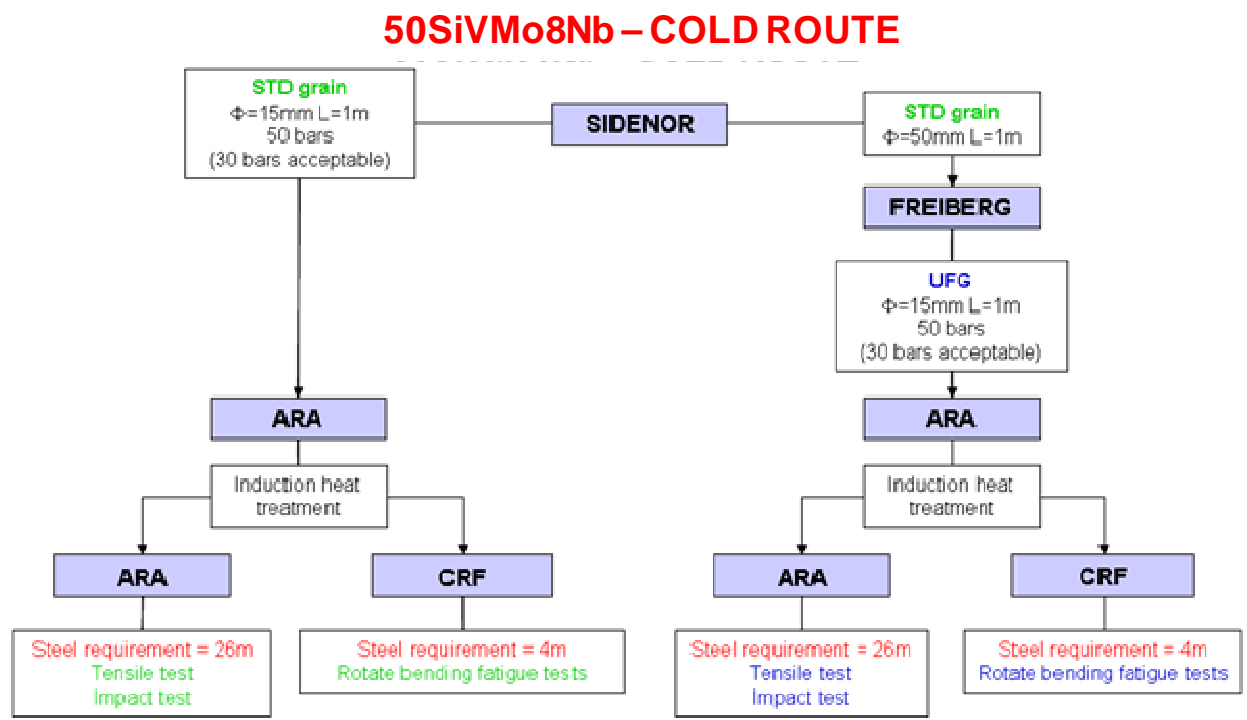


Figure 15: Spring steel flow for preliminary tests.

Automotive – spring (carbon range 0.40-0.60 %)

To compare the mechanical properties of the spring steel with two different grain sizes it has been decided to proceed in the way described as follows.

Preliminary test

The main results will come from basic mechanical characterization as tensile tests, impact tests, rotate bending fatigue tests. These tests will be done by using simple specimens whose production

50SiVMo8Nb – HOT ROUTE

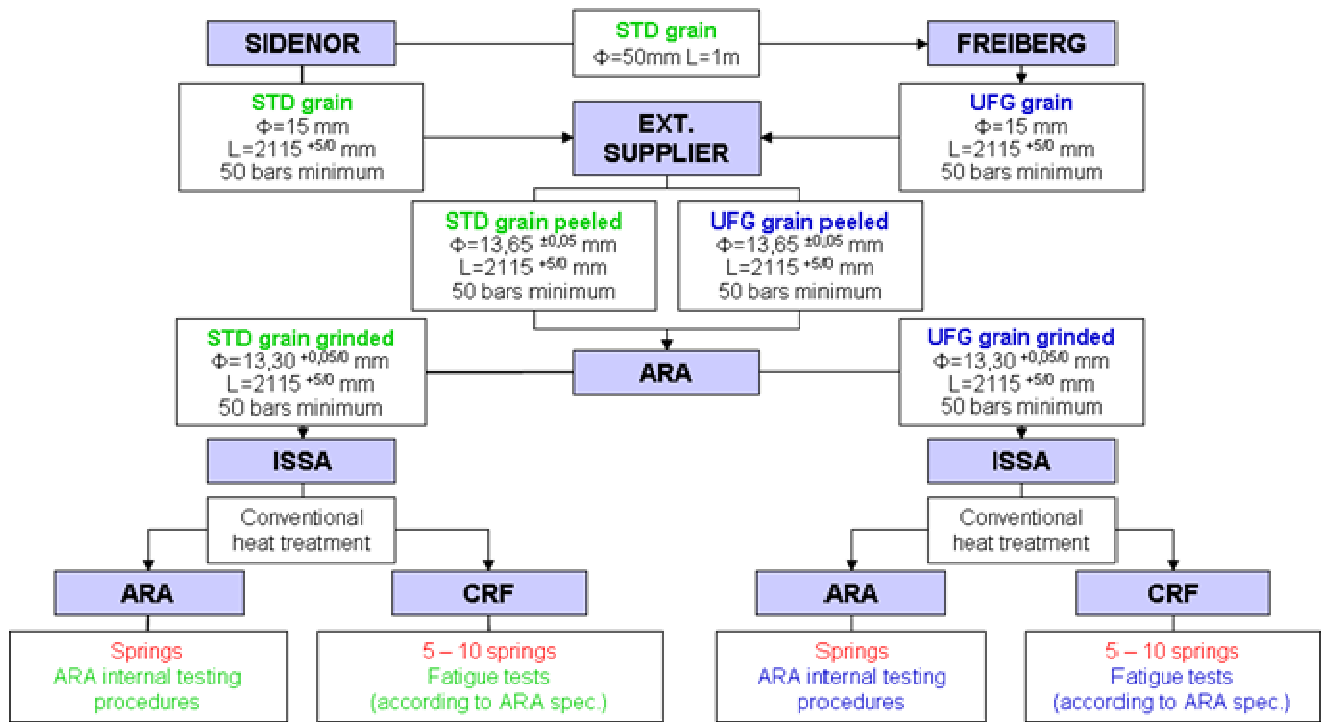


Figure 16: Spring steel flow for test on real component.

50SiVMo8Nb – COLD ROUTE

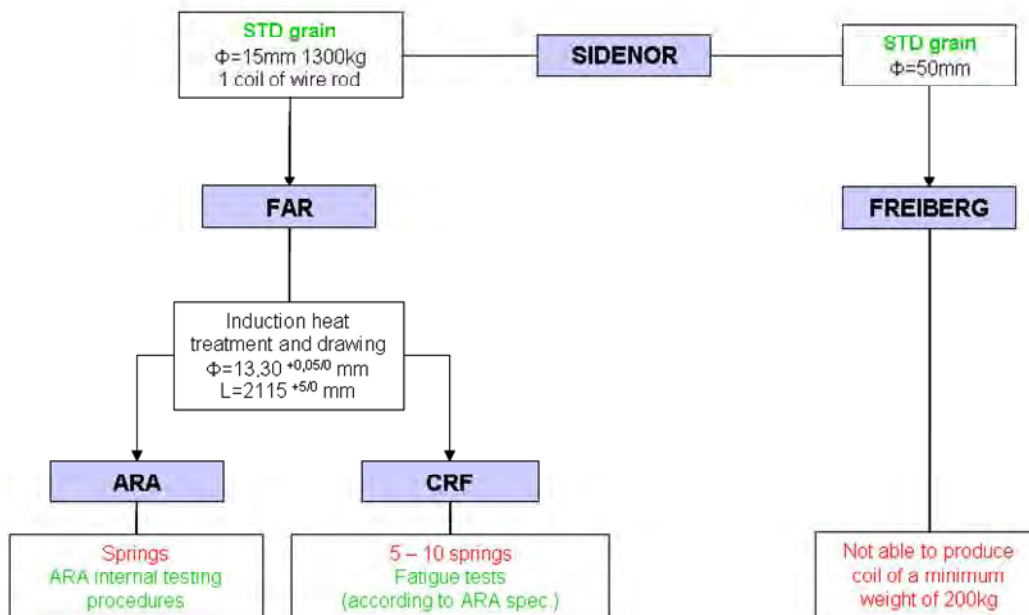


Figure 17: Spring steel flow for test on real component.

does not require coils or long bars. They can be produced by “Cold Route” in ARA preserving a finer grain structure. The steel bar manufacturing flow is described in Figure 15.

Two different grain sizes will be supplied to ARA. A steel with a standard grain size will come by Gerdau, UFG steel will come by Freiberg University.

ARA will be involved in the induction hardening treatment of the bars and of the standard tensile and impact tests that they normally do to characterize spring steels.

The fatigue properties of 50SiVMo8Nb UFG will be evaluated and compared with STDG 50SiVMo8Nb by using the rotate bending fatigue specimen.

If a significant increase of fatigue limit will be achieved, in comparison to standard 50SiCrMo8Nb, CRF will involve ARA for the production of real helicoidal suspension springs to be tested in CRF by following the fatigue assessment procedures of ARA.

Test on real components

Springs manufacturing by using the “Cold Route” need a coil of wire rod of almost 200kg. This coil cannot be produced in TU-Freiberg so it has been decided to compare STDG and UFG springs by using the “Hot Route” process.

The “Hot Route” process need just peeled bars of a length of 2m to produce real automotive springs. This length can be produced by TU-Freiberg with UFG Steel. The spring steel flow is shown in Figure 16.

Nevertheless there is a strong interest of GerdaU to evaluate STDG springs produced by “Cold Route” and to compare the results with the “Hot Route” process. Therefore it has been decided to produce a lot of SDTG springs following the manufacturing flow shown in Figure 17.

If “Cold Route” STDG steel will have better performance that “Hot Route” STDG steel, we could also assume that in the case of better performances achieved by UFG steel in comparison with STDG steel in “Hot Route” the same or better improvement can be achieved in a hypothetical “Cold Route” manufacturing process.

Summary

The materials for the experimentation in terms of chemical compositions were selected and the mechanical components for final applications were identified.

The prototype components to be manufactured by UFG steels have been identified among the following two families: fasteners applications (e.g. screws, bolts) whose C content ranged between 0.15-0.30%C, and automotive applications like gear shaft (0.15-0.20%C) and springs (0.40-0.60%C).

Materials for fastener application were produced by CSM and ORI Martin, while for powertrain applications from GERDAU.

The selected components for fastener applications are three screws of different shapes, sizes and final applications, produced by the company Agrati SpA. The expected advantages of UFG steel for fastener applications consist firstly of the chance to reduce or possibly avoid the annealing treatment, which is usually made before cold forming and is very expensive in terms of energy and time, and a further advantage could be the reduction of scraps caused by forging bursts in screw heads occurring during cold forming process

The prototype component automotive application selected by CRF, jointly to FIAT Powertrain Technologies, is the gear shaft. The part is currently produced by 17NiCrMo4 steel for high stressed application. The aim is to find an UFG steel without Ni, like 18CrMo4, able to replace the original 17NiCrMo4 steel.

In the case of automotive spring applications, the proposed steel is 50SiMoVNb8, which is a steel grade used for helicoidal suspension springs, at present produced with standard grain size. The aim of grain refinement is to increase the fatigue performances of high stressed spring steel.

The main critical aspects of the manufacturing cycles of the chosen powertrain components are related to the high temperature heat treatment after cold forming. The related phase transformation may reduce the advantages coming from UFG structure.

2.2 WORK PACKAGE 2:

SIMULATION OF THERMOMECHANICAL CYCLES FOR UFG STEELS PRODUCTION

DIFT (Deformation Induced Ferrite Transformation) and Heavy γ deformation mechanisms can be exploited to produce UFG steels. In this WP these routes have been tested and the most effective condition has been chosen for pilot plant trials.

In particular the objective of this WP are:

- Determination of thermomechanical conditions for DIFT occurrence versus range of C content, deformation temperature, prior austenite grain size, imposed strain, strain rate and effect of microalloying content (e.g. Nb).
- Determination of thermomechanical conditions for ultrafine grains formation by Heavy γ deformation mechanism.
- Identification of the best mechanism to be exploited for producing UFG long product.

Task 2.1. Determination of DIFT parameters for different C steels

Driving force for phase transformation depends on chemical composition and temperature.

The typical phase transformations in steels are austenite to ferrite, austenite to pearlite, austenite to bainite, austenite to martensite and precipitation of nitrides and carbides.

If an external load is applied to the system above the static transformation temperature, its free energy will be certainly raised. If the load (e.g. deformation) is applied to the austenite above transformation temperature and the free energy of austenite is raised to the extent over the free energy of ferrite at the same temperature, the transformation from austenite to ferrite will occur, which could not be found to happen without deformation.

This kind of ferrite transformation induced by deformation has been called Deformation Induced Ferrite Transformation (DIFT).

It was assessed that it is a dynamic phase transformation occurring during deformation at temperature slightly higher than Ar_3 , due to the strain energy accumulated in the austenite phase that induces an early γ - α phase transformation.

This mechanism has a critical strain to occur that depends on strain rate, deformation temperature, content of carbon, alloying elements, and prior austenite grain size.

The resulting ferritic grains are very fine and for this reason DIFT is considered one of the mechanisms which is proven to be an effective method for grain refinement in plain low carbon steels. The aim of this experimentation was to assess the hot deformation conditions in the austenite region for producing fine grain sizes through DIFT mechanism.

In addition it is necessary to point out that during the austenite deformation, DIFT and dynamic recrystallization (DRX) compete with each other, and one of them, the one that has the smaller critical strain, will take place ahead. When the deformation temperature is below Ae_3 the critical strain for DIFT is smaller than for DRX and DIFT becomes the predominant softening mechanism (Figure 18).

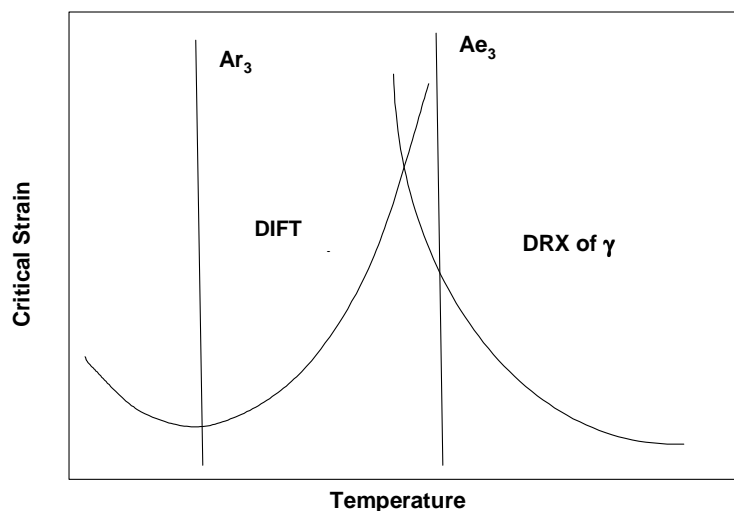


Figure 18: Schematic illustration of temperature dependencies of the critical strain for DIFT and DRX [4].

Dilatometric experiments were carried out both on the materials cast at CSM and on the materials industrially produced by Ori Martin. Cylindrical samples had 5mm diameter and 10mm length. The experiments were carried out in vacuum.

Two different austenitizing temperatures (900 and 1100°C) have been tested in order to produce different prior austenite grain sizes. Then, two different deformation temperatures ($A_{r3}+15^{\circ}\text{C}$ and $A_{r3}+40^{\circ}\text{C}$) and two different strain rates in the range 1 and 30 s^{-1} were performed.

Samples were deformed at 50% and after deformation the samples were quenched (at 150°C/s).

Samples for metallographic examination were prepared from the deformed specimens by polishing the longitudinal section down to centre of the sample. The scheme of the thermomechanical cycles is reported in Figure 19.

The aim of the experiment was to verify the effect of prior austenite grain size, deformation temperature and strain rate on critical strain for DIFT activation, as well to determine ferrite ultrafine grain size and volume fraction.

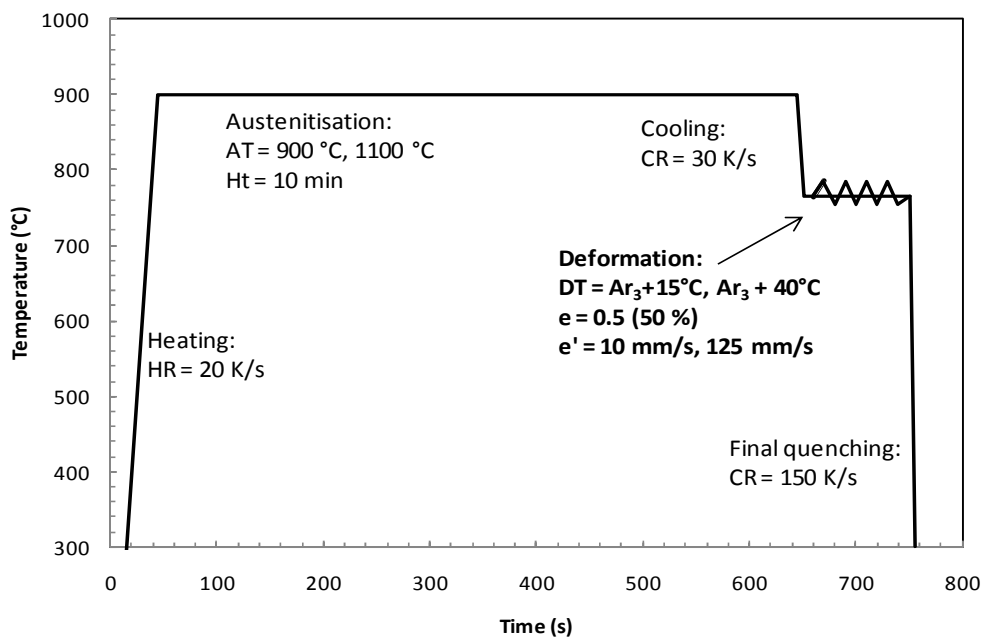


Figure 19: Thermomechanical cycles for determination of DIFT parameters.

Determination of DIFT Parameters for fasteners application (0.15-0.30%C)

In order to get different prior austenite grain sizes before deformation the samples were treated according to the cycles showed in Figure 20: after soaking they were cooled at a rate of 30°C/s to the deformation temperature of about $A_{r3}+15^{\circ}\text{C}$ and, after a short soaking at this temperature (approximately of the same order of the deformation time), quenched without deformation.

Table 14 shows the measured prior austenite grain sizes. It can be noted that independently on the steel grade, it was possible to obtain two different grain sizes changing only the soaking temperature.

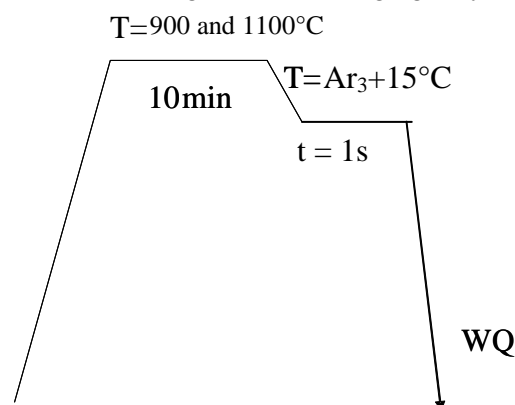


Figure 20: Thermomechanical treatments carried out by dilatometer for prior austenite grain size determination.

	T=900°C	T=1100°C
18Mn7/ VM2623	9.5	40.5
18MnB7/ VM2624	10.0	44.1
30MnB7/ VM2625	10.7	50.0
30MnB4/ AE1055	10.6	50.8
18MnB2/ AE4008	11.6	47.4

Table 14: Prior austenite grain sizes (μm) (PAGS) for all the steels at different soaking temperatures.

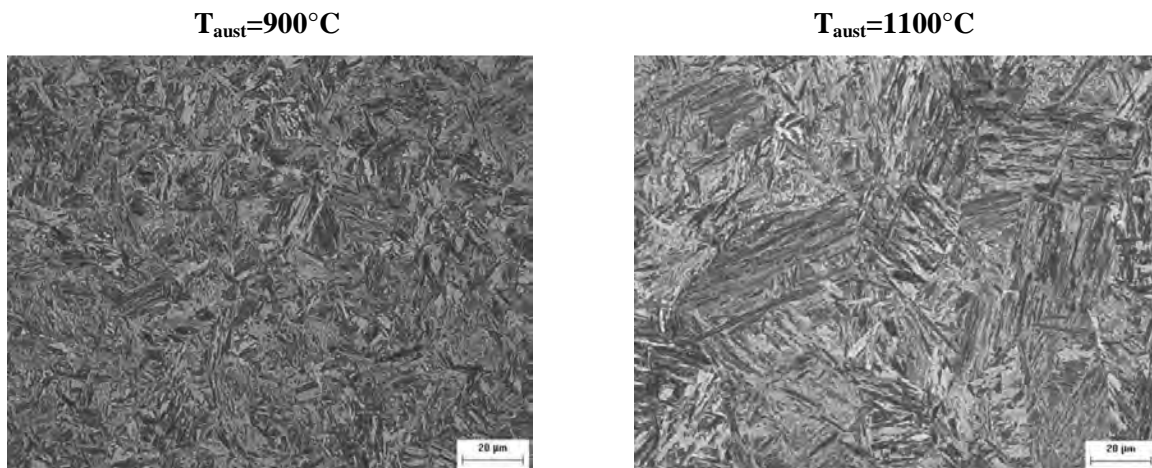


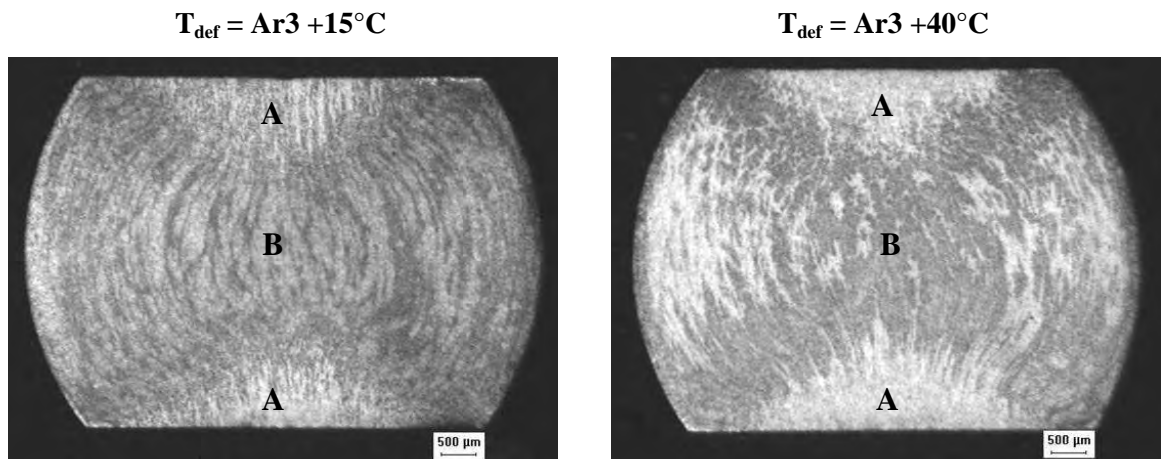
Figure 21 : Microstructure of 30MnB4 sample after the thermomechanical cycle without deformation with different austenitization temperatures.

An example of 30MnB4 microstructure (Figure 21), treated without deformation showed fully martensitic structure and absence of ferrite nucleation, excluding the possible formation of ferrite not due to DIFT for two different austenitization temperatures.

In Figure 22 the macrostructures of samples after the thermomechanical cycles showed in Figure 19 are reported. It is evident that the microstructure inside the samples with smaller PAGS is quite inhomogeneous. In the regions nearby the surfaces, where the load has been applied (indicated as “A” in Figure 22), no ferrite is present (Figure 23). Approaching the centre of the sample (regions indicated as “B”), ultra fine ferrite is present, meaning that DIFT occurred. Such inhomogeneity in microstructure is directly related to the variation of strain distribution inside the sample.

PAGS
(μm)

10



50

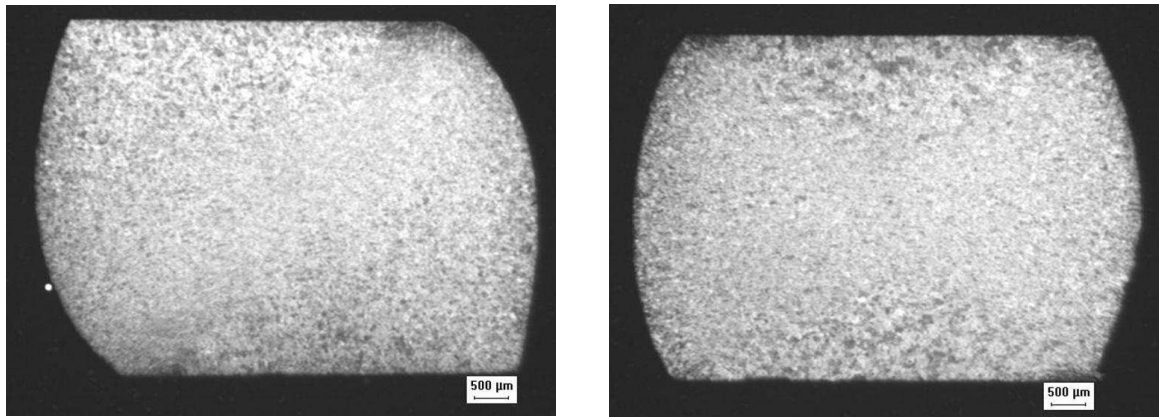


Figure 22: Macrostructures of deformed samples.

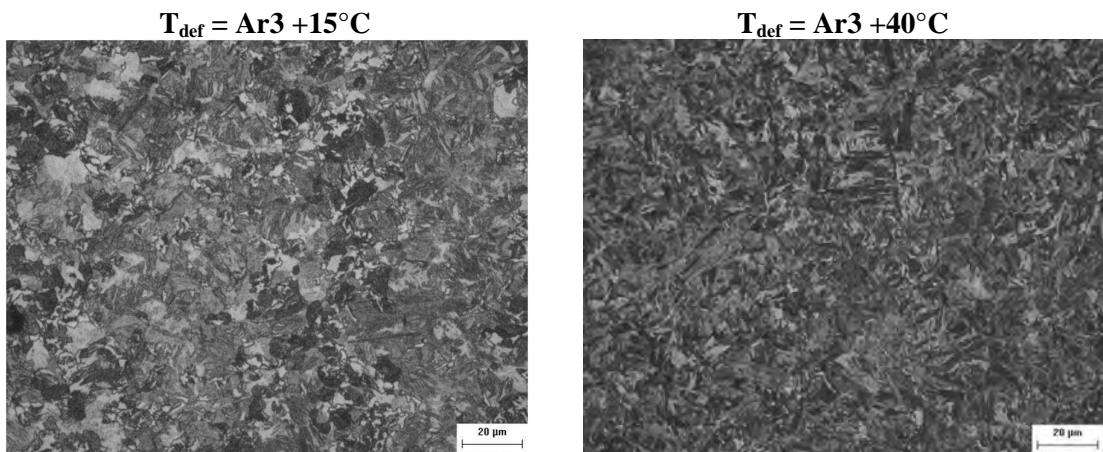


Figure 23: Microstructure in zone “A” for samples with PAGS=10 μ m.

Modeling of deformation

In order to understand the strain distribution inside the compressed sample and the correspondent microstructural behaviour, FEM simulations of the dilatometric compressive tests were carried out using MARC code. The hypotheses of the model have been:

- Rigid tools
- T=constant
- Axisymmetric model
- $\frac{1}{4}$ geometry modeled (2 symmetry planes)

Two steels with different C contents (close to the steel used in the tests) were simulated: C15 (0.15%C) and C35 (0.35%C). As inputs parameters for the models, stress-strain curves of these steels at T=830°C and T=780°C respectively have been used, which are very close to the deformation temperatures actually adopted for the experimental tests. Before simulation of compression, it was necessary to determine the friction coefficient of the test. An evaluation of the friction coefficient was carried out measuring the barreling of the real dilatometric sample as shown in Figure 24. The results of the measure compared with the barreling of simulation showed that the friction coefficient to insert in the model had to be 0.6. Simulated equivalent strain distributions inside the sample for the two different steels and strain rates are shown in Figure 25 and quantitative distribution along the axis of the sample is reported in Figure 26.

Figure 25 shows that for all cases the most deformed zone is in the central part of the sample and the most deformed sample is the one having high C content (0.35%) and low strain rate (gray zone).

In addition the shape of the zone having the maximum deformation changes with strain rate.

In Figure 26 quantitative distribution of equivalent strain through the thickness in the central line of the sample is reported. It can be noted that there are not significant differences among all the compression conditions and steels. At the same chemical composition the strain distribution difference at different strain rates increases with the C content.

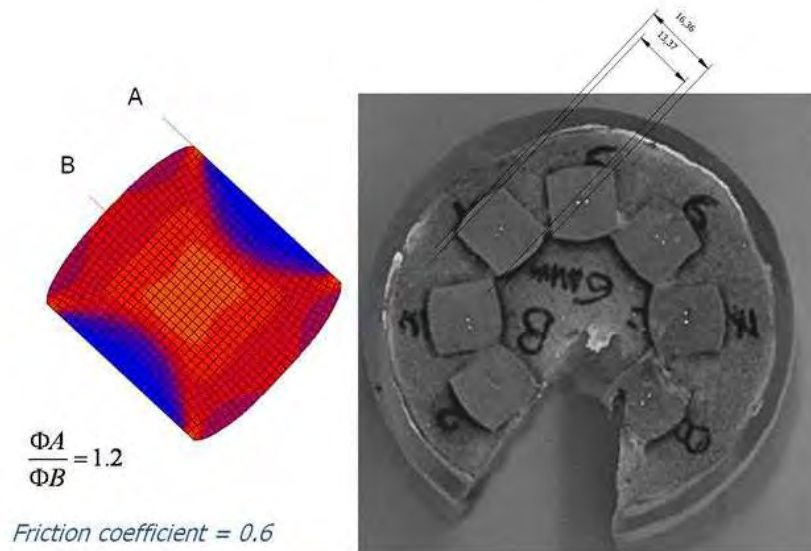


Figure 24: Determination of friction coefficient.

Strain distribution in compression test

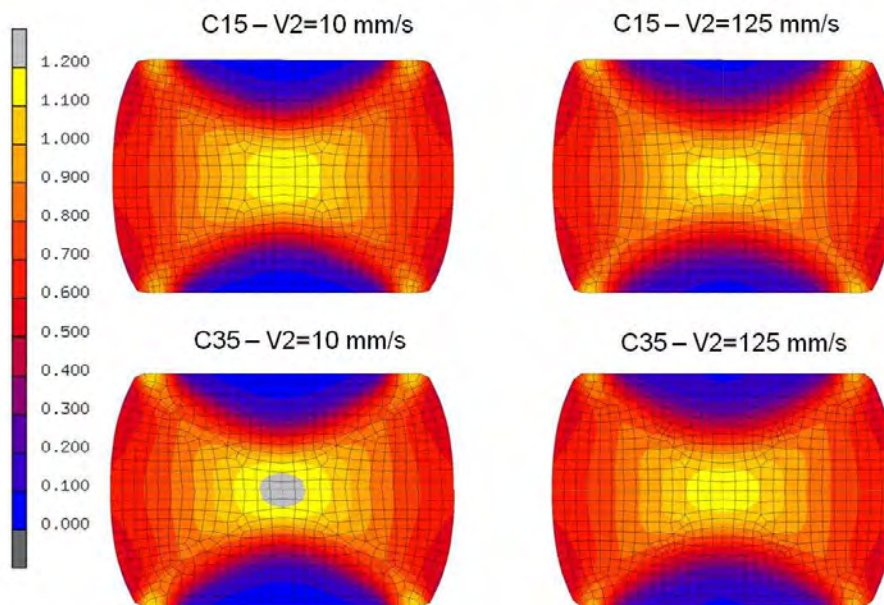


Figure 25: Equivalent strain distribution in compression tests.

Comparing the model results and the microstructure for the samples where DIFT occurred (PAGS = 10 μ m), it is clear that the microstructure follows the same trend of the strain. In particular, measuring the deepness at which DIFT starts to occur along the sample axis, it is possible to estimate the critical strain from Figure 26.

The results show that for sample 30MnB4 with deformation temperature $T_{def}=A_{r3}+15^{\circ}C$ the deepness of region “A” is about 1mm and the critical strain is $\epsilon=0.4$. For the sample with deformation temperature $T_{def}=A_{r3}+40^{\circ}C$ the deepness of region “A” is about 1.4 mm and the corresponding critical strain is $\epsilon=0.8$. It means that decreasing the deformation temperature the critical strain decreases while the increase of PAGS increases the critical strain. In our case a value of PAGS of 50 μ m was enough to inhibit the DIFT occurrence, even for strain values up to $\epsilon=1.2$.

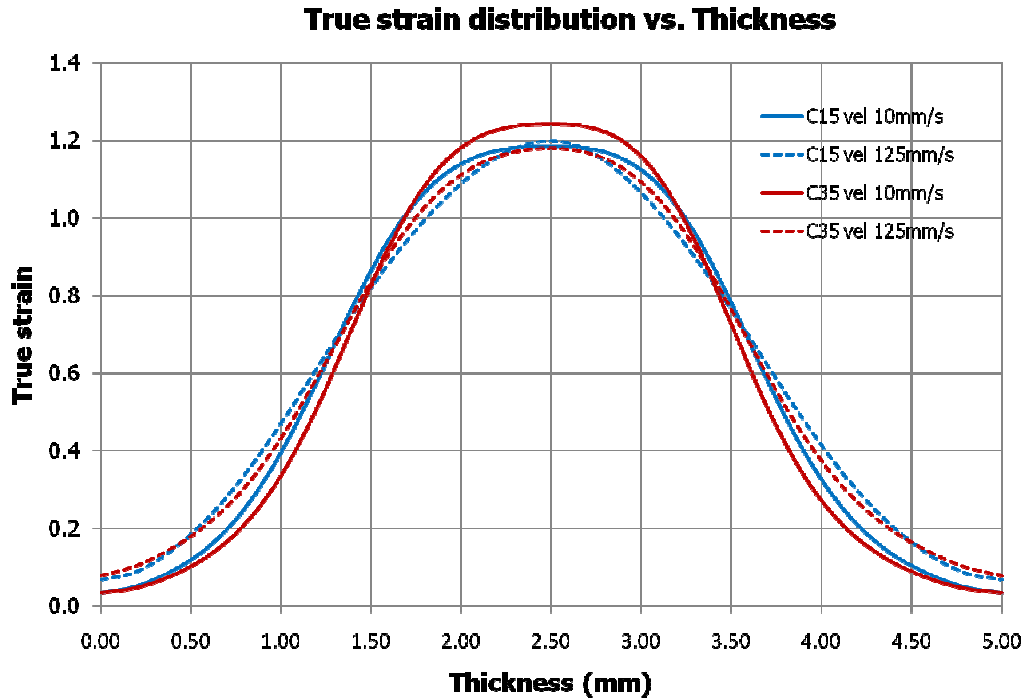
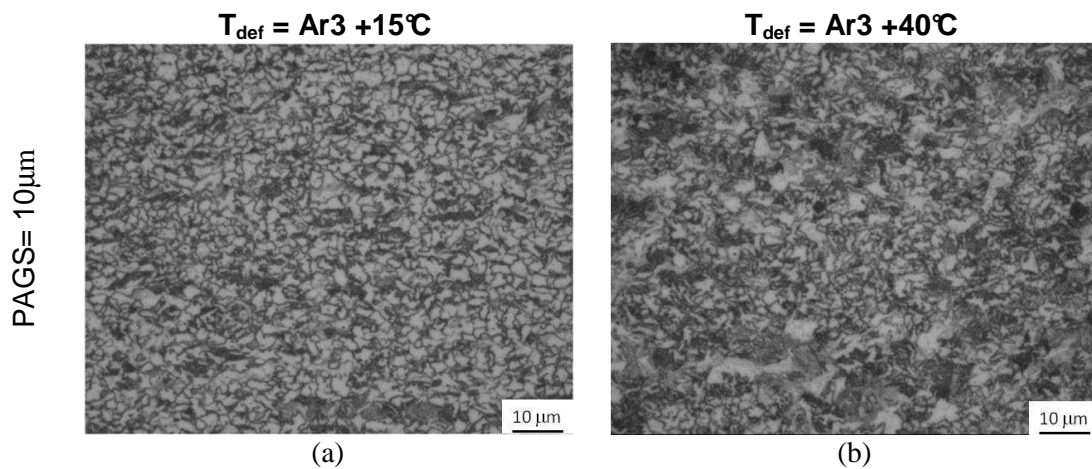


Figure 26: True strain distribution vs. thickness.

Determination of critical strain and grain size

In Figure 27, microstructures show that DIFT ferrite is formed both in the case of $A_{r3}+15^{\circ}C$ and $A_{r3}+40^{\circ}C$ with small PAGS. Volume fraction of deformation induced transformed ferrite at the centre of the sample is around 60% in the case of $T_{def}=A_{r3}+15^{\circ}C$ while for $T_{def}=A_{r3}+40^{\circ}C$ the ferrite volume fraction is between 40 and 50% (Figure 28a). The average ferrite grain size is 2-3 μm (Figure 28b). The microstructure inside the samples with larger PAGS is quite homogeneous and no ferrite is present through the whole specimens, meaning that DIFT did not occur. From the graphs is clear that increasing the deformation, grain size decreases and ferrite volume fraction increases.

For the sample 18MnB2, DIFT ferrite is formed mainly for small PAGS. For PAGS=50 μm only in the case of lower deformation temperature ($A_{r3}+15^{\circ}C$) there is some small ferrite volume fraction (Figure 29). In particular (Figure 30a) the ferrite volume fraction at the centre of the sample is around 70% in the case of $T_{def}=A_{r3}+15^{\circ}C$, while for $T_{def}=A_{r3}+40^{\circ}C$ is between 50 and 60%. The average ferrite grain size (Figure 30b) is 2-4 μm . However in the centre of the sample in the case of $T_{def}=A_{r3}+15^{\circ}C$ and PAGS=50 μm the ferrite volume fraction is around 30-40%.



PAGS= 50µm

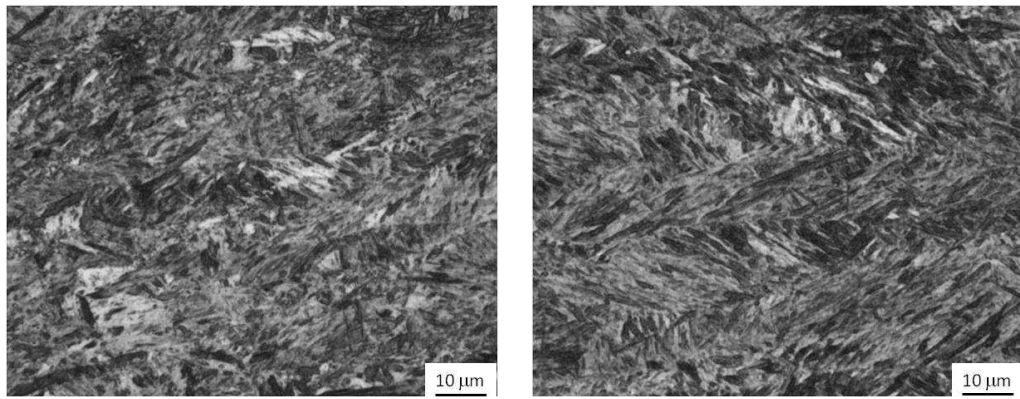


Figure 27: Microstructure for samples 30MnB4 (Steel B).

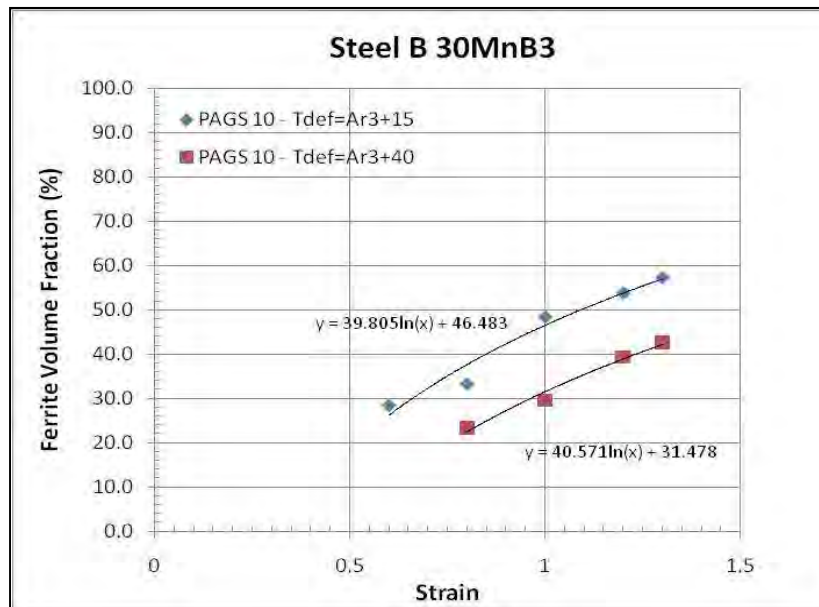
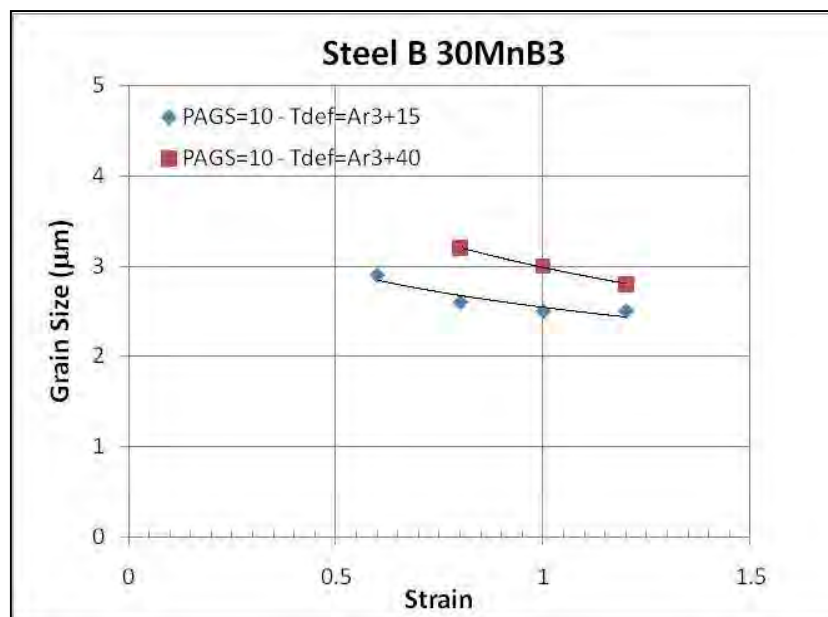


Figure 28a: Ferrite volume fraction versus strain for Steel 30MnB4.



(b)

Figure 28b: Grain size versus strain for Steel 30MnB4.

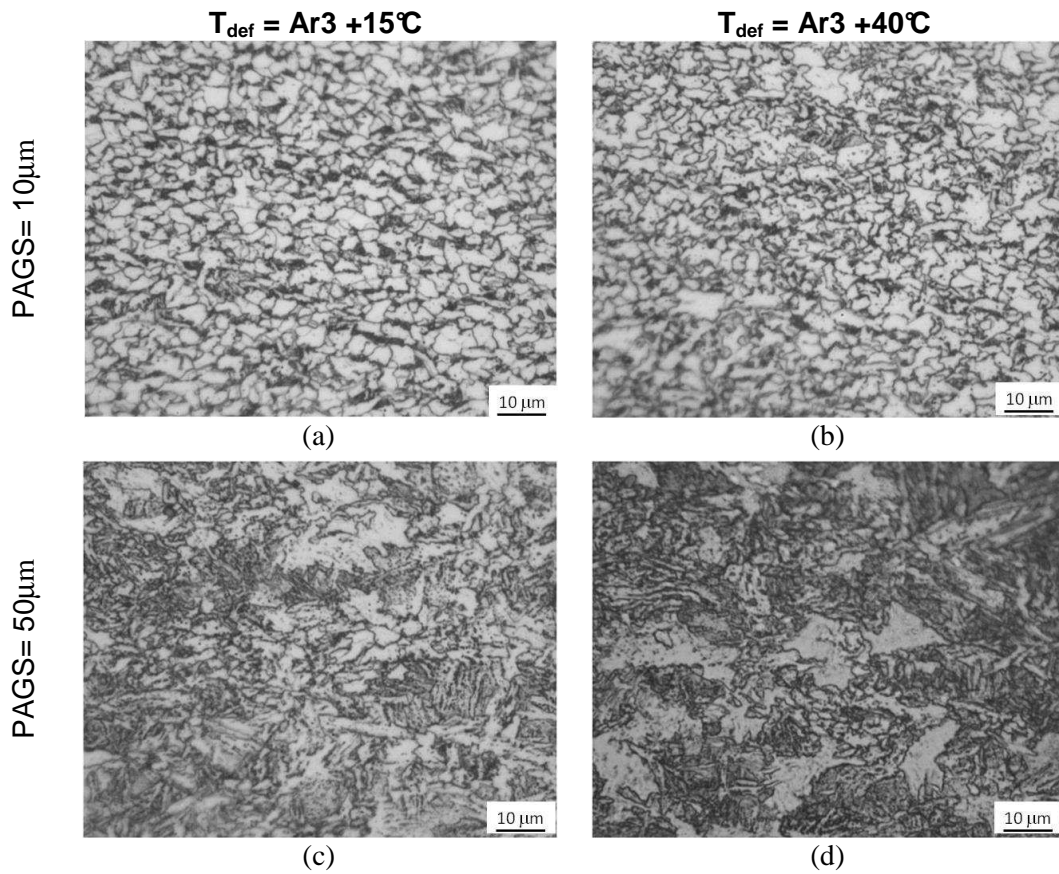


Figure 29: Microstructure for samples 18MnB2 (Steel A).

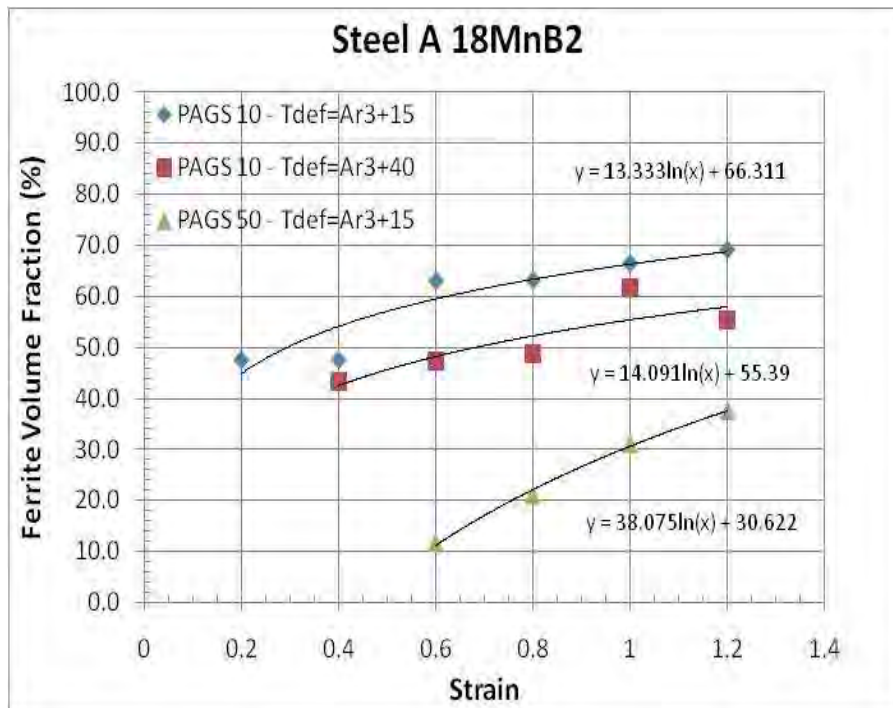


Figure 30a: Ferrite volume fraction versus strain for Steel A (18MnB2).

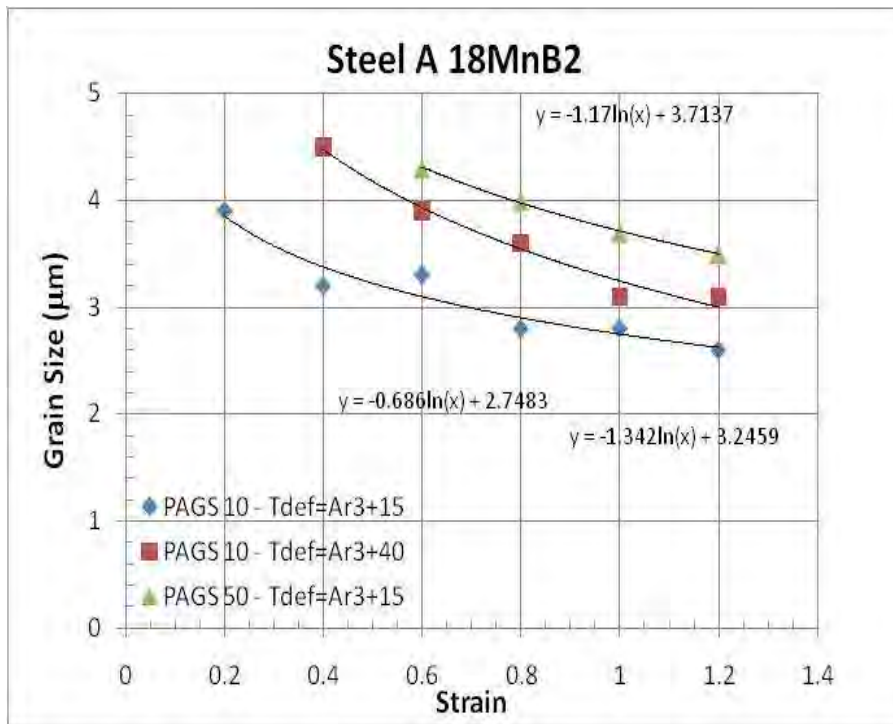


Figure 30b: Grain size versus strain for Steel A (18MnB2).

In Figure 31 the microstructure of the sample 18MnB7 (2624) is reported. Ferrite has formed only for small prior austenite grain size (Figure 31a and b). In the other cases (Figure 31c and d) only martensite is present through the whole sample thickness. Ferrite volume fraction is around 50-60% in Figure 31a while in Figure 31b is around 30%. Ferrite grain size is around 3 µm (Figure 32).

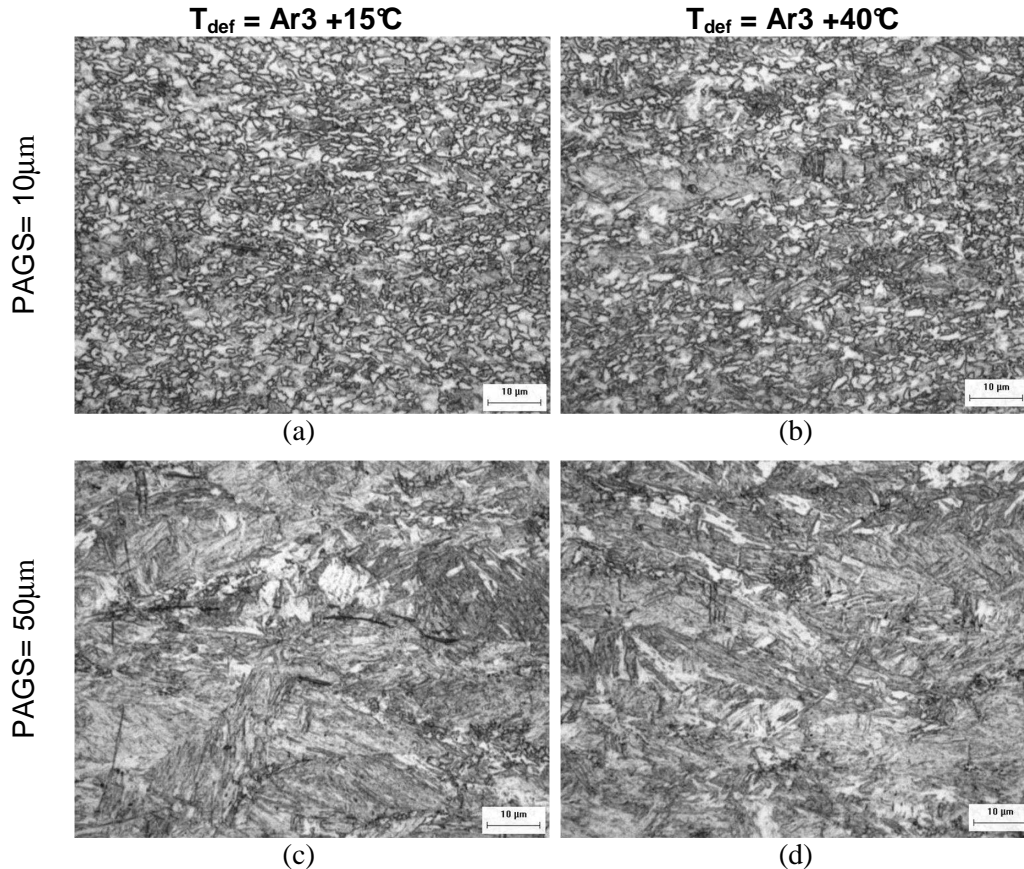


Figure 31: Microstructure for samples 18MnB7 (2624).

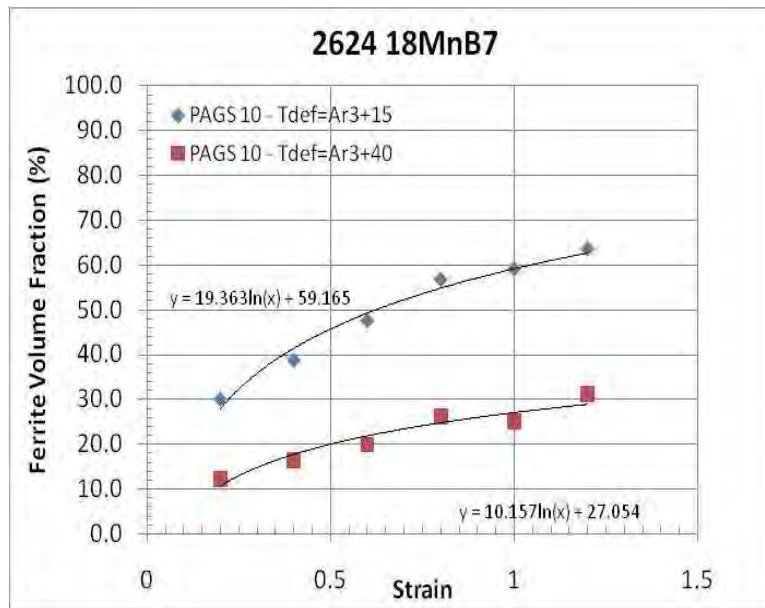


Figure 32a: Ferrite volume fraction versus strain 18MnB7 steel.

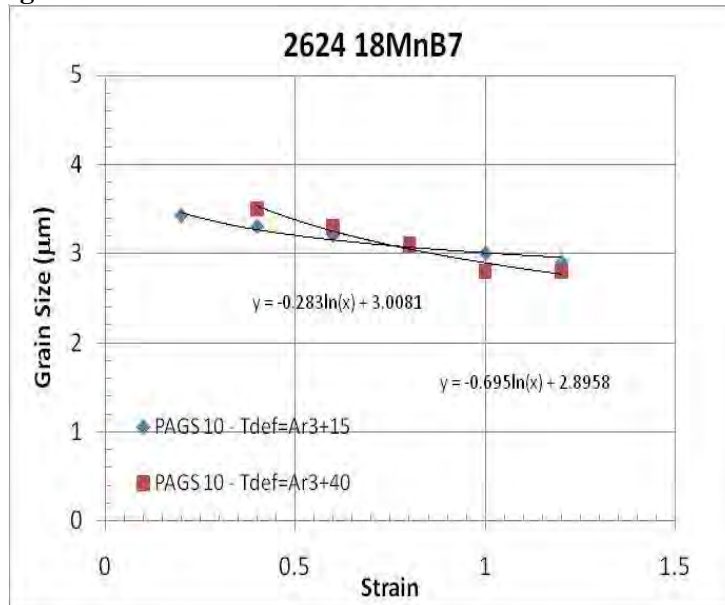
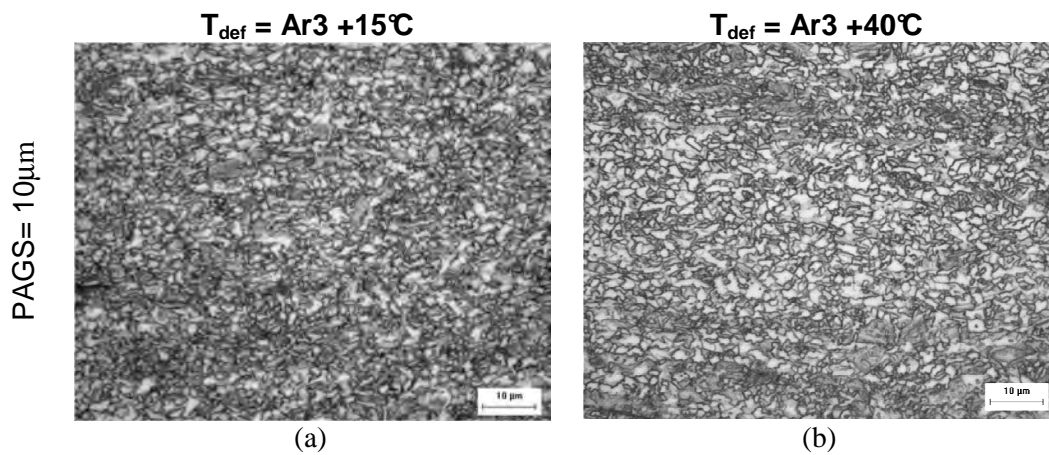


Figure 32b: Grain size versus strain 18MnB7 steel.



PAGS= 50 μ m

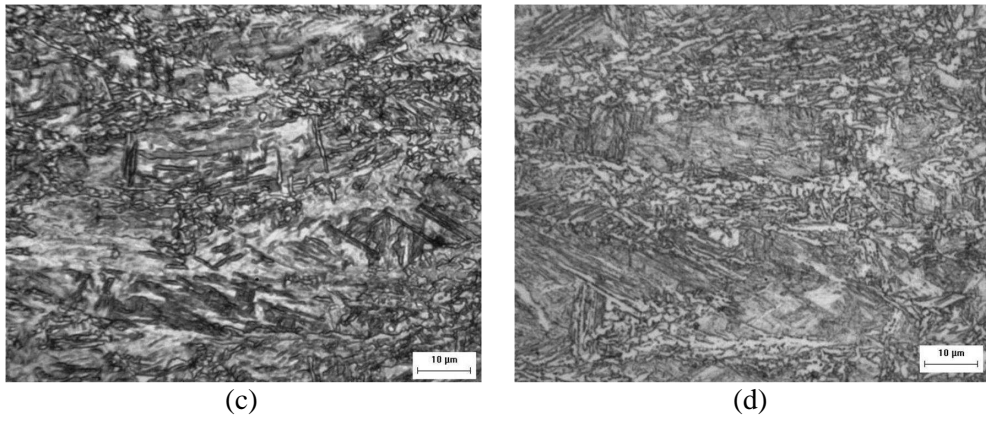


Figure 33 : Microstructure for samples 18Mn7 (2623).

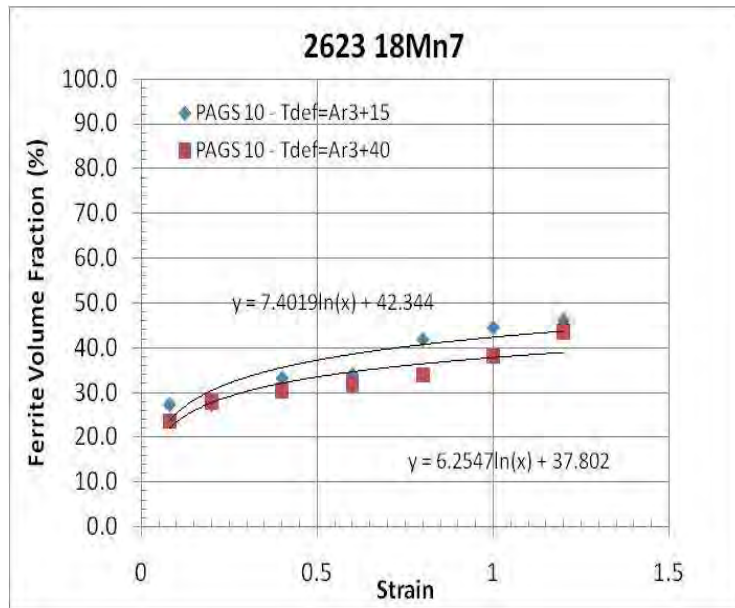


Figure 34a: Ferrite volume fraction versus strain for 18Mn7 steel.

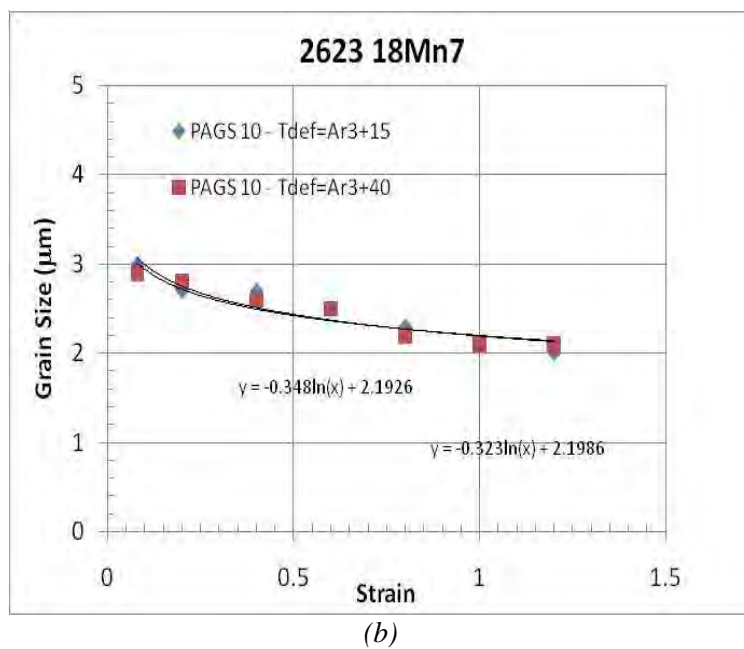


Figure 34b: Grain size versus strain for 18Mn7 steel.

In Figure 33 the microstructures of steel 18Mn7 are reported. Even in this case only for small prior austenite grain size formation of DIFT ferrite occurs, even if no evident differences in ferrite volume fraction and grain size due to deformation temperature are detected. In both cases the ferrite volume fraction is around 35-45% and the grain size is very similar and ranges from 2 to 3 μm (Figure 34). In Figure 35 microstructures of the sample 30MnB7 show that increasing the carbon content together with the Mn content DIFT ferrite formation is less favorite, showing only some grains in the case of small prior austenite grain size and only martensite and bainite for all the other cases. For this reason no graph regarding ferrite volume fraction and grain size is reported.

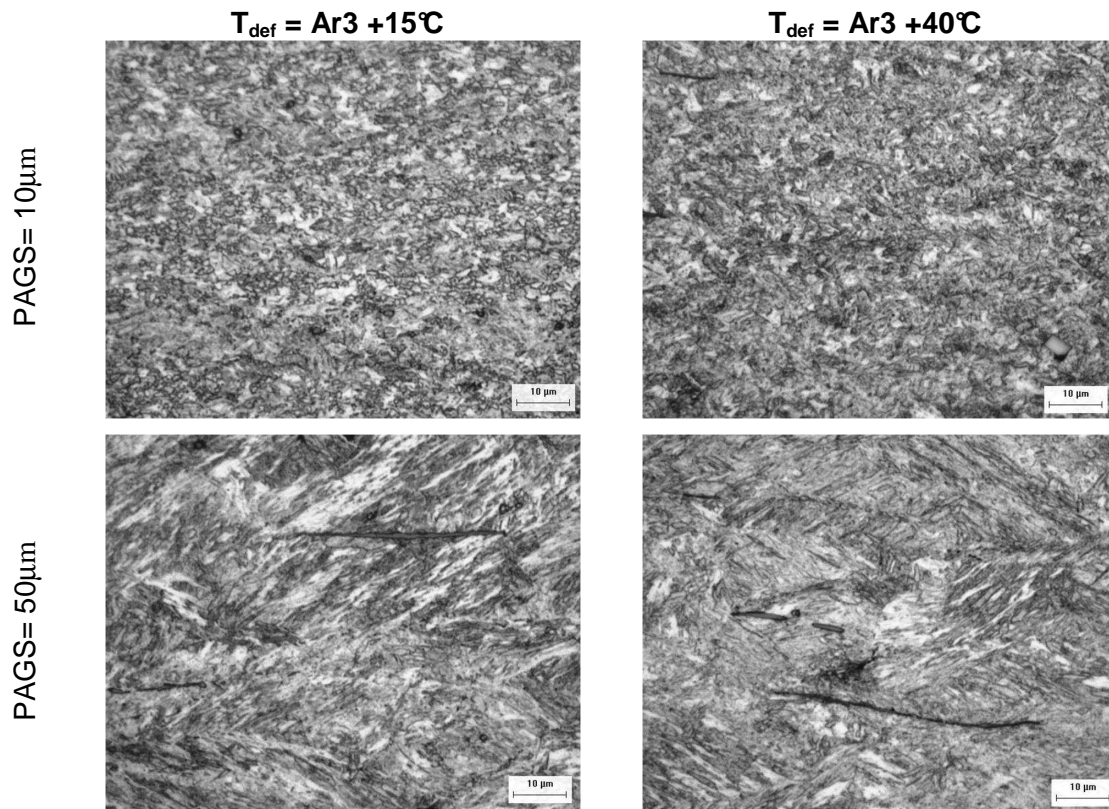


Figure 35: Microstructure for samples 30MnB7 (2625).

Steel B 30MnB3				2625 30MnB7			
Sample n.	PAGS (μm)	T_{def} ($^{\circ}\text{C}$)	ϵ_c	Sample n.	PAGS (μm)	T_{def} ($^{\circ}\text{C}$)	ϵ_c
1	10	$\text{Ar}_3 + 15$	0.4	21	10	$\text{Ar}_3 + 15$	0.9
3	10	$\text{Ar}_3 + 40$	0.8	23	10	$\text{Ar}_3 + 40$	>1.3
5	50	$\text{Ar}_3 + 15$	>1.3	25	50	$\text{Ar}_3 + 15$	>1.3
7	50	$\text{Ar}_3 + 40$	>1.3	27	50	$\text{Ar}_3 + 40$	>1.3

(a) (b)

Table 15: Critical strain for medium-C steels.

In Tables 15 and 16 the critical strain measured for each deformation condition are reported. As explained previously, the measure of critical strain has been carried out by comparing the microstructure in the compressed sample at a given distance from the surface with the results of FEM simulation of compression tests.

By this comparison it is possible to determine the strain after that the ferrite is formed.

In Table 15 results for 0.3%C steels are reported. In the green lines results of samples having small prior austenite grain size are reported while in the yellow lines are reported results related to big PAGS. It can be noted that the critical strain strongly depends on the prior austenite grain size. In fact there is a big difference between the critical strain at the same deformation temperature but at different PAGS. At

the same PAGS higher is the deformation temperature higher is the critical strain. These results are always valid independently on the chemical composition.

In Table 15 the difference of the chemical compositions is the Mn content. So it is clear that at the same thermomechanical conditions, increasing the Mn content the critical strain for DIFT occurring increases. That means that the higher content of Mn inhibits the DIFT occurrence.

In Table 16 the critical strains for the steels with 0.18% C content and different content of Mn and B are reported. The effect of Mn is still confirmed (Table 16a and 16b) even if to a lesser extent than for 0.3%C content in the case of small PAGS. In the case of big PAGS the effect seems to be stronger if compared with small PAGS but difficult to assess if compared with 0.3%C content because in this case the critical strain was so high that was impossible to be determined.

Table 16c shows that even the B content seems to have an effect on critical strain (comparison between Table 16b and 16c), in particular its presence increases the critical strain. However it must be noted that the tests of Table 16c have been carried out at lower deformation temperature (about 10°C less) for a problem of the machine.

Steel A 18MnB2				2624 18MnB7			
N. camp.	PAGS (μm)	T _{def} (°C)	ε _c	N. camp.	PAGS (μm)	T _{def} (°C)	ε _c
11	10	Ar ₃ + 15	0.18	31	10	Ar ₃ + 15	0.21
13	10	Ar ₃ + 40	0.28	33	10	Ar ₃ + 40	0.35
15	50	Ar ₃ + 15	0.58	35	50	Ar ₃ + 15	>1.2
17	50	Ar ₃ + 40	>1.2	37	50	Ar ₃ + 40	>1.2

(a)

(b)

2623 18Mn7			
N. camp.	PAGS (μm)	T _{def} (°C)	ε _c
41	10	Ar ₃ + 05	0.08-0.11
43	10	Ar ₃ + 30	0.11-0.15
45	50	Ar ₃ + 05	>1.2
47	50	Ar ₃ + 30	>1.2

(c)

Table 16: Critical strain for low C steels.

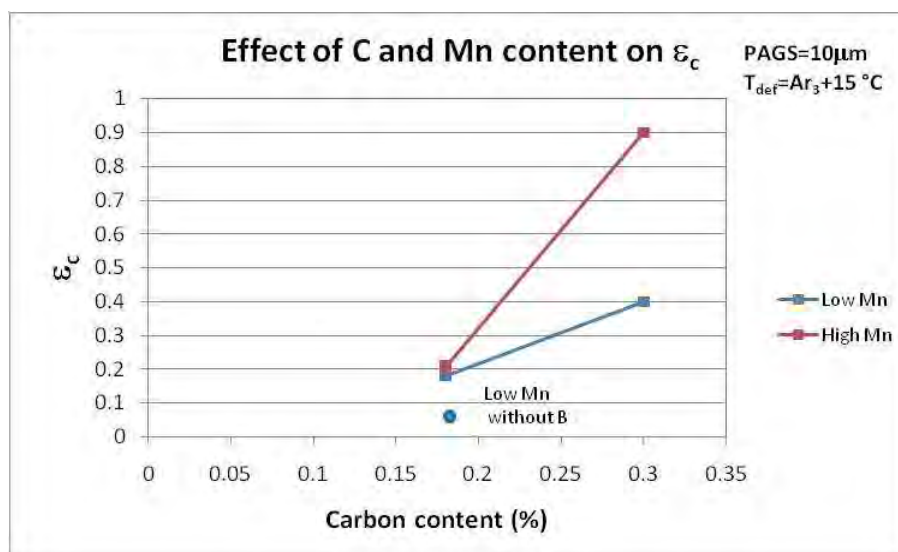


Figure 36: Effect of C and Mn content on ε_c.

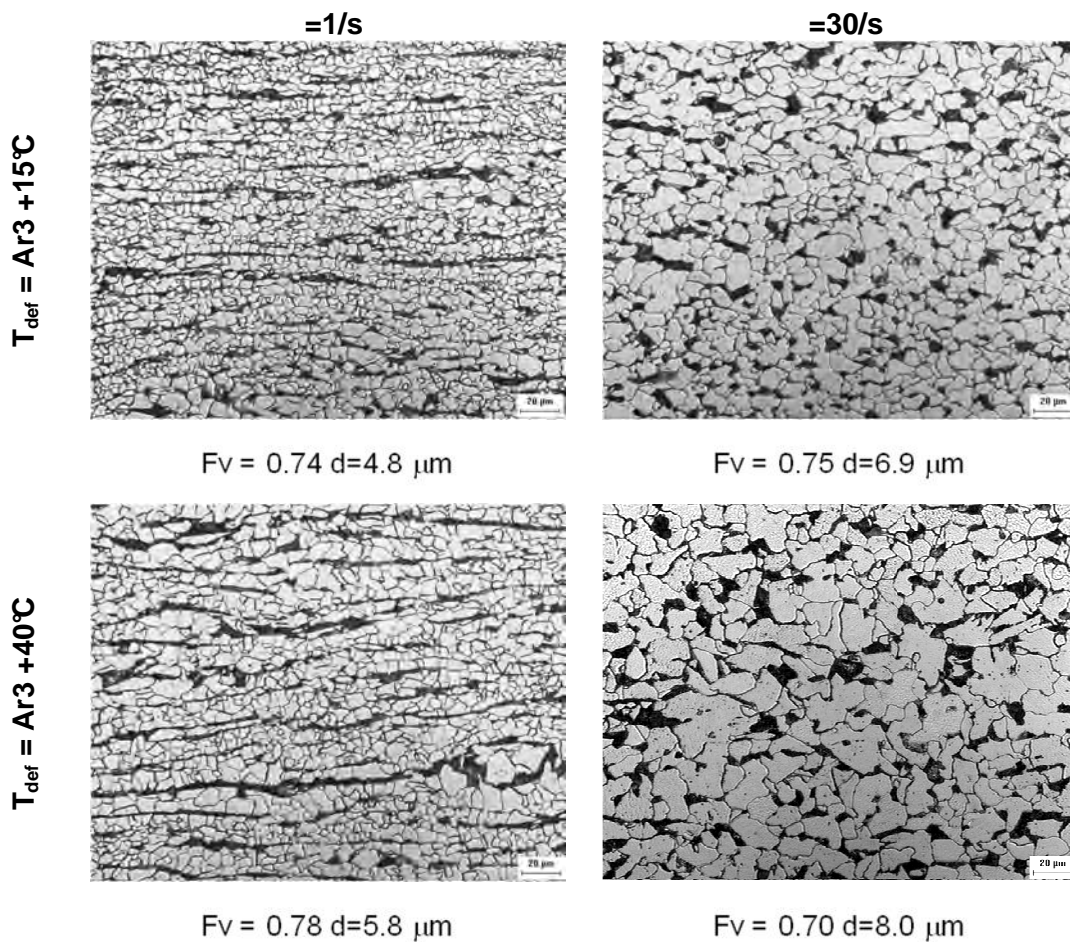
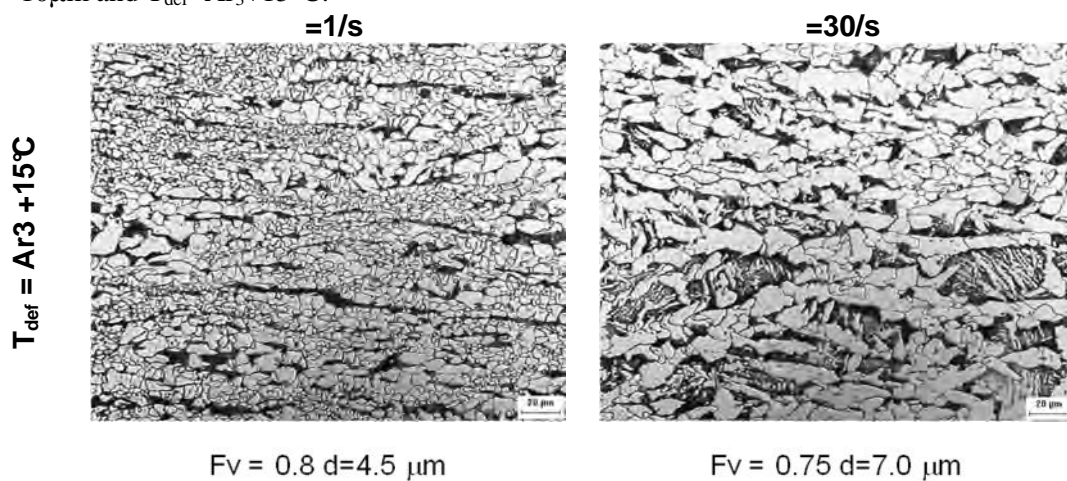


Figure 37: Microstructure for 18MnB2 samples PAGS= 10 μm (Steel A).

The comparison between Table 15 and Table 16 shows that the effect of C content is quite important. The critical strain decreases significantly when C content decreases.

This effect is true both varying the PAGS and T_{def} . The decrease of critical strain due to C content increases the DIFT ferrite volume fraction at the centre of the sample but not relevant difference in grain size is noted. Figure 36 summarizes the effect of the alloy elements on critical strain for PAGS=10μm and $T_{\text{def}}=\text{Ar}_3+15^\circ\text{C}$.



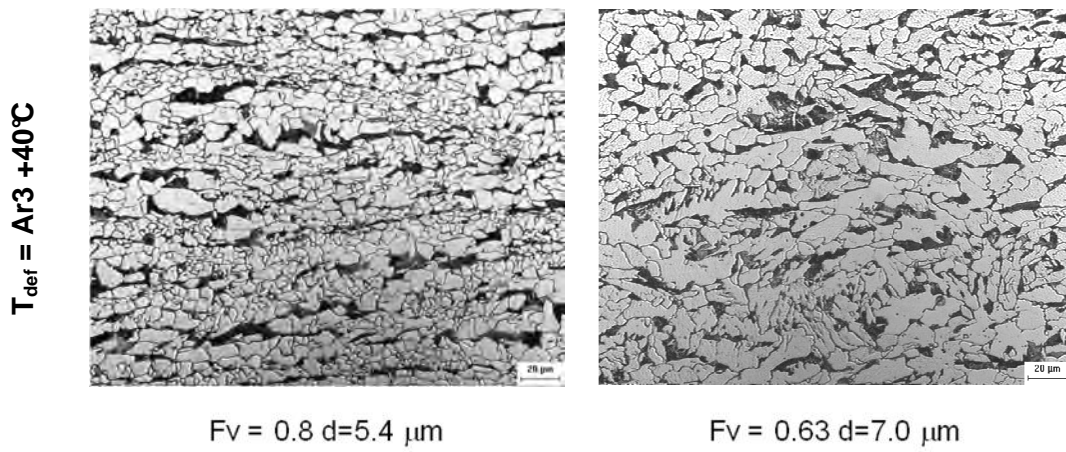


Figure 38: Microstructure for samples 18MnB2 PAGS= 50 μm(Steel A).

The effect of strain rate has been investigated by means of a number of tests on a Gleeble machine. These tests were carried out at TUBAF. In Figures 37-40 the microstructures of 30MnB4 and 18MnB2 at different T_{def} , PAGS and strain rates (1 and 30 s^{-1}) are reported.

In Figures 41 and 42 the results concerning the ferrite volume fraction and grain size versus strain rate for samples 18MnB2 (steel A) and 30MnB4 (steel B) are summarized. The dotted lines are related to the deformation temperature $Ar_3+40^\circ C$ while the continuous lines to $Ar_3+15^\circ C$.

The red lines are related to 10 μm prior austenite grain size (PAGS) and the blue lines to 50 μm PAGS. The effect of strain rate on ferrite volume fraction seems to be not significant, at least in the analyzed range (1-30 s^{-1}). The grain size tends to increase when strain rate increases in most of the investigated samples. Such effect is in contrast to what reported in literature.

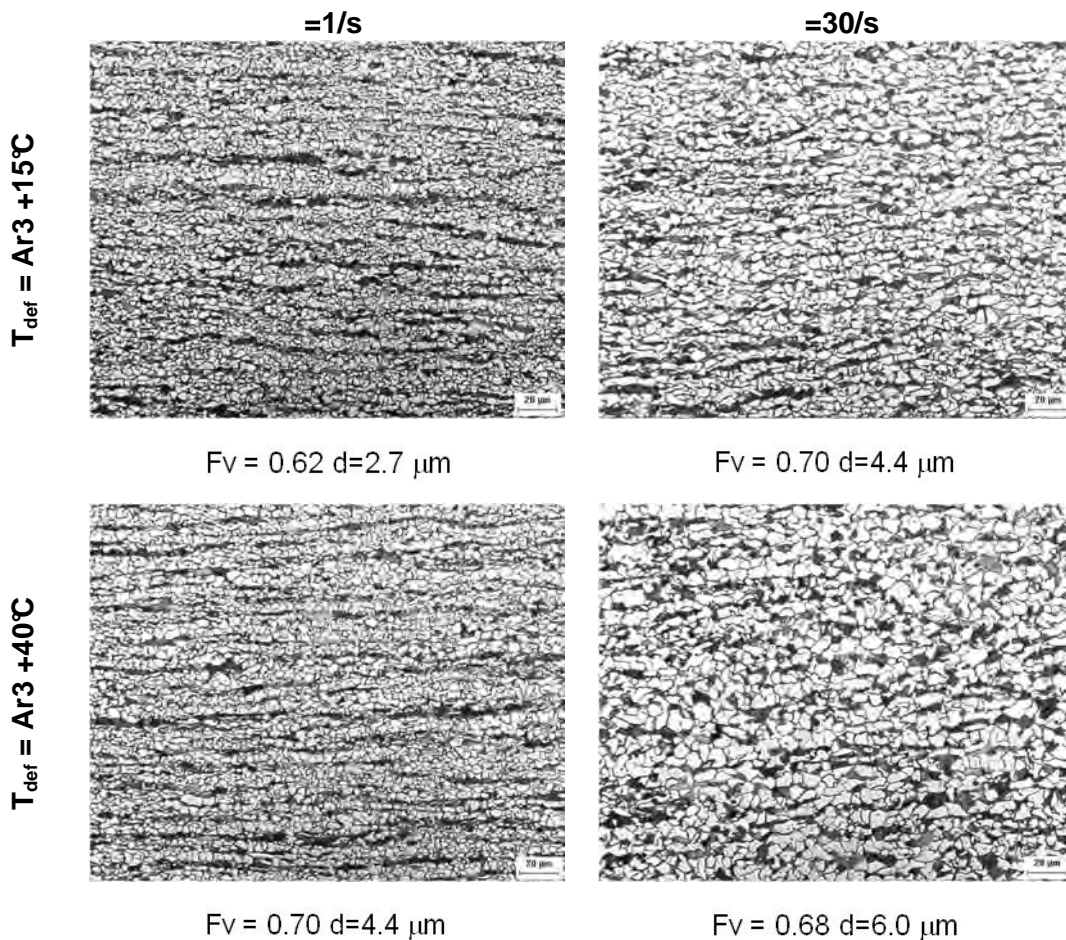


Figure 39: Microstructure for samples 30MnB4 PAGS= 10 μm(Steel B).

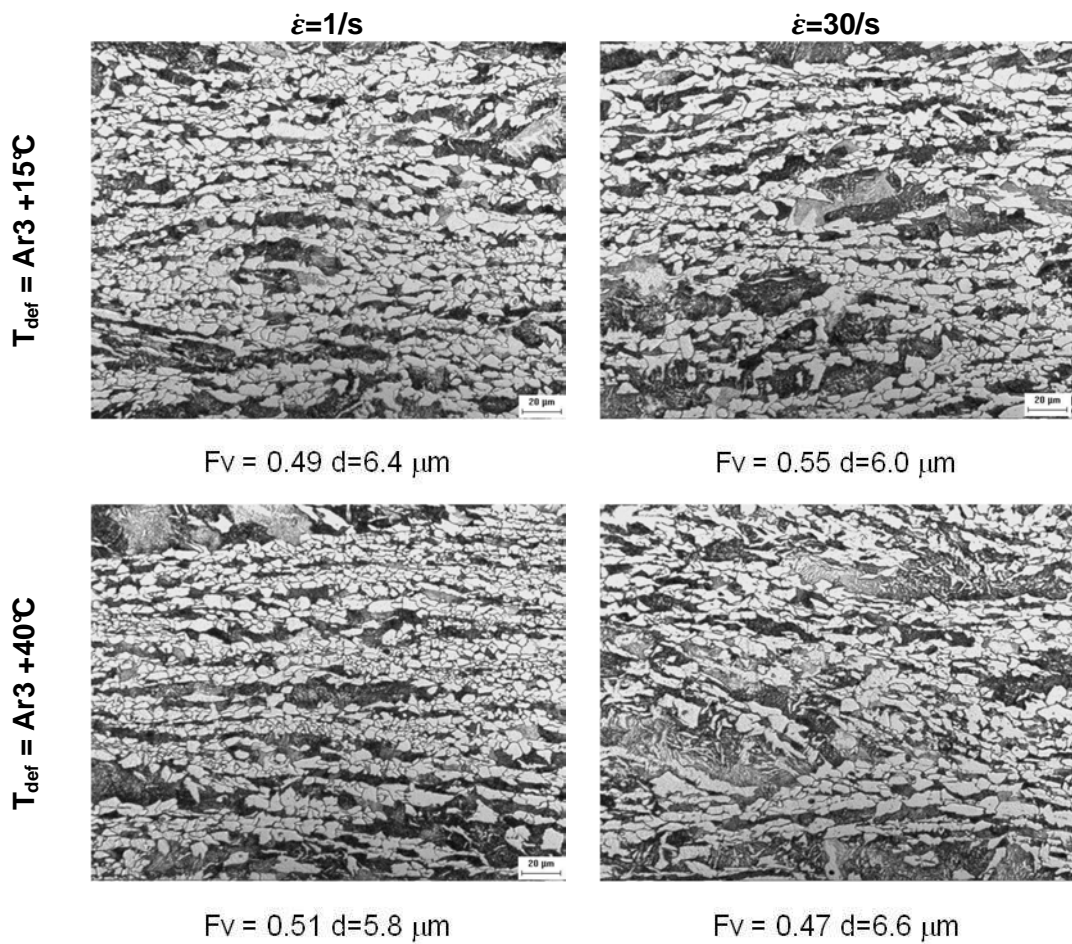


Figure 40: Microstructure for samples 30MnB4 PAGS= 50 μm (Steel B).

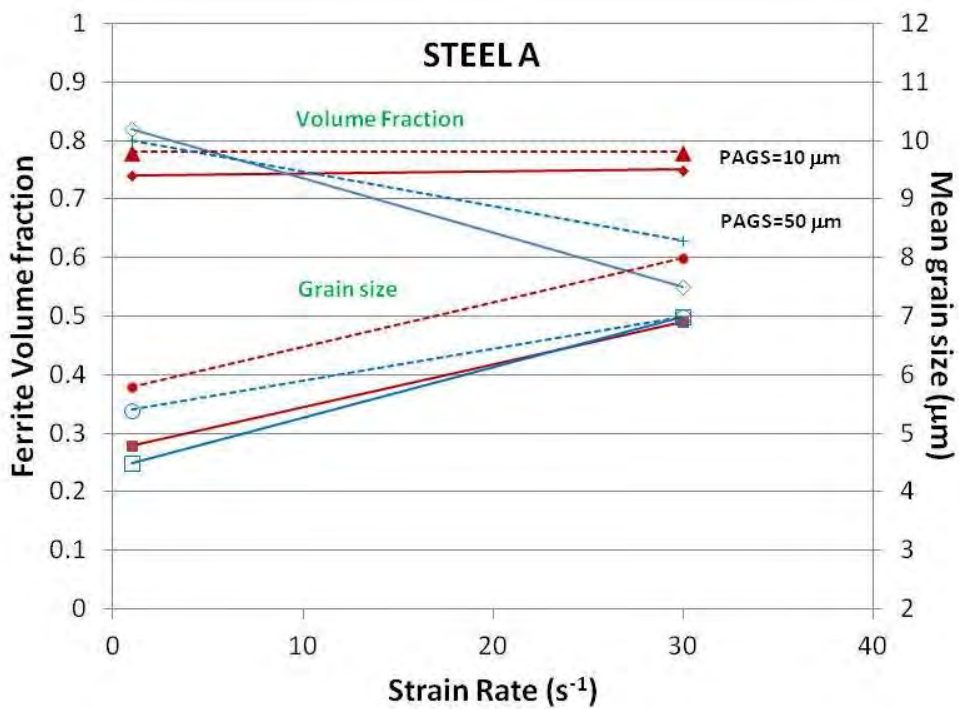


Figure 41: Ferrite volume fraction and grain size versus strain rate for samples 18MnB2.

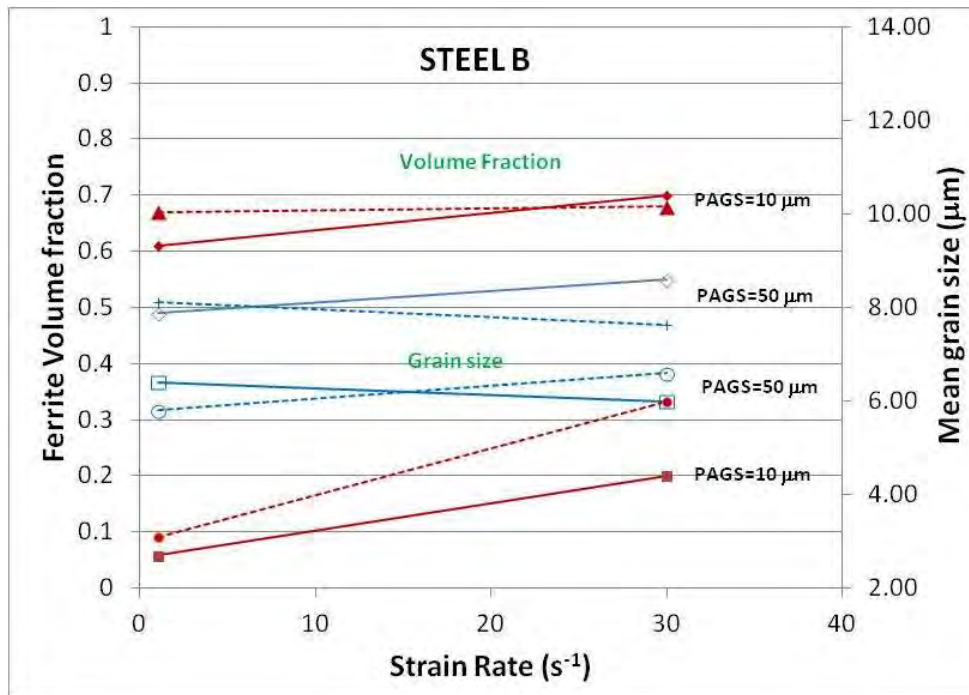


Figure 42: Ferrite volume fraction and grain size versus strain rate for samples 30MnB4.

Summary of DIFT results

From the results it is evident that the processing parameters and initial microstructure can influence the occurrence of DIFT and the DIFT ferrite grain size and volume fraction.

(a) - Critical strain

As explained before, deformation accelerates the phase transformation kinetics. However if the imposed strain is too small the dynamic transformation is not activated.

Therefore, it is clear that there is a critical strain required for DIFT to occur and it is related to the deformation conditions and chemical composition. Decreasing the prior austenite grain sizes and deformation temperature the critical strain value decreases. The increase of alloying element as C, Mn and B increase the critical strain.

(b) - Strain

It can be confirmed that increasing strain (beyond the critical strain), more DIFT grains can be obtained. When the strain is small, DIFT ferrite starts to form along the prior austenite grain boundaries. As the strain is increased, the interiors of austenite grains are activated as nucleation sites for DIFT ferrite, which are probably deformation bands or twin boundaries.

About the grain size it was noted that increasing the strain the grain size decreases. However for all the tested chemical compositions for $\epsilon > 1$ the refining rate of ferrite grain size is very low.

(c) - Prior austenite grain size

From the results shown it is evident that the smaller prior austenitic grain size, the higher is the volume fraction of DIFT ferrite under a given deformation condition. This is mainly because the prior austenite grain boundary is a preferential nucleation site for DIFT ferrite.

A smaller prior austenite grain size has the longer grain boundary area in a given volume of material, and this results in the larger volume fraction of ferrite and consequently finer grain size.

(d) - Deformation Temperature

Deformation temperature influences the critical strain, and ferrite volume fraction. Lower the deformation temperature, lower is the critical strain. If the critical strain for DIFT is reduced, a finer ferrite grain size and more volume fraction at given strain are observed.

The effect of low deformation temperature is important when the strain is relatively small, because decreasing the deformation temperature is very effective in increasing the amount of DIFT, but at relatively high strains decreasing the deformation temperature will affect only slightly the amount of DIFT.

(e) - Strain rate

The effect of strain rate on ferrite volume fraction seems to be not significant, at least in the analyzed range ($1-30 \text{ s}^{-1}$). The grain size tends to increase when strain rate increases in most of the investigated samples. Such effect is in contrast to what reported in literature.

(f) – Chemical composition

Critical strain increases with C and Mn content. The Mn content increases the critical strain necessary for DIFT occurrence at the same C content. However it has a weaker effect if compared with the C content. The level of ferrite refinement increases slightly with the carbon content. The presence of B increases the critical strain.

Determination of DIFT parameters for powertrain steel

One of the aims of this project is to produce ultrafine-grained steel long products in a conventional hot rolling mill. The first simulated thermomechanical cycles have tried to approach industrial conditions. For this reason, firstly, some tests were performed heating the samples at $1200^\circ\text{C} \times 5$ minutes but the prior austenite grain size was more than $80 \mu\text{m}$ so it was not possible to get DIFT ferrite grain size even changing the number of deformation passes and the deformation temperature.

18CrMo4 Experimental Production Run

Other thermo-mechanical tests were performed by heating the samples at 1000°C for 15 min. The number of passes was 3. The last deformation pass was introduced at 810°C to favour DIFT. The amount of deformation of each pass ranged between 0.1 and 0.75, without exceeding the deformation limit of $\epsilon_{\text{total}} = 1$.

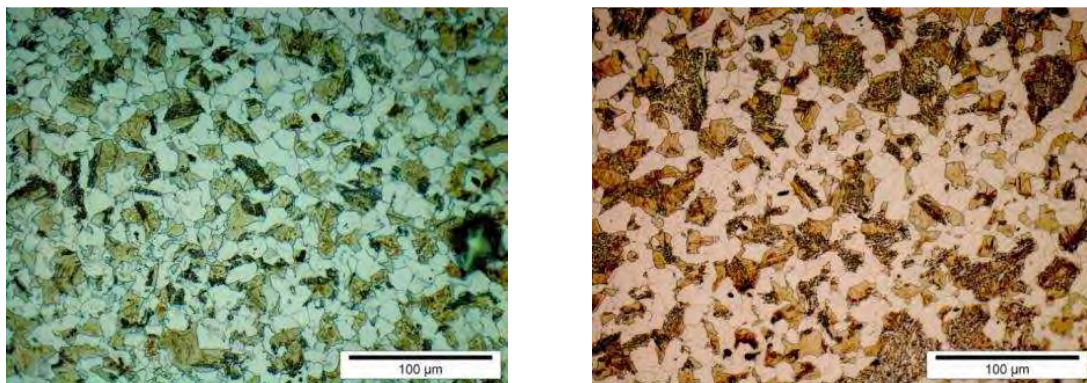


Figure 43: Microstructure of samples (left) #16 and (right) #17 of 18CrMo4 Experimental (etched in 2% Nital for 5-10 s).

Cooling rate varied from 5°C/s , between deformation passes, and 0.7°C/s , during the final cooling. Figure 43 shows the microstructures achieved in these thermo-mechanical cycles. Figure 44 shows the two cycles performed.

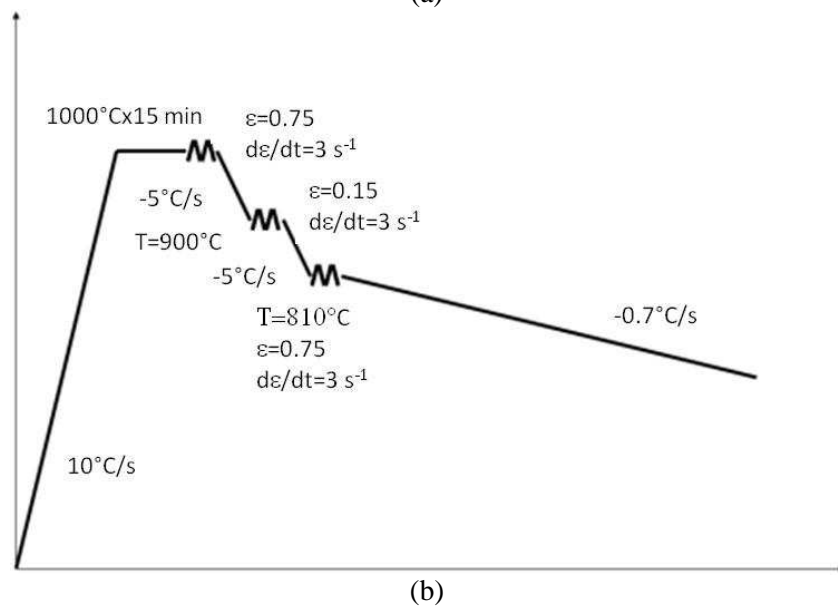
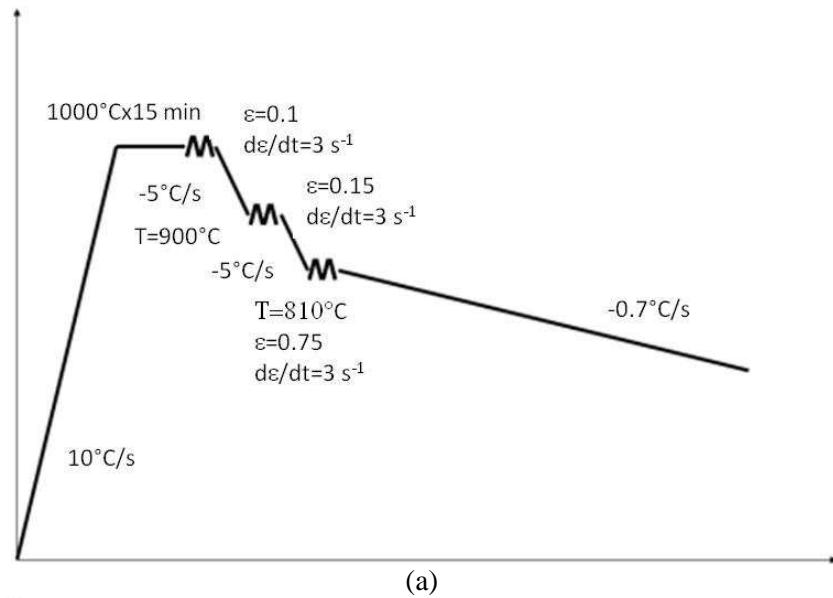


Figure 44: Thermomechanical cycles corresponding to samples (a) #16 and (b) #17 of 18CrMo4 Experimental.

Grade	18CrMo4 Experimental			
Sample	Microstructure	Parameter		HV (0.5 kg)
#16	Ferrite	Vol. fract.	0.43 ± 0.02	250 ± 10
		Size (μm)	7.3 ± 0.1	
	Bainite			
	Martensite			
#17	Ferrite	Vol. fract.	0.45 ± 0.02	259 ± 8
		Size (μm)	8.6 ± 0.3	
	Bainite			
	Martensite			

Table 17: Microstructural composition (phases, amount and size) and Vickers hardness (0.5 kg) of the DIFT cycles of 18CrMo4 Experimental.

Table 17 summarizes the microstructural composition and the Vickers hardness (0.5 kg) of these samples. The microstructures are still very complex and the presence of a brittle phase, such as martensite, can be found, too.

Figure 45 shows the thermo-mechanical cycle corresponding to the best result (finest microstructure) obtained with the experimental grade of 18CrMo4. Table 18 summarizes the present phases, and amount and size of the present phases in the best cycle.

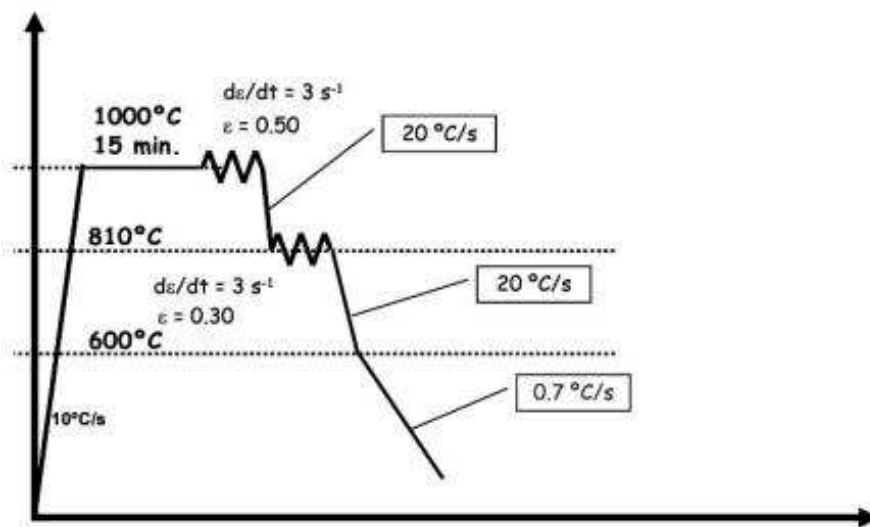


Figure 45: Thermo-mechanical cycle corresponding to the best result obtained with the 18crMo4 Experimental (sample #10).

Steel grade	18CrMo4 Experimental		
Specimen	Microstructure	Measured parameter (<u>ferrite</u>)	
#10	Ferrite / Bainite	Vol. fract.	0.44 ± 0.04
		Size (µm)	1.8 ± 0.1

Table 18: Microstructural composition (phases, amount and size) of the best result obtained with the 18CrMo4 Experimental.

18CrMo4 Industrial Production Run

Some thermo-mechanical tests were performed with this steel, with different austenitization conditions and number of passes. The last one was introduced at 810 °C to favour DIFT. The total amount of deformation was 1. The final cooling rate was 0.7 °C/s. Figure 46 shows two of the cycles performed. Figure 47 shows the microstructures achieved in these thermo-mechanical cycles.

Table 19 summarizes the microstructural composition and the Vickers hardness (0.5 kg) of these samples. As for the other materials, the microstructures are still very complex and include martensite. Some improvement has been obtained in this set of experiments, as the ferrite grain size has been reduced to 3.9 (sample #23), very close to the ultrafine range (2-3 µm).

As for the other materials, the microstructures are still very complex and include martensite.

50SiMoVNb8

Several thermo-mechanical tests were performed to assess the effect of different parameters that configure the cycles, on the final grain size. In all cases, the austenitization process was at 1000 °C and 15 min. The number of passes was 2 or 3. At least one pass took place at 810 °C to favour DIFT. The total amount of deformation was equal to 1, which is the maximum allowed by the dilatometer. Cooling rate varied from 5 °C/s, between deformation passes, to 0.7 °C/s, during the final cooling. Figure 48 shows the cycles performed.

Figure 49 shows the microstructures achieved in these thermo-mechanical cycles. Table 20 summarizes the microstructural composition and the Vickers hardness (0.5 kg) of these samples.

The microstructures are still very complex and several phases (martensite in particular) can be found. Nevertheless, we are now closer to the objective of the project, as ferrite size is in the ultrafine range (2-3 μm).

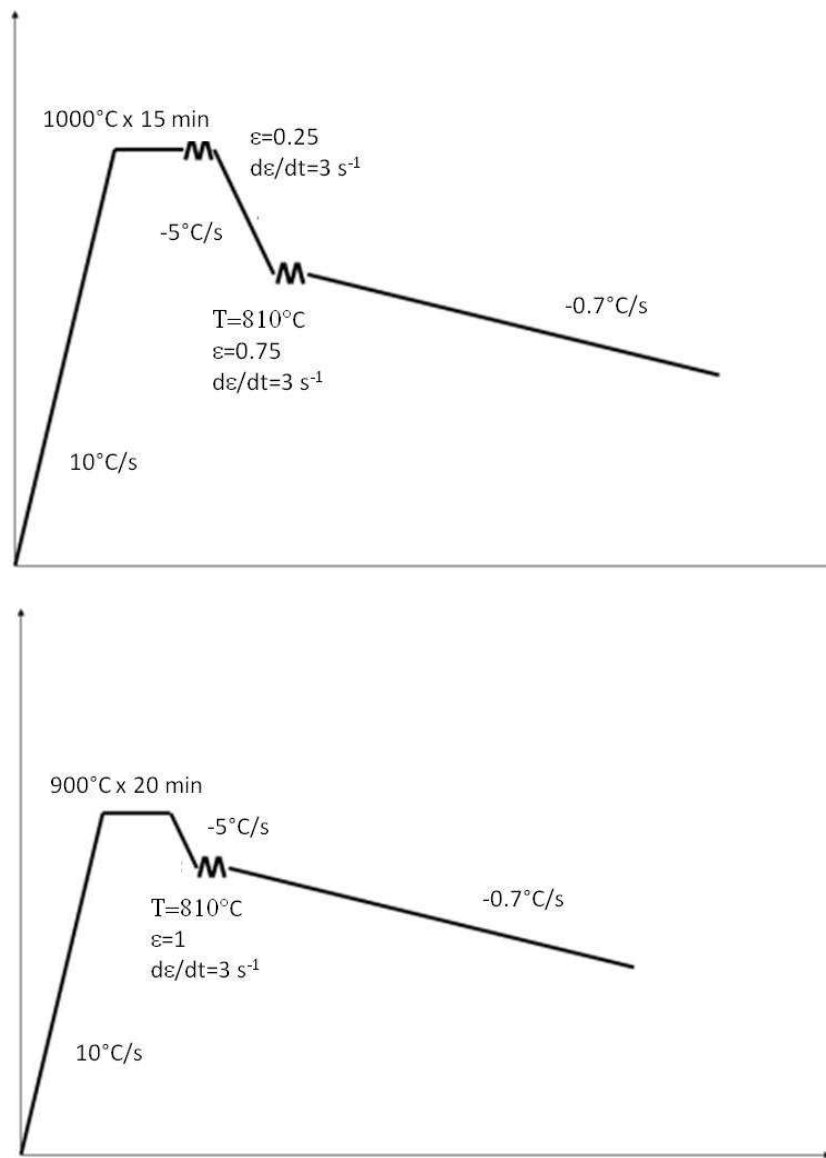


Figure 46: Thermo-mechanical cycles corresponding to samples (top) #23 and (bottom) #24 of 18CrMo4 Industrial.

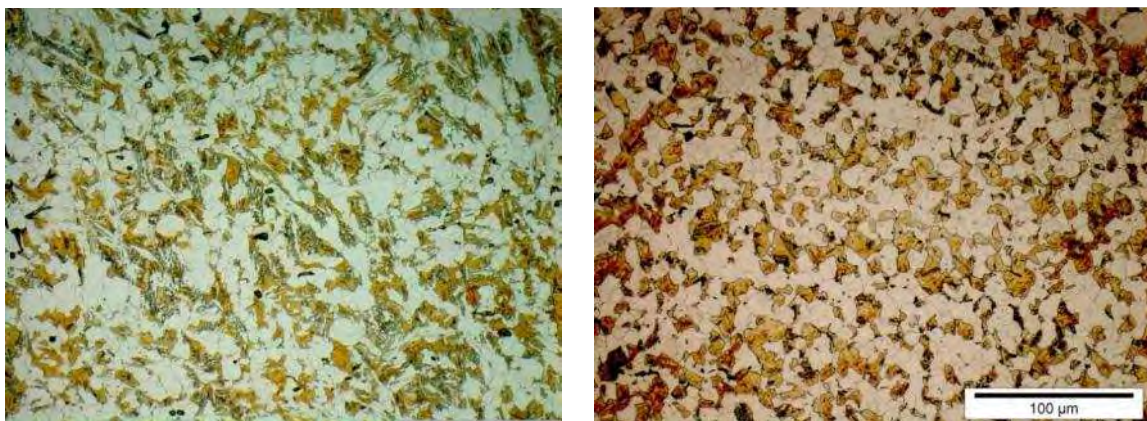


Figure 47: Microstructure of samples (left) #23 and (right) #24 of 18CrMo4 Industrial (etched in 2% Nital for 5-10 s).

Grade	18CrMo4 Industrial			
Sample	Microstructure	Parameter		HV (0.5 kg)
#23	Ferrite	Vol. fract.	0.41 ± 0.06	260 ± 10
		Size (μm)	3.9 ± 0.1	
	Bainite			
	Martensite			
#24	Ferrite	Vol. fract.	0.54 ± 0.02	280 ± 10
		Size (μm)	6.6 ± 0.2	
	Bainite			
	Martensite			

Table 19: Microstructural composition (phases, amount and size) and Vickers hardness (0.5 kg) of the DIFT cycles of 18CrMo4 Industrial.

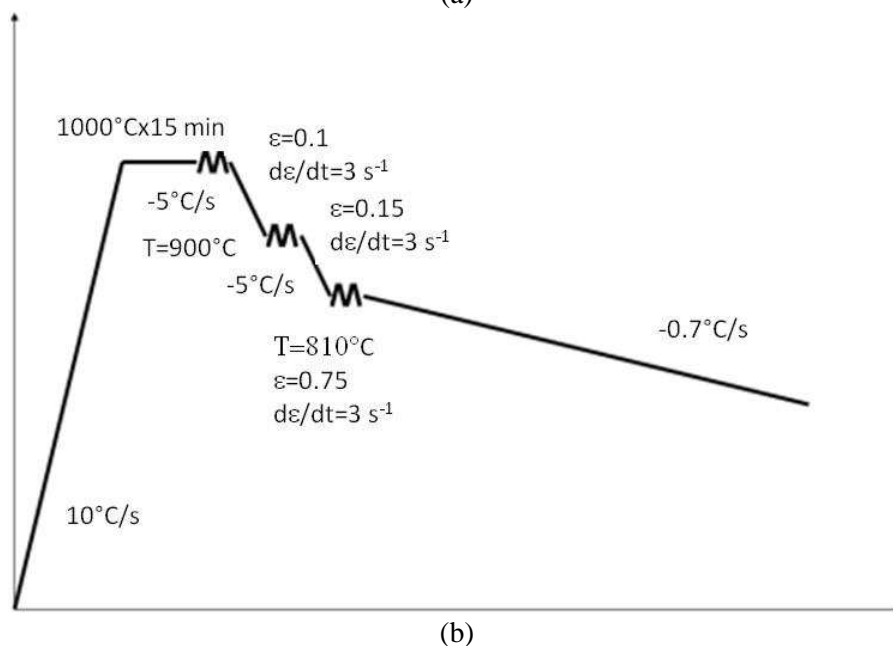
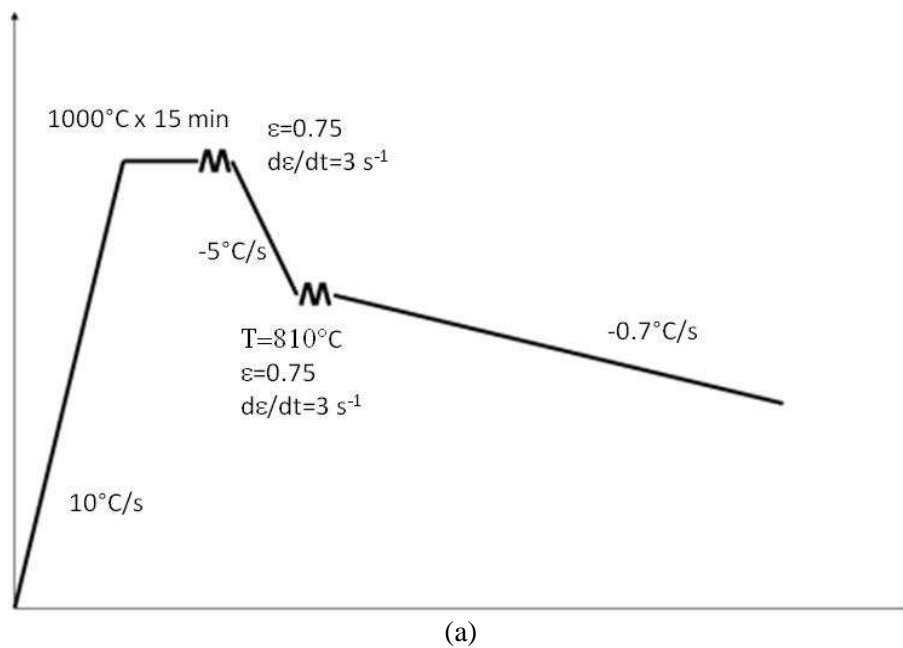


Figure 48: Thermo-mechanical cycles corresponding to samples (a) #16, (b) #18 of 50SiMoVNb8.

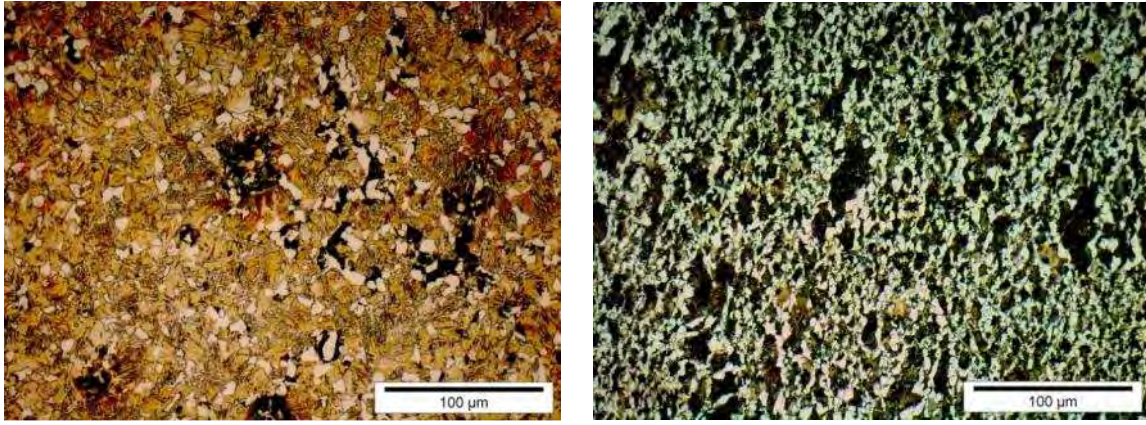


Figure 49: Microstructure of samples (left) #16 and (right) #17 of 50SiMoVNb8 (etched in 2% Nital for 5-10 s).

Grade	50SiMoVNb8			
Sample	Microstructure	Parameter		HV (0.5 kg)
#16	Ferrite	Vol. fract.	0.08 ± 0.01	480 ± 30
		Size (μm)	4.1 ± 0.1	
	Pearlite			
	Martensite			
#17	Ferrite	Vol. fract.	0.26 ± 0.01	354 ± 9
		Size (μm)	2.2 ± 0.1	
	Pearlite			
	Martensite			

Table 20: Microstructural composition (phases, amount and size) and Vickers hardness (0.5 kg) of the DIFT cycles of 50SiMoVNb8.

Figure 50 shows the thermo-mechanical cycle corresponding to the best result (finest microstructure) obtained with the 50SiMoVNb8 (sample #14). Table 21 summarizes the present phases, and amount and size of the present phases in the best cycle.

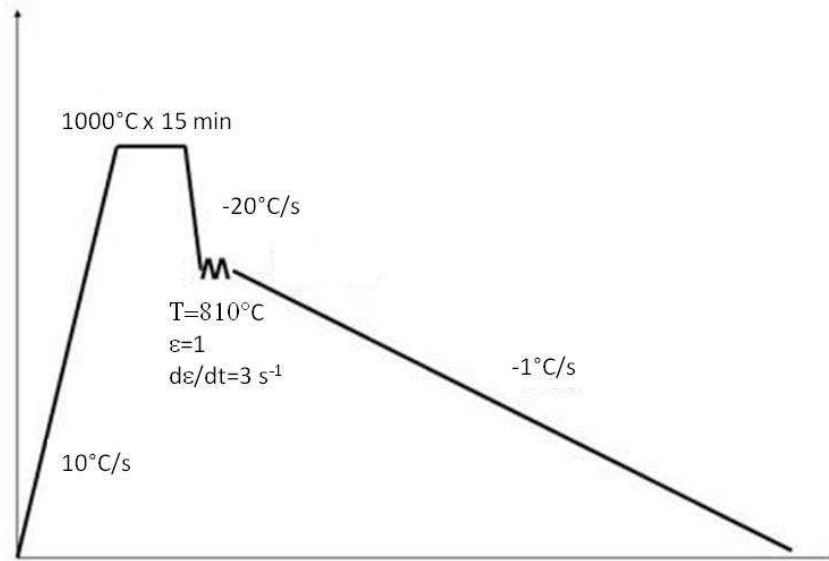


Figure 50: Thermo-mechanical cycle corresponding to the best result obtained with the 50SiMoVNb8 (sample #14).

Steel grade	50SiMoVNb8		
Specimen	Microstructure	Measured parameter (ferrite)	
#14	Ferrite + Pearlite + Martensite	Vol. fraction	0.32 ± 0.02
		Size (mm)	2.4 ± 0.2

Table 21: Microstructural composition (phases, amount and size) of the best result obtained with 50SiMoVNb8.

Task 2.2: Heavy γ deformation: Determination of parameters for different C steels

Another approach to obtain ultra fine grains in steels is to give severe plastic straining during hot rolling in order to have deformed austenite that transforms in ferrite during cooling.

Most of the ultra-fine ferrite comes from nucleation on the grain boundaries in the deformed austenite. With the increase of the accumulated strain, the pancaking of deformed grains increases and therefore the number of nucleation sites for ferrite increases.

The use of low temperature rolling combined with high reductions leads to low volume fraction of recrystallized austenite microstructures just prior to ferrite transformation. The ultrafine ferrite formed is a consequence of a significant fraction of deformed grains in the austenite microstructure.

The industrial hot rolling process varies from plant to plant but generally can be described by the schematic in Figure 51 [5].

In the process shown above, firstly, the austenite is deformed at high Zener-Hollomon parameter to cause austenite refinement by dynamic recrystallization ($T > T_{nr}$ = non recrystallization temperature). Decreasing the rolling temperature (below T_{nr}), the austenite is deformed in the no-recrystallization temperature region. This gives elongated austenite grains, helpful for ferrite grain refinement during. When the retained austenite transforms during cooling gives fine ferrite.

In the temperature range between A_{e3} and A_{r3} , also DIFT can occur if the critical strain is achieved.

In this task the activity has been focused on the identification of the conditions to obtain grain refinement through transformation of heavily deformed austenite to ferrite during cooling.

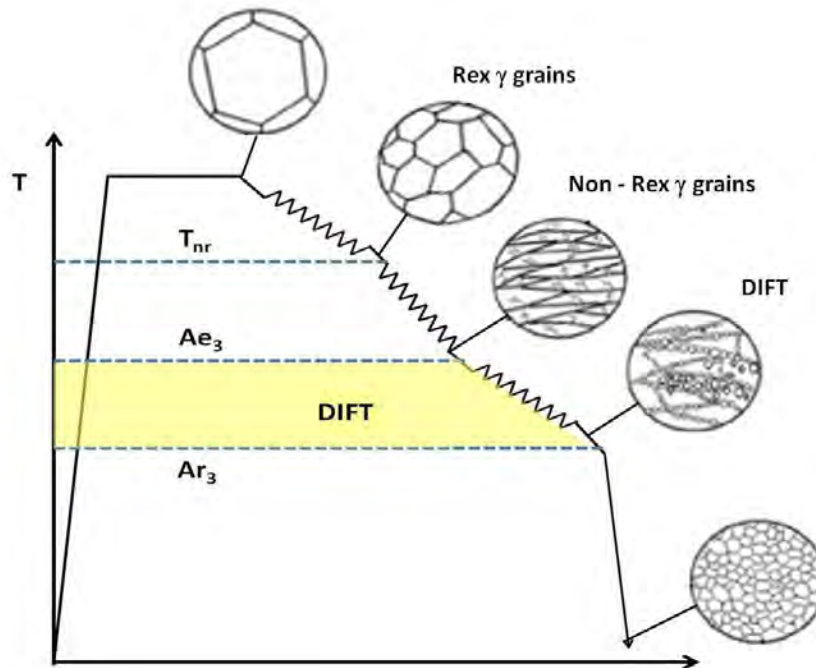


Figure 51: Scheme of mechanisms occurring during rolling [5].

Fasteners (carbon range 0.15-0.30 %)

For each steel, dilatometry experiments were planned to determine CCT diagrams.

The thermal schedule consisted in heating to 900°C, soaking for 600s and then cooling at 8 different rates, ranging from 0.5-150°C/s. Note that the reheating temperature was the same for all steels.

In addition for Steel A (18MnB2) and Steel B (30MnB4) even CCT with 2 different deformations (30 and 50%) were tested in order to measure how the diagrams change if deformation is carried out. In

these cases samples were heated to 900°C, soaking for 600s, deformation at 30 or 50% at T=900°C and then 8 different cooling rates were tested.

For each test, start and finish transformation temperatures were obtained from the observed dilatation. In addition samples were analyzed via optical microscopy to determine the phases percentage present after cooling. CCT diagrams were obtained from the combination of optical microscopy and dilatometry results. In Figures 52-56 the CCT diagrams for non deformed samples are reported.

For the non-deformed samples determination of prior austenite grain size (PAGS) was carried out by helium quenching at 150°C/s. After quenching, samples were mechanically ground and polished followed by etching to reveal the prior austenite grain boundaries. Figure 57 shows the microstructures obtained for all steels. It can be observed that the PAGS is generally equiaxed and mean size is about 9µm. Only 18MnB2 steel shows a coarser PAGS, however its microstructure is quite inhomogeneous.

Comparing the CCT diagrams it can be noted that (as expected) the increase of C content decreases the austenite-ferrite transformation temperatures, the addition of B and the increase of Mn content move the CCT diagram to the right side, giving to the steel a higher hardenability and a decrease of the austenite-ferrite transformation temperatures. The resulting microstructures ranged from polygonal ferrite and pearlite for slow cooling rates and low alloying element contents, to bainite accompanied by martensite for fast cooling rates and high concentrations of alloying elements. Combined additions of B and Mn with the same C content were found to be most effective in increasing steel hardenability.

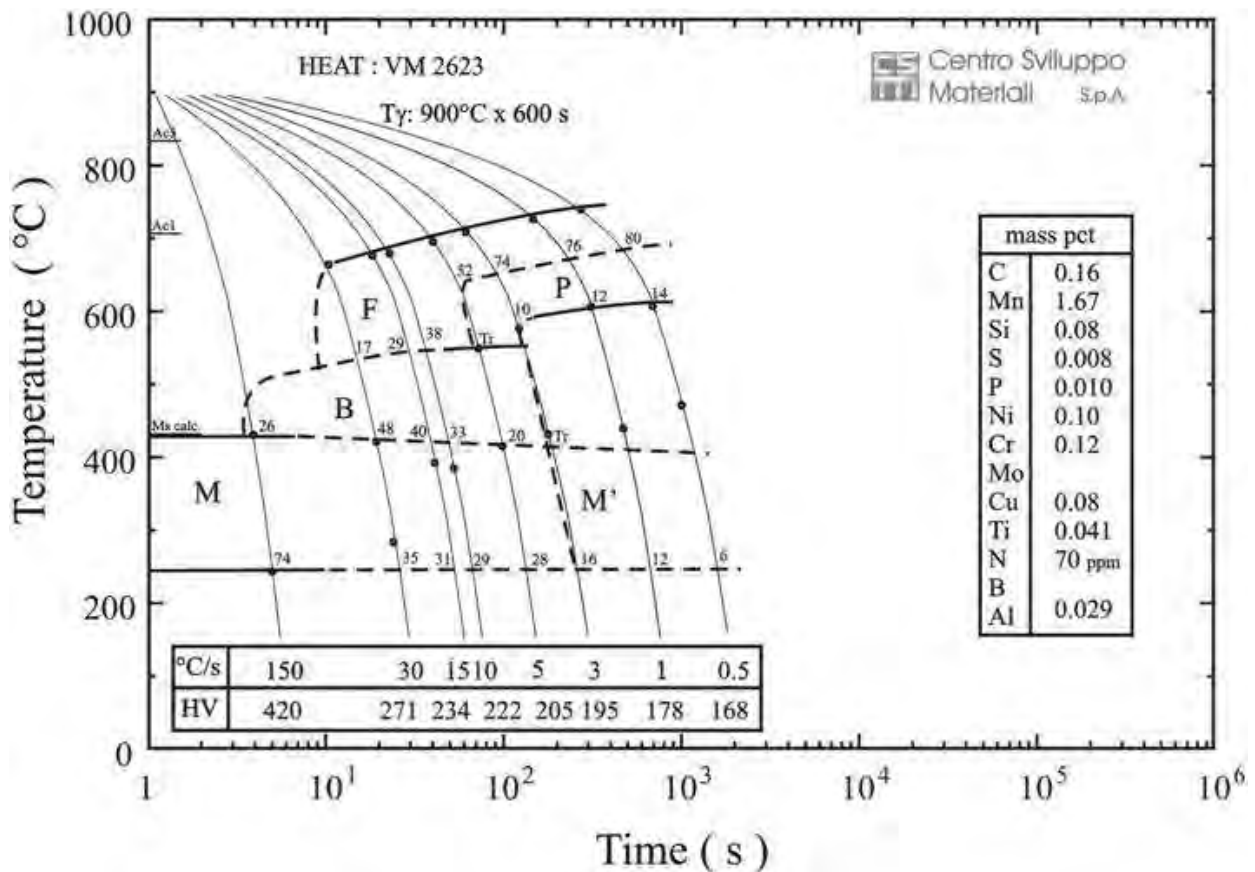


Figure 52: CCT diagram of VM2623 (18Mn7 steel).

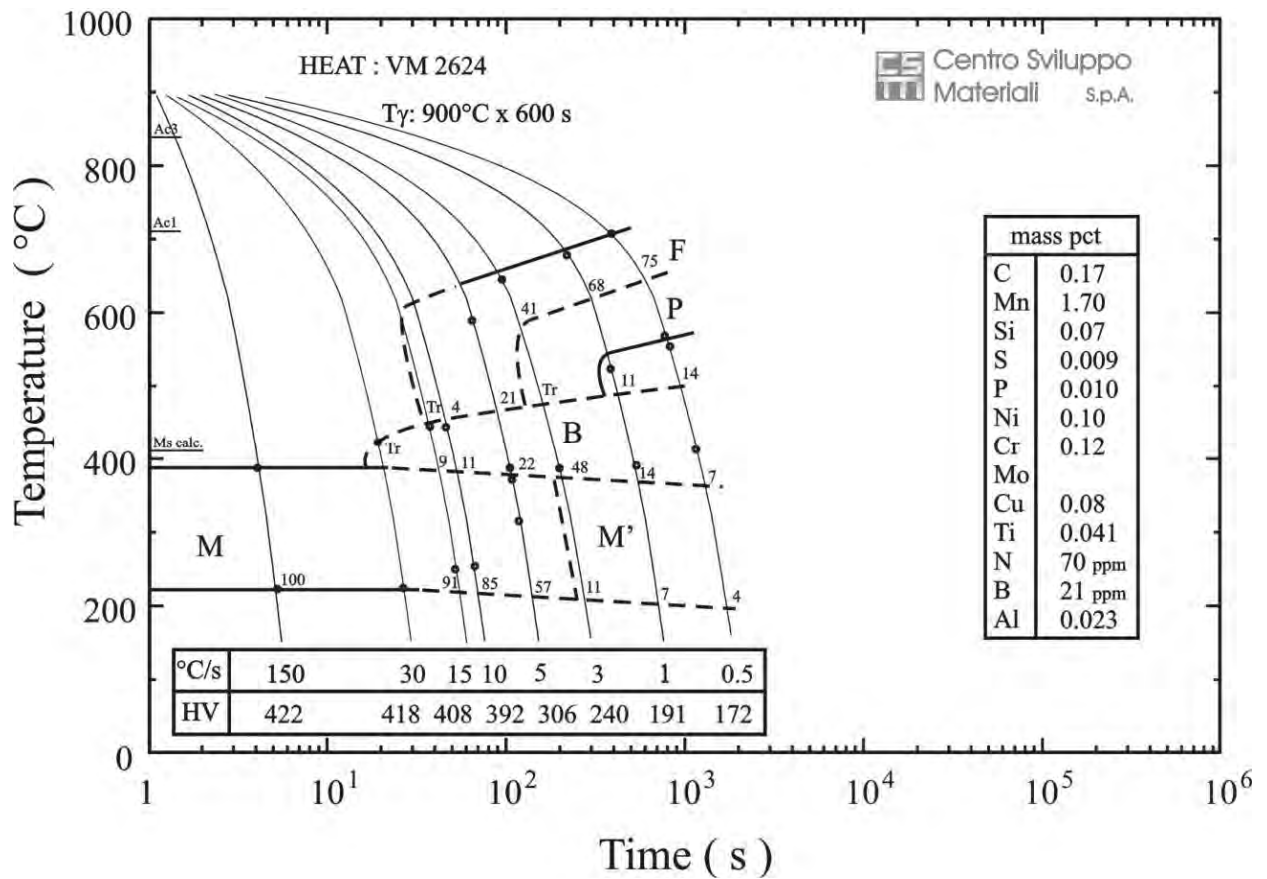


Figure 53: CCT diagram of VM2624 (18MnB7steel).

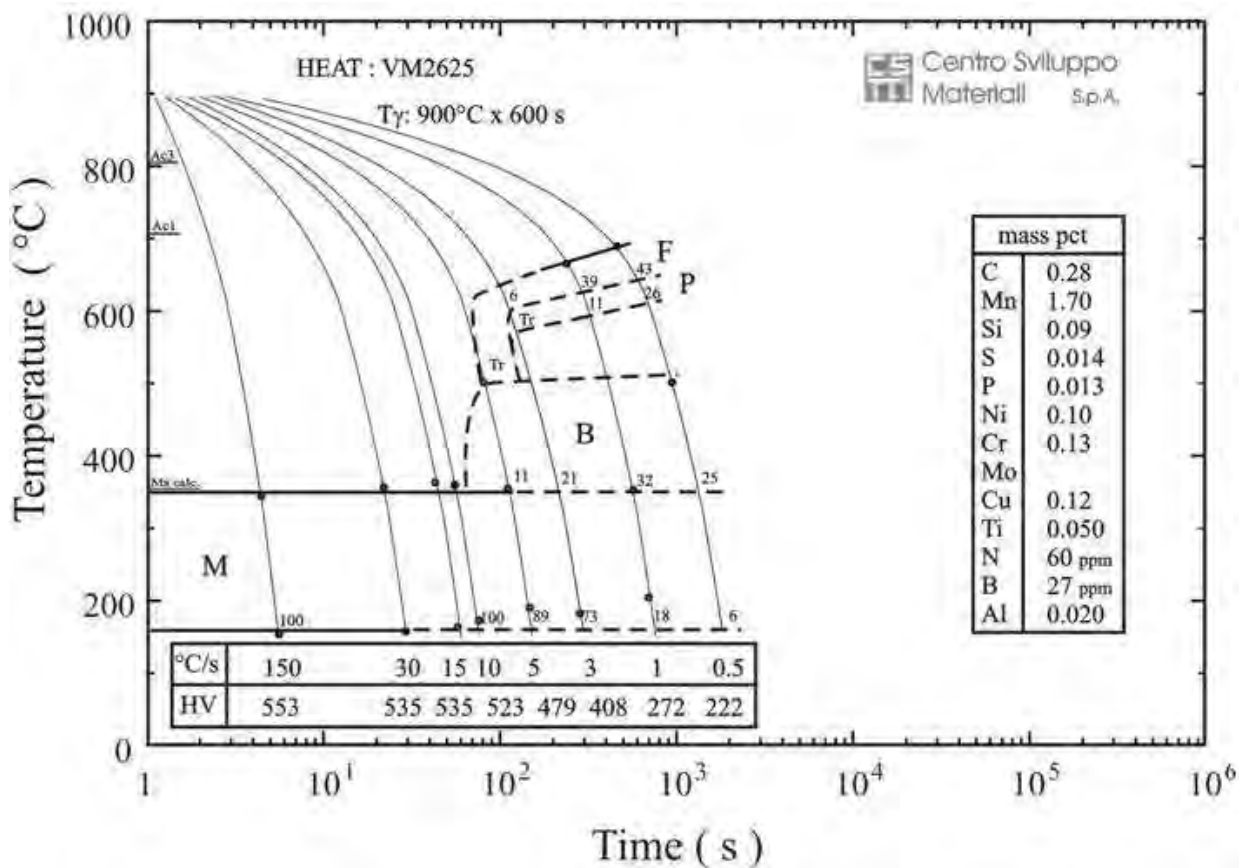


Figure 54: CCT diagram of VM2625 (30MnB7steel).

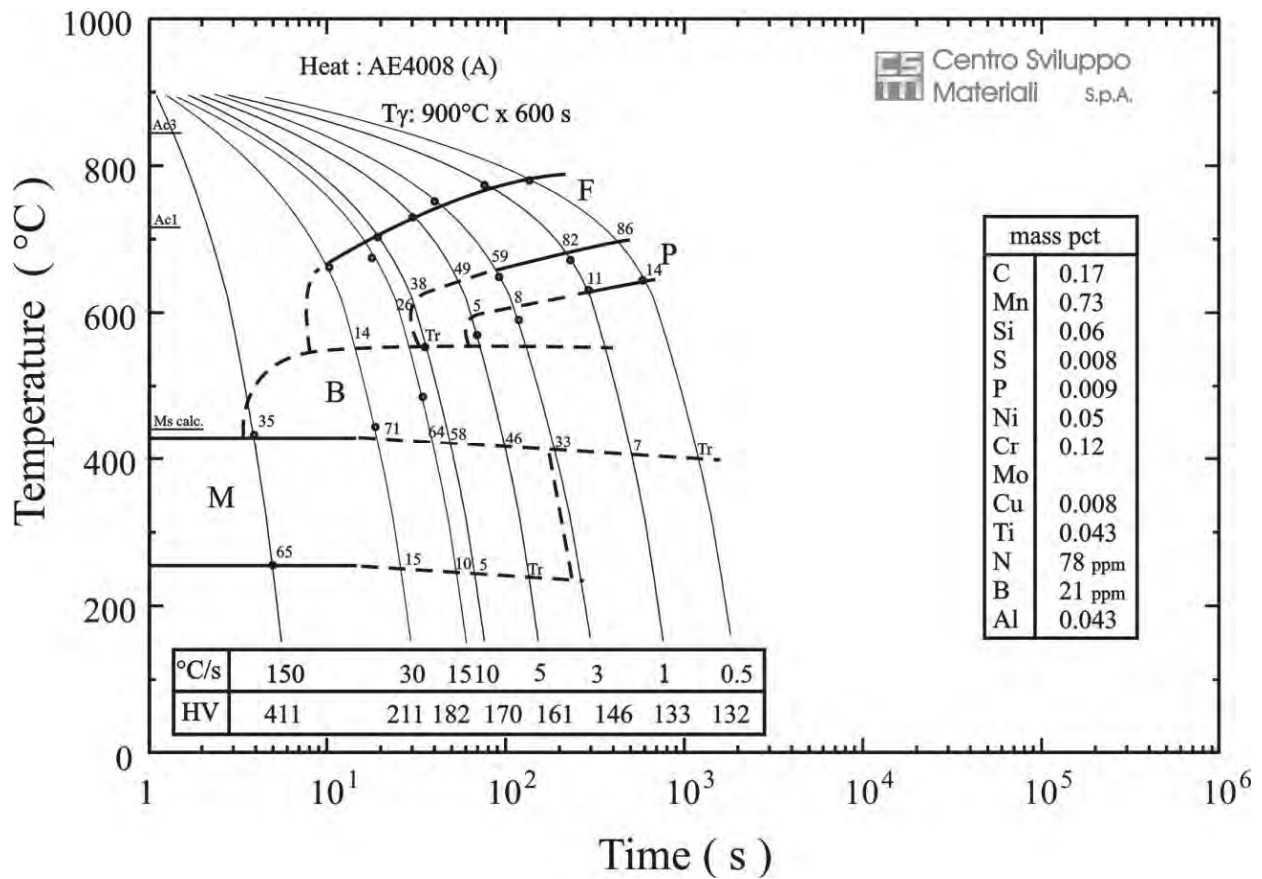


Figure 55: CCT diagram of A steel (18MnB2 steel).

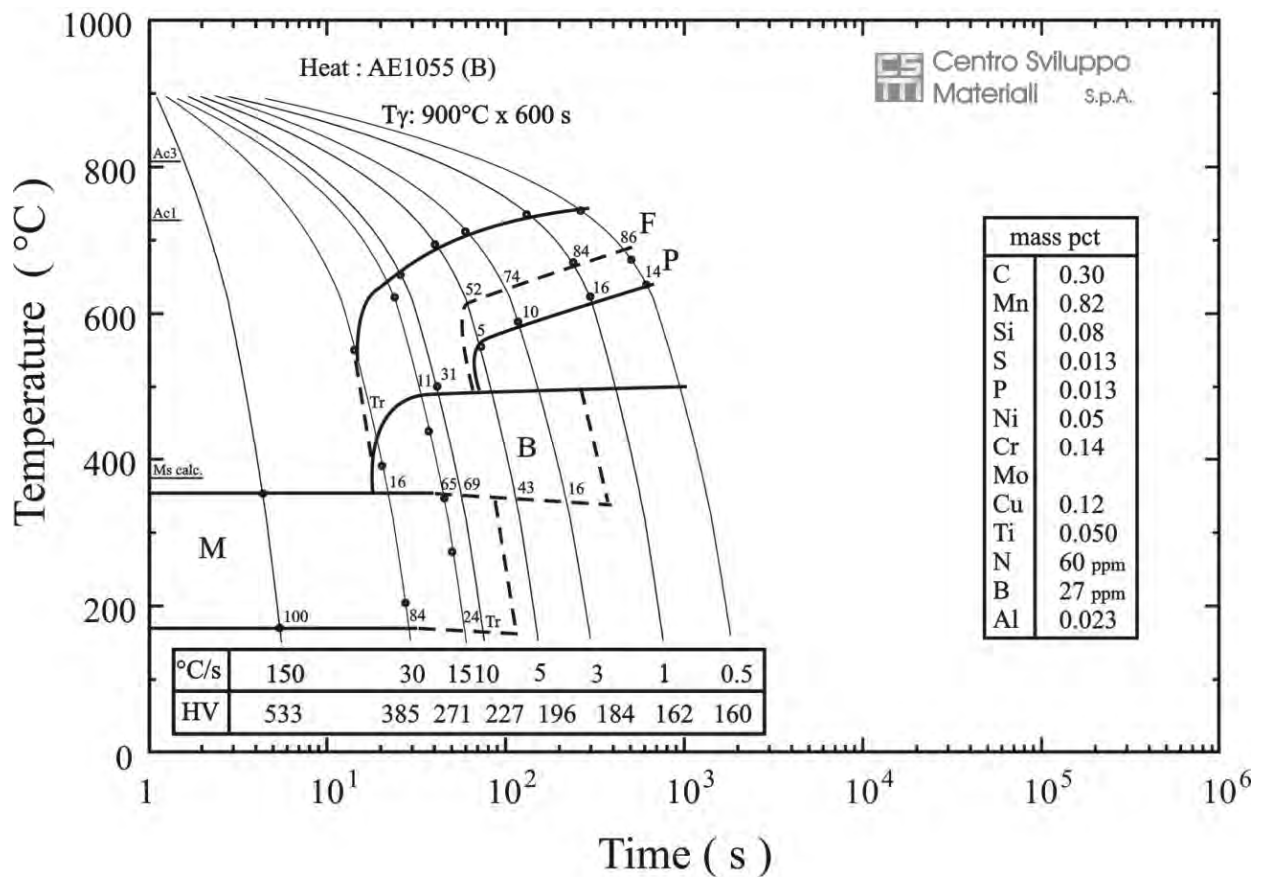


Figure 56: CCT diagram of B steel (30MnB4 steel).

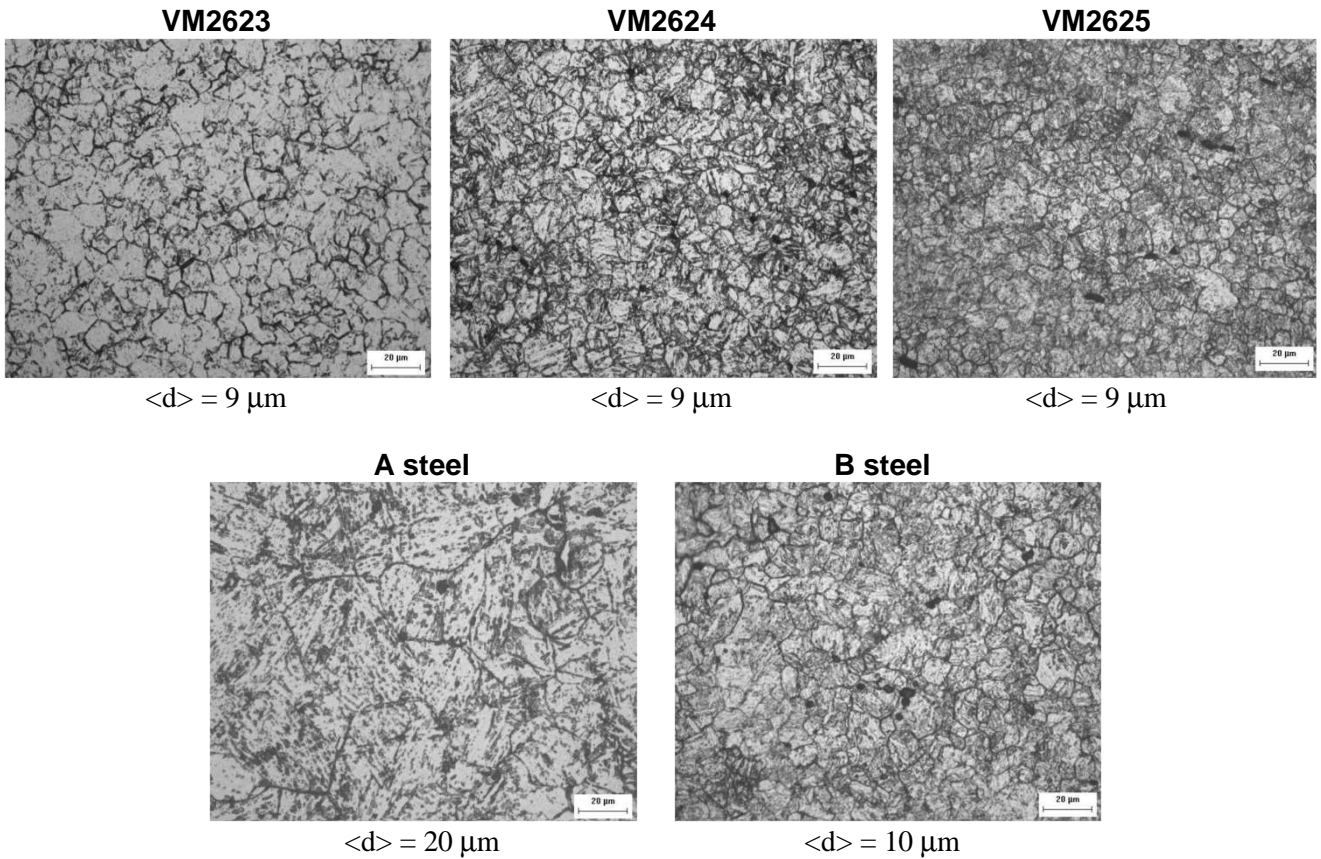


Figure 57: Prior austenite grain boundaries (PAGS) as revealed by quenching non-deformed samples. $\langle d \rangle$ is the mean value of PAGS.

PAGS (μm)	T_{def} ($^{\circ}\text{C}$)	Strain rate (s^{-1})	Ferrite vol. fract. (%)	FGS (μm)
10	867	1	80	5.6
10	867	30	77	6.7
50	867	1	63	7.9
50	867	30	65	9.0

Table 22: Summary of results for steel A (18MnB2) ($A_{r_3} + 70^{\circ}\text{C} = 867^{\circ}\text{C}$, def.= 50%).

PAGS (μm)	T_{def} ($^{\circ}\text{C}$)	Strain rate (s^{-1})	Ferrite vol. fract. (%)	FGS (μm)
10	820	1	80	3.3
10	820	30	65	5.4
50	820	1	49	6.4
50	820	30	51	6.7

Table 23: Summary of results for steel B (30MnB4) ($A_{r_3} + 70^{\circ}\text{C} = 820^{\circ}\text{C}$, def.= 50%).

The mechanism of heavy γ deformation has been investigated by means of a number of tests carried out on a Gleeble equipment on samples of 18MnB2 (steel A) and 30MnB4 (steel B), deformed of 50% at temperature $A_{r_3} + 70^{\circ}\text{C}$ at two different strain rates (1 s^{-1} and 30 s^{-1}) and two different prior austenite grain sizes ($10 \mu\text{m}$ and $50 \mu\text{m}$).

In Tables 22 and 23 the results of these tests are summarised, while the related microstructures are shown in Figures 58 and 59.

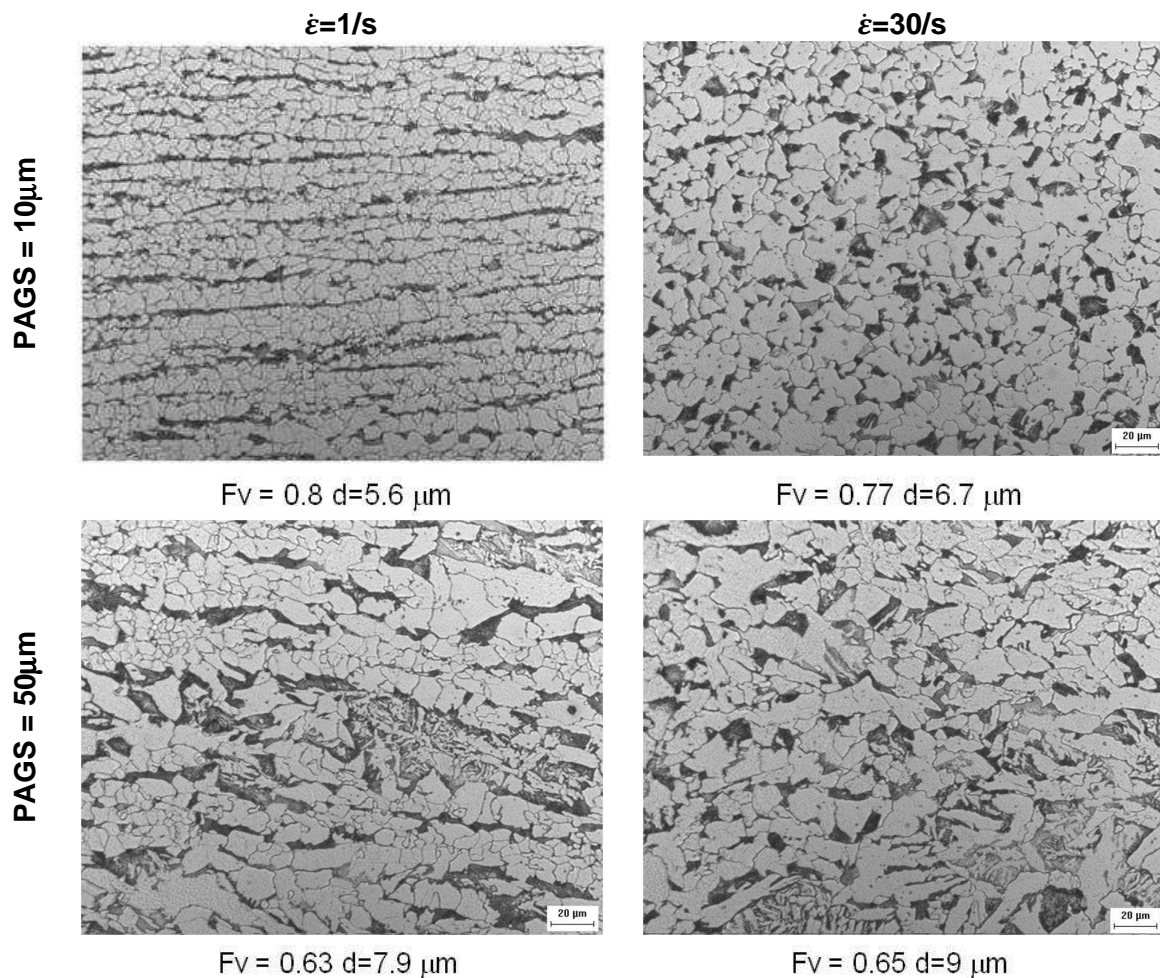


Figure 58: Microstructure for 18MnB2 samples deformed of 50% at $T=867^{\circ}\text{C}$ ($A_{r3}+70$) (Steel A).

As in the case of DIFT, a significant influence of PAGS has been found: when PAGS is finer, also ferrite grain sizes are finer and ferrite volume fraction increases. Such effect is true for both steel, but ferrite grain size values are smaller for 30MnB4 (steel B). Increasing strain rate is not effective on grain size refining: on the contrary, ferrite grain size tends to increase when strain rate rises. As in the case of DIFT Gleeble tests, this effect need to be better clarified.

Summarising, the results found proved that it is possible, by means of high deformations imposed in a temperature range where the dynamic recrystallization is inhibited and strain is accumulated in austenite structure, to obtain grain refinement. The microstructures obtained are characterised by fine ferrite grain size and high ferrite volume fractions, especially when the prior austenite grain size is held at sufficiently small values. However, at the same deformation conditions (strain and prior austenite grain size) DIFT showed a more refining power.

Automotive – powertrain (carbon range 0.15-0.20 %)

A number of dilatometry tests have been performed to determine the CCT curves of the industrial 17CrV6 (Table 24 and Figures 60 and 61). As it is shown in Table 24, the critical quenching rate is a bit higher than 30°C/s , as at this cooling rate almost the 100% of the microstructure is martensite.

As for the industrial heats, some dilatometry tests have been performed to determine the CCT curve of the experimental heats 17CrV6 and 17CrVNb6 (Tables 25, 26 and Figures 62-65). In the CCT curves obtained for the 17CrV6 and 17CrVNb6, it has been observed that experimental heat with Nb shows higher percentage of bainite and martensite than the heat without Nb.

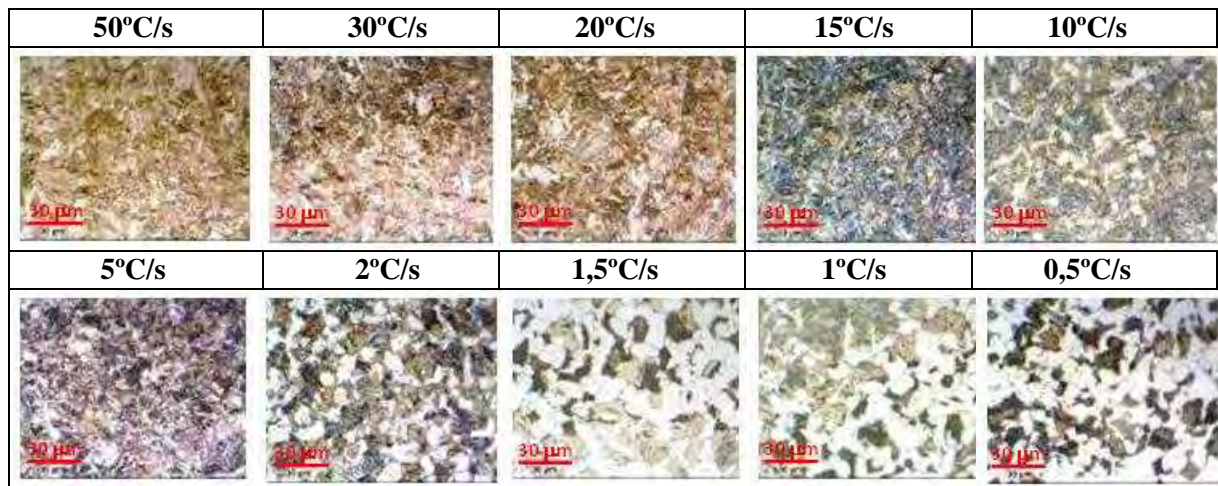


Figure 60: Microstructures obtained at the different cooling rates of the CCT curve.

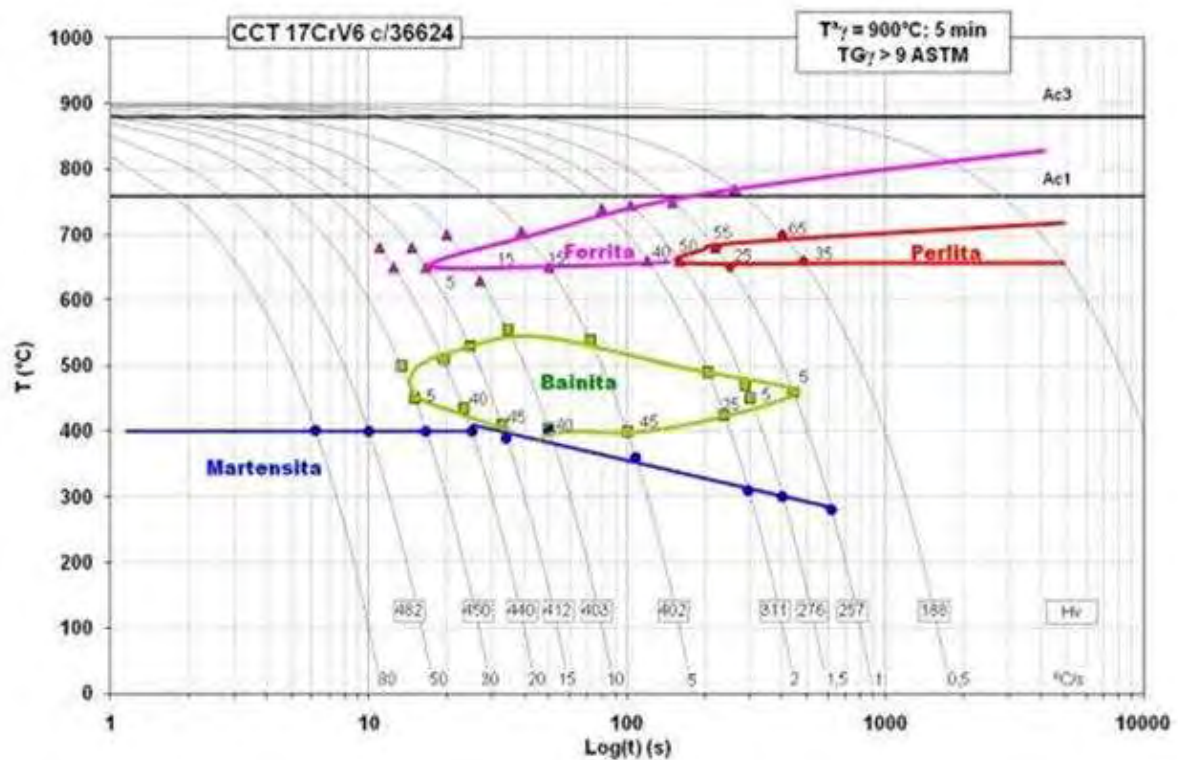


Figure 61: CCT curve of the industrial heat of 17CrV6 (36624).

Cooling rate (°C/s)	Microstructure (%)				Hardness (HV 30)
	ferrite	Pearlite	bainite	martensite	
20	10	0	25	65	347
5	40	0	30	30	298
1	60	25	5	10	204
0,2	65	35	0	0	182

Table 25: Results of dilatometry tests of the Experimental heat of 17CrV6.

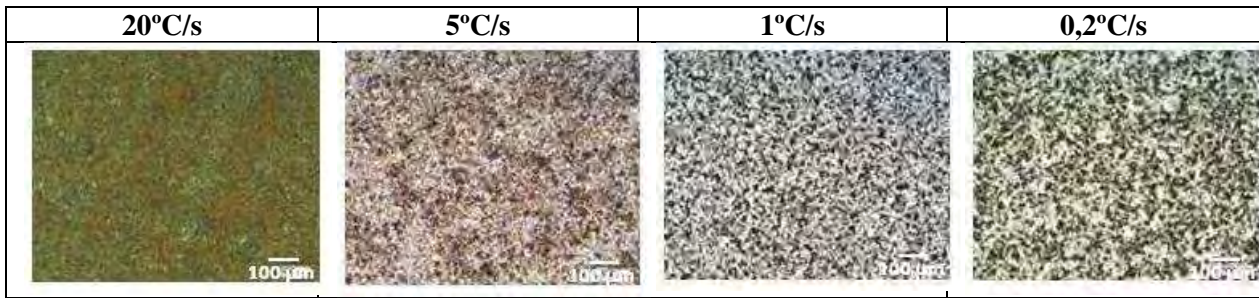


Figure 62: Microstructures obtained at the different cooling rates for the Experimental heat of 17CrV6.

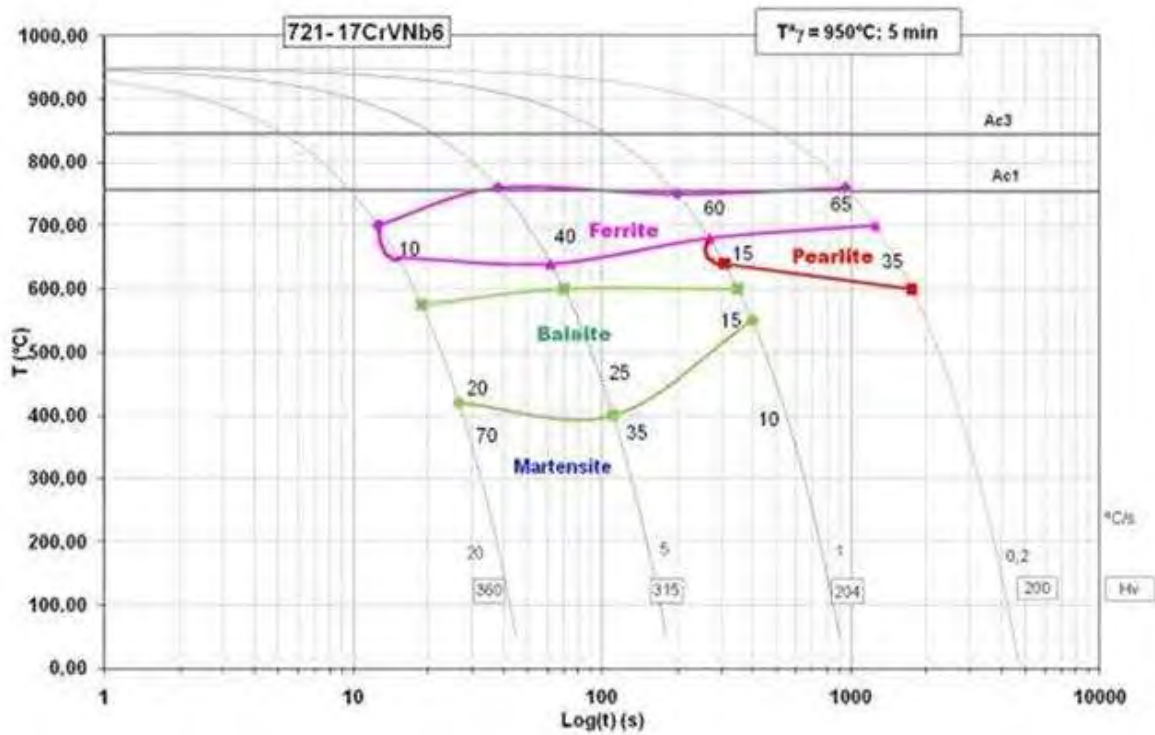


Figure 63: CCT diagram of the experimental heat of 17CrV6.

Cooling rate (°C/s)	Microstructure (%)				Hardness (HV 30)
	ferrite	pearlite	bainite	martensite	
20	10	0	20	70	360
5	40	0	25	35	315
1	60	15	15	10	204
0,2	65	35	0	0	200

Table 26: Results of dilatometry tests of 17CrVNb6.

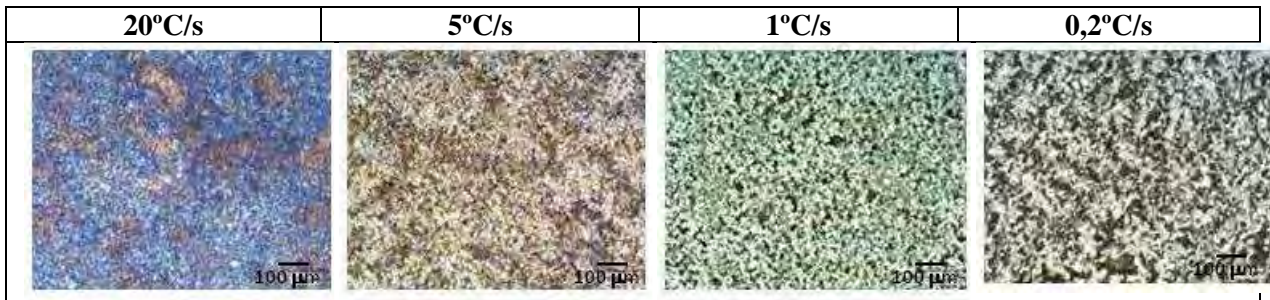


Figure 64: Microstructures obtained at the different cooling rates for the 17CrVNb6.

Thermomechanical cycles by Gleeble

The hot forming test machine “GLEEBLE 3800C” was used in LUNA project with the objective of determining the best thermomechanical route to promote the formation of ultrafine-grained microstructures. To perform these thermomechanical tests, prismatic test samples of 15x20x15mm have been used. In all the tests, two thermocouples have been welded to the specimen to control its temperature. After the test, the hardness and the microstructure have been analysed in the zone of maximum deformation (Figure 66).

Even in this case, since the aims of the project was to produce ultrafine-grained long products in a conventional hot rolling mill, the first simulated thermomechanical cycles have tried to approach industrial conditions.

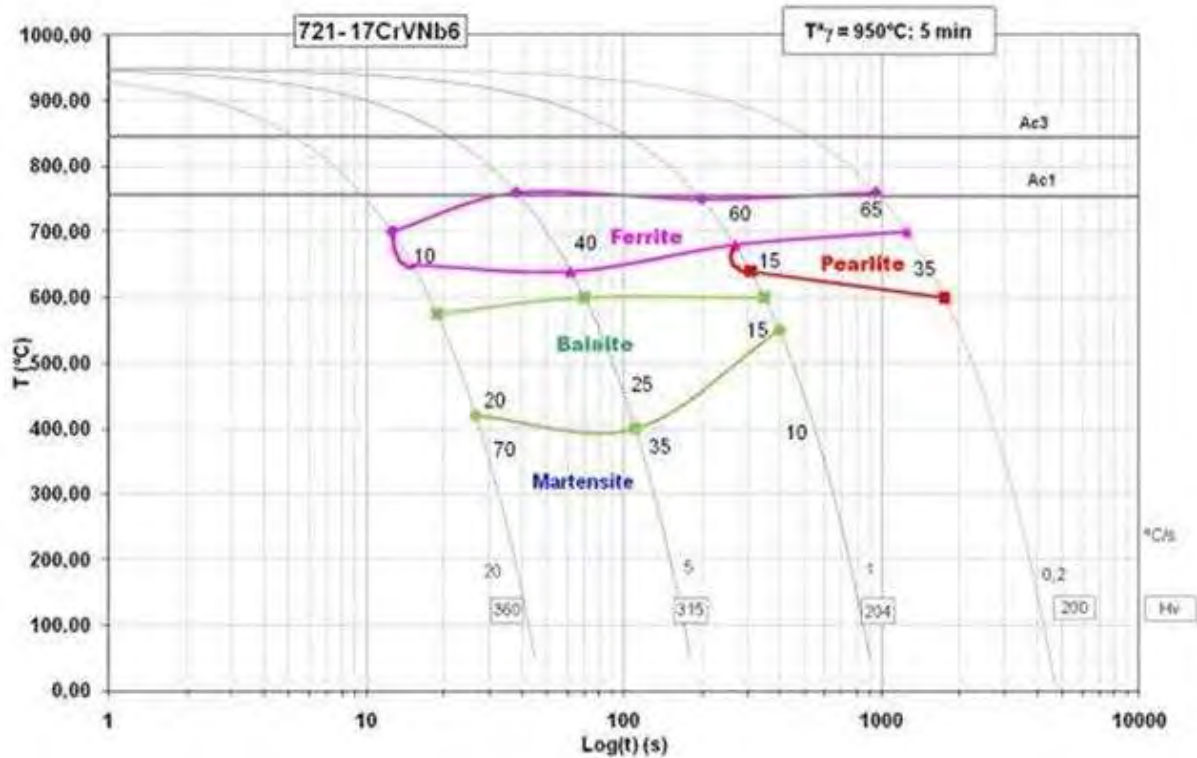


Figure 65: CCT diagram of the experimental heat of 17CrVNb6.

GERDAU has mostly performed the thermomechanical tests with the carburizing steel grades because a lot of problems happened with the thermocouples of the spring steel grade. Firstly, some tests were performed heating the samples at 1200°C during 2 minutes in order to know the prior austenite grain size. This austenite grain size has been revealed with the application of a thermal cycle: this methodology is based on the heating of the samples after being carefully polished until austenization temperature in an inert atmosphere. Afterwards, the sample is cooled down until room temperature and immediately the grain boundaries are observed (Figure 67).

In all the cases the austenite grain size is between 40 and 105 μm.

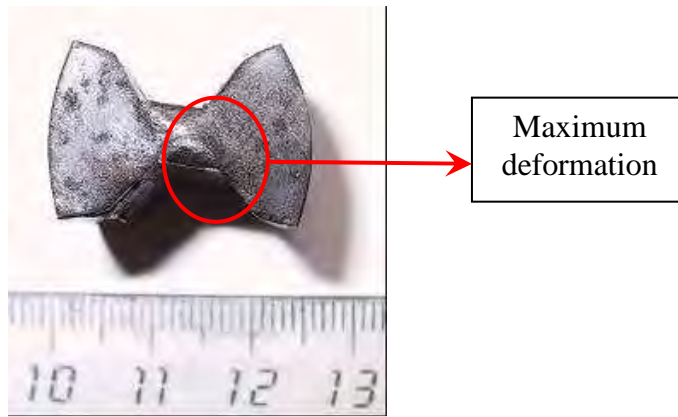


Figure 66: Geometry of the sample after the compression test.

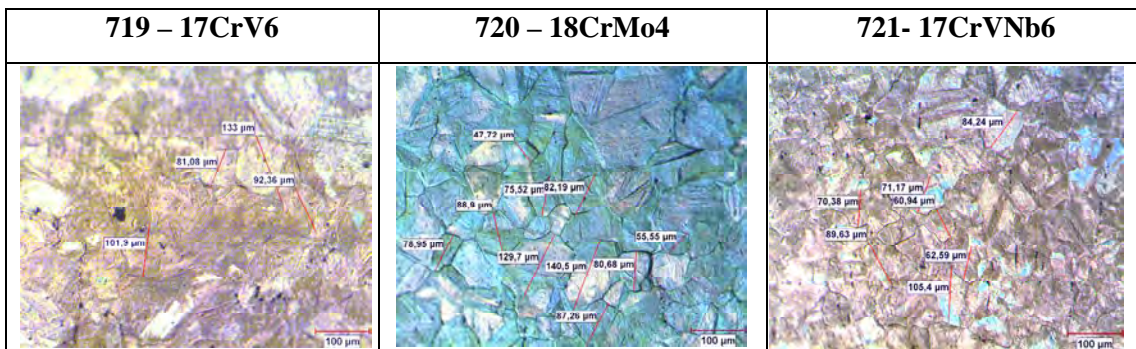


Figure 67: Prior austenite grain size after soaking during 2 minutes at 1200°C.

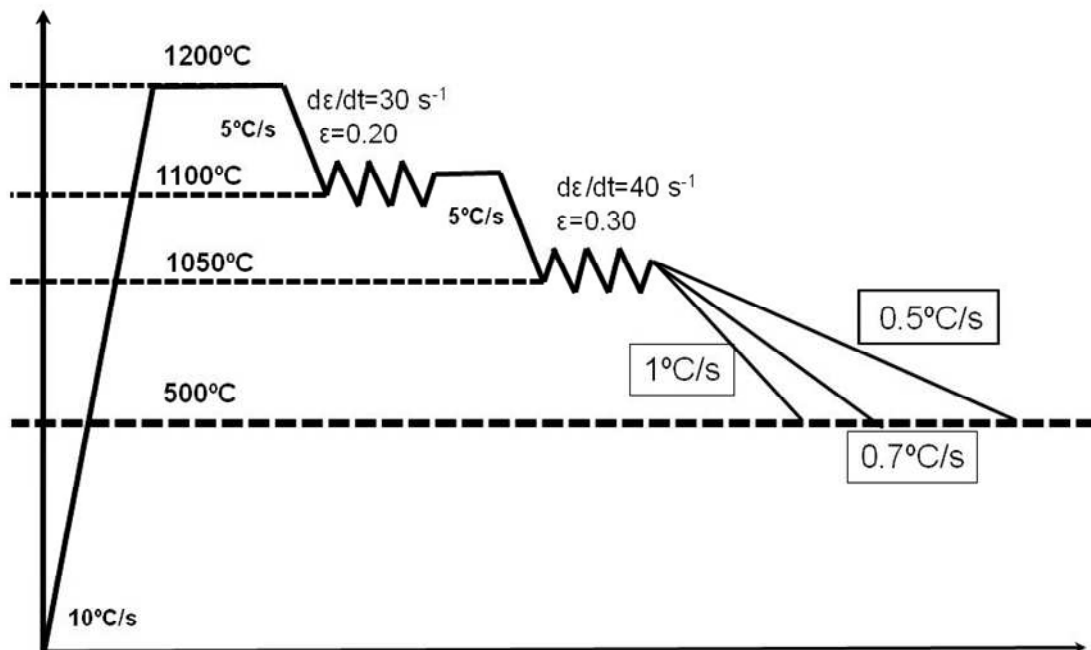


Figure 68: First thermomechanical cycle performed in the GLEEBLE machine.

The results obtained after the first thermomechanical cycle of Figure 68 are shown in Table 27 and Figure 69. The ferrite grain size values are in the range 20-30 μm and hard phases (bainite and martensite) are always found. Afterwards, in order to try to obtain a smaller grain size and a higher percentage of ferrite and pearlite, in the 2nd thermomechanical cycle the temperature of the second deformation was decreased as well as the final cooling rate (Figure 70).

Experimental heat	Cooling rate (°C/s)	Ferrite grain size (µm)	Hardness (HV)	Microstructure
719 (17CrV6)	0.5	20	232	Ferrite + pearlite + bainite + martensite
	0.7	20	260	Ferrite + pearlite + bainite + martensite
	1	20	284	Ferrite + bainite
720 (18CrMo4)	0.5	20 - 30	236	Ferrite + bainite + martensite
	0.7	20	238	Ferrite + bainite + martensite
	1	20	252	Ferrite + bainite + martensite
721 (17CrVNB6)	0.5	20	295	Ferrite + bainite + martensite
	0.7	20 - 30	301	Ferrite + bainite + martensite
	1	20 - 30	303	Ferrite + bainite + martensite

Table 27: Results obtained after the 1st thermomechanical cycle.


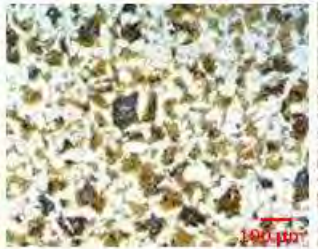

	719 – 17CrV6	720 – 18CrMo4	721 – 17CrVNB8
Ferrite grain size (ASTM)	7 - 8	6 - 7	7 - 8
Hardness (HV)	215	250	255
			

Figure 69: Microstructures obtained of the first thermomechanical cycle.

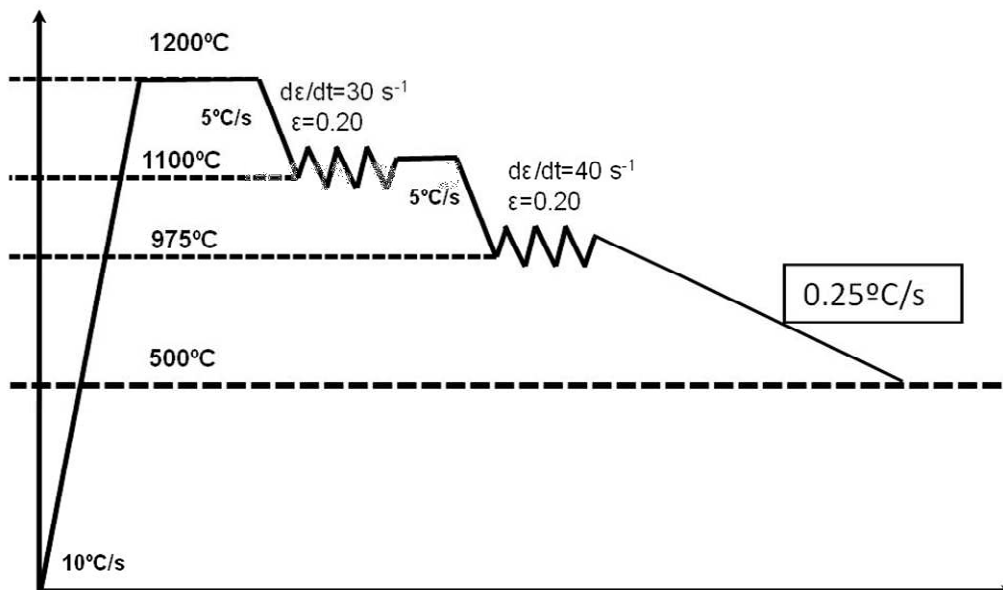


Figure 70: Second thermomechanical cycle performed in the GLEEBLE machine.

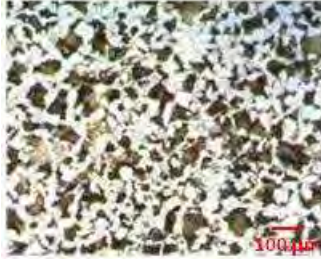


	719 – 17CrV6	720 – 18CrMo4	721 – 17CrVNB6
Ferrite grain size (μm)	20 - 30	28 - 40	20 - 30
Hardness (HV)	215	250	255
			

Figure 71: Microstructures obtained after the second thermomechanical cycle.

The microstructure obtained for the three experimental heats has been a mix of ferrite, pearlite, bainite and martensite in all the experimental heats (Figure 71) and not very significant differences have been found.

From a theoretical point of view there are two different possibilities to obtain a fine grain size. On one hand, it is possible to get a very fine grain size if the transformation starts with an austenite recrystallized grain, not higher than 20 μm .

In this case, in order to perform hot rolling with control of recrystallization, it is necessary to finish the rolling process at a temperature higher than the non-recrystallization temperature T_{nr} (cycle of Figure 72). The other possibility is to finish the rolling process at a temperature lower than the non-recrystallization temperature). In this way it should be possible to obtain an austenite grain size with a high grade of deformation and obtain a very fine ferrite grain size after cooling (Figure 73).

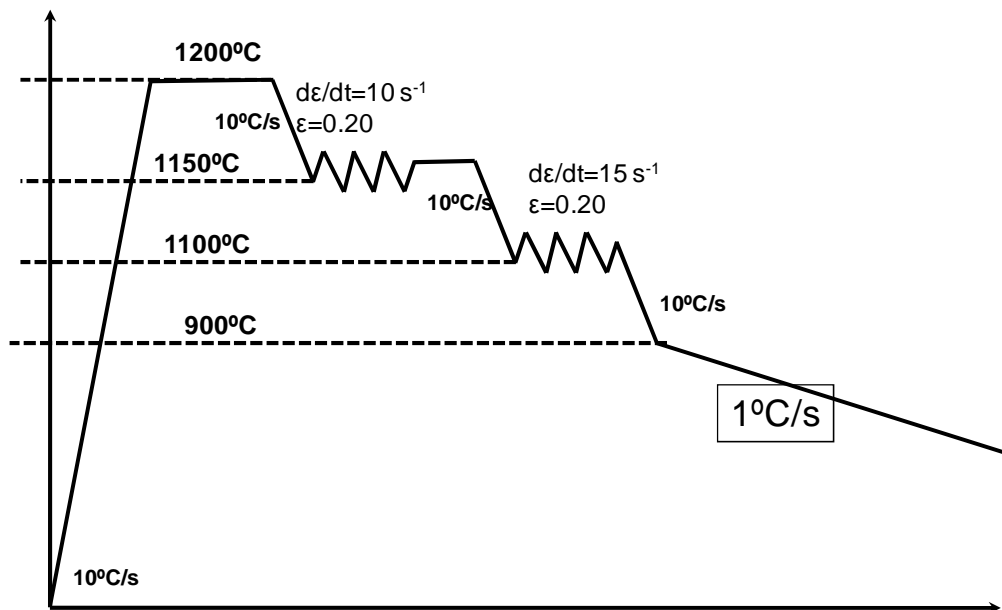


Figure 72: Third thermomechanical cycle performed in the GLEEBLE machine.

The results obtained following the cycles of the Figures 72 and 73 are shown in Table 28, and Figures 74 and 75, where it can be observed that the best grain size has been got with the thermomechanical cycle number IV (final deformation at low temperature) and with the experimental heat 721 with the Nb addition.

In particular results show that:

- No significant change in the ferritic grain size has been observed changing the temperature of the second deformation and the cooling rate in thermomechanical cycles I and II;

- The thermomechanical cycles III and IV to obtain finer grain size show a microstructure of ferritic grain 8-9 ASTM (14 – 20 μm), instead of the 7-8 ASTM (20 – 30 μm), obtained in the first cycles:
- For the experimental heat of 17CrVNB6 a ferritic grain size 9-10 ASTM (10-15 μm), has been observed, which shows the good influence of the Nb in the control of the final grain size.

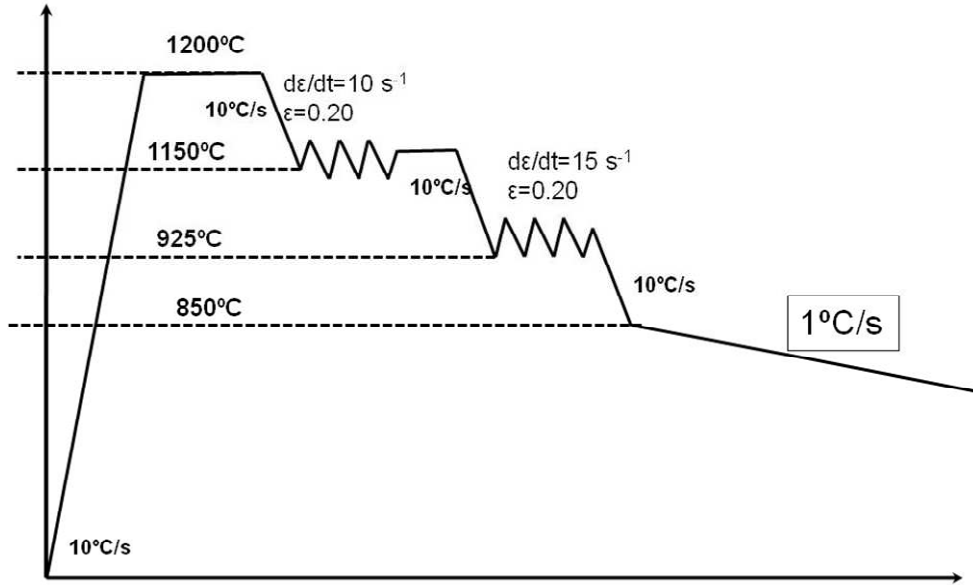


Figure 73: Fourth thermomechanical cycle performed in the GLEEBLE machine.

Heat	Final deformation (°C)	Ferrite grain size (μm)	Hardness (HV)	Microstructure
719 (17CrV6)	1100	20	274	Ferrite + bainite + a bit of martensite
	925	14-20	276	Ferrite + pearlite + bainite + martensite
720 (18CrMo4)	1100	20	241	Ferrite + bainite + a bit of martensite
	925	14-20	238	Ferrite + bainite + martensite
721 (17CrVNB6)	1100	20	298	Ferrite + bainite + martensite
	925	10-15	298	Ferrite + bainite + martensite
36624 (17CrV6)	1100	20	291	Ferrite + bainite + martensite
	925	14-20	295	Ferrite + bainite + martensite
50654 (18CrMo4)	1100	20	252	Ferrite + bainite + martensite
	925	14-20	249	Ferrite + bainite + martensite

Table 28: Results obtained for the different samples after the thermomechanical cycles III and IV.

The non recrystallization temperature has been calculated in order to know the most suitable temperature for the last deformation of the thermomechanical cycle. To get this aim, the Jonas' relationship has been used:

$$T_{nr} = 887 + 464x(\%C) + (6445x(\%Nb) - 644x\sqrt{\%Nb}) + (732x(\%V) - 230x\sqrt{\%V}) + 890x(\%Ti) + 363x(\%Al) - 357x(\%Si).$$

So, according this relationship, the values of T_{nr} obtained for the different industrial and experimental heats are the following:

18CrMo4(50654): 845°C
 17CrV6 (36624): 857°C
 17CrV6 (719): 858°C
 18CrMo4 (720): 864°C
 17CrVNb6 (721): 916°C
 50SiMoVNb8: 529°C

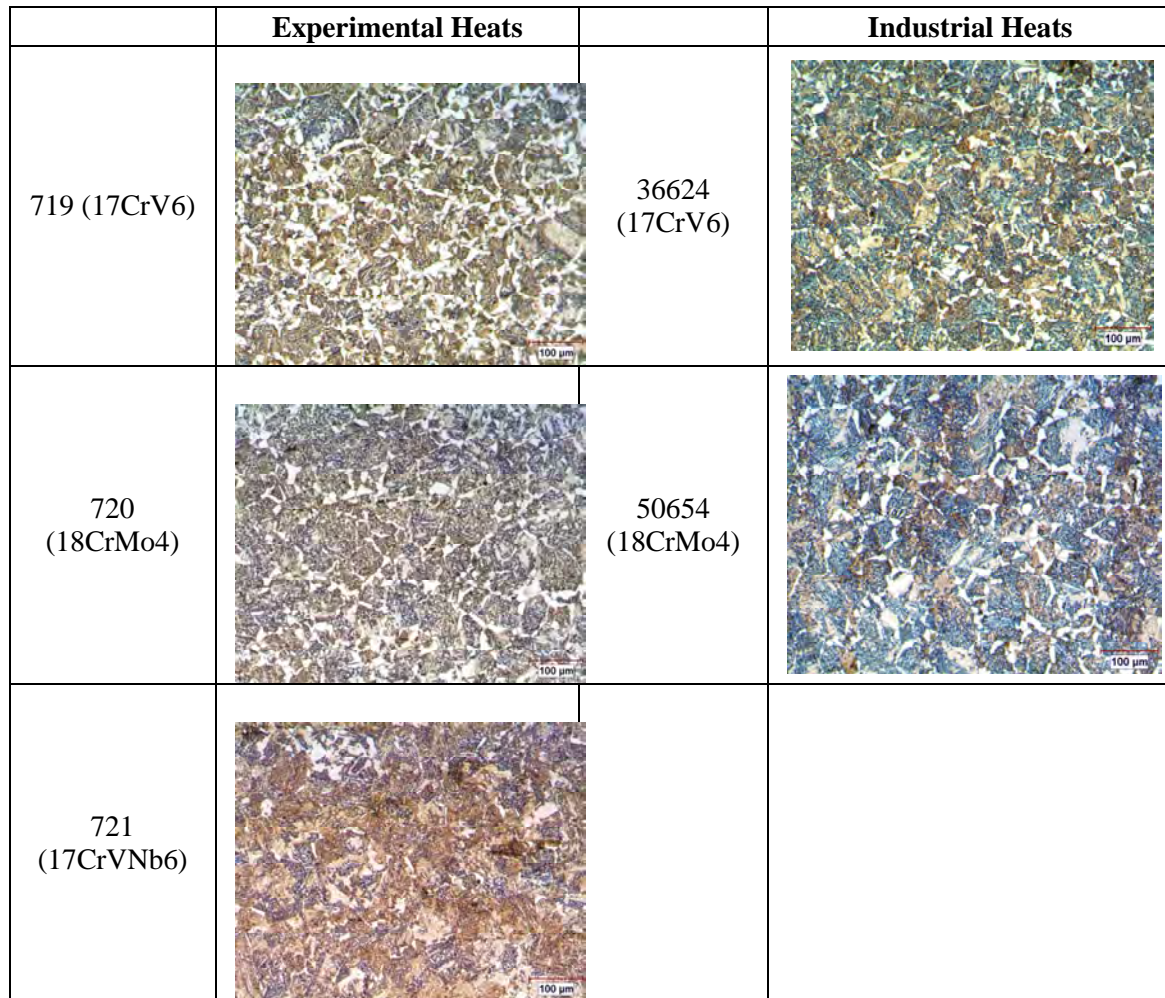


Figure 74. Microstructures obtained for the thermomechanical cycle number III.

Heat	Ferrite grain size (µm)	Hardness (HV)	Microstructure
720 (18CrMo4)	9 – 25	274	Ferrite + bainite + martensite
721 (17CrVNb6)	10 – 25	308	Ferrite + bainite + martensite
36624 (17CrV6)	5 – 20	303	Ferrite + bainite + martensite and a bit of pearlite
50654 (18CrMo4)	7 – 23	248	Ferrite + bainite + a bit of martensite
48988 (50SiMoVNb8)	8 - 14	484	Martensite + bainite + a bit of ferrite

Table 29: Results obtained for the different samples after the thermomechanical cycle VII.

The 7th thermomechanical cycle has been designed taking into account the non recrystallization temperature of all the experimental and industrial heats, except the 50SiMoVNb8. In this way, the last deformation has been tried to be performed at 850°C, temperature lower than the non recrystallization temperature. This cycle is shown in Figure 76.

Results and microstructures are reported in Table 29 and Figure 77.

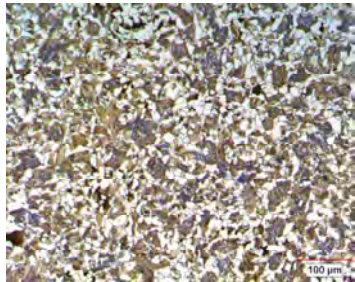
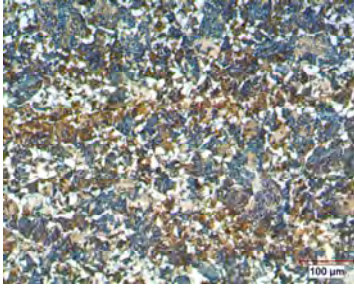
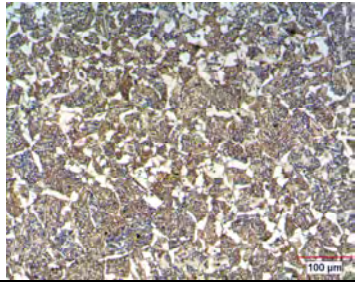
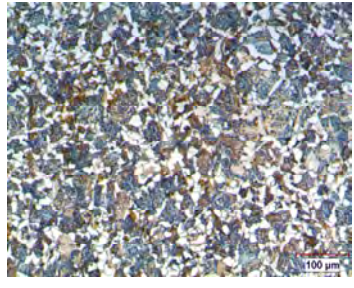
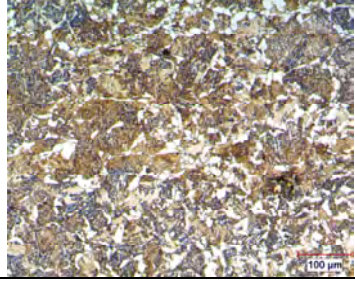
	Experimental Heats		Industrial Heats
719 (17CrV6)		36624 (17CrV6)	
720 (18CrMo4)		50654 (18CrMo4)	
721 (17CrVNb6)			

Figure 75. Microstructures obtained for the thermomechanical cycle number IV.

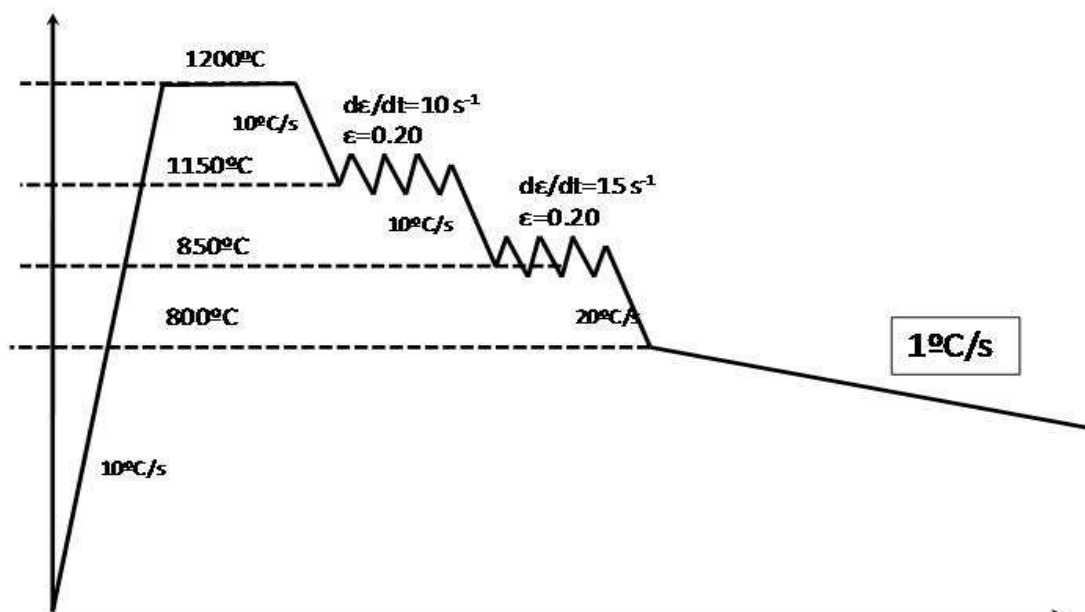


Figure 76: 7th thermomechanical cycle performed in GLEEBLE machine.

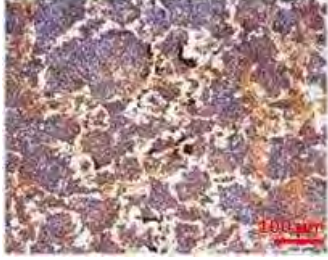
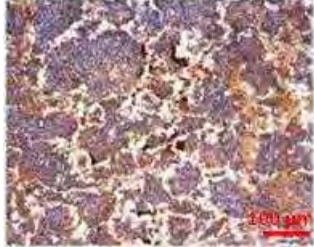
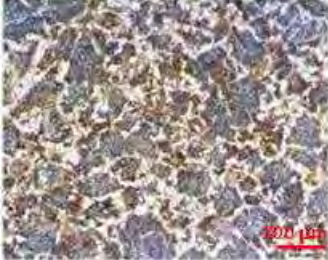
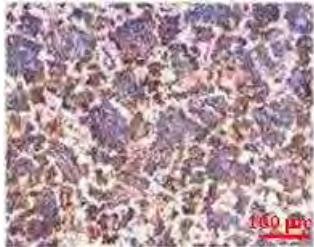
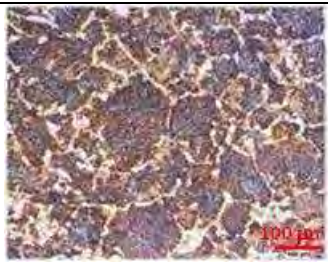

	Experimental Heats		Industrial Heats
719 (17CrV6)		36624 (17CrV6)	
720 (18CrMo4)		50654 (18CrMo4)	
721 (17CrVNB6)		48988 (50SiMoVNB8)	

Figure 77: Microstructures obtained for the thermomechanical cycle number VII.

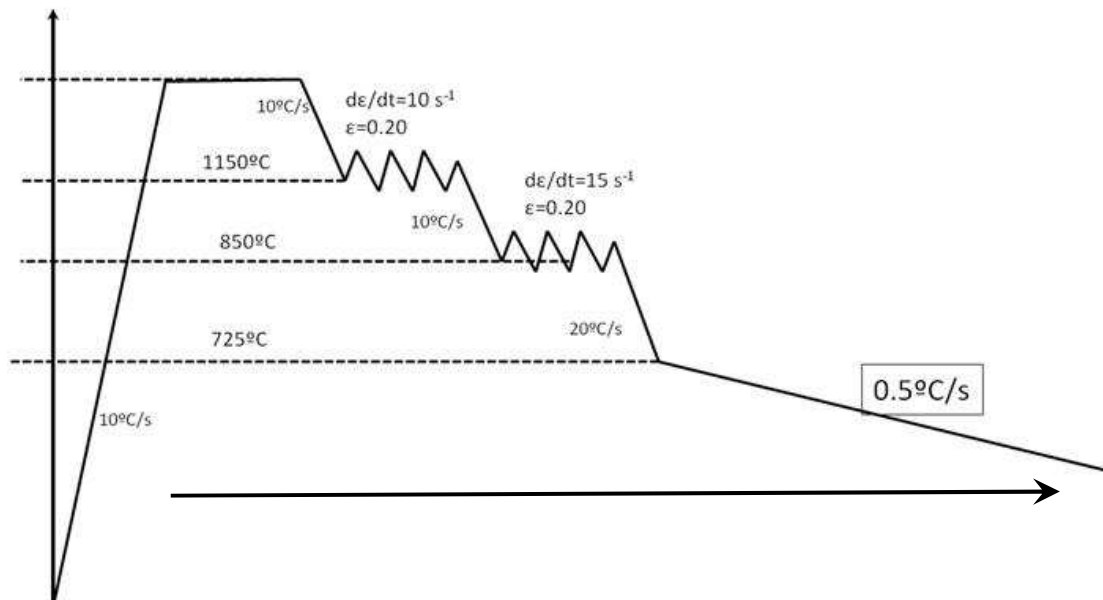


Figure 78: The 8th thermomechanical cycle.

After all these results, new thermomechanical tests have been planned to be carried out. Firstly, it has been thought that after the last deformation at 850°C the temperature will be decreased until 700°-750°C at high rate; afterwards, it will be decreased slower about 0.2°C/s in order to try to obtain more nucleation points for the ferrite transformation and in this way, to obtain a finer grain size (Figure 78). This cycle was only carried out with the industrial heats, obtaining the following ferrite grain sizes, values of hardness and microstructures (Figure 79).

As no important improvement has been obtained with this thermomechanical cycle, it has not been carried out with the experimental heats.

Afterwards, it was tried to decrease the temperature of the second deformation at 800°C, in order to try to perform the 2nd deformation at a temperature lower than the recrystallization stop temperature. The 9th thermomechanical cycle is shown in the Figure 80.

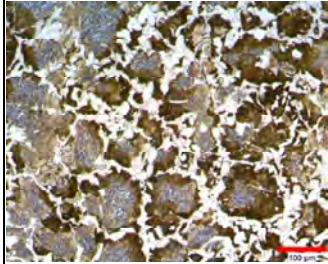
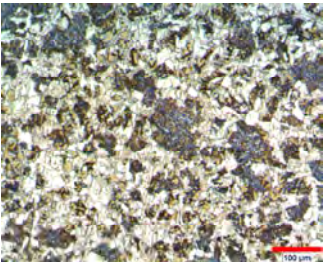
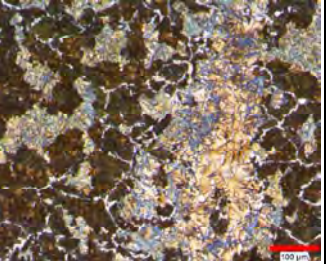
	36624 (17CrV6)	50654 (18CrMo4)	48988 (50SiMoVNb8)
Ferrite grain size (µm)	12 - 25	7 - 20	-
Hardness (HV)	255	229	424
			
	Ferrite + bainite + pearlite + a bit of martensite	Bainite + ferrite + martensite	Pearlite + martensite + bainite

Figure 79: Microstructures of grain size, hardness and microstructure obtained with the 8th thermomechanical cycle.

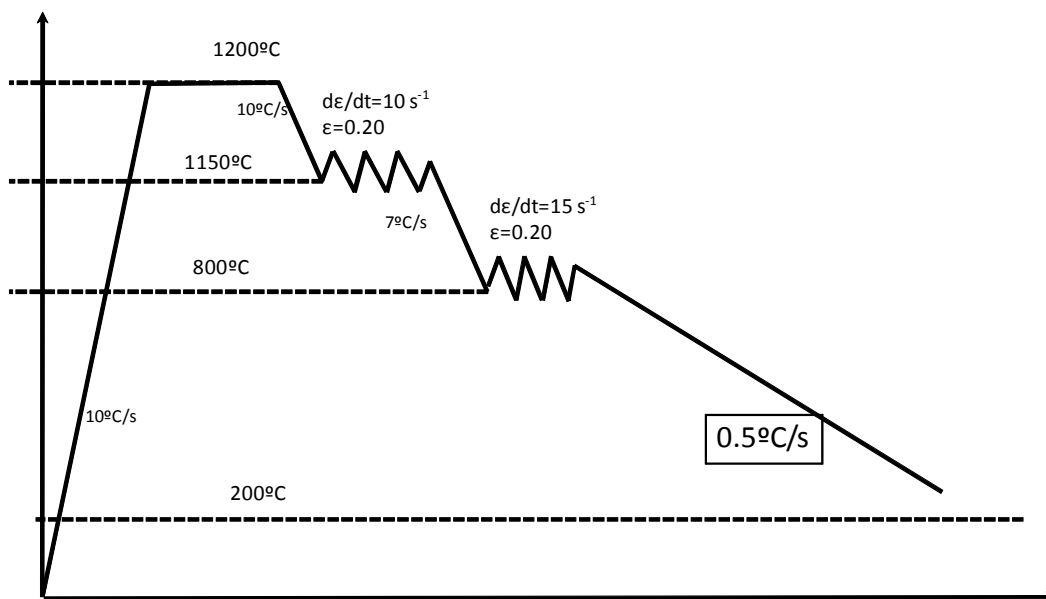


Figure 80: The 9th thermomechanical cycle.

This cycle has been carried out with the industrial heats and two of the experimental heats. For the heat 48988, the cooling rate has been 0.25°C/s in order to obtain a higher percentage of ferrite and pearlite, due to its higher hardenability. The obtained microstructures are shown in Figure 81 and Table 30.

Afterwards, it was tried to perform the second deformation at 800°C but decreasing the temperature from the first to the second deformation at higher rate ($\approx 20^\circ\text{C/s}$); however, it has not been possible to decrease the temperature at this rate, therefore the second deformation has been carried out at 900°C (Figure 82). Results are shown in Figure 83 and Table 31.

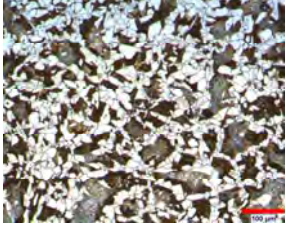
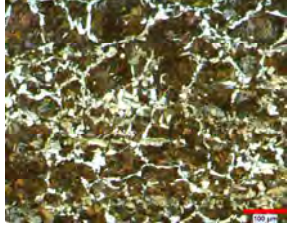
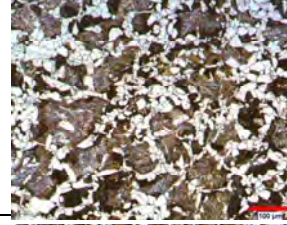

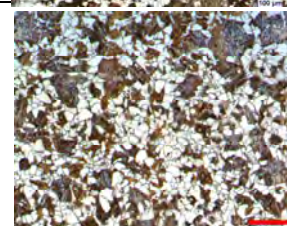
	Experimental Heats		Industrial Heats
719 (17CrV6)		36624 (17CrV6)	
		50654 (18CrMo4)	
721 (17CrVNB6)		48988 (50SiMoVNB8)	

Figure 81: Microstructure obtained after the 9th thermomechanical cycle.

Heat	Ferrite grain size (μm)	Hardness (HV)	Microstructure
719 (17CrV6)	13 - 19	238	Ferrite + pearlite + bainite + martensite
721 (17CrVNB6)	9 - 30	285	Ferrite + pearlite + bainite + martensite
36624 (17CrV6)	5 - 20	350	70% pearlite + 30% ferrite
50654 (18CrMo4)	8 - 20	225	Ferrite + bainite + martensite
48988 (50SiMoVNB8)	7 - 25	275	Ferrite + pearlite + bainite + martensite

Table 30: Results of grain size, hardness and microstructure obtained with the 9th thermomechanical cycle.

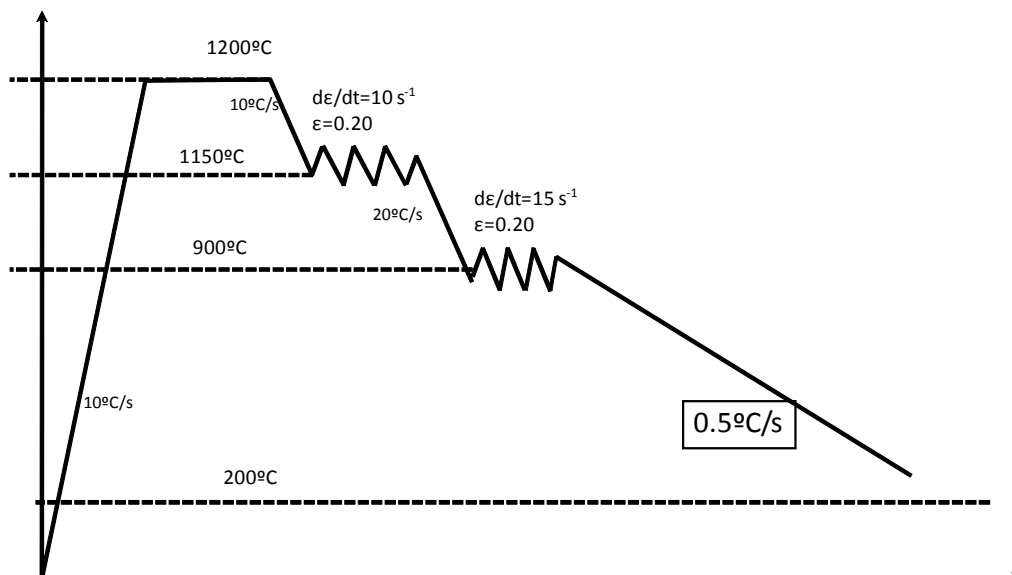


Figure 82: The 10th thermomechanical cycle.


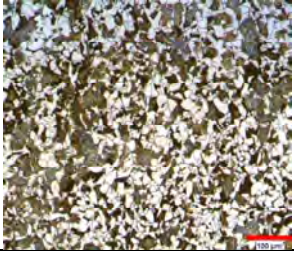
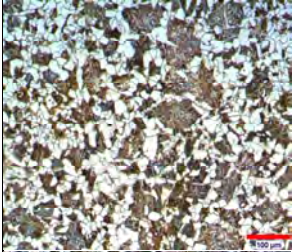
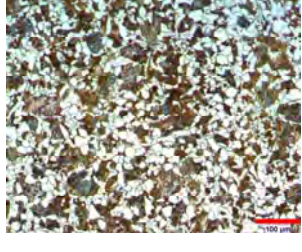

	Experimental Heats		Industrial Heats
719 (17CrV6)		36624 (17CrV6)	
		50654 (18CrMo4)	
721 (17CrVNb6)		48988 (50SiMoVNb8)	

Figure 83: Microstructures obtained after the 10th thermomechanical cycle.

Heat	Ferrite grain size (µm)	Hardness (HV)	Microstructure
719 (17CrV6)	7 – 14	256	Ferrite + bainite + pearlite + martensite
720 (18CrMo4)	7 – 25	216	Ferrite + bainite + martensite
721 (17CrVNb6)	7 – 20	293	Bainite + ferrite + pearlite + martensite
36624 (17CrV6)	8 – 22	244	Ferrite + bainite + pearlite + martensite
50654 (18CrMo4)	6 - 20	230	Ferrite + bainite + pearlite + martensite

Table 31: Results of grain size, hardness and microstructure obtained with the 10th thermomechanical cycle.

In the 11th thermomechanical cycle (Figure 84), the temperature has been decreased as fast as possible from 1150° to 700°C obtaining the results shown in Figure 85 and Table 32.

Although almost all the grains are finer than 12 µm, there are some coarse grains which can reach the 20 µm; therefore, it has been tried to know the relationship of the ferrite grain size after the last thermomechanical cycle.

If the different figures are observed (Figures 86÷90), the best heat where the highest percentage of fine grain size has been observed is the heat 50654 (18MoCr4). For this heat almost the 50% the ferrite grains are finer than 8 µm.

On the other hand, the maximum forces obtained at the different temperatures of the last deformation have been measured; the results are shown in Table 33.

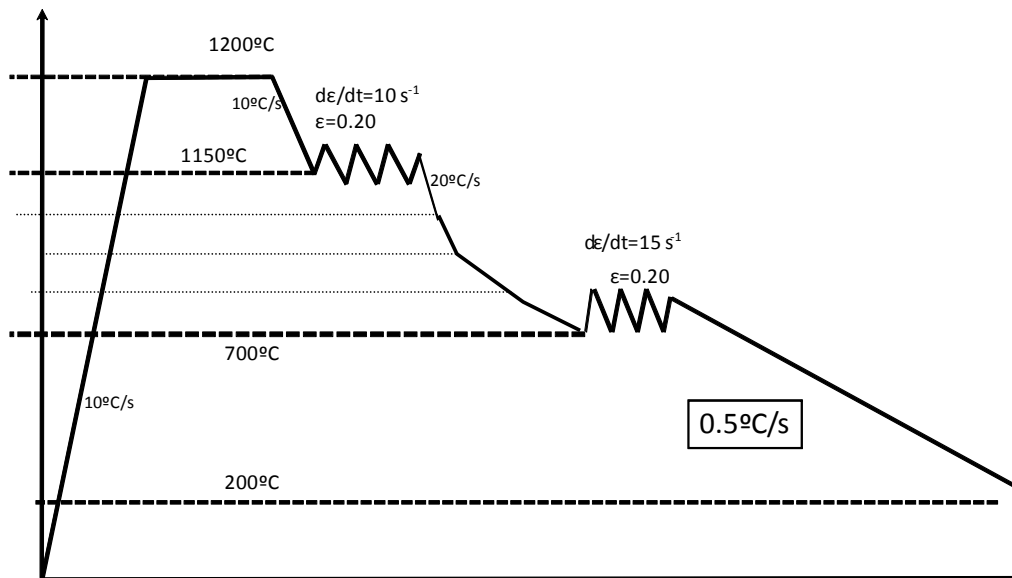


Figure 84: The 11th thermomechanical cycle.

Heat	Ferrite grain size (μm)	Hardness (HV)	Microstructure
719 (17CrV6)	4 – 28	237	Ferrite + pearlite + some of martensite and bainite
721 (17CrVNb6)	4 – 25	300	Bainite + ferrite + some of martensite and pearlite
721 $def=0.4$ (17CrVNb6)	4 – 25	284	Ferrite + pearlite + bainite + martensite
36624 (17CrV6)	4 – 20	265	Ferrite + bainite + a bit of pearlite and martensite
50654 (18CrMo4)	5 – 18	236	Ferrite + bainite + martensite and a bit of pearlite
48988 (50SiMoVNb8)		381	100% martensite and bainite

Table 32: Results of grain size, hardness and microstructure obtained with the 11th thermomechanical cycle.

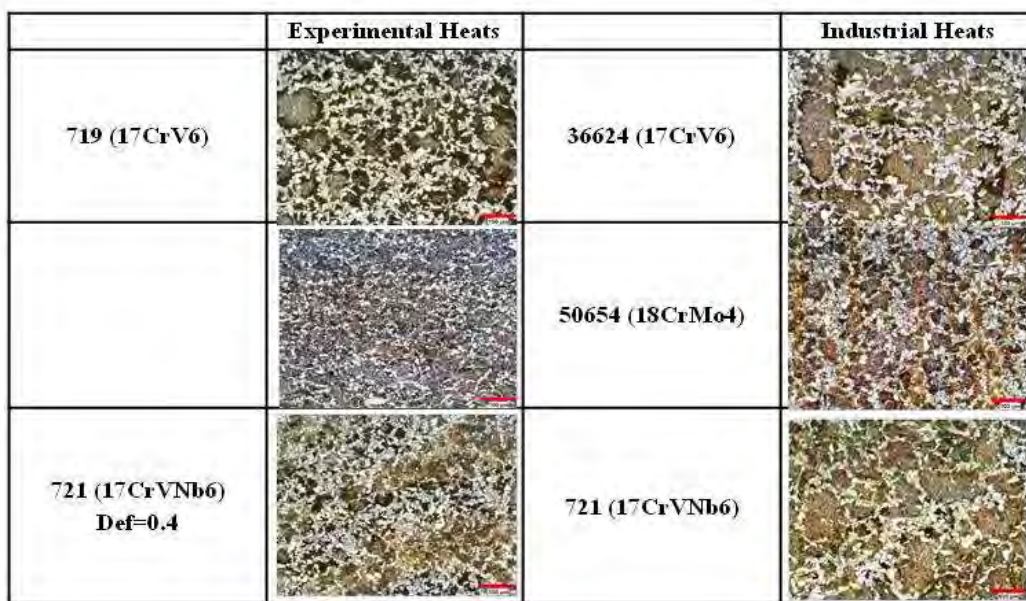


Figure 85: Microstructures obtained after the 11th thermomechanical cycle.

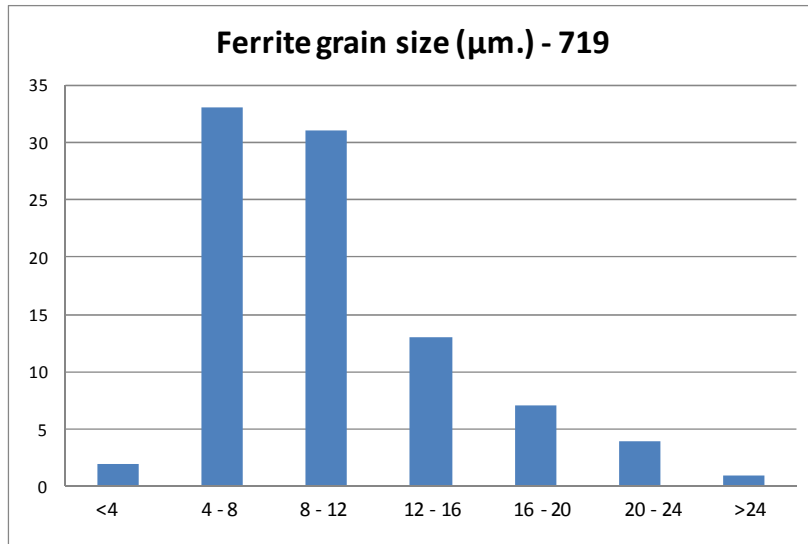


Figure 86: Percentage of ferrite grain sizes for heat 719 (17CrV6) after the 11th thermomechanical cycle.

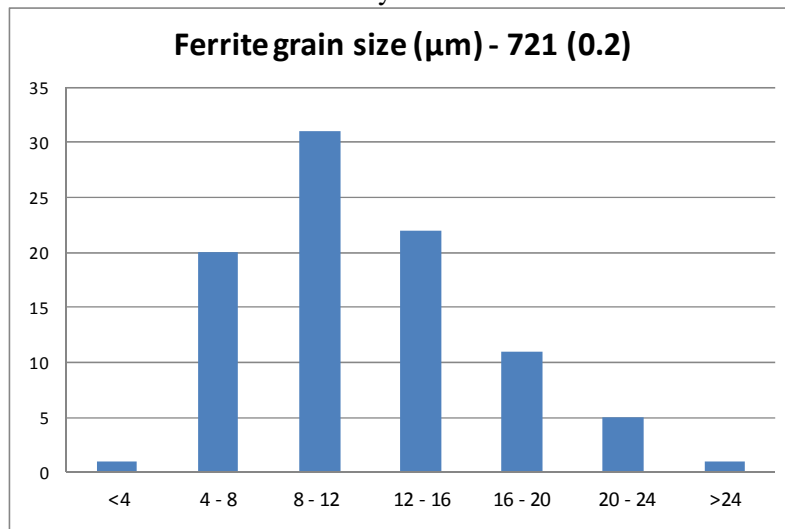


Figure 87: Percentage of ferrite grain sizes for heat 721 (17CrVNb6) after the 11th thermomechanical cycle and a deformation grade of 0.2.

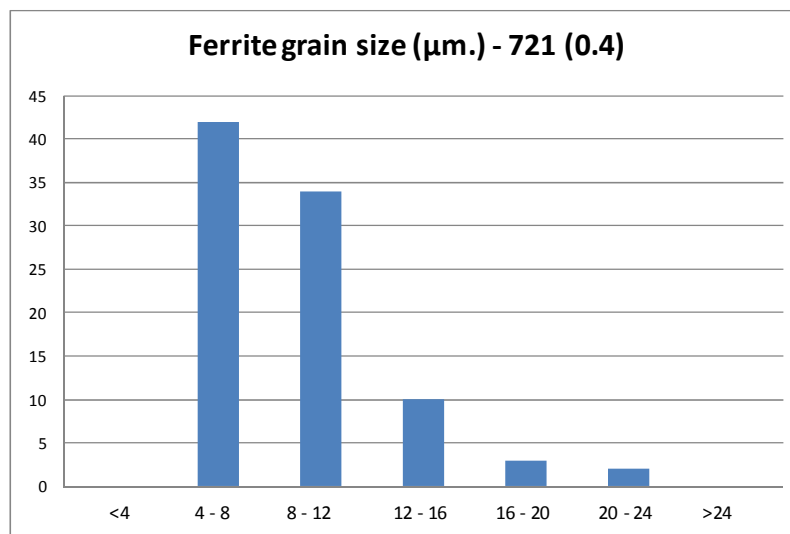


Figure 88: Percentage of ferrite grain sizes for heat 721 (17CrVNb6) after the 11th thermomechanical cycle and a deformation grade of 0.4.

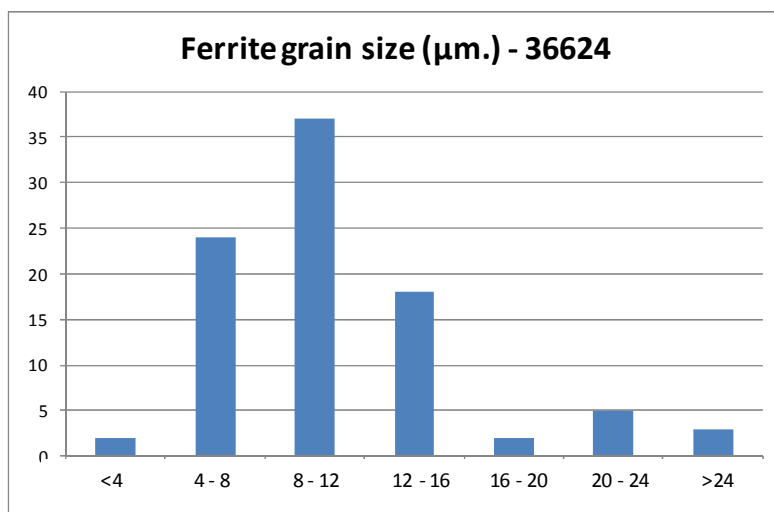


Figure 89: Percentage of ferrite grain sizes for heat 36624 (17CrV6) after the 11th thermomechanical cycle.

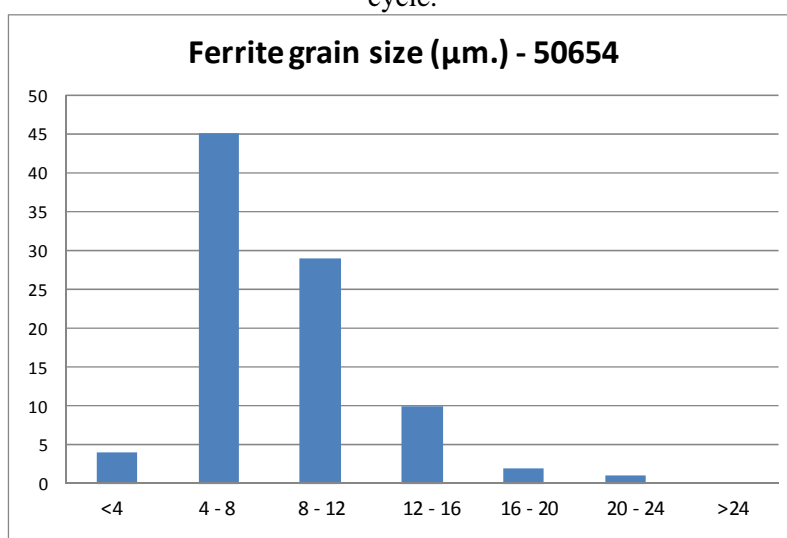


Figure 90: Percentage of ferrite grain sizes for heat 50654 (18CrMo4) after the 11th thermomechanical cycle.

The different values of forces increased when the temperature is decreased, as it was expected. Otherwise, all the heats show similar values of force except the heat 48988, which has a higher tensile strength than the other ones.

Another study carried out has been the analysis of the austenite grain sizes in the different steps of the thermomechanical cycles. Firstly, the austenite grain size after the heating at 1200°C for 5 minutes has been measured by chemical analysis; the results are shown in the Figure 91.

Cycle	Last deformation T (°C)	Forces (Kgf) for each heat					
		17CrV6 719	18CrM04 720	17CrVNb 721	17CrV6 36624	50SiMoVNb8 48988	18CrM04 50654
III	1100	2133	2125	2078	2142		1850
I	1050	2704	2850	2782			
II	975	3000	3117	2994			
V	900	3064	3375	3047	3368	3171	3166
VII	850		3609	3904	3642	3715	3342
VIII	800	3922		4112	4208	5100	4026
IX	700	4715	5690	4739	4761	7583	4648
X	700 (0.4)			5384			

Table 33: Maximum forces obtained at the different temperatures of the last deformation.

The austenite grain size has been quite coarse in all the cases:

- between 87 and 154 μm . for heat 719
- between 87 and 154 μm . for heat 721
- between 134 and 203 μm . for 36624
- between 72 and 130 μm . for 50654

Afterwards, the measurement of the austenite grain size after heating at 1200°C and the first deformation at 1150°C was carried out in order to analyse the evolution of the austenite grain size. The results are shown in Figure 92.

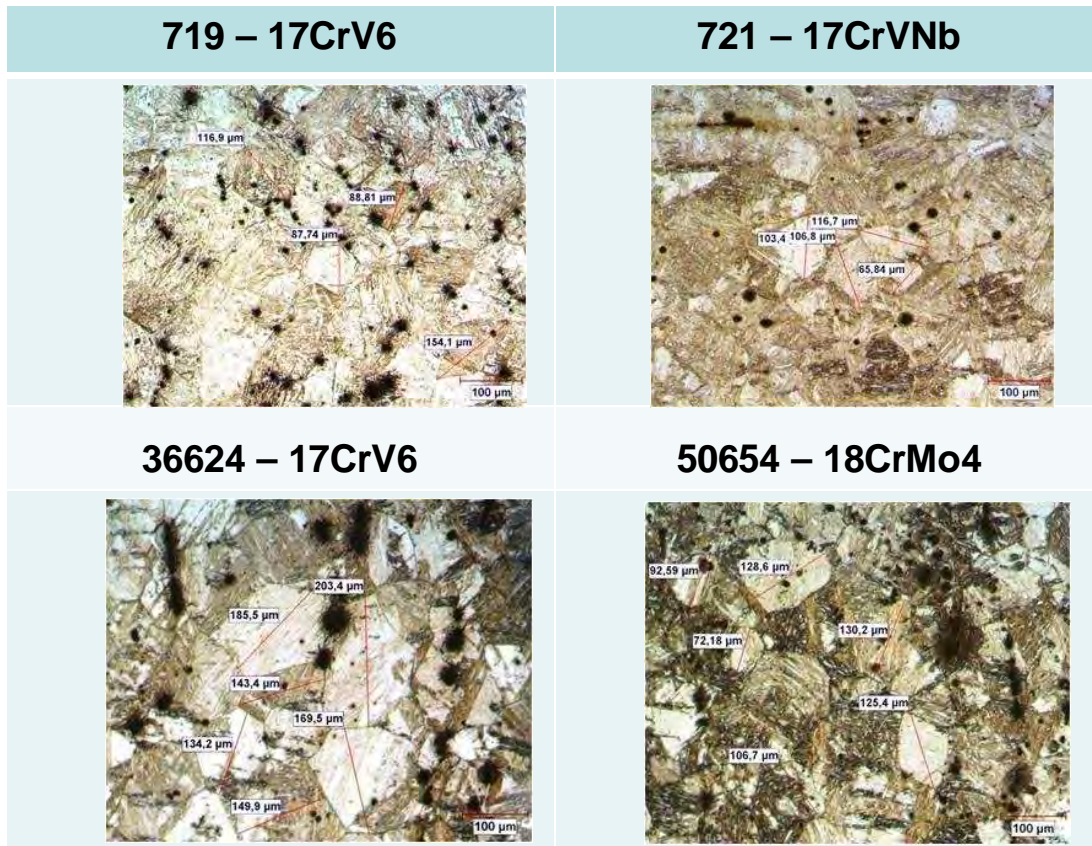


Figure 91: Austenite grain size obtained by chemical analysis after heating at 1200°C for 5 minutes.

Finally the austenite grain size after the two deformations at 1150° and 800°C have been measured and the results are shown in Figure 93.

A summary of the different austenite grain sizes obtained for the experimental and industrial heats is shown in Table 34.

A comparison of the best results obtained in the different thermomechanical tests after an austenization temperature of 1200°C has been carried out; this summary is shown in Table 35.

In general, it can be assumed that the 50SiMoVNb8 is the steel grade where the finest values of grain size of ferrite are obtained; however the percentage of ferrite obtained in this steel grade has been very small and its influence on the general mechanical properties, almost insignificant. On the other hand, the experimental heat 721, 17CrVNb6, despite being one of the most promising steel grade because of Nb addition, has not been able to show grain sizes finer than 10 – 15 μm .

Finally, a new thermomechanical cycle with an austenization temperature of 1000°C has been carried out, which is shown in Figure 94 and the resulting microstructure are reported in Figure 95.

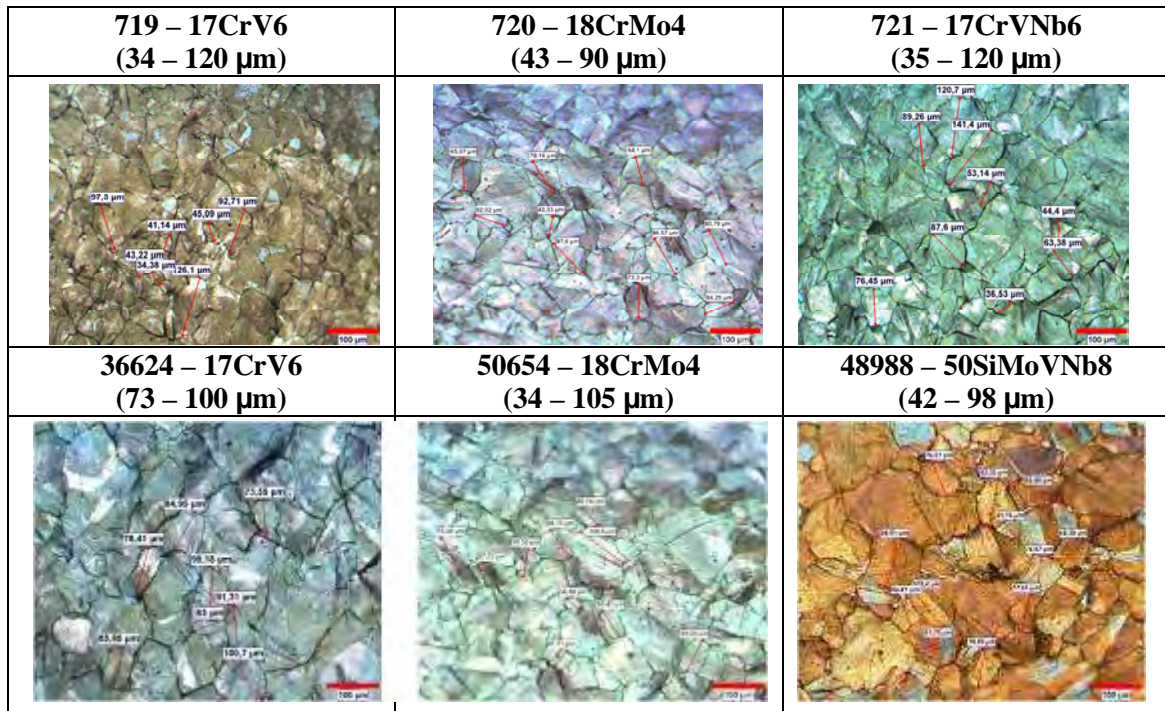


Figure 92: Austenite grain size obtained by thermal etching in Gleeble machine after heating at 1200°C for 5 minutes and the first deformation at 1150°C.

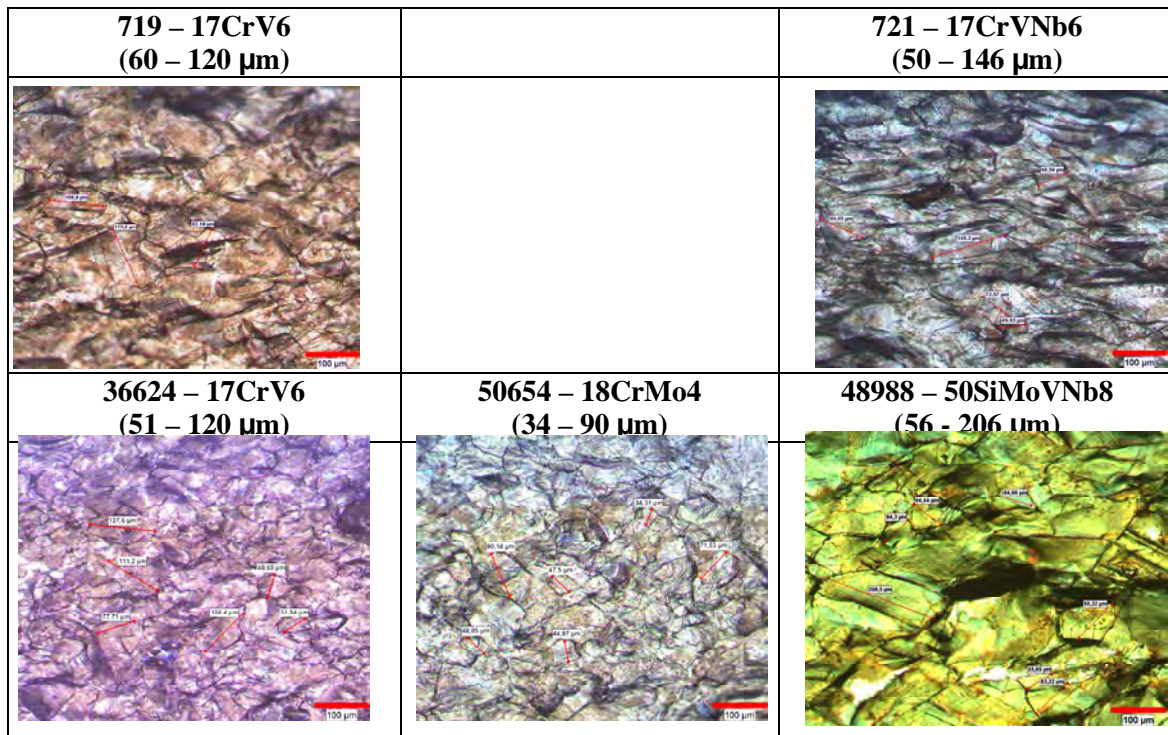


Figure 93: Austenite grain size obtained by thermal etching in Gleeble machine after heating at 1200°C and the two deformation at 1150°C and 800°C.

Heat	Heating at 1200°C (µm)	After 1 st deformation at 1150°C (µm)	After 2 nd deformation at 800°C (µm)	Final ferrite grain size (µm)
719	80 - 150	34 - 120	60 - 120	13 - 19
721	65 - 120	35 - 120	50 - 146	9 - 30
36624	130 - 200	73 - 100	51 - 120	5 - 20
48988		42 - 98	56 - 206	7 - 25
50654	72 - 130	34 - 105	34 - 90	8 - 20

Table 34: Summary of results for the different experimental and industrial heats after the last thermomechanical cycle.

Steel grade	Temperature of the last deformation (°C)	Cooling rate (°C/s)	Grain size (µm)
17CrVNB6	1050	0,5	13 – 23
17CrV6 and 17CrVNB6	975	0,25	20 – 30
18CrMo4	1100	1	13 – 23
17CrVNB6	925	1	10 – 15
17CrV6	900 (two deformations)	1	7 – 23
50SiMoVNB8			9 - 16
17CrV6	900 (three deformations)	1	9 - 20
17CrV6	850	1	5 - 20
50SiMoVNB8			8 - 14

Table 35: Summary of the best results obtained in the different thermomechanical tests with an austenization temperature of 1200°C.

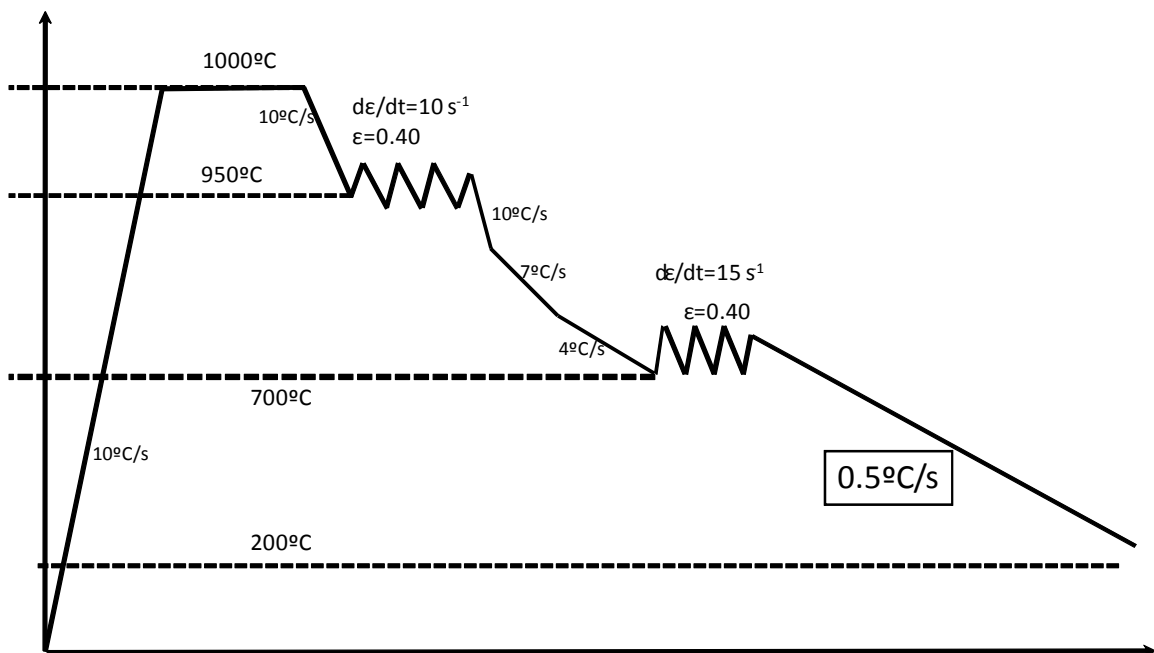


Figure 94: The 12th thermomechanical cycle.

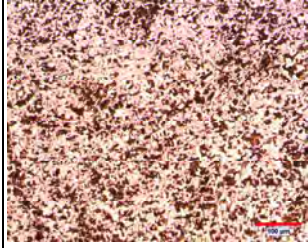
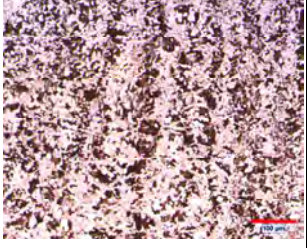
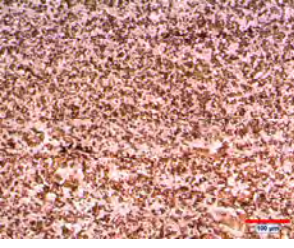
	36624 (17CrV6)	50654 (18CrMo4)	719 (17CrV6)
Hardness (HV)	212 - 215	195	214 - 215
			
	Ferrite + pearlite	Ferrite + pearlite with some traces of bainite	Ferrite + pearlite

Figure 95: Microstructures obtained after the 12th thermomechanical cycle.

As it is shown in Figure 96, the ferrite grain size is, in general, much finer than in the previous thermomechanical cycles. In this case, the most of ferrite grains (>50%) are finer than 4 μm. (Figures 97÷99) and in the previous tests (Figures 86÷90), the most of the ferrite grains (>50%) are between 4 and 12 μm.

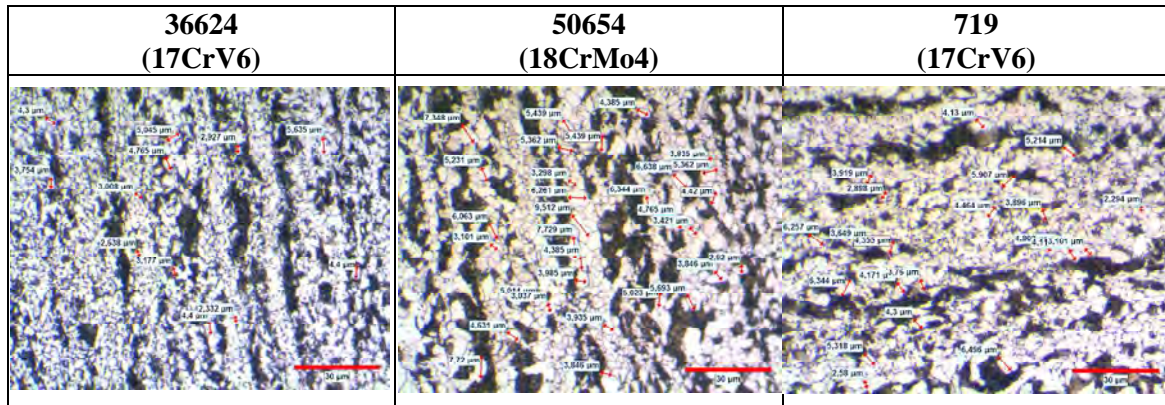


Figure 96: Ferrite grain size for the three tested heats.

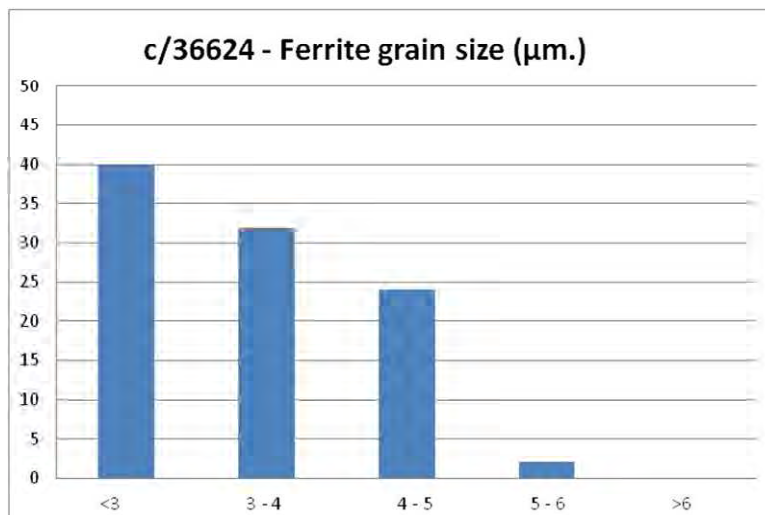


Figure 97: Percentage of ferrite grain sizes for heat 36624 (17CrV6) after the 12th thermomechanical cycle.

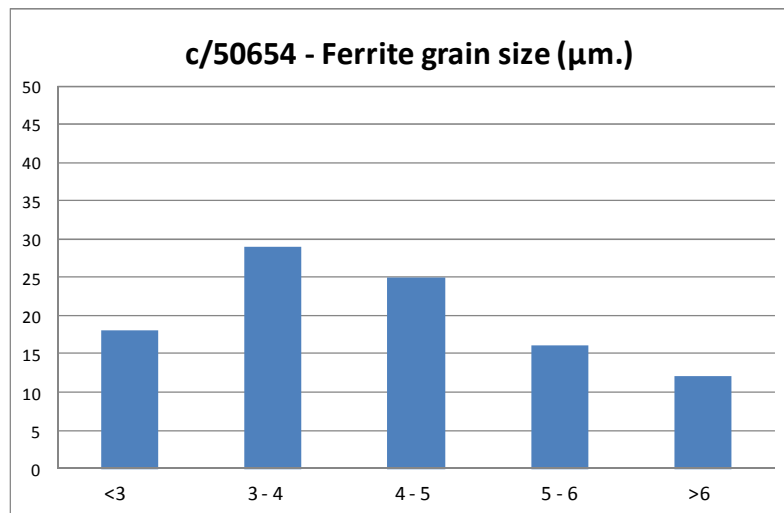


Figure 98: Percentage of ferrite grain sizes for heat 50654 (18CrMo4) after the 12th thermomechanical cycle.

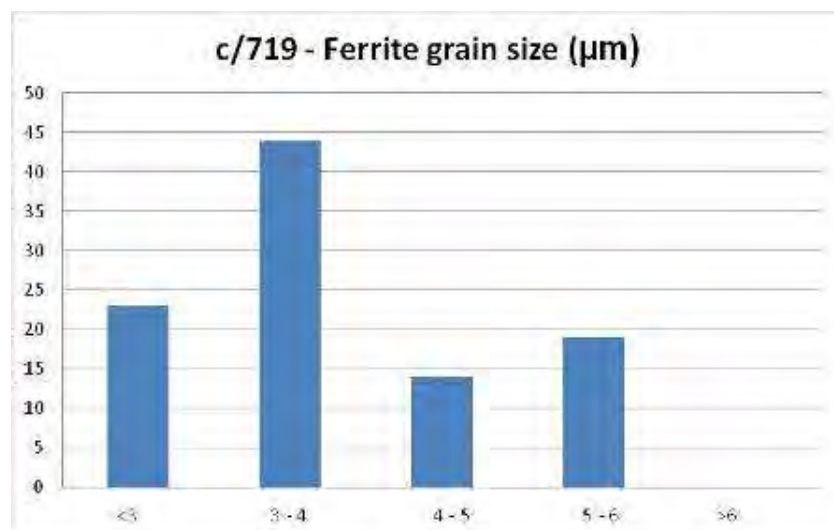


Figure 99: Percentage of ferrite grain sizes for heat 719 (17CrV6) after the 12th thermomechanical cycle.

The austenite grain size is between 10 and 26 µm which is much finer than the austenite grain size obtained after the austenization at 1200°C, which, in general, is coarser than 100 µm.

The best results obtained in the different thermomechanical tests has been carried out, this summary is shown in Table 37.

Steel grade	Austenization temperature (°C)	T. of the last deformation (°C)	Cooling rate (°C/s)	Grain size (µm)
17CrV6	1200	850	1	5 - 20
17CrV6	1000	700	0.5	2 - 6

Table 37: Comparison of the best results after an austenization temperature of 1000° and 1200°C.

Conclusions

- In the Gleeble tests, in which the austenization temperature has been decreased to 1000°C, instead of 1200°C of the previous tests, the austenite grain size has been clearly finer and also the final ferrite grain size.
- In the first Gleeble tests, with an austenization temperature of 1200°C, it has not been possible to obtain a ferrite grain size finer than 4 µm. However, in the last Gleeble tests, with austenization at 1000°C, grain sizes of 2 µm have been obtained.

Task 2.3 – Identification of the mechanisms to be exploited for producing UFG long product

On the basis of the results reported in the previous sections, both DIFT and Heavy γ deformation mechanisms can be exploited to obtain UFG long product steels.

Very promising results in terms of grain size has been achieved both exploiting DIFT mechanism (occurring at deformation temperature between $Ar_3 + 15^\circ\text{C}$ and $Ar_3 + 40^\circ\text{C}$) and Heavy γ deformation (deformation temperature at around $Ar_3 + 70^\circ\text{C}$).

DIFT mechanism has a higher refining power, however it is not possible to fully exploit it using industrial configurations because of high deformation level required at low temperature.

So, for industrial production steel, the final microstructure will be a mix DIFT ferrite and Heavy γ deformation ferrite. Since the refining power of DIFT is greater than the refining power of Heavy γ deformation mechanism, it is necessary to optimize the thermomechanical cycle in order to maximize DIFT.

Main parameters that control the formation of ultrafine ferrite are the following:

- C content : DIFT occurs at $C < 0.35\%$. For higher C contents the critical strain becomes too high to be applied in a industrial mill. However heavy γ deformation allows to obtain fine ferrite grains even at medium C content (0.3-0.5%).
- Mn content: a Low Mn content ($< 1\%$) is favourable for DIFT.
- Small Prior Austenite grain size: it is the most important parameter that can be tuned in an industrial plant. Small prior austenite grain size is always beneficial for both DIFT and Heavy γ deformation mechanisms and should be held lower than $20\ \mu\text{m}$ (better around $10\ \mu\text{m}$) in order to achieve fine ferrite grains and high ferrite volume fraction.
- Deformation: High strain level in the last rolling pass (possibly higher than $\epsilon=0.35$) or high accumulated deformation in austenite at this stage are required to obtain UFG ferrite.
- Strain rate: The effect of strain rate for both mechanisms is not clear for the investigated range ($1-30\ \text{s}^{-1}$) that is not comparable with the one used in industrial mill. However from literature its increase seems to be beneficial for increasing the ultrafine ferrite volume fraction.

An example of the possible conditions for a thermomechanical cycle aimed to produce UFG steel is:

- Low C content ($< 0.35\%$)
- Low Mn content ($< 1\%$)
- Small PAGS ($< 20\ \mu\text{m}$)
- Low T_{def} in last pass ($< Ar_3 + 25^\circ\text{C}$)
- Last pass strain or accumulated strain at last pass greater than 0.35.

2.3 WORK PACKAGE 3:

EXPERIMENTAL PRODUCTION OF LONG UFG STEELS ON PILOT MILL AND INDUSTRIAL PLANT

The objectives of this WP are:

- Realization of different routes at pilot mill in order to verify the feasibility of the process on pilot plant scale
- Identification of constraints and general guidelines for transfer to industrial production mills.
- Industrialization trials and production of prototype UFG steels.

Experimental production set-up of long UFG products has been chosen after defining the best mechanism to exploit for UFG long products. Different thermomechanical processes have been tested in order to optimize the material properties and the production process.

In addition a parametric investigation of relationship between grain size and cold formability in the new UFG long steels by FEM modeling has been carried out.

Task 3.1 – Definition of thermomechanical processes to be tested on pilot plant

Before hot rolling at pilot mill in Freiberg, in order to better determine the thermomechanical cycle to test, some tests by Gleeble at TUBAF were carried out, simulating for 18MnB2 and 30MnB4 the hot rolling passes defining the reductions and the temperatures for each pass. The aim of these Gleeble tests was to evaluate the microstructural evolution after each pass (quenching was carried out just after each single pass).

The MaxStrain system allows to realize a bi-axial deformation (Figure 100). With respect to other methods used (uniaxial compression) it simulates a more homogenous deformation, because the test specimen rotates after each operation pass of 90°. In this way the same conditions of rod and wire rolling occur. On the other hand the deformed specimen can be cooled after each process step (both normal as rapidly). So it is possible, both to simulate a rolling schedule for long products, as to follow the temperature-time regime in a real rolling mill.

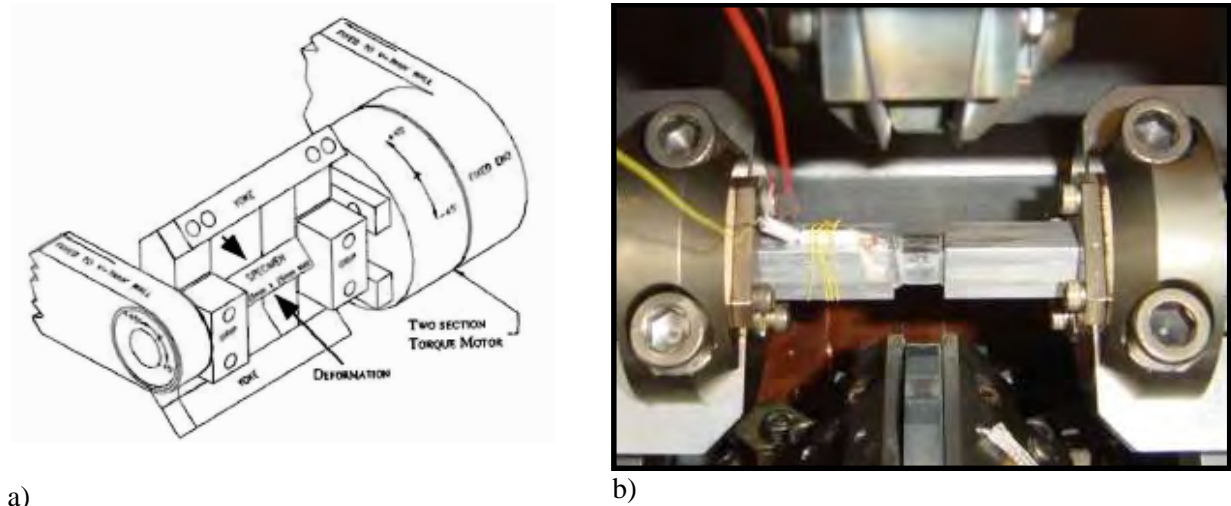


Figure 100: (a) Schematic drawing of the rotation assembly of the MaxStrain System and (b) MaxStrain system.

For steels 18MnB2 and 30MnB4 (Tables 38 and 39) the sequence of hot rolling passes was planned in such a way that the last pass increased the reduction and the deformation temperature was in the range of DIFT occurrence. Figures 101 and 102 show the microstructural evolution of the samples at each pass.

In Figure 101 a microstructural evolution of 18MnB2 after the simulated hot rolling passes is shown. Measures of ferrite volume fraction and grain size have been carried out from the second pass where the volume fraction is higher and the final volume fraction after the 6th pass is around 87%. Increasing the number of passes the grain size decreases and after the last pass it is about 6.5 μm that is fine but not ultrafine.

In Figure 102 the microstructural evolution of 30MnB4 after the simulated hot rolling passes is shown. In this case the ferrite volume fraction is less than the previous steel (65% max), and the grain size after the 6th pass is around 6.6 μm), similar to the previous steel.

From these results it can be concluded that it is necessary a further decrease in the temperatures of the passes or an increase of the deformations at 4th and 5th passes in order to further refine the prior austenite grain size.

Steel A							
SPECIMEN	1° Pass	2° Pass	3° Pass	4° Pass	5° Pass	6° Pass	
7	1000°C						Quenching
8	1000°C	970°C					Quenching
9	1000°C	970°C	920°C				Quenching
10	1000°C	970°C	920°C	870°C			Quenching
11	1000°C	970°C	920°C	870°C	840°C		Quenching
12	1000°C	970°C	920°C	870°C	840°C	810°C	Quenching
Deformation per pass (%)	36	36	34	34	34	41	Quenching

Table 38: Thermomechanical conditions simulated at Gleeble for steel 18MnB2.

Steel B							
SPECIMEN	1° Pass	2° Pass	3° Pass	4° Pass	5° Pass	6° Pass	
1	1000°C						Quenching
2	1000°C	950°C					Quenching
3	1000°C	950°C	900°C				Quenching
4	1000°C	950°C	900°C	850°C			Quenching
5	1000°C	950°C	900°C	850°C	800°C		Quenching
6	1000°C	950°C	900°C	850°C	800°C	765°C	Quenching
Deformation per pass (%)	36	36	34	34	34	41	

Table 39: Thermomechanical conditions simulated at Gleeble for steel 30MnB4.

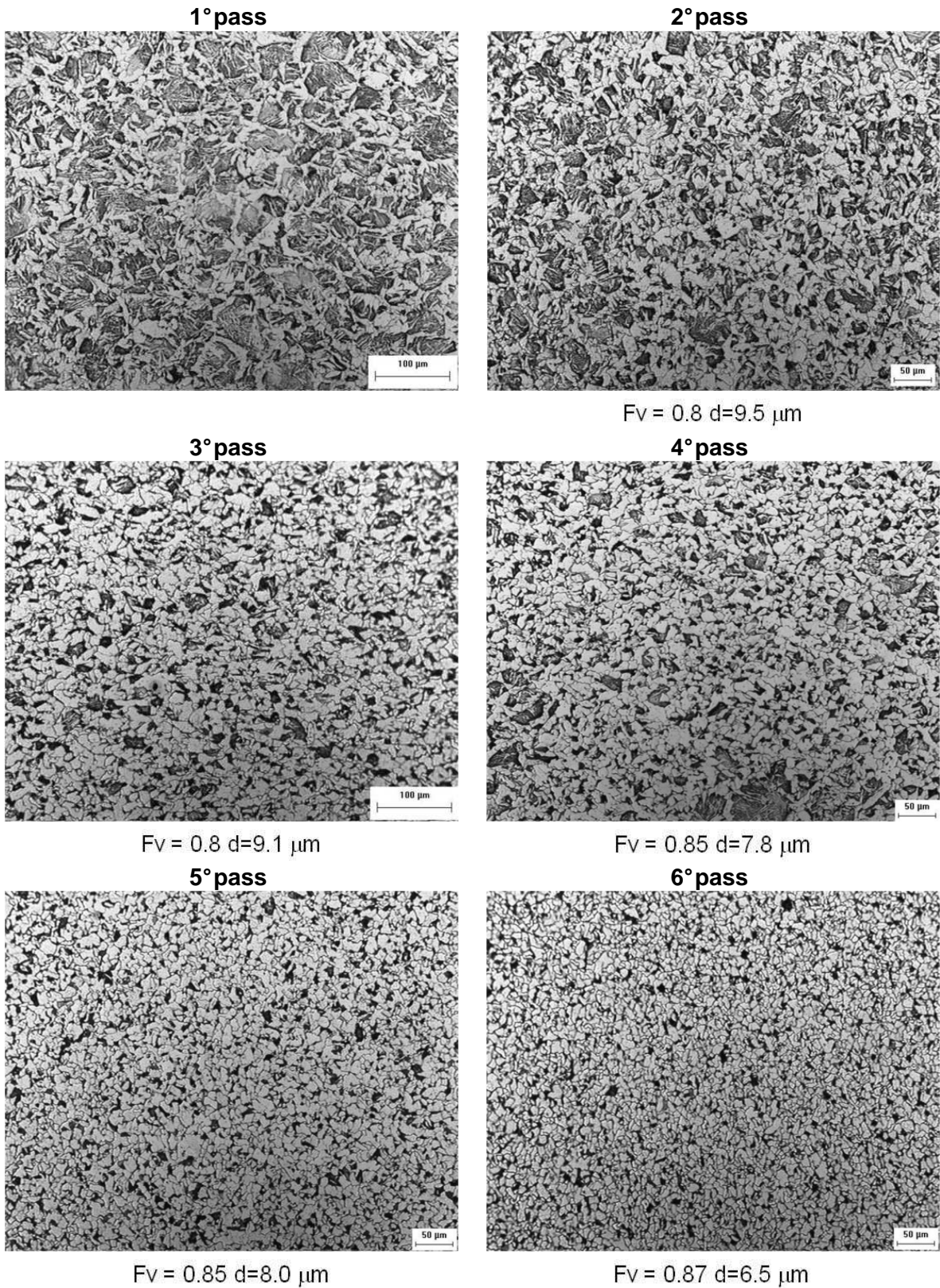
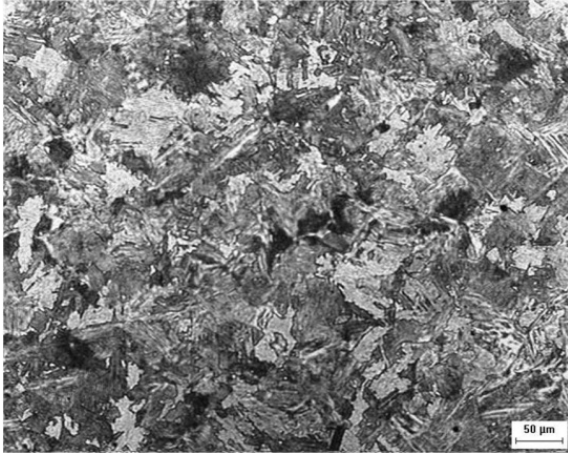
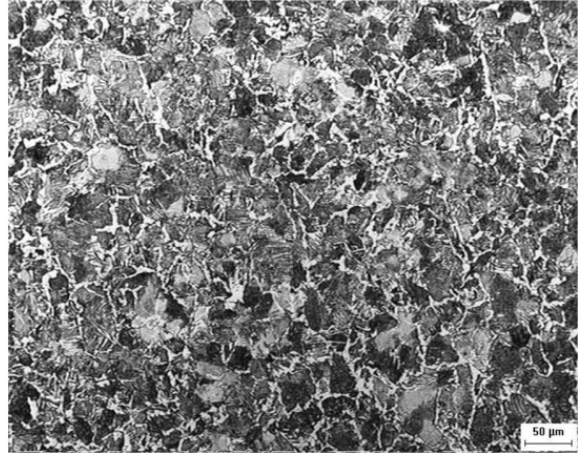


Figure 101: Microstructural evolution of 18MnB2 after each hot rolling pass.

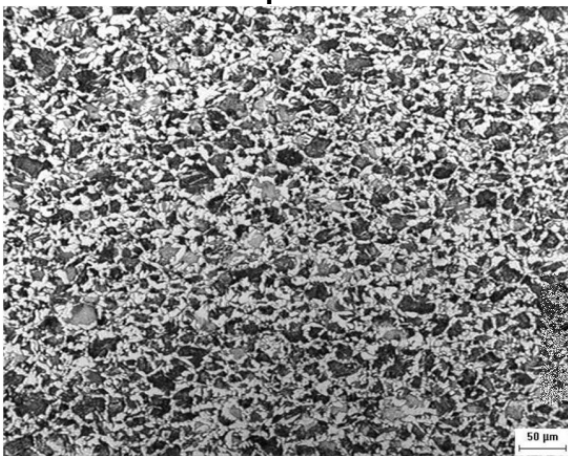
1° pass



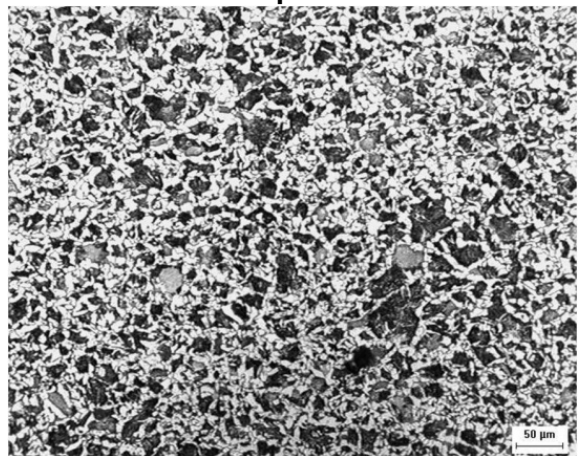
2° pass



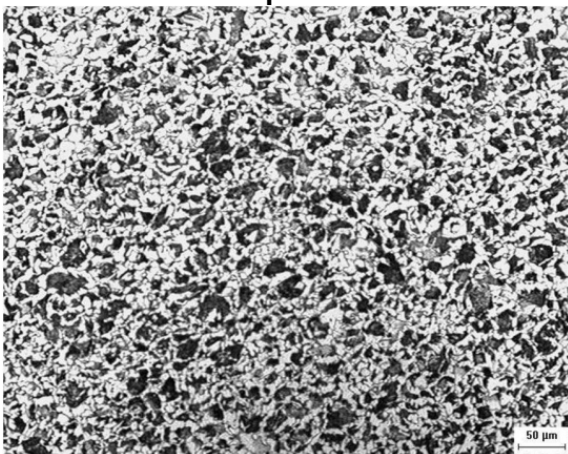
3° pass



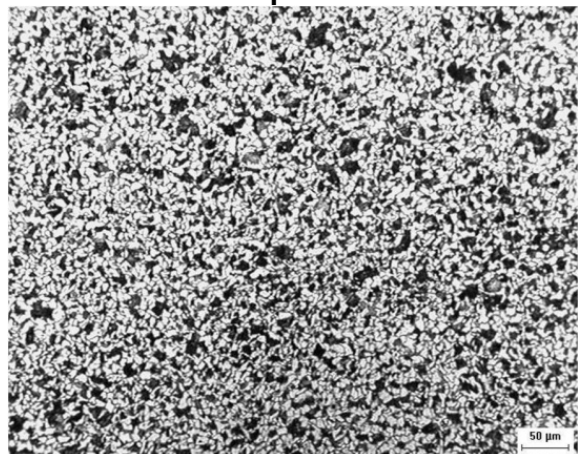
4° pass



5° pass



6° pass



Fv = 0.5 d=8.7 μm

Fv = 0.5 d=7.5 μm

Fv = 0.65 d=6.6 μm

Figure 102: Microstructural evolution of 30MnB4 after the simulated hot rolling passes.

Preliminary tests on TUBAF pilot mill

For 18CrMo4 preliminary tests on Tubaf pilot mill were carried out. Objective of these pilot tests on the Two-high rolling mill (Figure 103a) was to investigate the effects of different start and end rolling temperatures and different cooling rates on grain refinement. Three start rolling temperatures were selected from the non-recrystallisation region. The recrystallisation temperature for the steel 18CrMo4 was calculated according to [6]. Start and finish rolling temperature was measured with the pyrometers before the first and after the last passes corresponding Figure 103b and 103c respectively. Measured temperatures (which are underestimated due to external oxidation and to the faster cooling at the surface) are shown in Table 40. Air and water cooling were tested.

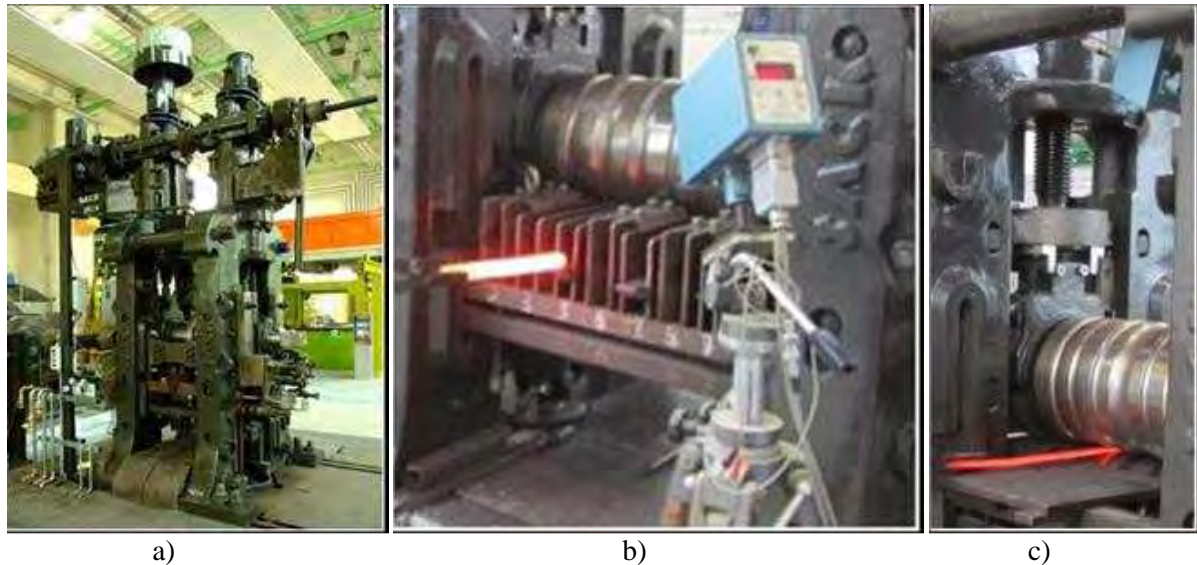


Figure 103: (a) Two-high rolling mill, (b) measurement of the start and (c) finish rolling temperature.

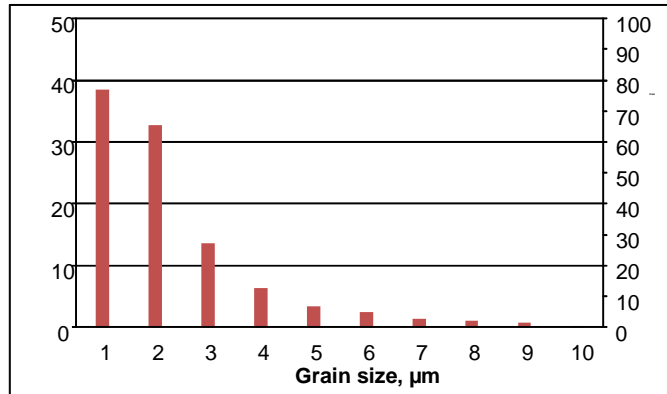
Start rolling temperature, °C	Finish rolling temperature, °C	Cooling
850	840	Air
850	840	Water
800	805	Air
800	800	Water
690	748	Air
690	737	Water
670	740	Air
670	730	Water

Table 40: Measured start and finish rolling temperatures (by pyrometer).

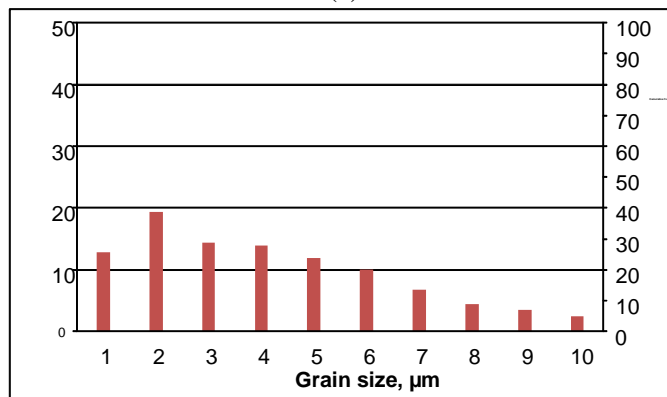
It was found that with the reduction of the finish rolling temperature, the average grain size decreases and the percentage of phases changed according to Table 41. The quantitative measurement of grain size has been carried out automatically by the image processing. The parameter selected for describing the grain size has been the chord length. Figure 104 depicts the grain size distribution chart for each case. In Figure 105 micrographs of the specimens after air cooling are shown.

Start/finish rolling temperature, °C	Average grain size, μm	HV10	Microstructure, %		
			Ferrite	Pearlite	Bainite/Martensite
670/740	2	255	71	25	4
690/748	3	244	72	15	12
800/805	4	243	63	10	27
850/840	6	242	60	12	28

Table 41: Average grain size, microstructure and hardness of the steel 18CrMo4 versus finish rolling temperature after air cooling.



(a)



(b)

Figure 104: Grain size distribution after rolling for steel 18CrMo4 a) finish rolling temperature 740°C, air cooling, b) finish rolling temperature 840°C, air cooling.

Start/finish rolling temperature, °C	Average grain size, μm	HV ₁₀	Microstructure, %		
			Ferrite	Pearlite	Bainite/Martensite
670/730	2	386	37	0	63
690/737	2	424	33	0	67
800/800	3	522	7	0	93
850/840	4	518	5	0	92

Table 42: Average grain size, microstructure and hardness of the steel 18CrMo4 in dependence on the finish rolling temperature after the water cooling.

Investigation of the influence of cooling rate on the microstructure development showed that increasing of the cooling rate results in the reduction of the average grain size (Table 42). Figure 106 depicts the grain size distribution chart for each case.

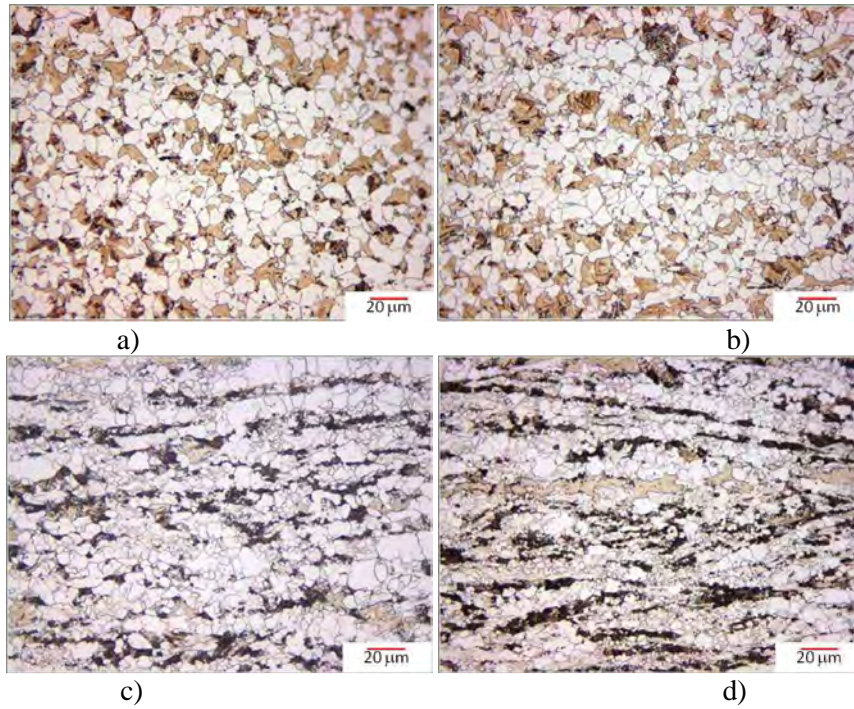
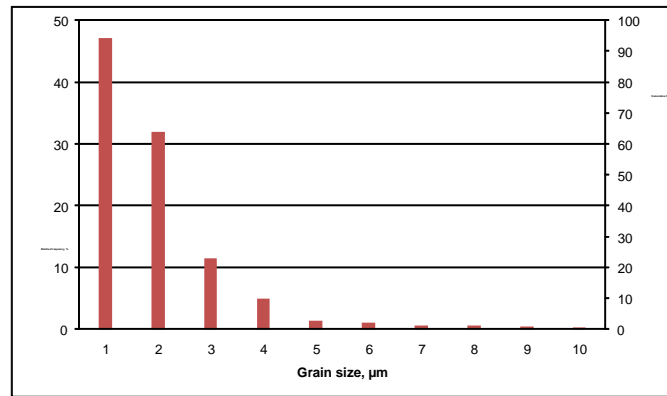
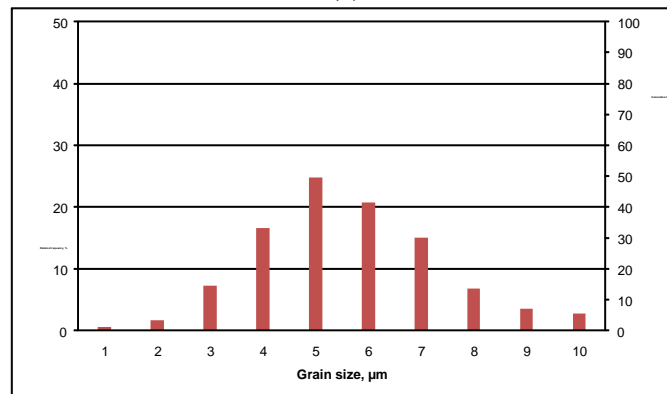


Figure 105: Micrographs of the structure in air cooled after the rolling specimens. Finish rolling temperature a) 840°C, b) 805°C, c) 748°C and d) 740°C.



(a)



(b)

Figure 106: Grain size distribution chart for the metallographic samples extracted from steel 18CrMo4 after rolling: a) finish rolling temperature 740°C, water cooling and b) finish rolling temperature 840°C, water cooling.

In addition it was determined that the strain induced ferrite forms on the prior austenite grain boundaries (Figures 107b, 107c, 107d). Dependence of grain size and hardness on the finish rolling temperature for air and water cooling is reported in Figure 108.

Summarizing, after the hot rolling of bars to the final diameter of 19 mm at different temperatures, the following results were obtained:

- average grain size was 2-6 μm after air cooling and 2-4 μm after water cooling;
- microstructure consisted of ferrite, pearlite and bainite/martensite after air cooling and of ferrite and martensite/bainite and after water cooling;
- for air-cooled samples hardness HV_{10} was 240-250, meanwhile for water-quenched samples hardness was 390-520. These values correspond to the tensile strength of 780-820MPa (air cooling) and 1240-1710MPa (water cooling).

From these preliminary results, it is possible to say that the final rolling must be about 700-750°C (temperature determined by pyrometer) in order to obtain ultrafine ferrite (2-6 μm) by DIFT process.

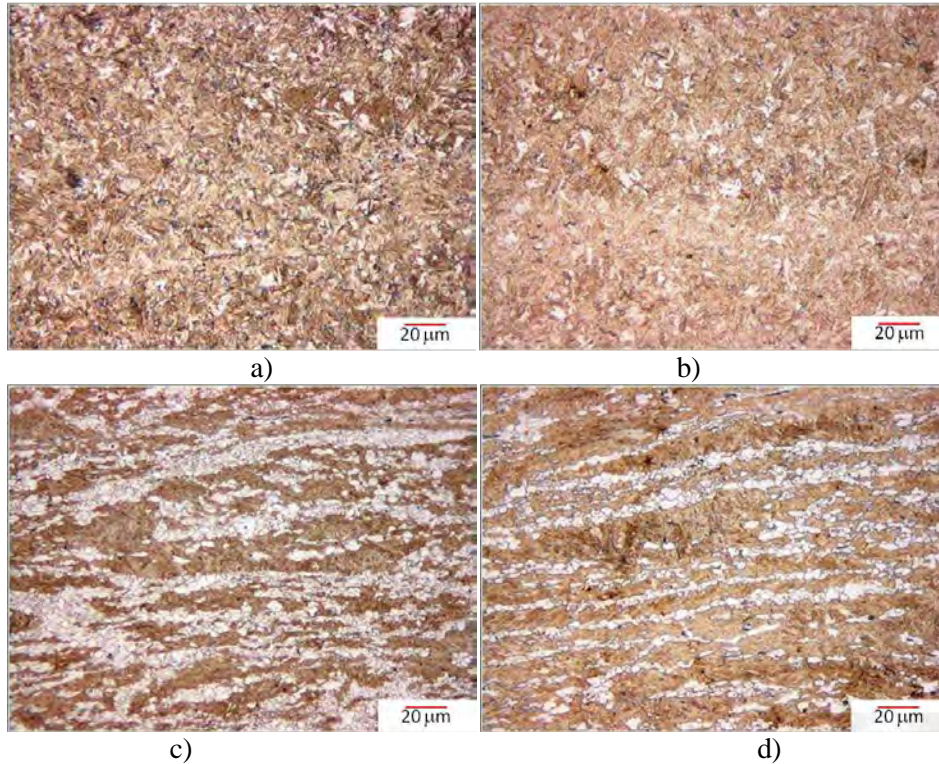


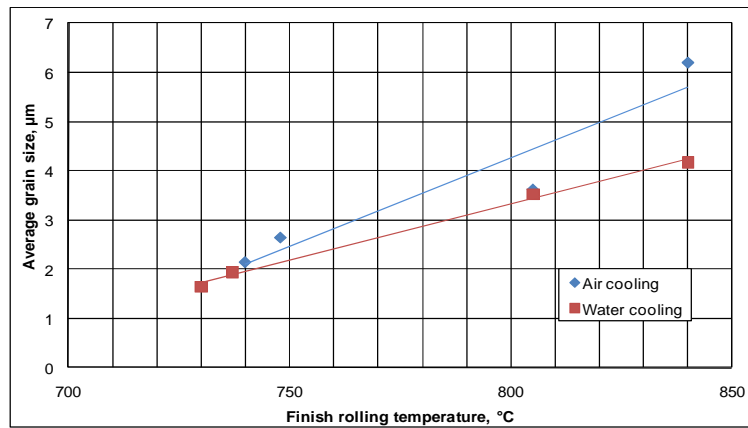
Figure 107: Micrographs of the structure in water cooled after the rolling specimens. Finish rolling temperature a) 840°C, b) 805°C, c) 737°C and d) 730°C.

Task 3.2 – Experimental production of long UFG steels

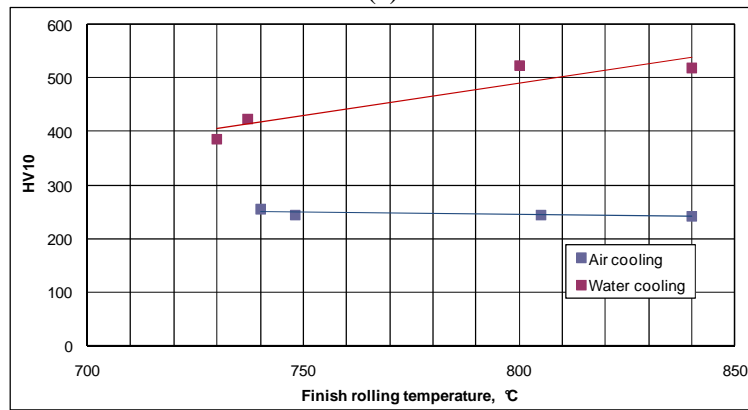
Experimental production of long UFG steels was carried out on pilot rolling on the Two-high rolling mill and continuous rolling mill at TUBAF.

The rolling trials were divided in two groups:

- Rolling of steels 18CrMo4 and 50SiMoVNb8 on the continuous rolling mill (Figure 109) whose aim was to study the influence of the rolling speed and finish rolling temperature on the microstructure and mechanical properties;
- Rolling of steels 18MnB2 and 30MnB4 on the roughing reversing mill of the continuous line whose aim was to study the influence of finish rolling temperature on the microstructure and mechanical properties.



(a)



(b)

Figure 108: Average grain size (a) and hardness (b) of the steel 18CrMo4 in dependence on the finish rolling temperature after the air and water cooling.

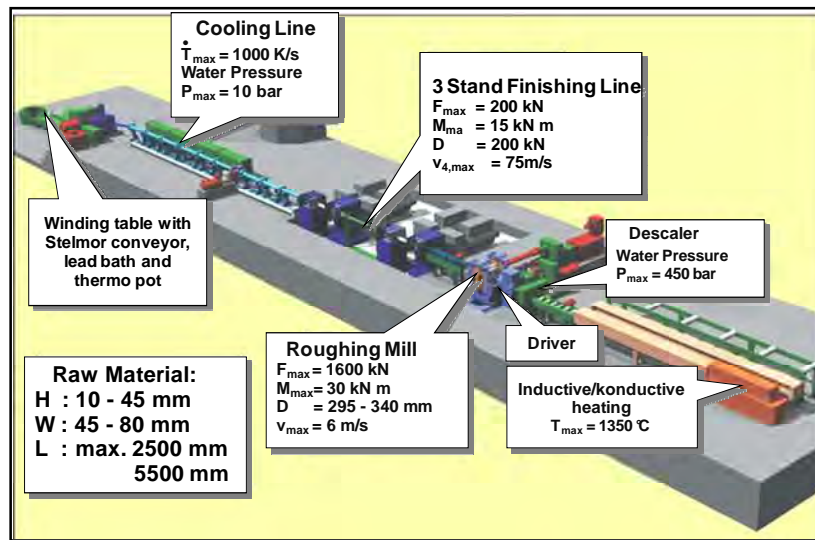


Figure 109: Continuous rolling mill.

Rolling speed, m/s	Finish rolling temperature, °C	Rolling speed, m/s	Finish rolling temperature, °C
Steel 18CrMo4		Steel 50SiMoVNb8	
6	850	12	880
	800		850
	750		800
	730		-
12	850	16	880
	800		850
	750		800
	730		-
20	850	20	880
	800		850
	750		800
	730		-

Table 43: Rolling schedule of steels 18CrMo4 and 50SiMoVNb8.

Rolling trials of 18CrMo4 and 50SiMoVNb8 steels

Steels 18CrMo4 and 50SiMoVNb8 were rolled on the continuous rolling mill in 12 passes (Table 43). The aim of this rolling was to investigate the influence of rolling speed and finish rolling temperature on the microstructure development of studied steels. Calculated parameters of the rolling are summarized in Table 44.

				6m/s				12m/s				16m/s				20m/s			
St.	Groove	Ap	l	vw	φ	ld	phip	vw	φ	ld	phip	vw	φ	ld	phip	vw	φ	ld	phip
		mm ²	-	m/s	mm	mm		m/s	mm	mm		m/s	mm	mm		m/s	mm	mm	
F0	Swedish-Oval	1228	1	1	0,62	53,60	11,60	1	0,62	53,60	11,60	1	0,62	53,60	11,60	1	0,62	53,60	11,60
F0	Round 36mm	923	1	1	0,61	62,97	9,76	1	0,61	62,97	9,76	1	0,61	62,97	9,76	1	0,61	62,97	9,76
F0	Swedish-Oval	658	1	1	0,88	57,90	15,27	1	0,88	57,90	15,27	1	0,88	57,90	15,27	1	0,88	57,90	15,27
F0	Round 27mm	479	1	1	0,82	67,19	12,23	1	0,82	67,19	12,23	1	0,82	67,19	12,23	1	0,82	67,19	12,23
F0	Oval	358	1	1	0,78	45,93	16,89	1	0,78	45,93	16,89	1	0,78	45,93	16,89	1	0,78	45,93	16,89
F0	Round 20mm	289	1	1	0,79	55,98	14,08	1	0,79	55,98	14,08	1	0,79	55,98	14,08	1	0,79	55,98	14,08
F0	Oval	202	1	1	1,05	45,57	23,03	1	1,05	45,57	23,03	1	1,05	45,57	23,03	1	1,05	45,57	23,03
F0	Round 15mm	163	1	1	0,94	56,46	16,71	1	0,94	56,46	16,71	1	0,94	56,46	16,71	1	0,94	56,46	16,71
F0	Oval	132	1	1	0,68	33,79	20,15	1	0,68	33,79	20,15	1	0,68	33,79	20,15	1	0,68	33,79	20,15
F0	Round 12mm	115	1	1	0,71	40,71	17,41	1	0,71	40,71	17,41	1	0,71	40,71	17,41	1	0,71	40,71	17,41
F0	Death pass																		
F1	Oval	88,6	1	4,62	0,91	28,02	150,41	9,23	0,91	28,02	300,81	12,31	0,91	28,02	401,09	15,38	0,91	28,02	501,36
F2	round 9,8mm	75	1	6,00	0,86	33,51	154,12	12,00	0,86	33,51	308,24	16,00	0,86	33,51	410,99	20,00	0,86	33,51	513,73

Table 44: Calculated parameters of the rolling of steels 18CrMo4 and 50SiMoVNb8 versus rolling speed.

Specimens were heated up to 1200°C and maintained at this temperature for 45min. Roughing occurred from diameter 50 mm up to 12mm. Finish rolling was carried out up to diameter of 10 mm, then the specimens were air or water cooled. The aim of the water cooling was to investigate the microstructure after the last pass. Temperature was measured before and after every pass of the roughing and after the last finish pass by pyrometers.

In order to obtain heating curve in rod before rolling, thermocouple was welded in its core.

After the rolling, cooling curve was measured only on the surface of the rod by pyrometer. The thermomechanical cycle consisted in:

- Heating: 1200°C x 30 min;
- Roughing: Ø50mm → Ø12mm
- Finish rolling Ø12mm → Ø10mm
- Air and water cooling after the rolling

Microstructure of air cooled specimens of steel 18CrMo4 versus finish rolling temperature and rolling speed is shown in Figure 110. It is composed by ferrite + pearlite + bainite. Ferrite grain size and hardness of each sample are reported in Table 45.

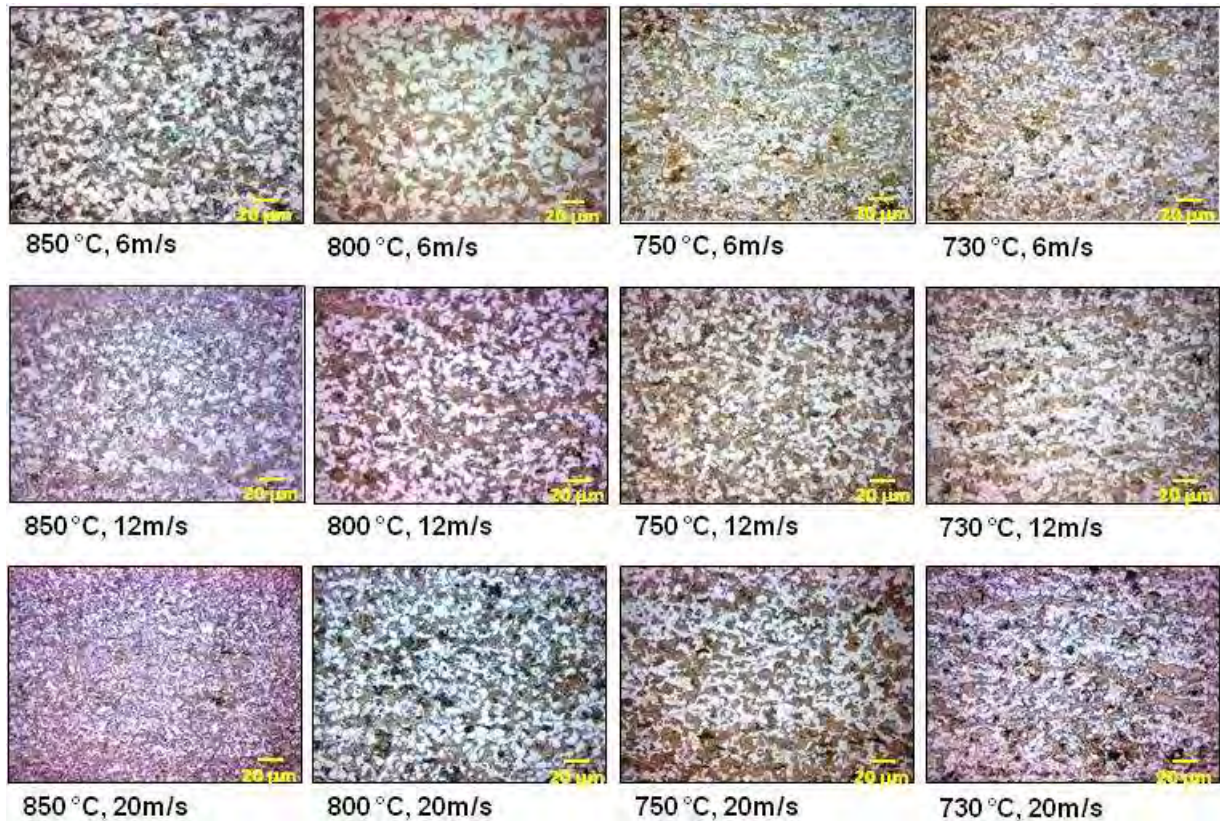


Figure 110: Microstructure of air cooled specimens of steel 18CrMo4 versus finish rolling temperature and rolling speed.

Roll. speed, m/s	6				12				20			
	850	800	750	730	850	800	750	730	850	800	750	730
Finish rolling temperature, °C	850	800	750	730	850	800	750	730	850	800	750	730
Ferrite Grain size, µm	3.9	4.0	2.5	2.7	2.8	3.4	3.2	2.7	2.7	3.3	2.6	2.5
Average Grain size, µm	6.6	4.9	5.9	6.7	6.5	6.1	7.2	8.9	4.8	5.5	7.5	6.6
Hardness HV ₁₀	264	258	255	254	279	279	278	258	285	276	278	252

Table 45: Ferrite grain size, average grain size and hardness of air cooled specimens of steel 18CrMo4.

It can be noted that decreasing the finish rolling temperature and increasing the rolling speed the ferrite grain size decreases. The average grain size, that is the mean value among ferrite, pearlite and bainite grain size always shows an increase at 12 m/s rolling speed.

In Figure 111 and Table 46 microstructural evolution, austenite grain size and hardness for samples water quenched are reported. The microstructure is formed by ferrite + bainite.

The trends of average grain size are not so clear, while the trend of hardness shows that if the samples are water quenched, independently on the hot rolling temperature the hardness HV₁₀ decreases with

rolling speed (except the one rolled at 800°C). If the samples are air cooled hardness remains almost the same for the whole range of hot rolling speed.

Roll. speed, m/s	6				12				20			
Finish rolling temperature, °C	850	800	750	730	850	800	750	730	850	800	750	730
Austenite Grain size, µm	6.6	4.9	5.9	6.7	6.5	6.1	7.2	8.9	4.8	5.5	7.5	6.6
Hardness HV ₁₀	531	496	547	550	452	513	508	515	420	521	381	385

Table 46: Austenite grain size and hardness of water quenched specimens of steel 18CrMo4.

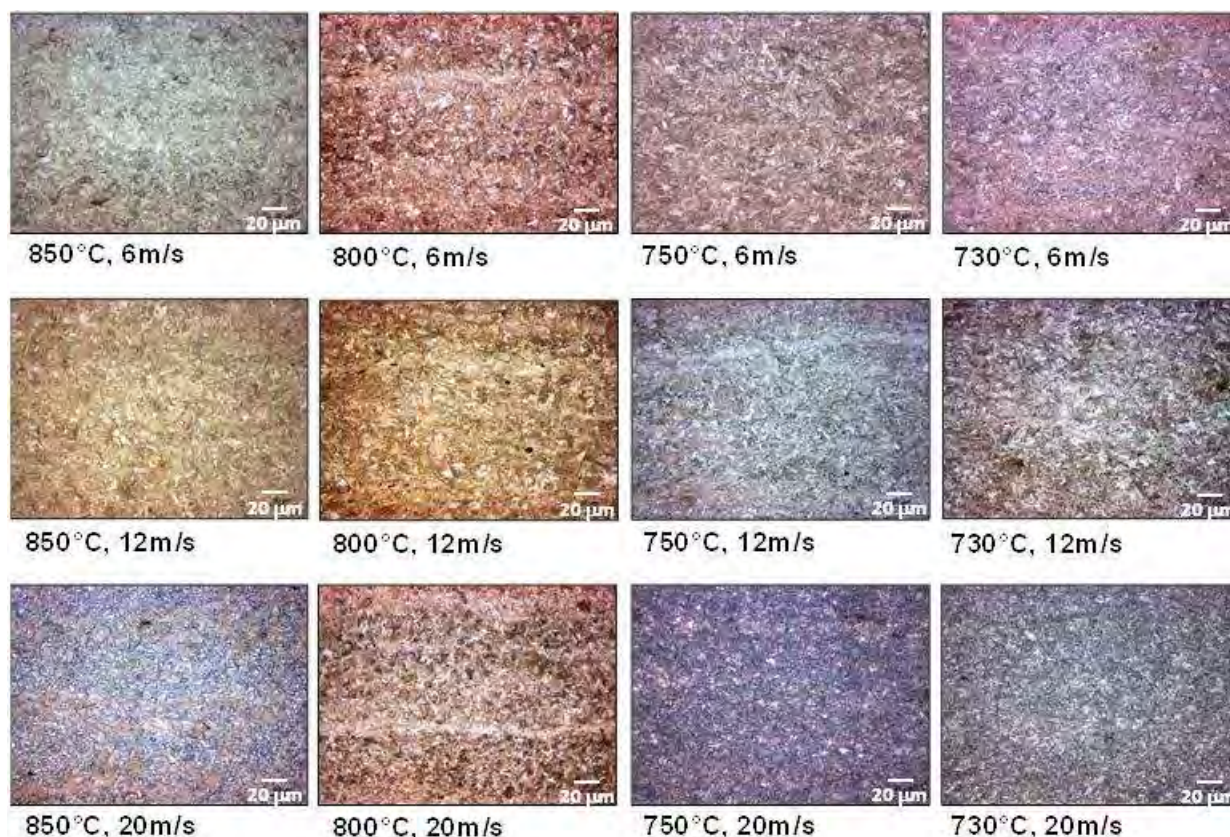


Figure 111: Microstructure of water cooled specimens of steel 18CrMo4 versus finish rolling temperature and rolling speed.

In Table 47 and in Figure 112 ferrite and average grain size, hardness and microstructural evolution for 50SiMoVNb8 samples after air cooling are reported. Microstructure is formed by ferrite + pearlite + bainite + martensite. Figure 113 and Table 48 refer to the water quenched samples. In this case microstructure is formed by ferrite + martensite.

In Figure 114 the average grain size and the hardness versus rolling speed are shown. All the tests are reported, both after air cooling and water quenching.

Rolling speed, m/s	12			16			20		
Finish rolling temperature, °C	880	850	800	880	850	800	880	850	800
Ferrite Grain size, µm	1.4	1.5	2.0	1.6	1.9	2.0	1.9	2.5	2.1
Average Grain size, µm	3.0	3.8	4.3	9.2	7.0	6.8	8.3	6.2	3.6
Hardness HV ₁₀	541	524	518	522	502	568	456	585	519

Table 47: Ferrite and average grain size and hardness of air cooled specimens of steel 50SiMoVNb8.

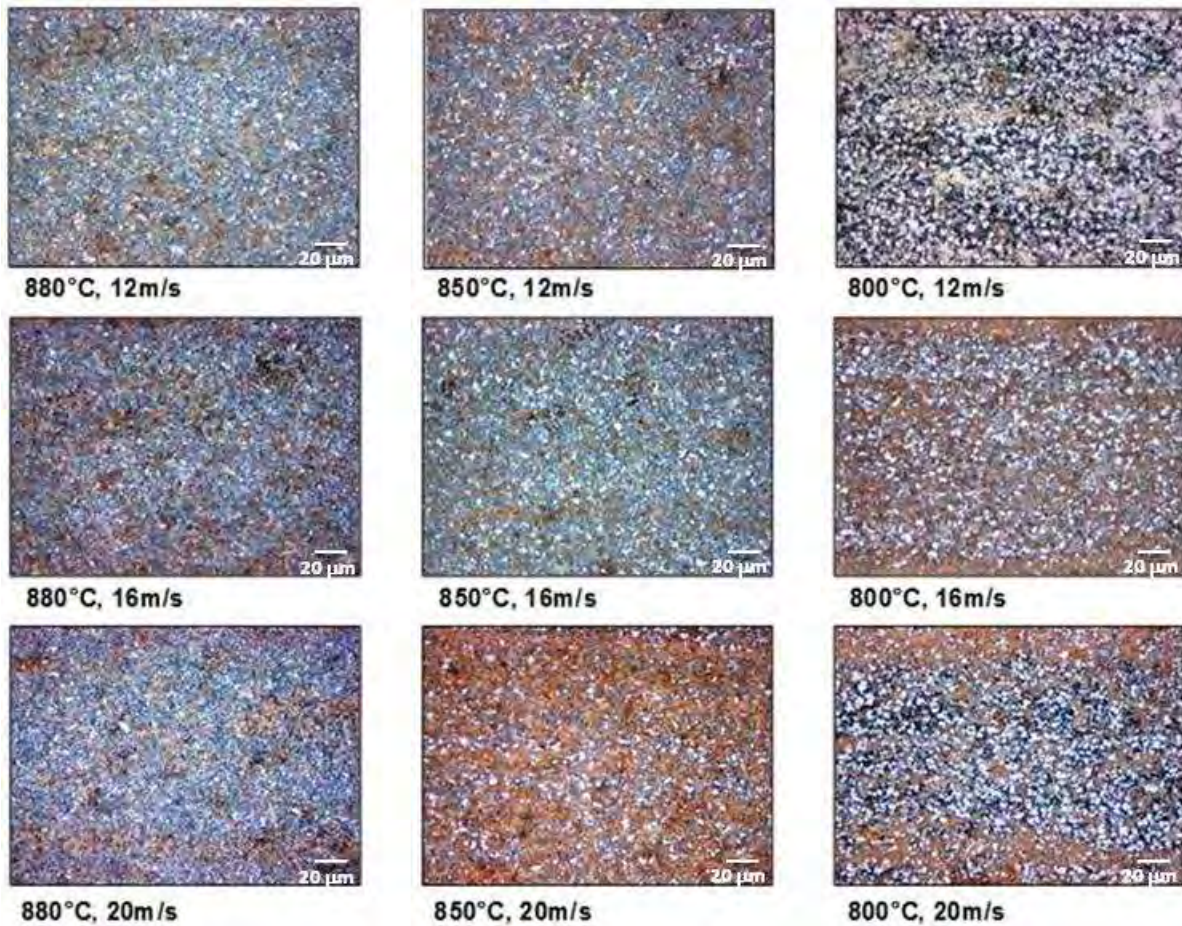


Figure 112: Microstructure of air cooled specimens of steel 50SiMoVNb8 versus finish rolling temperature and rolling speed.

Rolling speed, m/s	12				16				20			
Finish rolling temperature, °C	880	850	800	750	880	850	800	750	880	850	800	750
Austenite Grain size, µm	5.0	4.6	5.4	5.0	4.8	4.7	5.0	5.6	5.2	5.9	4.4	5.2
Hardness HV ₁₀	697	820	754	758	758	750	780	780	782	844	782	835

Table 48: Austenite grain size and hardness of water cooled specimens of steel 50SiMoVNb8.

The trends of average grain size are not so clear in the case of water quenched samples while the graph of hardness shows that if the samples are water quenched, the hardness HV₁₀ slightly increases with rolling speed. If the samples are air cooled both hardness and average grain size have not a clear trend, however the difference for the hot rolling speed 12-20 m/s is not meaningful.

Two billet of 50SiMoVNb8 have been rolled.

a) One of the billet has been rolled to bar of 50 mm in Gerdau

Afterwards, these bars have been rolled to Ø=15 mm in Freiberg.

Some of the bars have been cut to 1.10 m of length for preliminary induction treatment and other ones have been peeled to Ø=13.3 mm. and cut to 2.115 mm of length in Gerdau.

b) One of the billet has been rolled to wire rod of 15 mm and has been annealed in Gerdau.

Afterwards, some of the bars have been cut to 1.10 m of length for preliminary induction treatment and other ones have been peeled to Ø=13.3 mm and cut to 2.115 mm of length in Gerdau.

The mechanical properties of the bars with induction treatment, standard grain size and ultra fine grain size, will be compared in WP4.

Some springs have been manufactured by hot route, with standard material and with ultra fine grain material, in order to perform the fatigue tests reported in WP4.

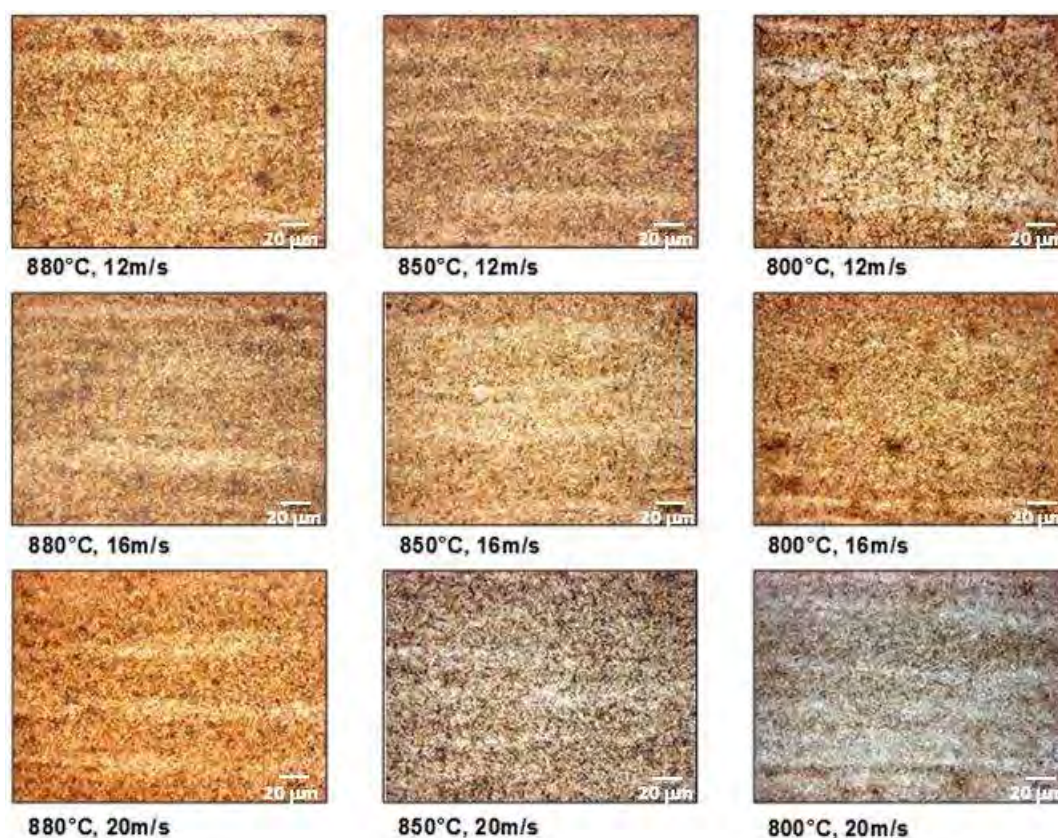


Figure 113: Microstructure of water quenched specimens of steel 50SiMoVNb8 versus finish rolling temperature and rolling speed.

Rolling trials of steels 18MnB2 and 30MnB4

Steels 18MnB2 and 30MnB4 were hot rolled at TUBAF pilot mill according the following scheme:

- Heating: 1200°C x 30 min;
- Rolling on roughing mill: Ø50mm → Ø12mm
- Finish rolling temperatures: Ar3-50°C, Ar3+15°C, Ar3+50°C
- Air and water quenching after finish rolling

Temperature was measured before the first and after the last pass. The rolling pass design refers to Table 44 where roughing mill F0 finishes at Round Ø12.0mm.

In Figure 115 the microstructure of air cooled specimens of steel 18MnB2 versus finish rolling temperature are shown. Microstructure is formed by ferrite + pearlite + bainite.

In Table 49 the corresponding grain size and hardness are reported. Ferrite grain size is fine and constant for all the hot rolling temperatures as the corresponding hardness.

Ferrite grain size, µm			
Finish rolling temperature, °C	847	812	750
Ferrite Grain size, µm	3.3	3.6	3.2
Average Grain size, µm	3.8	3.6	2.9
Hardness HV ₁₀	151	145	150

Table 49: Ferrite, average grain size and hardness of air cooled specimens of steel 18MnB2.

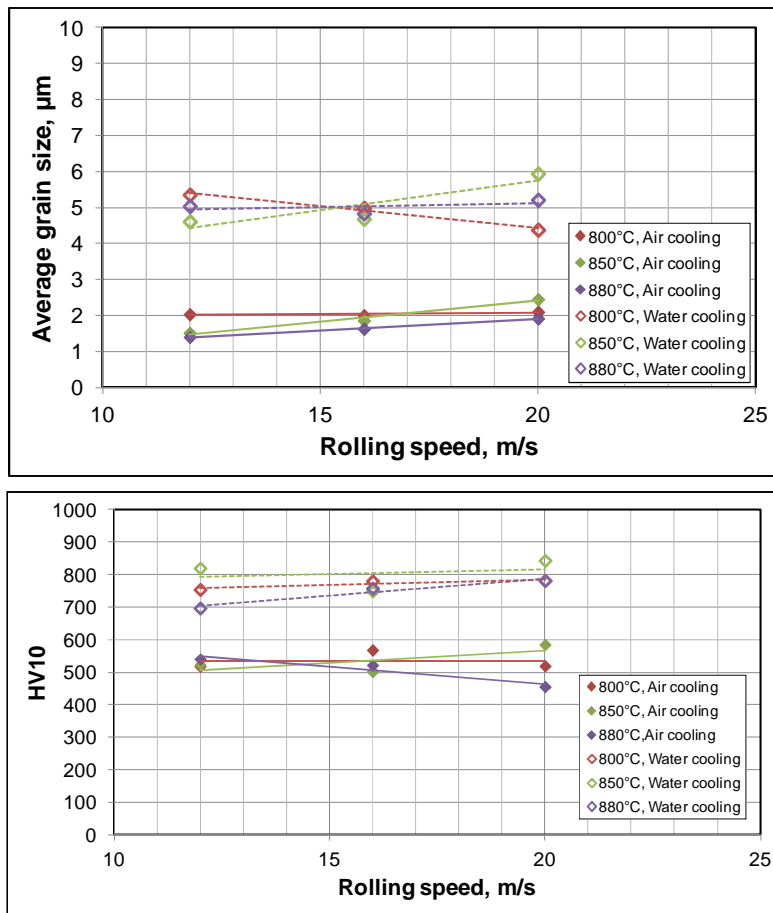


Figure 114: Average grain size and hardness of air and water quenched specimens of steel 50SiMoVNb8.

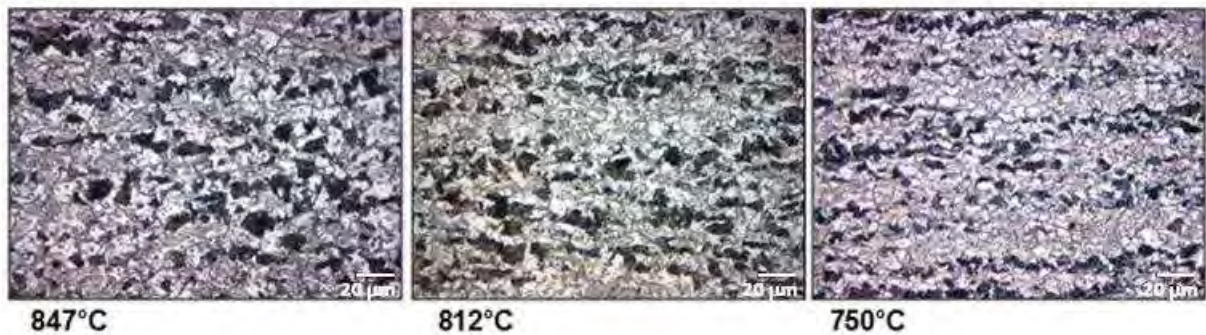


Figure 115: Microstructure of air cooled specimens of steel 18MnB2 versus finish rolling temperature.



Figure 116: Microstructure of water cooled specimens of steel 18MnB2 versus finish rolling temperature.

Finish rolling temperature, °C	847	812	750
Austenite Grain size, μm	4.5	5.5	4.4
Hardness HV ₁₀	432	472	337

Table 50: Austenite grain size and hardness of water cooled specimens of steel 30MnB4.

In Figure 116 the microstructure of water quenched specimens of steel 18MnB2 versus finish rolling temperature are shown. Microstructure is formed by ferrite + bainite + martensite. In Table 50 the corresponding grain size and hardness are reported. Austenite grain size is fine for all the hot rolling temperatures but it varies with a maximum a 812°C as the corresponding hardness.

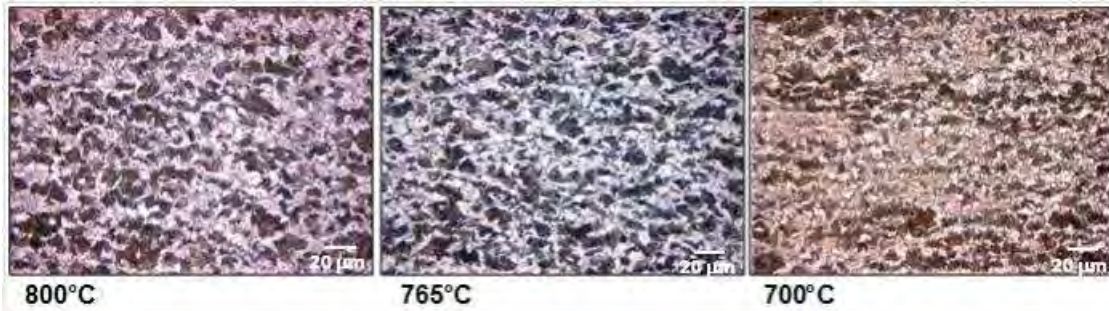


Figure 117: Microstructure of air cooled specimens of steel 30MnB4 versus finish rolling temperature.

Ferrite grain size, μm			
Finish rolling temperature, °C	800	765	700
Ferrite grain size, μm	3.4	3.5	3.0
Average grain size, μm	3.9	3.9	3.6
Hardness HV ₁₀	196	195	199

Table 51: Ferrite grain size, average grain size and hardness of air cooled specimens of steel 30MnB4.

In Figure 117 the microstructures of air cooled specimens of steel 30MnB4 versus finish rolling temperature are shown, while in Table 51 the corresponding grain size and hardness are reported. Microstructure is formed by ferrite + pearlite. Ferrite grain size is fine for all the hot rolling temperatures and decreases with the hot rolling temperature.

In the case of water quenched specimens (Figure 118 and Table 52) the microstructure is formed by martensite and the austenite grain size decreases with the lowest hot rolling temperature (700°C).

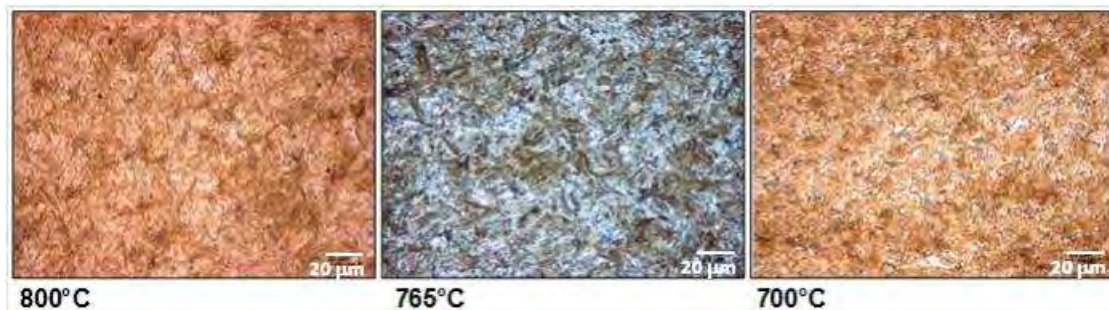


Figure 118: Microstructure of water cooled specimens of steel 30MnB4 in dependence of finish rolling temperature.

Austenite grain size, μm			
Finish rolling temperature, $^{\circ}\text{C}$	800	765	700
Austenite Grain size, μm	5.1	5.6	3.9
Hardness HV_{10}	602	573	532

Table 52: Austenite grain size and hardness of water quenched specimens of steel 30MnB4.

Task 3.3: Parametric investigation of relationship between microstructural features and cold formability in the new UFG long steels

The aim of this task was to investigate the relationships between steel microstructure and plastic deformation behavior of the material. The main feature to be considered is ferrite grain size, in particular the study focused on the comparison between steel with conventional and ultrafine microstructure. Among the steel grades which are the subject of the project, medium-carbon steel for fastener has been selected (30MnB4).

The flow chart of Figure 20 shows the followed approach. Firstly a selected forming process – in this case, the cold forming of a screw – has been analyzed and simulated by means of FEM. On the basis of the results of FE analysis, in order to define the specimen designs and a test plan able to reproduce conditions comparable to those experienced in the forming process, both stress and strain evolution at the most critical point in the screw head has been studied. The results of the mechanical tests, performed according such experimental plan, allow to build the ductility curves (strain to failure vs. triaxiality) related to the different microstructures (conventional vs. UFG). Finally, the ductility curves may be used to simulate cold forming taking into account the material damage.

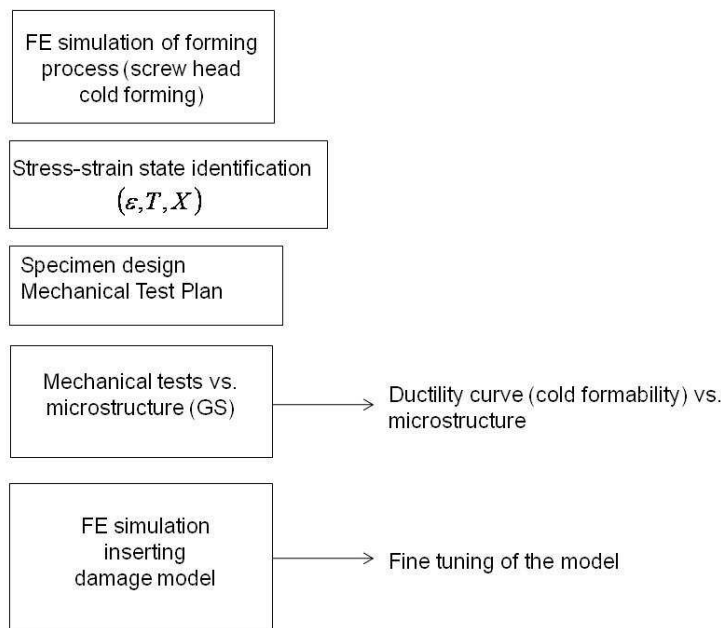


Figure 119: Flow chart of the investigation of relationship between microstructural features and cold formability.

C	Mn	Si	S	Cr	Mo	Al	Ti	B	N
%	%	%	%	%	%	%	%	ppm	ppm
0.28	1.18	0.29	<0.001	0.48	0.02	0.032	0.031	30	43

Table 53: Chemical composition of 33MnB5 from CSM database.

Material stress-strain curve

The material selected is the steel for fastener 30MnB4. To perform the numerical studies on the stress state developed during the screw head forming, it is necessary to have the complete stress-strain curve of the material.

Due to the elevated plastic strain reached during cold forming, the conventional tensile testing post processing is not suited to the aim, so a different approach is needed. In particular the so called extended stress-strain curve has to be determined. Different techniques may be used, according to [7].

As preliminary material curve, data on 33MnB5, a steel with a composition close to the one under study, were available in the CSM database. The chemical composition of the material is listed in Table 53. The original material was in the form a seamless pipe. The delivery state was annealed.

The extended stress-strain curve is shown in Figure 120 [8]. For the preliminary process simulations no strain rate effect or temperature dependence of the stress-strain curve was considered.

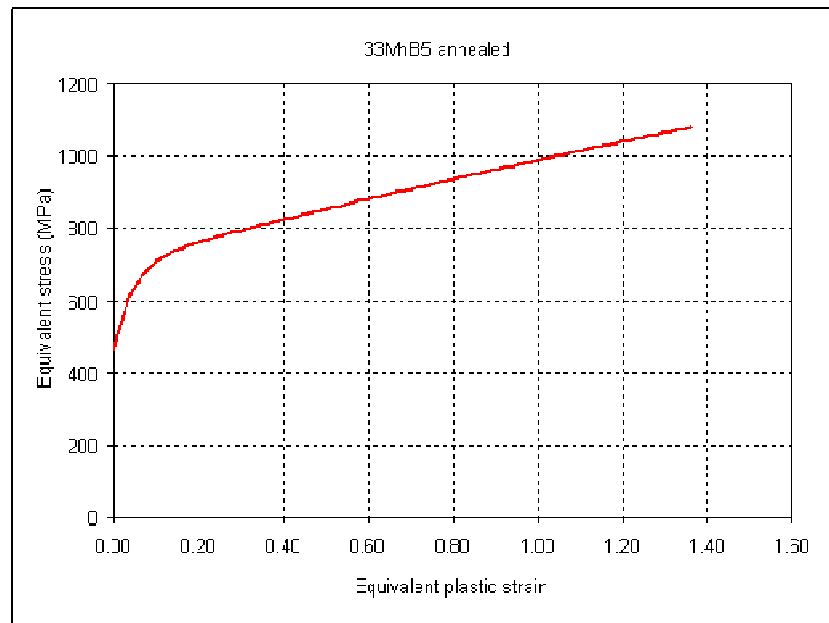


Figure 120: Extended stress-strain curve for 33MnB5.

Process data collection for screw head forming

The selected component for the project is a M12 screw with triple square head (type XZN). The geometry has been selected by Agrati and the general screw drawing is shown in Figure 121. The screw head is formed through a number of steps described in the following.

The four steps are (Figure 122):

- Step 1: extrusion in die
- Step 2: first heading
- Step 3: second heading
- Step 4: flange and key hole forming

In step 1, the initial rod, having a diameter of about 13.6 mm, is extruded into a die of 12.75 mm diameter, leaving a portion of defined length that will be formed by heading in the next steps.

In step 2 and 3 there is a progressive upsetting with a corresponding barreling. In each step a specific tooling is used, as shown in Figure 121. In the fourth step a net shape forming is performed by a nearly closed die configuration. In this stage both the flange and the key hole are formed.

The process runs at 80 strokes/min, which has been estimated to result in a mean ram speed of 10 m/s.

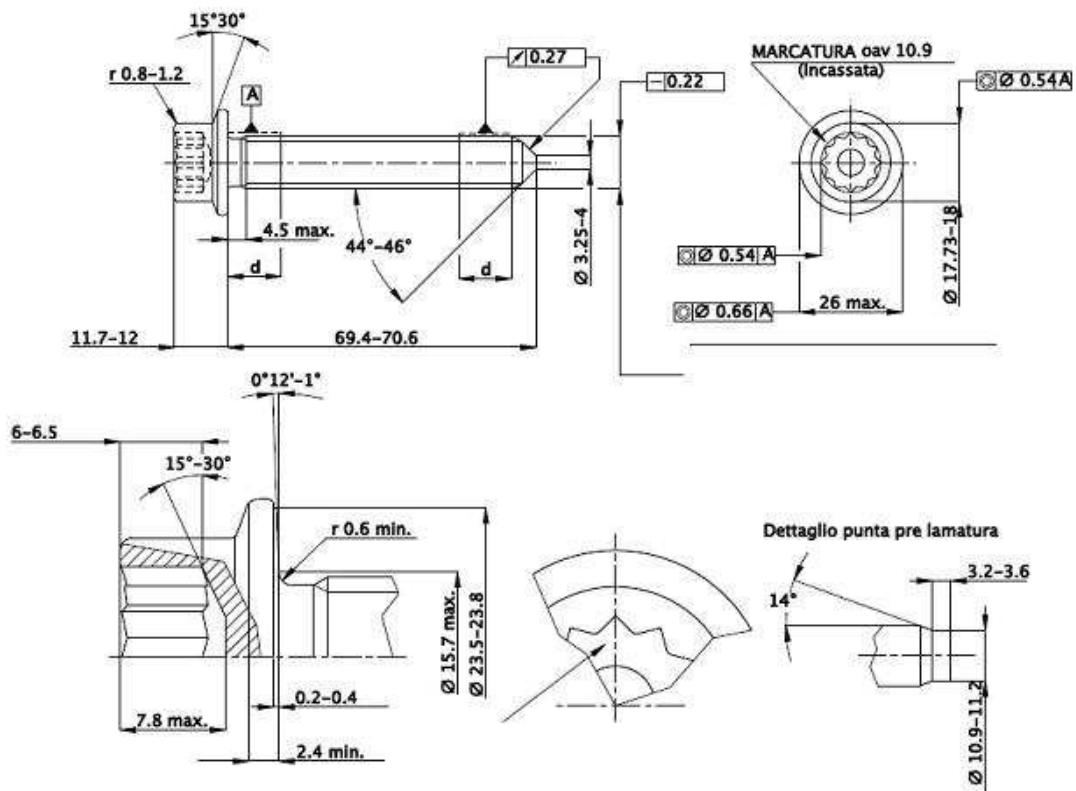


Figure 121: Screw dimensions.

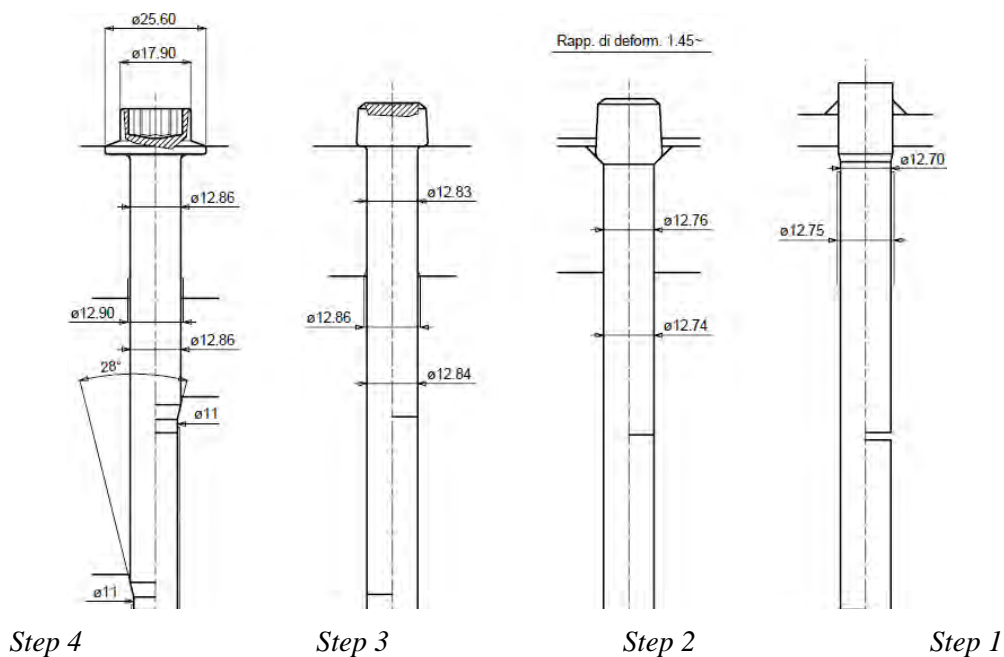


Figure 122: Screw head cold forming steps.

Finite element modeling of head forming

To determine the strain and stress field evolution during forming, the process has been modeled by means of finite element. As the main objective of the activity was the stress-strain history in the critical points, some simplifications were adopted in order to speed up the analysis but by keeping at the same time the essential features of the process. The adopted hypotheses for the FE analysis are listed below:

- Tool constant speed $v=10$ m/s
- Rigid tools with friction

- Step 1 not modelled (head is not involved in forming)
- Elastic-plastic material, no strain rate dependency, no heat generation due to plastic work (isothermal). Extended stress-strain curve obtained from standard tensile tests [7]
- 2D axisymmetric modelling
- Automatic remeshing
- Key hole modelled as cylindrical (mean radius applied)
- FE code: *MSC.Marc* (2010 release)

The results of the FE analysis are summarized in Figures 123, 124 and 125, where the equivalent plastic strain at the end of each step is shown respectively for steps 2, 3 and 4. Step 1 is not modeled as no plastic strain is applied to the head material in this step.

According to the manufactures experience, there may be some criticalities in the process, briefly listed below:

- Lack of filling
- Tolerances not obtained
- Die wear
- Die fracture
- Defects in the flange due to material failure.

The first four points are related to process control and tooling and do not refers specifically to the material. Only the last one is strictly related to the material behavior and to the excessive strain level reached during forming. The most critical point according to manufacturer is the flange tip (point “A” in Figure 125) where a free surface expansion during flange forming is experienced by the material.

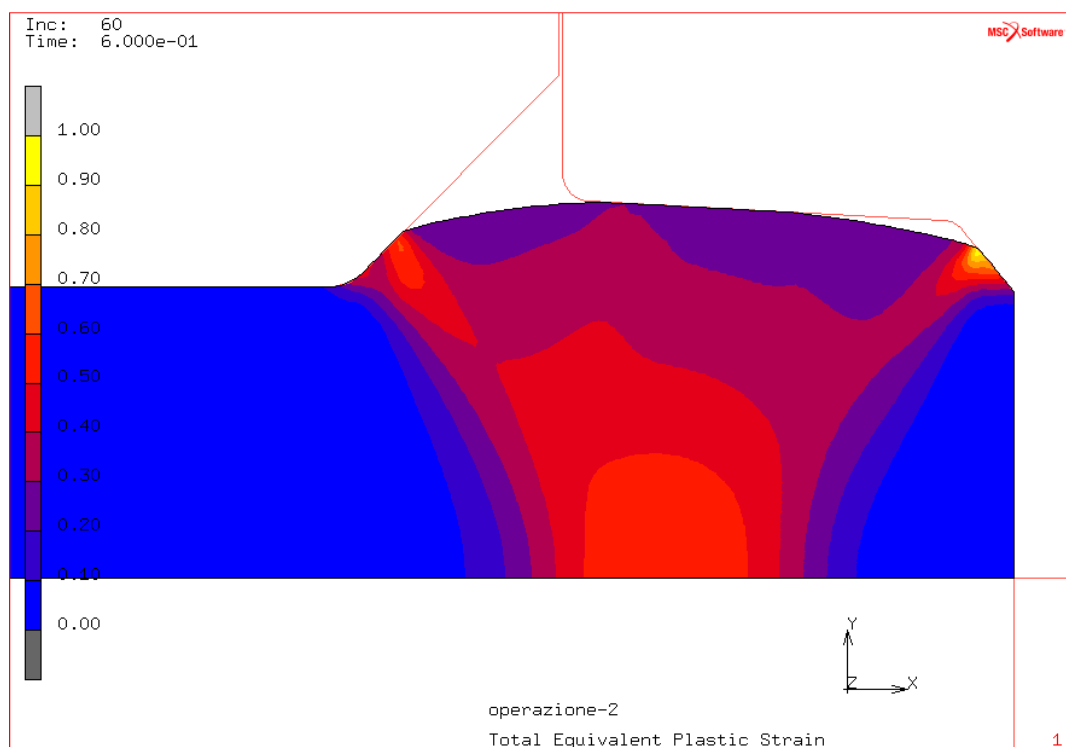


Figure 123: Equivalent plastic strain field at the end of step 2.

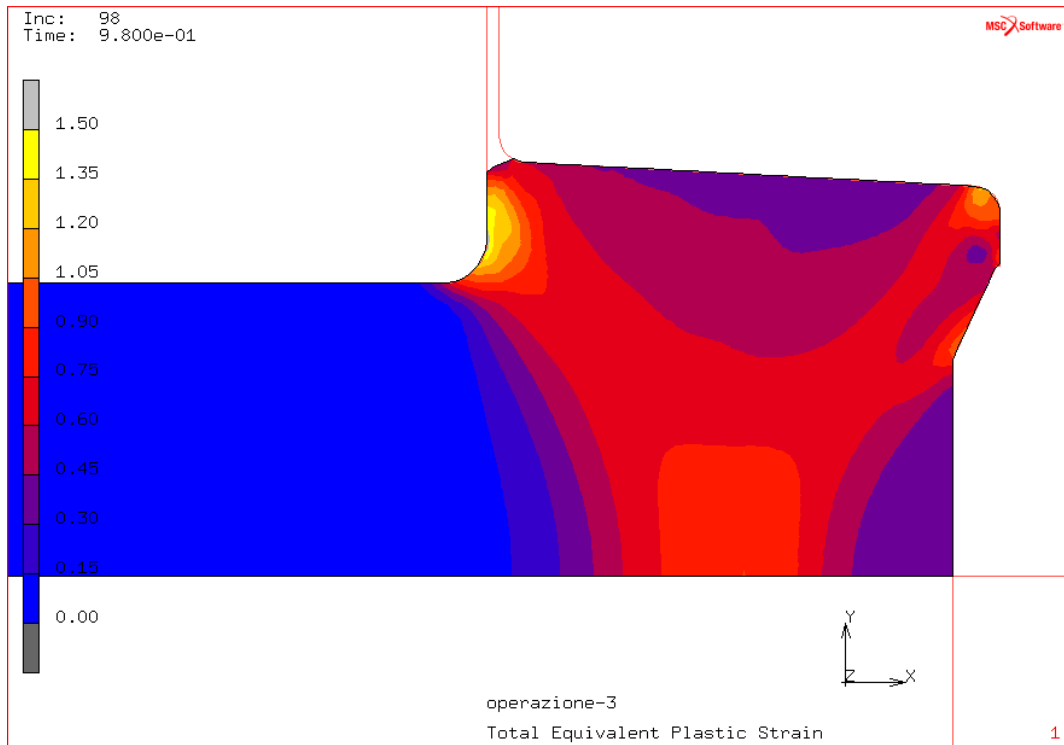


Figure 124: Equivalent plastic strain field at the end of step 3.

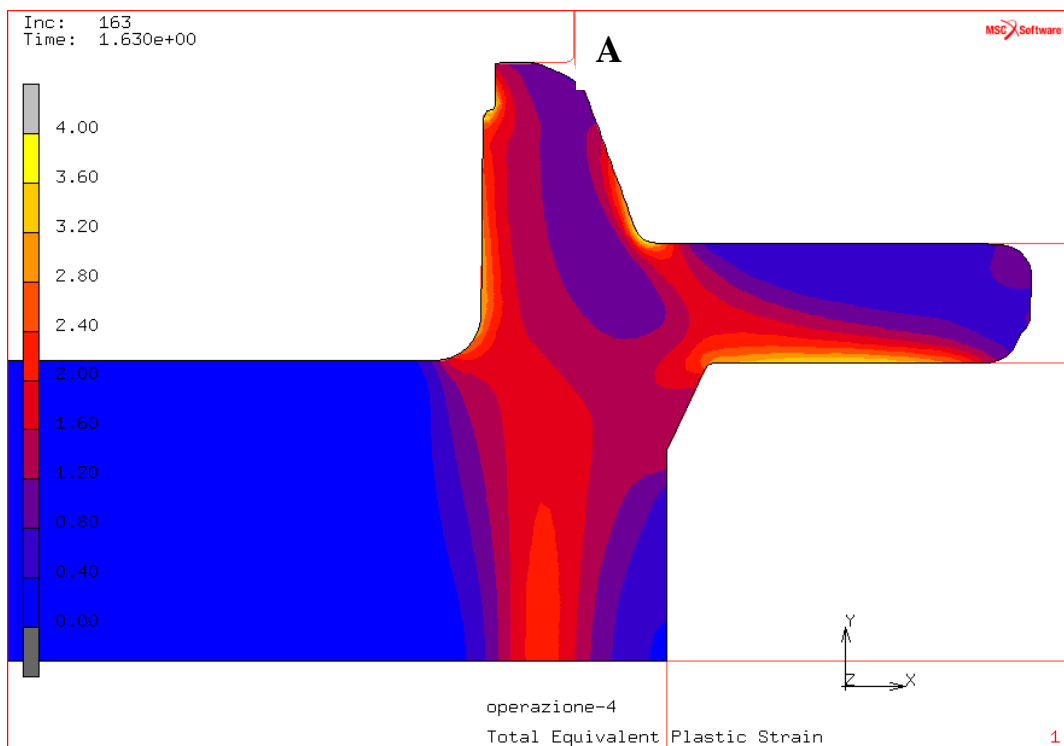


Figure 125: Equivalent plastic strain field at the end of step 4.

Stress and strain state identification

In order to define the most proper experimental laboratory test able to reproduce the material stress or strain limit in conditions comparable to those experienced in the forming process, it is necessary to study both stress and strain evolution at the most critical point in the screw head.

Having defined, according to experience, the typical critical area in the flange tip, the main tensor parameters have been plotted at that point as function of the process step.

The following stress/strain tensor parameters have been considered for the analysis:

- Maximum and minimum principal strain
- Stress triaxiality parameter (T)
- Deviatoric stress parameter (X)

The first two (max/min principal strain) are used in relation to investigate the material workability in compressive stress states. During upsetting the axial strain is compressive and hoop strain is tensile. These two components are usually plotted as in Figure 126. A range of strain combination may be obtained by simply altering the friction coefficient.

To extend the range of surface strains available toward the vertical, tensile axis, different specimen geometries may be used. By using a tapered bulge or a flange on the cylindrical surface (Figure 127), the axial compression causes expansion of core portion which expand the rim in hoop direction. So it is possible to amplify the axial effect on the hoop direction. Each combination of height h and thickness t gives a different ratio of axial to hoop strain, with different strain paths during the upsetting test. The different strain paths developed are summarized in Figure 128.

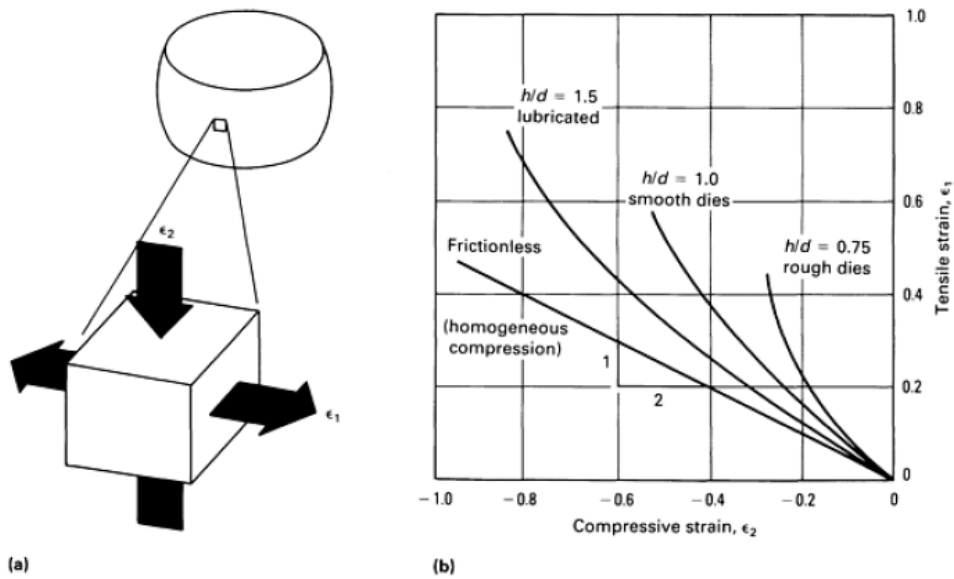


Figure 126: Strain evolution in the upsetting test.

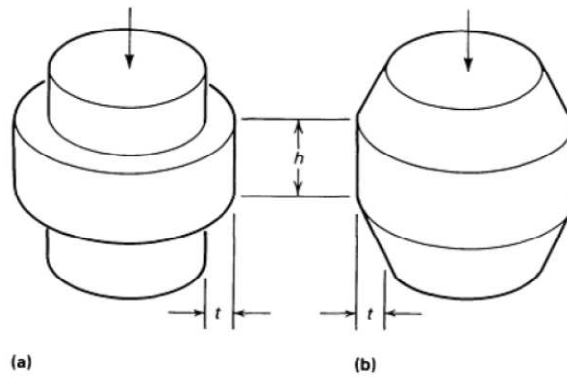


Figure 127: Flanged (a) and tapered bulged (b) specimens.

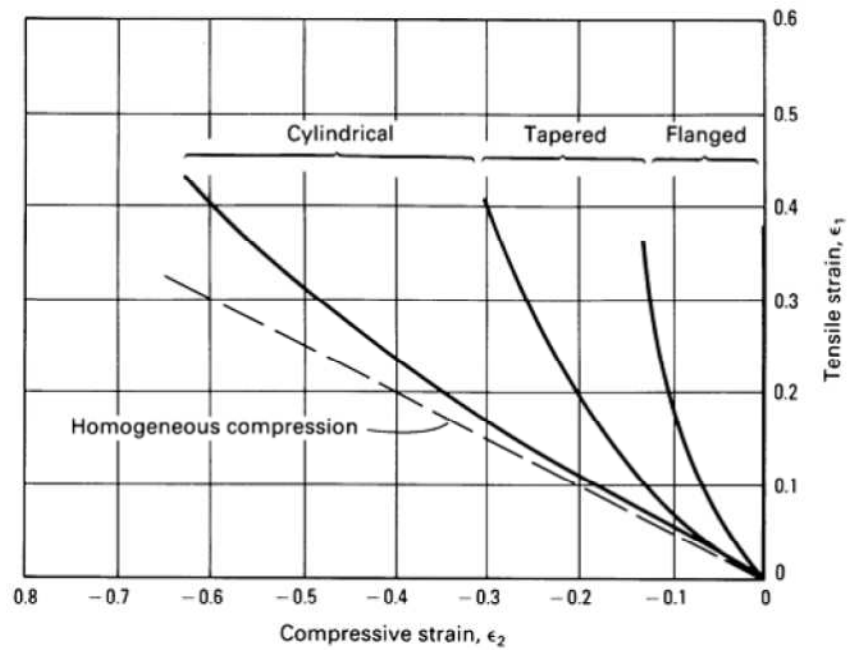


Figure 128: Strain evolution for different upsetting specimens.

By plotting the axial and hoop strain developed during the head forming steps at the flange tip, it is possible to obtain the actual strain history (Figure 129). Each forming step is identified by a different colour. So it is possible to observe that in step 2 and 3 the strain path is very similar to the ideal upsetting with small friction (axial to hoop strain ratio is a bit less than theoretical 2:1), while in step 4 becomes near to 1:2, so very similar to that of the tapered specimen.

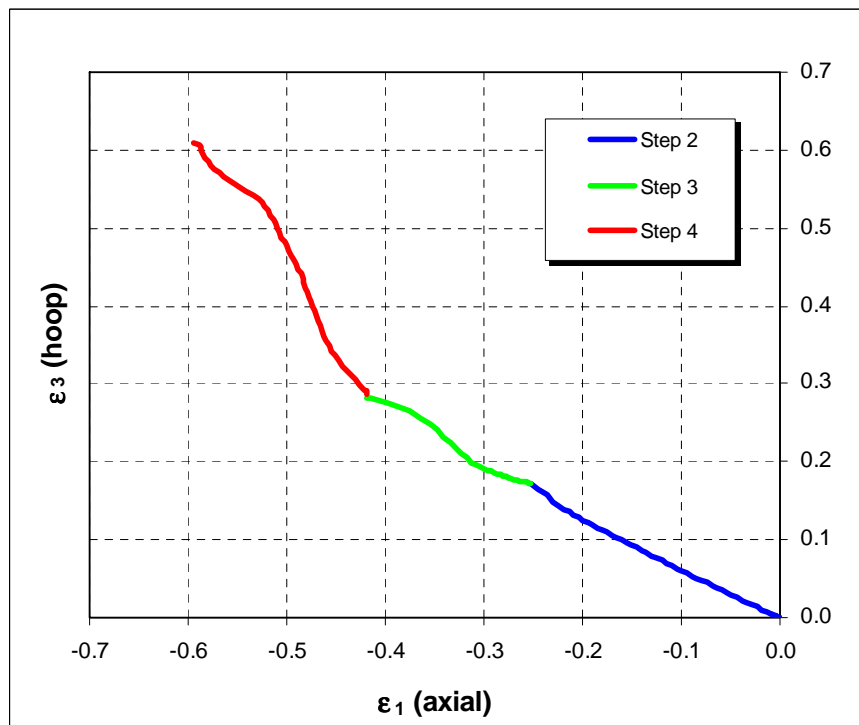


Figure 129: Strain evolution at the flange tip in screw head forming.

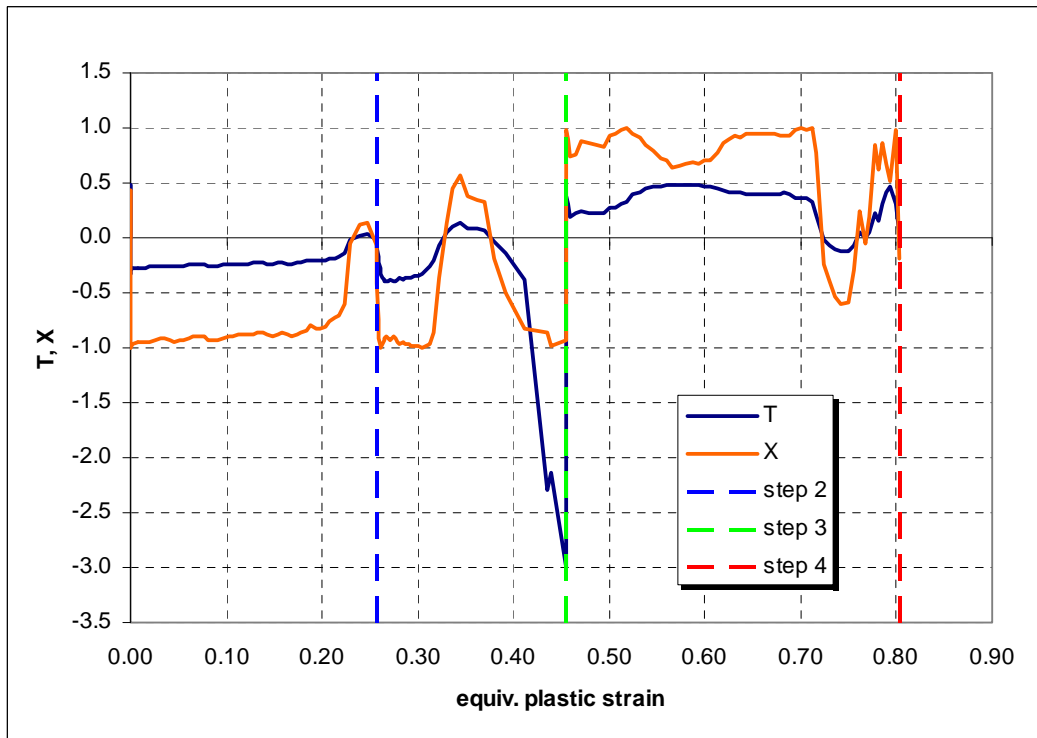


Figure 130: Stress parameters T and X evolution at flange tip during head forming.

The two other parameters investigated are the stress triaxiality (T) and the stress deviatoric parameter (X). For a detailed description of these two, refer to ref. [8]. As far as their influence on material ductility concerns, refers to next section. The two parameters evolution is plotted in Figure 130. it should be noted that:

- In step 4 (the critical one), the stress state is mostly at $0 < T < 0.5$ and $0.5 < X < 1$.
- In step 2 and 3 the stress state is mostly T near zero or highly compressive (end of step 3).

Mechanical test plan and specimen design

The specimen test plan to investigate the material ductility should be strictly linked to the aimed stress and strain state experienced at the material critical point in the forming process.

According to classical theories, plastic damage and ductile fracture limits depend on the triaxiality level of stress applied during the straining of the material. The first to recognize that the equivalent plastic strain to failure is influenced by the hydrostatic pressure was Bridgman. Recently proposed interpretations have introduced a more complete fracture strain dependence from the stress tensor by introducing a second stress parameter, named deviatoric, related to third invariant of the stress tensor deviator, or Lode angle. For a discussion on ductile fracture theories refers to [8].

Having understood that the stress state influences in a complex way the plastic damage evolution and the fracture strain, it is of primary importance to completely characterize the material in a wide range of stress conditions, different from the uniaxial one obtained in conventional tensile tests. Namely, it is important to apply different stress states during deformation; this to vary the triaxiality and deviatoric parameters respectively into an as wide range as possible.

We can recall here that any stress state may be represented by two stress parameters, called triaxiality (T) and deviatoric (X), defined as:

$$T = \frac{p}{\bar{\sigma}} = \frac{\sqrt{2}}{3} \frac{\xi}{\rho} \quad (1)$$

$$X = \cos(3\theta) = \frac{27}{2} \frac{J_3}{\bar{\sigma}^3} \quad (2)$$

To be noted that T may span in the full range $\pm\infty$, while X is confined in the interval $[-1; 1]$. For the same triaxiality T , we have at $X=1$ the maximum ductility (axysymmetric stress states, tensile tests), while at $X=0$ we have the minimum ductility (pure shear and plane strain states). So ductility, represented by the equivalent plastic strain to failure ϵ_f , is bounded between two limits in the plane $\epsilon_f - T$, named ϵ_1 (upper bound) and ϵ_0 (lower bound) corresponding to the extreme values of X . In a synthetic form, an example of ductile fracture limits are represented in Figure 131, together the main laboratory test types applicable to identify the strain limits.

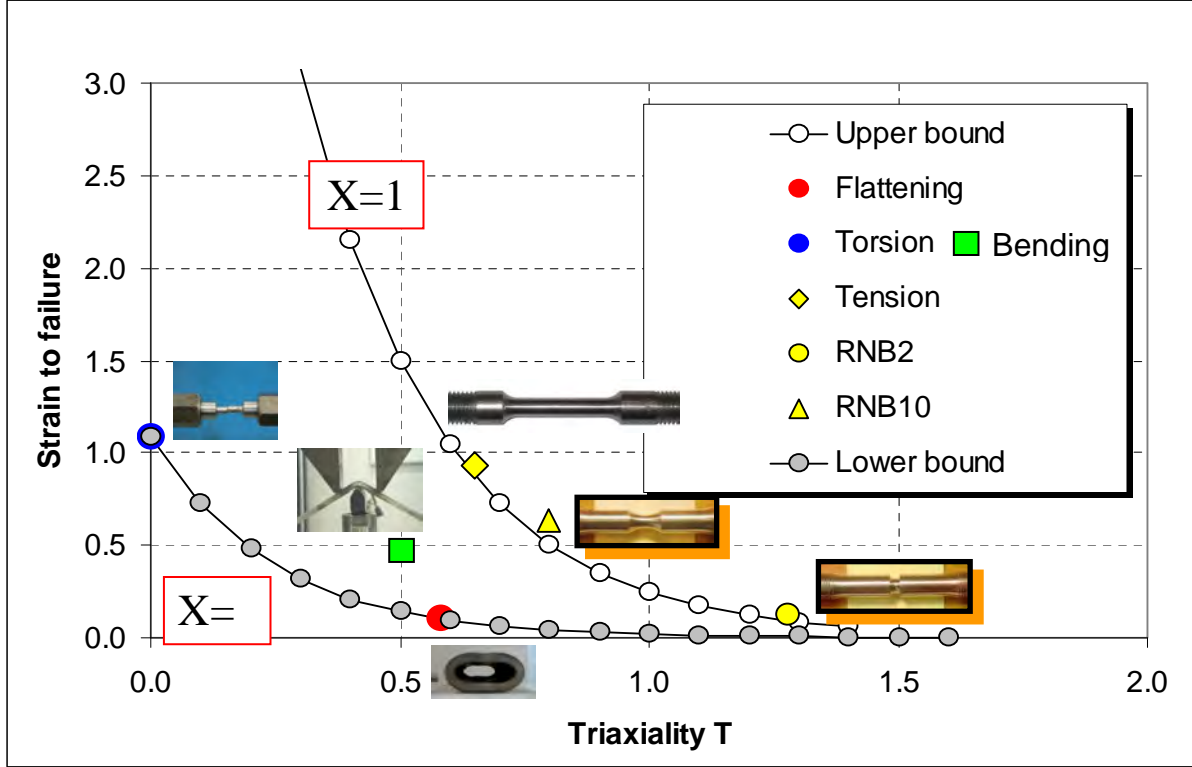


Figure 131: Example of ductile fracture locus.

Once the limits are identified, it is possible to associate to them a damage evolution law, which in the CSM proposed formulation is given by [8]:

$$D = \int_0^{\epsilon_f} \frac{f(T)}{g(X)^{1/n}} d\epsilon_p \quad (3)$$

where the two functions $f(T)$ and $g(X)$ are defined as:

$$f(T) = C_1 e^{C_2 T} \quad (4)$$

$$g(X) = \frac{\alpha}{\cos \left[\beta \frac{\pi}{6} - \frac{1}{3} \cos^{-1}(\gamma X) \right]} \quad (5)$$

When D reaches the value of 1 we have the failure, that is the material has reached its ductile fracture limit.

To be noted the typical values for T and X obtained in some typical specimen geometries, briefly listed in Table 54. Beside the stress parameters values, additional info are included. For instance, the tensile test is also used to obtain the complete stress-strain extended curve beyond necking. To note also the values for the compression-tapered specimen, which have been preliminarily obtained by some finite element simulations. In Figure 132 the strain path calculated for such specimen is plotted together the strain path at the flange tip in screw head forming. To be noted the same strain ratio (slope in the plot) in step 4.

The list of tests in Table 54 represents the guide for the mechanical test program aiming to obtain the strain limits for the candidate material.

Test type/specimen	Aim	T	X
Tensile – round bar	True stress – true strain curve Fracture strain	0.33 - 0.5	1
Torsion – round bar	Fracture strain	0	0
Tensile – round notched bar	Fracture strain	> 0.5	1
Compression – tapered	Fracture strain	0<T<0.3	1

Table 54: Test type and related stress parameters.

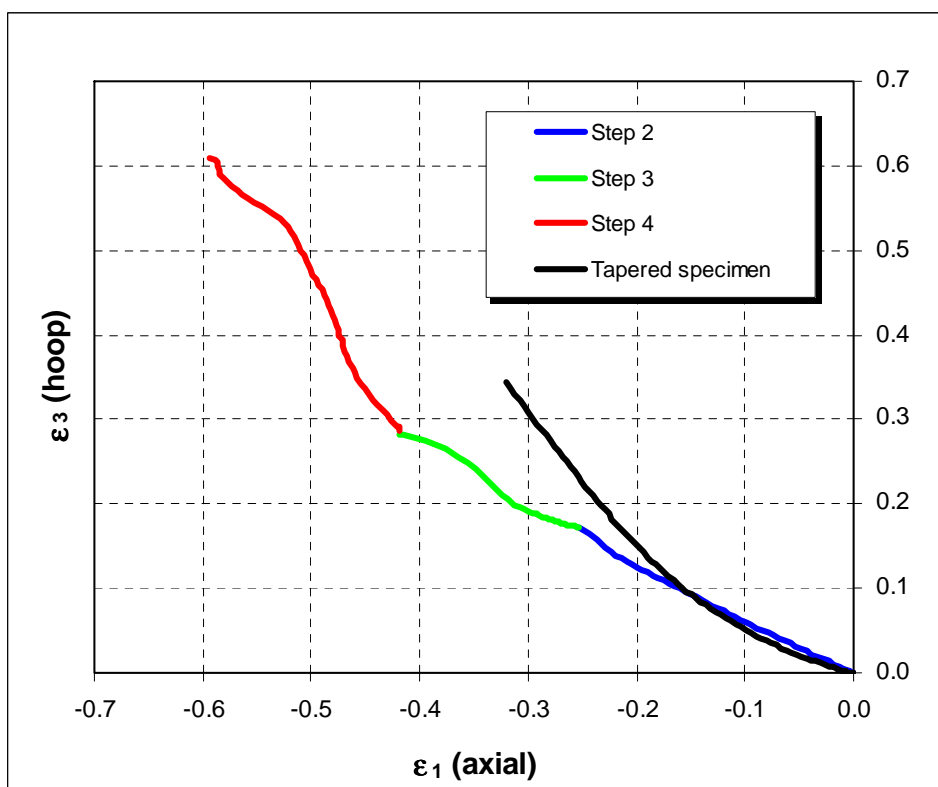


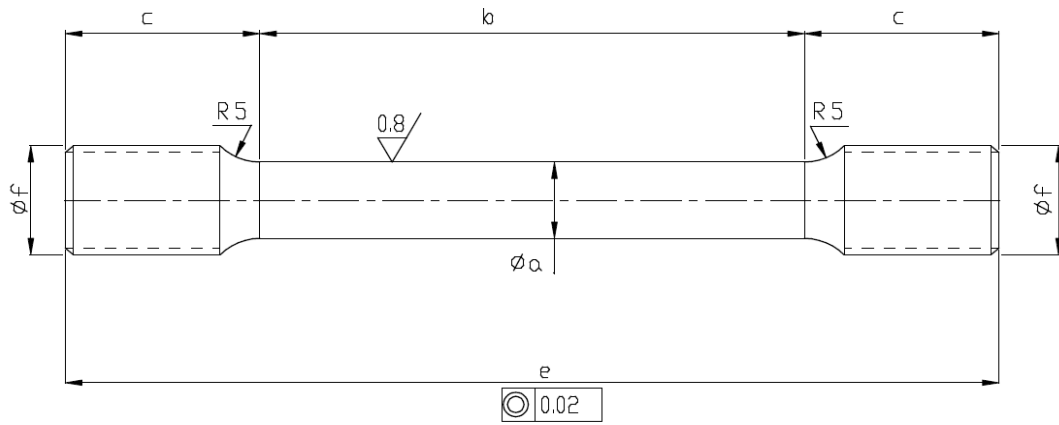
Figure 132: Strain path comparison for screw head forming and tapered specimen.

Material characterization

The steels under study are a 30MnB4 with UFG microstructure (named LN in the following) and the same steel with conventional microstructure (named ST). The first one has been rolled at TUBAF, and is supplied in as rolled and air cooled condition, with a resulting microstructure mean size of 3-4 μm . The second one is a standard wire rod in the as rolled and controlled cooling state, with a resulting microstructure mean size of 12 μm .

According to the available wire rod diameter, the following specimens have been prepared:

- Cylindrical smooth tensile (Figure 133)
- Tensile with round notch of 10 mm (RNB10, Figure 134)
- Tensile with round notch of 2 mm (RNB2, Figure 135)
- Torsion (Figure 136)
- Tapered compression (Figure 137)



tipo quote	A	B	C	D	E	F	G	H	I	L	M	N	O	P	Q	R	S	T
a	6	7	8	9	5	7	5	4	4	6.35	2.8	3	4	5	6	7	8	9
b	42	49	56	63	35	63	50	30	20	35	14	18	24	30	36	42	48	54
c	16	17.5	20	21.5	11	21.5	-	15	16	17.5	11.75	12.5	13	13	17	17	16	15.5
e	74	84	96	106	57	106	50	60	52	70	37.5	43	50	56	70	76	80	85
f	M10*	M10*1	M12	M12	M10*1	M12	M10*1	M6*0.75	M6*0.75	M10*1	M4	M6	M10	M10	M14	M14	M14	M14

Figure 133: Tensile test specimen.

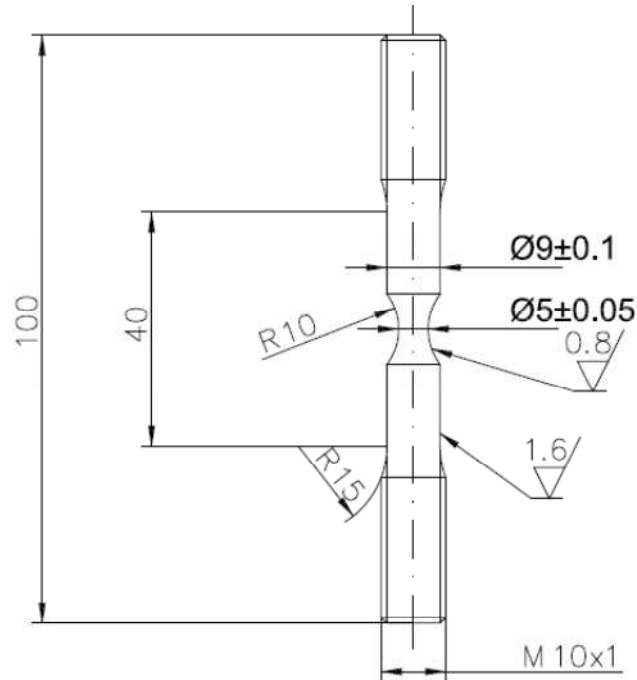


Figure 134: Tensile Round notched specimen RNB10.

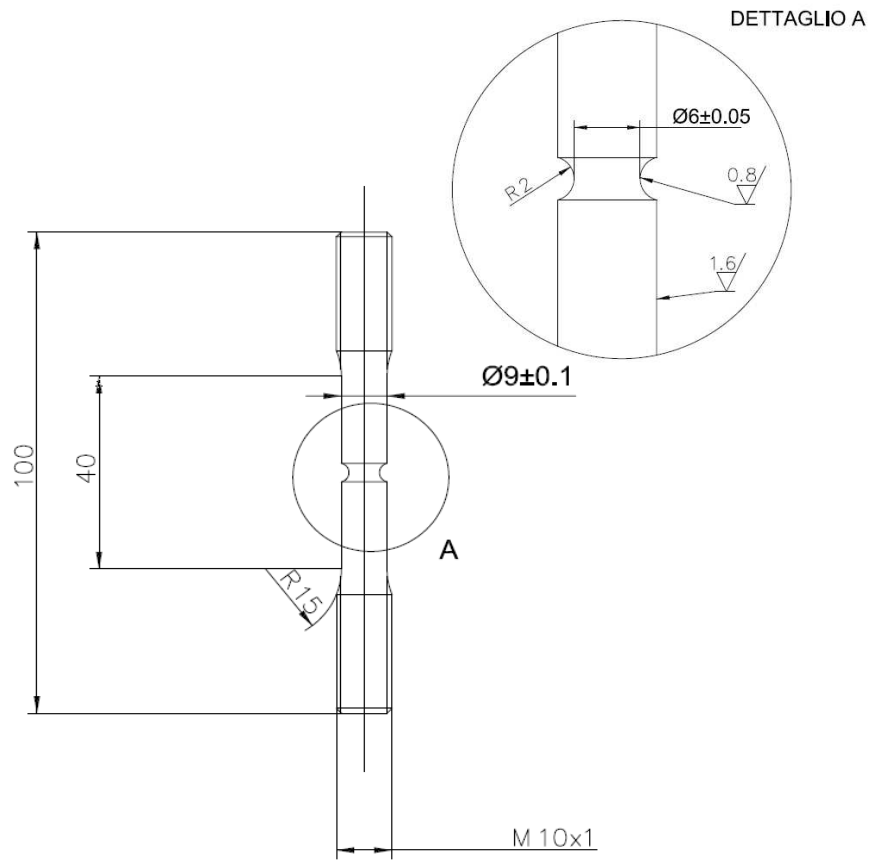


Figure 135: Tensile Round notched specimen RNB2.

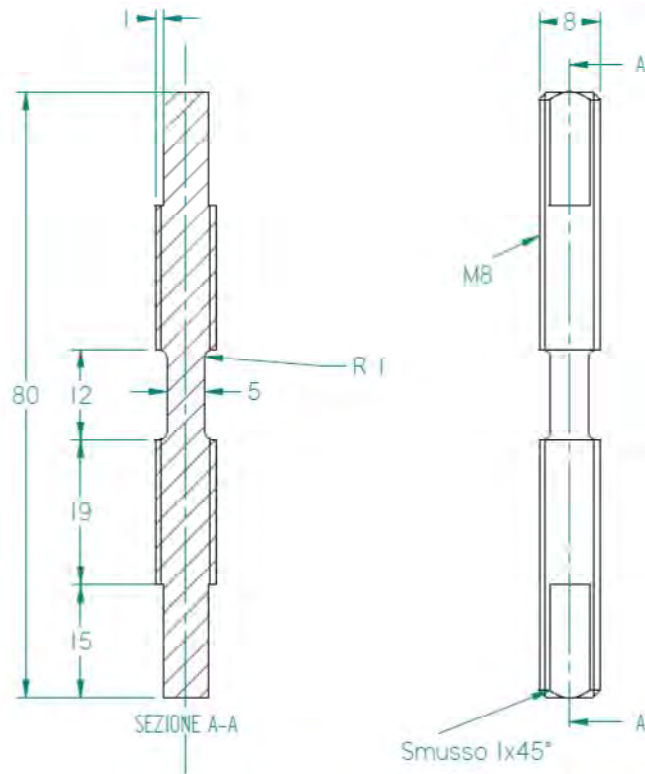


Figure 136: Torsion test specimen.

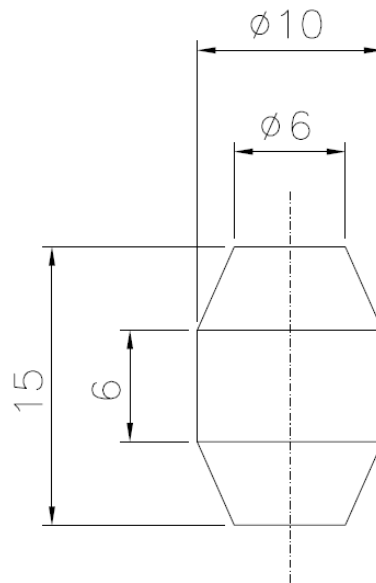


Figure 137: Compression tapered specimen.

Tensile tests on smooth and RNB specimens have been performed on a conventional testing frame. The following data have been recorded during the test: time, load, crosshead displacement, extensometer on the gauge length displacement. All signals have been acquired all along the test up to fracture, including the extensometer which wasn't removed after UTS, but maintained up to the end of the test. The aim is to obtain as first the true stress-true stress material curve extended up to fracture and the fracture strain at different triaxiality levels, induced by the different notch severity. The nominal strain rate applied is targeting the mean rate developed during the screw head forming.

Torsion tests have been performed on a dedicated frame. Time, torque and rotation angle have been recorded all along the test up to fracture. The aim is to obtain the fracture strain at zero triaxiality and deviatoric parameters.

Finally, the tapered specimens have been compressed at several height reductions and speed. The objective is to verify the material fracture limit in stress conditions similar to the forming process. Two specimens minimum for each test type have been performed. Tensile test results on smooth specimens are reported in Table 55.

Specimen id	LN-RB-1	LN-RB-2	ST-RB-1	ST-RB-2
Strain rate (1/s)	1.0	1.0	1.0	1.0
Yield point High (MPa)	679	696	562	555
Yield point Low (MPa)	646	659	514	493
UTS (MPa)	739	756	694	693
Plateau extension	2.4%		1.9%	
A%	19	20	23	20
Z%	63	59	58	57

Table 55: Tensile test results.

The load-extensometer data from tensile test have been elaborated in terms of logarithmic stress and strain up to necking in the conventional way. To determine the extended beyond necking stress-strain curve the inverse calibration method has been adopted [7].

The extended curves for the two steels are reported in Figure 138.

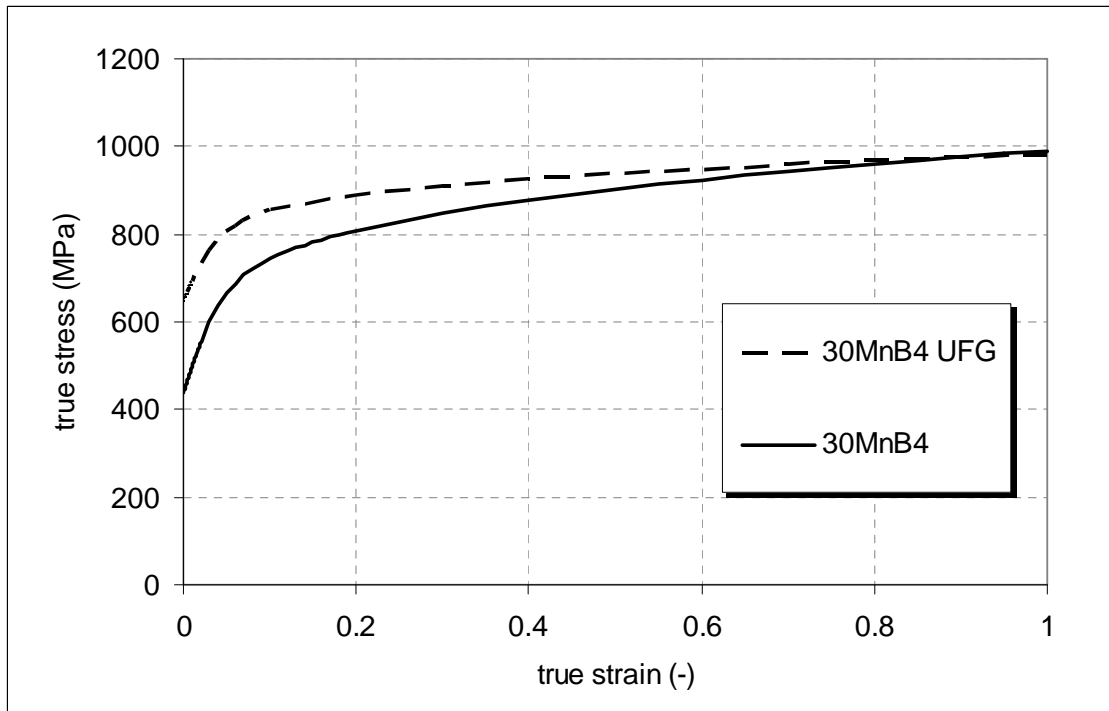


Figure 138: Extended true stress-true strain curve.

RNB2 and RNB10 tests don't need data manipulation, as only the load-displacement curve is needed to be compared with the finite element simulation. The measured displacement at fracture is used to stop the simulation and evaluate from the same the stress parameter history and the equivalent plastic strain. As triaxiality is not perfectly constant through the tensile tests, the mean value as to be evaluated, according to the procedure indicated in [7].

About torsion tests, torque-rotation angle data are converted directly in strain, and in particular only the final value at fracture is used for the damage model identification. In this case Triaxiality and deviatoric parameter are always zero, all along the test.

Compression tests have been performed at different height reductions and speed, to investigate possible strain rate effects on fracture tendency (Table 56). The final height is used as reference point to stop the simulation and, as before, to evaluate the stress parameters and strain history during the loading path.

Specimen id	TAP-1	TAP-2	TAP-3	TAP-4	TAP-5
Strain rate (1/s)	0.1	0.1	0.5	0.1	1.0
Height reduction $100 \times \Delta H / H_0$	80%	55%	80%	65%	65%

Table 56: Compression test results.

Height reduction 80%

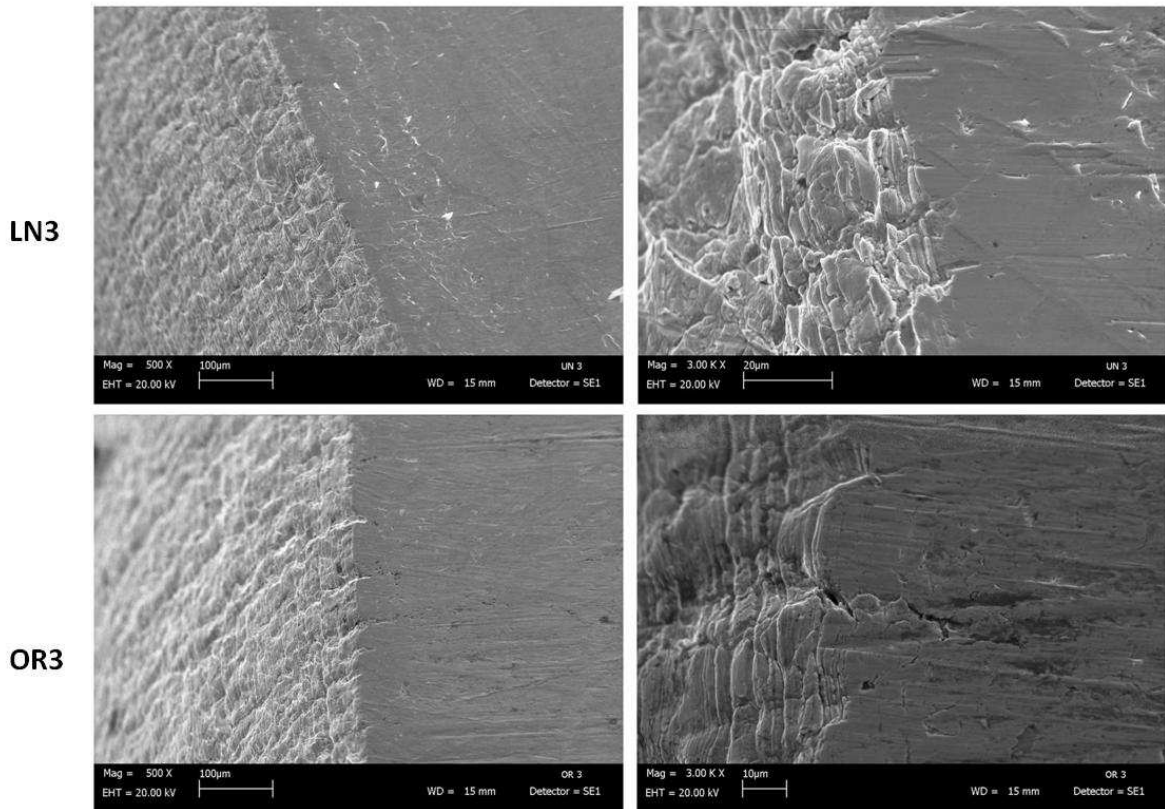


Figure 139: Visual cracks for different compression conditions and materials.

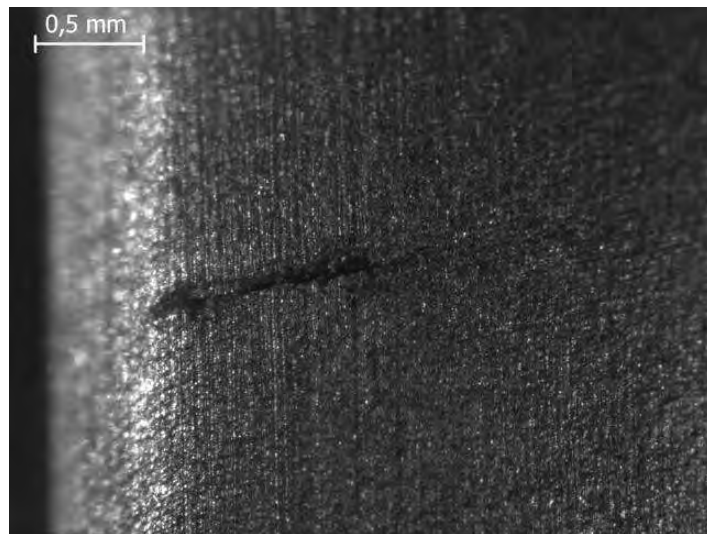


Figure 140: Visual cracks for TAP 1 standard sample.

No visual macro cracks have been observed in any of the LN specimens (Figure 139), while a crack was detected in specimen TAP-1 of steel ST (Figure 140).

In addition from SEM observation it was noted that the ST material presented more micro-cracks on the edge if compared to LN one (Figure 139).

Plastic damage evaluation

The parameters for the damage model in eq. (3) and functions in eq. (4) and (5) have to be identified by fitting on experimental data obtained from the fracture tests described previously.

By using the finite element modelling, each test type for both materials has been simulated to calculate the stress parameters T and X evolution together the equivalent plastic strain. By using mean values

along the loading path according to [7, 8], the following results have been obtained, summarized in Tables 57 and 58.

	Tm	Xm	$\bar{\epsilon}_{pl}$
Tension	0.59	1	0.99
RNB10	0.77	1	0.72
RNB2	1.24	1	0.43
Torsion	0	0	1.07

Table 57: Fracture strain summary for steel LN.

	Tm	Xm	$\bar{\epsilon}_{pl}$
Tension	0.51	1	0.84
RNB10	0.69	1	0.69
RNB2	1.1	1	0.4
Torsion	0	0	1.0

Table 58: Fracture strain summary for steel ST.

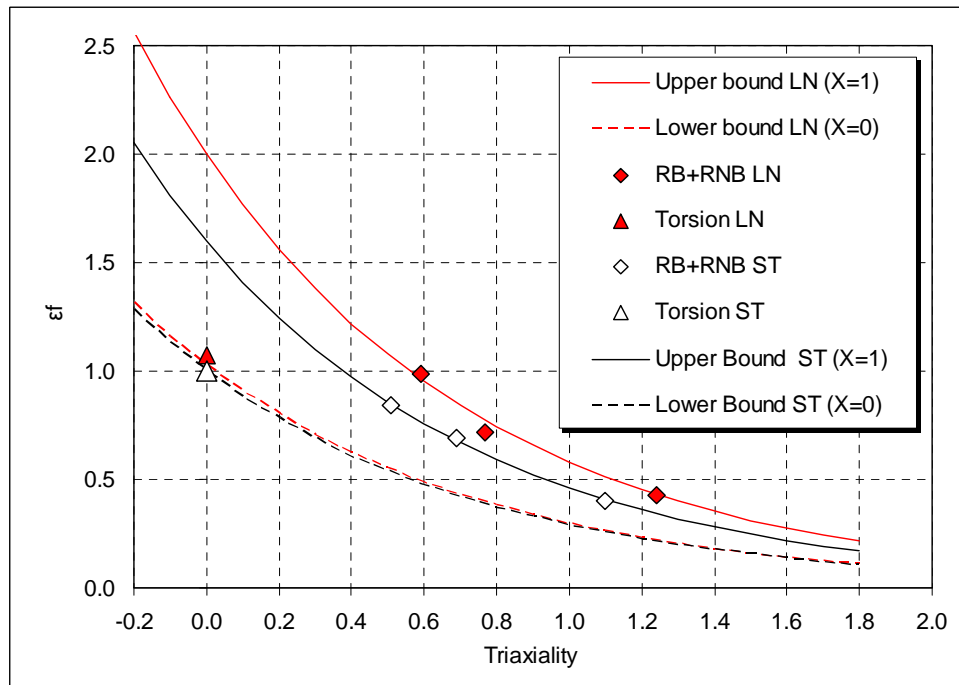


Figure 141: Fracture locus for steel LN and ST.

The six damage parameters in eq. (1) to (3) are obtained by fitting on all the four tests in Tables 57 and 58, except for n which is obtained directly from the tensile test. The fracture locus for the two steels, described analytically by eq. (1), is represented in Figure 141. The list of parameters for the fracture locus of the two steels LN and ST is reported in Table 59.

By using the identified damage model, it is possible to evaluate the plastic damage accumulation during the head screw forming and in the compression tapered specimen.

The loading path for both cases is elaborated calculating the damage parameter D accumulation, according to eq. (1) and using the constants in Table 59. The plots of the damage parameter D evolution as function of equivalent plastic strain during the compression test or the head screw forming are reported in Figure 142 and 143.

	<i>LN</i>	<i>ST</i>
C_1	0.51	0.41
C_2	1.24	1.24
n	0.07	0.15
α	0.955	0.866
β	1.0	0.754
γ	0.79	1.0

Table 59: Damage model parameters for steels LN and ST.

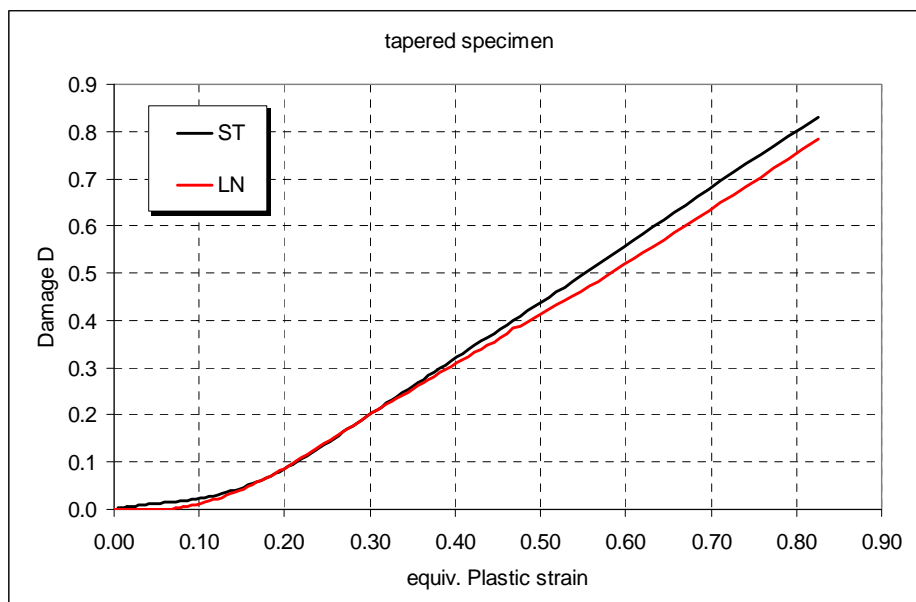


Figure 142: Damage evolution for steel LN and ST during compression test.

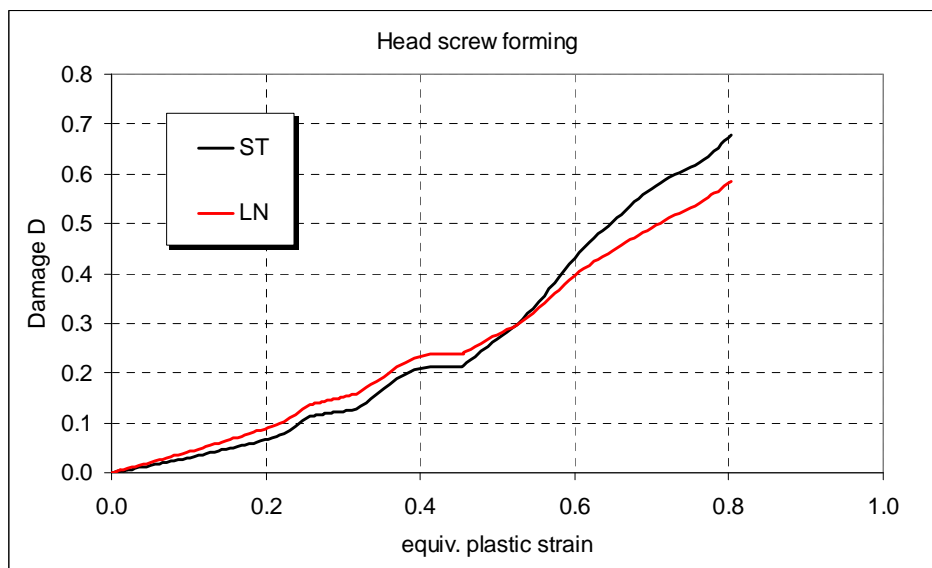


Figure 143: Damage evolution for steel LN and ST during head screw forming.

It can be noted that the material ST accumulates more plastic damage respect to material LN in both cases. It is also noted the compression test is more severe respect to the forming process, leading to an higher damage in the critical point. The parameter D doesn't reach the value of $D=1$ (which means failure) in any case, but it is more than 0.8 for ST material in compression test. This means that any small deviation in geometry or any small local defect in the material may generate a crack initiation more likely in the ST steel respect to the LN steel. This is confirmed by the compression test results. In fact LN steel didn't show any defect in any condition, while ST steel exhibited a surface crack in the barrelled region in test TAP-1.

The forming process is less critical, also confirmed by the fact that the conventional 30MnB4 steel (ST) is usually formed without criticalities. Also in this case it has to be noted that the UFG steel (LN) should have an higher safety margin respect to the conventional ST.

Task 3.4 – Industrialization trials on pilot plants and/or industrial plants

An experimental industrial heat of 30MnB4 (UNI EN 10263-4), has been produced at ORI MARTIN and the material was hot rolled to wire-rods of 8 and 14 mm as agreed with Agrati for the future production of prototype screws. The steel was hot rolled according to the process indications suggested from the results after hot rolling in TUBAF pilot mill.

Together with Agrati and CSM it was decided to hot roll wire-rods of 8 and 14 mm for fabrication of M8 e M14 prototype screws, in particular were produced:

- 8 billets for 14 mm diameter coil
- 6 billets for 8 mm diameter coil

The industrial plant of ORI MARTIN is reported in Figure 144.

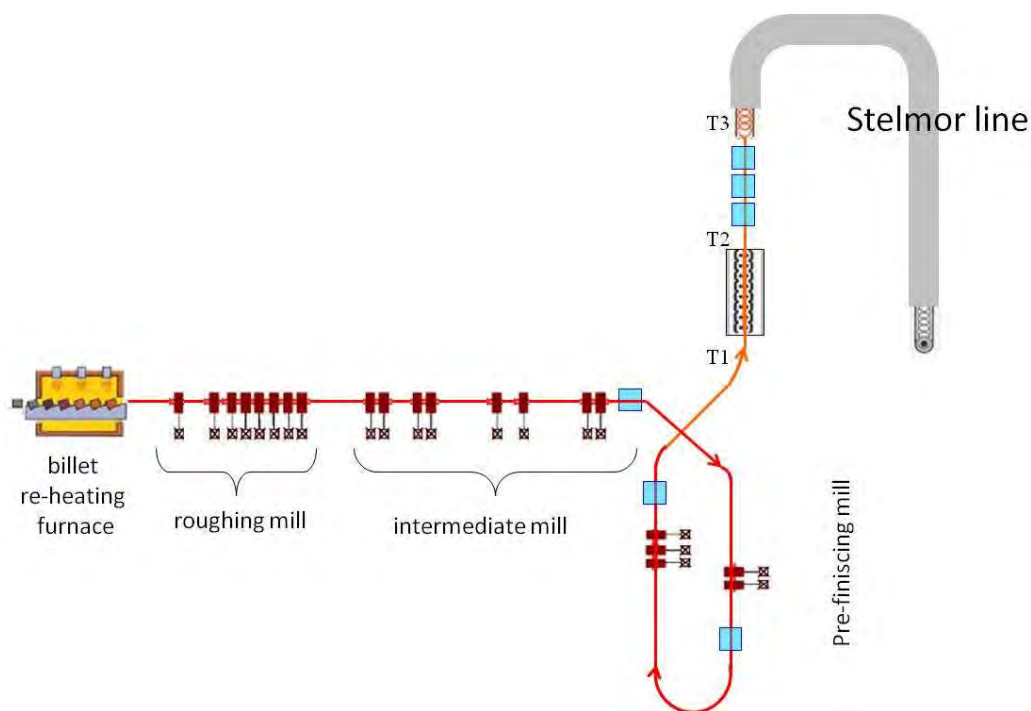


Figure 144: ORI Martin Industrial Plant.

It is formed by a reheating billet furnace, a roughing mill, intermediate mill, pre-finishing mill and a finishing mill (BGV) identified in Figure 144 between T1 and T2, and before entering in the Stelmor line there are some cooling systems. The temperature at finishing mill entry (T1) can be controlled by tuning the cooling devices before BGV (light blue boxes) in order to get at the entrance the requested temperature.

The indication come out from the pilot mill experimentation was to lower the temperature at finishing mill entry (T1 at BGV) in order to obtain a finer prior austenite grain size. The finishing mill has enough power to roll at low temperatures (up to 750°C). After the finishing mill and a cooling device, a Stelmor line allows to control the cooling (in particular, to perform slow cooling).

ORI MARTIN hot rolled the billets monitoring the following temperatures (indicated in Figure 144)

- BGV entry (T1), whose target temperature was 780°C
- BGV exit (T2)
- Laying Head - Stelmor entry (T3)

The Figures 145a and 146a show the evolution of the T1, T2 and T3 temperatures for all the produced billets and the Figures 145b and 146b show a more detailed graph of a single billet.

Samples from all the billets were sent to CSM for microstructural characterization. The billet chosen for a deeper characterization are indicated by the arrows in the figures. All the billets were sent to AGRATI to be transformed in screws as reported in (WP5).

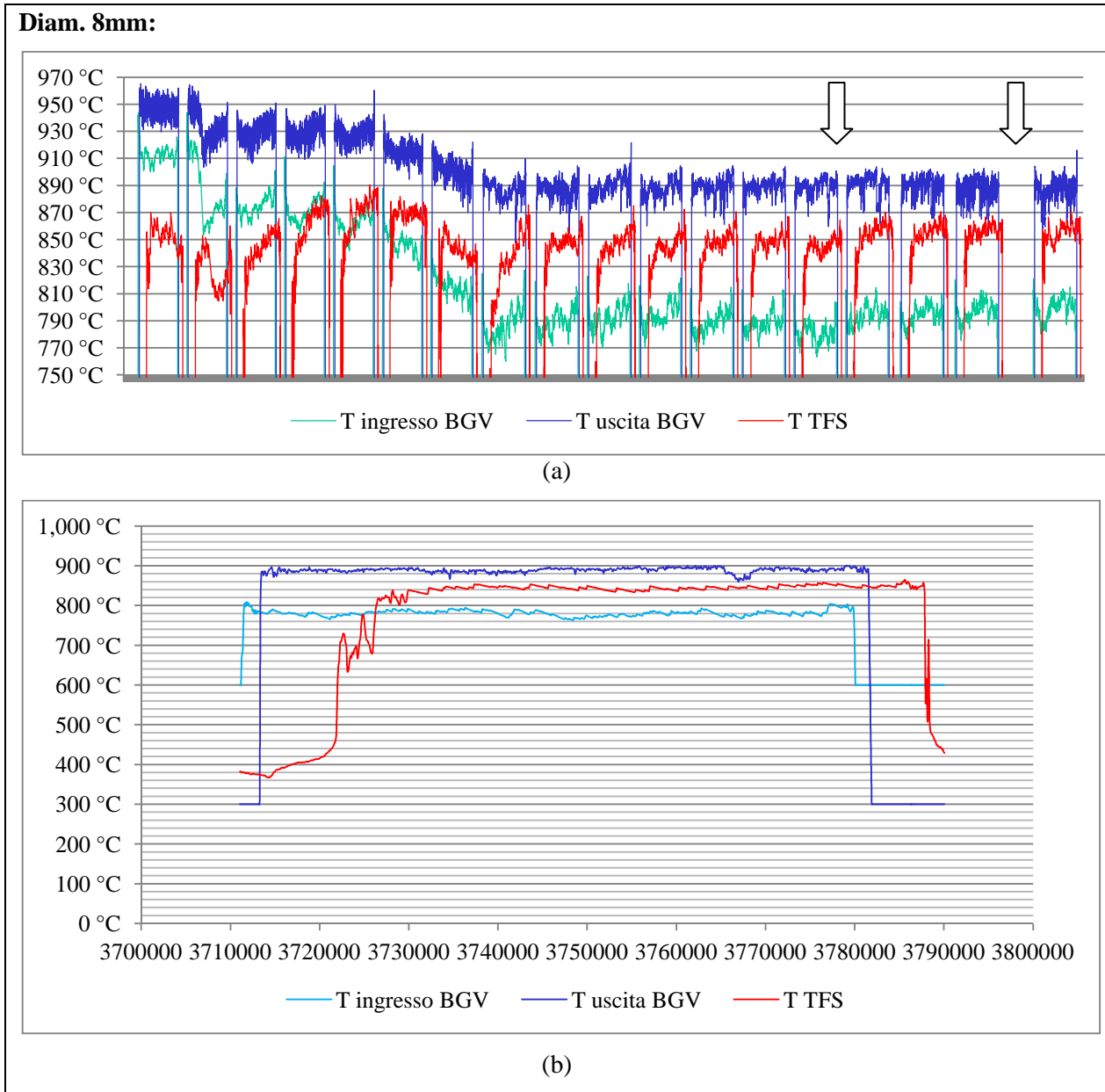
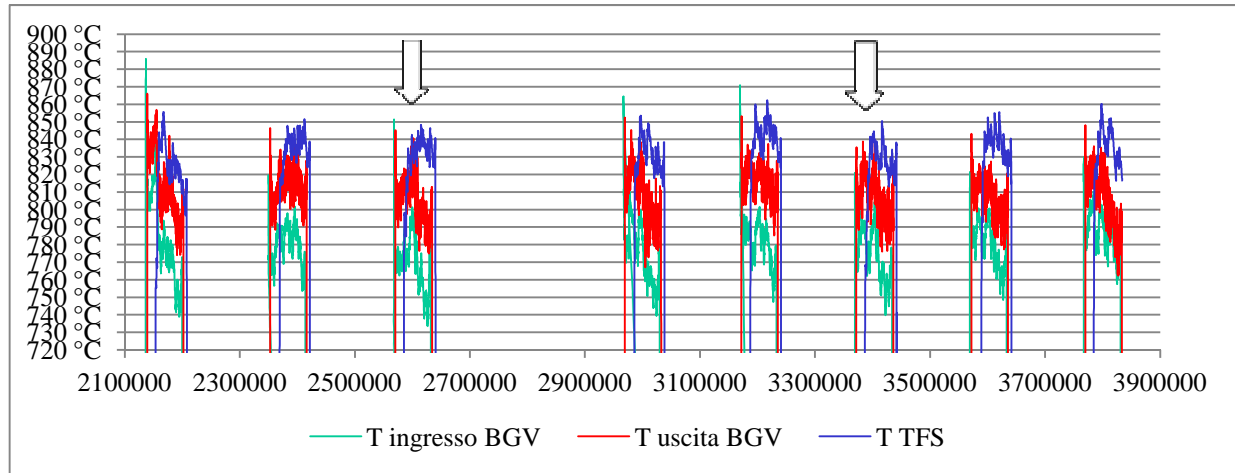
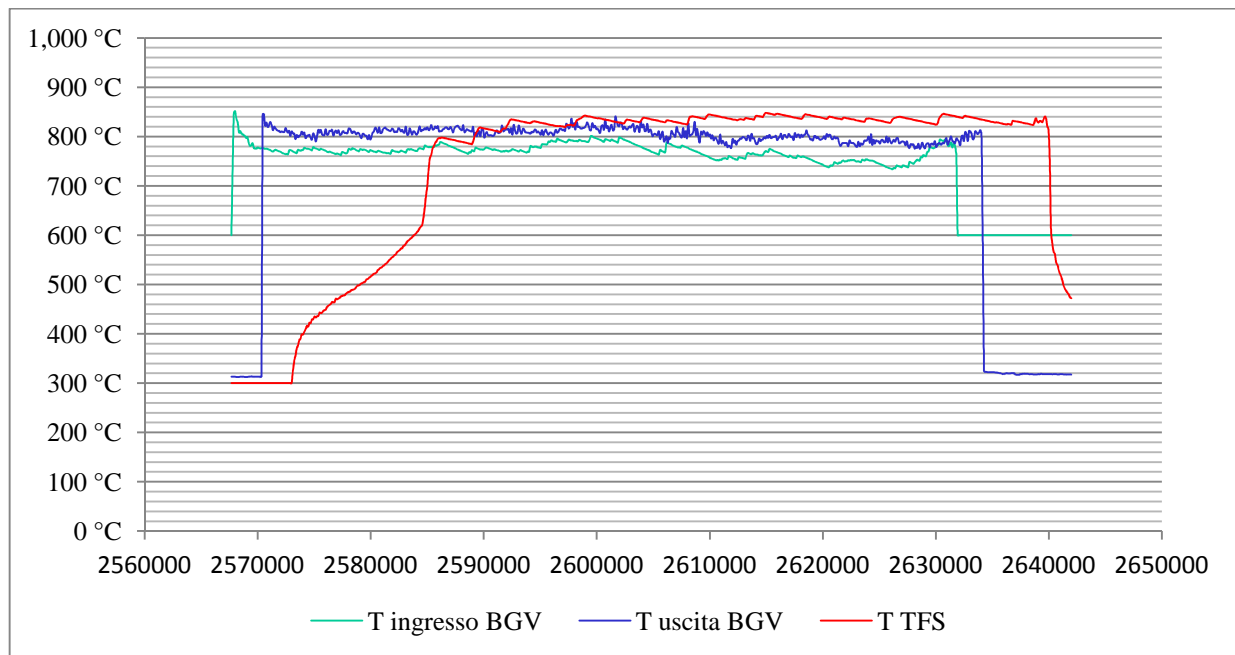


Figure 145: (a) Temperature evolution for each fabricated billet of 8mm diameter (T1 green line, T2 blue line, T3 red line), (b) example of temperature evolution of a single billet (T1 light blue line, T2 blue line, T3 red line).

Diam. 14mm:

(a)



(b)

Figure 146: (a) Temperature evolution for each fabricated billet of 14mm diameter (T1 green line, T2 blue line, T3 red line), (b) example of temperature evolution of a single billet (T1 green line, T2 blue line, T3 red line).

Samplings at T1, T2, T3 points were carried out in order to analyse the microstructural evolution at different points. In Figure 147 the microstructural characterization of material before entering in the finishing line (BGV) is reported. Measured temperature was around 780°C and the samples were cut and quenched. Prior austenite grain size ranged around 10-12 μm and it was the desired size.

In Figure 148 the microstructures of quenched samples after the finishing line (BGV), after passing the cooling devices and before entering the Stelmor line are reported. Microstructures are different ranging from martensite to ferrite to pearlite.

In Figures 149 and 150 microstructures of wire rods final product of 14 mm and 8mm diameter respectively, for different coils sampling, are reported. Microstructure is fully composed by ferrite and pearlite, in particular the 14mm wire rod showed 63% ferrite and 37% of pearlite. The average ferrite grain size was 7.2 μm . For the 8mm wire rod showed 79% ferrite and 21% of pearlite. The average ferrite grain size was 7.0 μm .

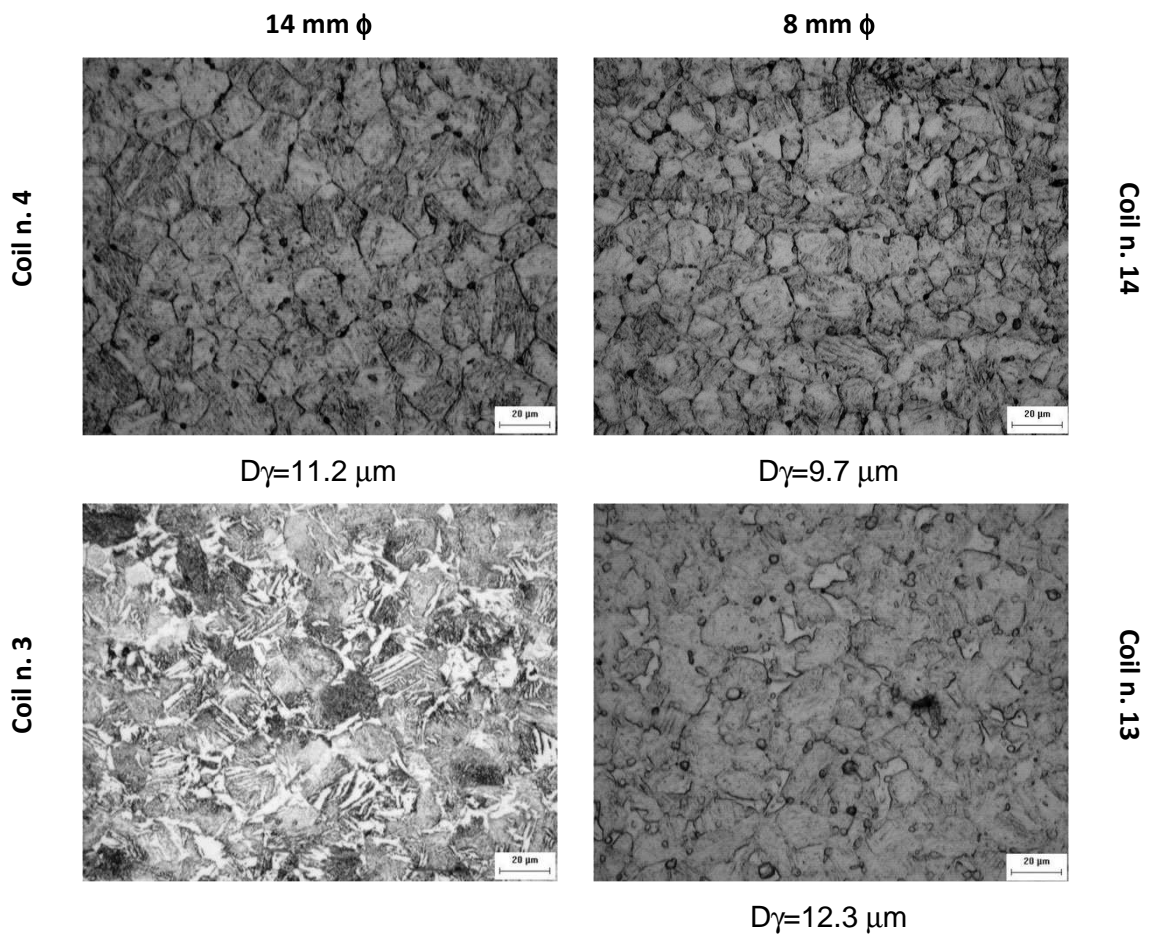


Figure 147: Prior austenite grain size of quenched samples before entering in the finishing line (BGV).

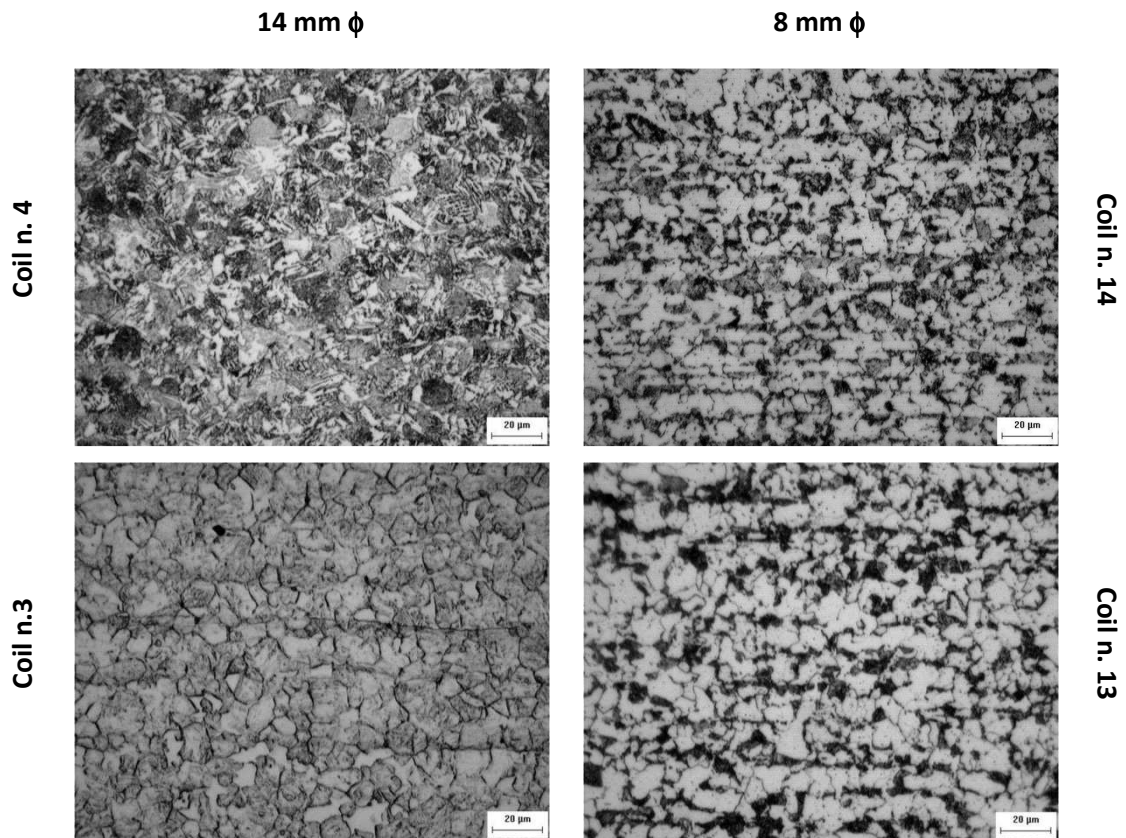


Figure 148: Microstructure of quenched samples after the finishing line (BGV) and before entering the Stelmor line.

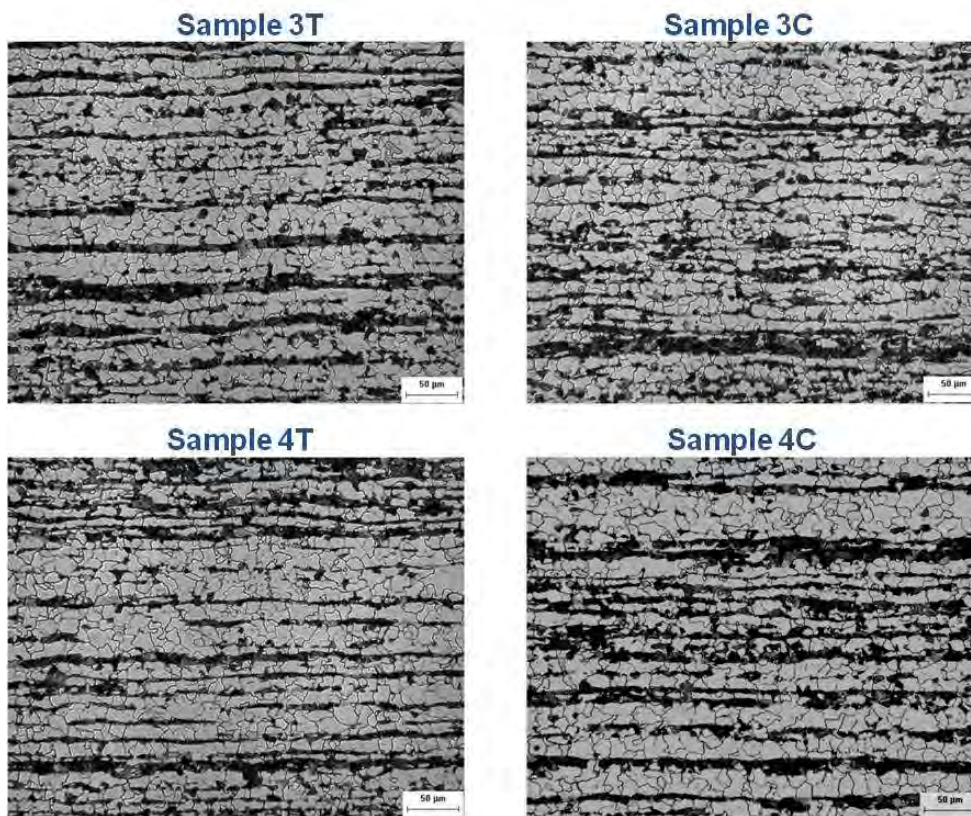


Figure 149: Microstructure of wire rods final product of 14 mm diameter (different coils sampling).
 $D_{\text{ferr}}=7.2\mu\text{m}$, $Fv_{\text{ferr}}=63\%$, $Fv_{\text{pearlite}}=37\%$.

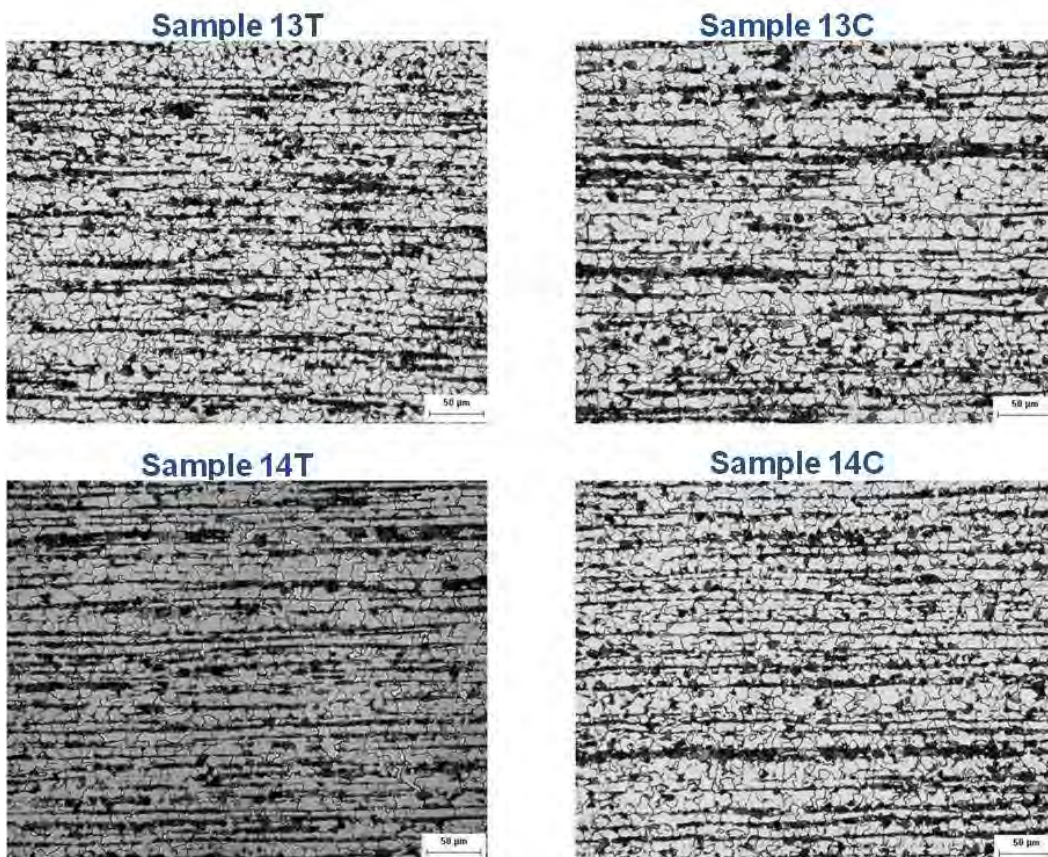


Figure 150: Microstructure of wire rods final product of 8 mm diameter (different coils sampling).
 $D_{\text{ferr}}=7.0\mu\text{m}$, $Fv_{\text{ferr}}=79\%$, $Fv_{\text{pearlite}}=21\%$.

The conventional material grain size produced by ORI Martin is around 12 μm . It means that only decreasing the entrance temperature at finishing mill helps to almost halve the final grain size, even if it is not enough to arrive at ultrafine range ($< 4\mu\text{m}$). To further decrease the grain size it is necessary to act on the deformation at finishing mill and to modify the cooling pattern.

Conclusions

Production of UFG steels at TUBAF pilot mill

Experimental production of long UFG steels was carried out on pilot rolling on the Two-high rolling mill and continuous rolling mill at TUBAF

The rolling trials were divided in two groups:

- Rolling of steels 18CrMo4 and 50SiMoVNb8 on the continuous rolling mill whose aim was to study the influence of the rolling speed and finish rolling temperature on the microstructure and mechanical properties;
- Rolling of steels 18MnB2 and 30MnB4 on the roughing reversing mill of the continuous line whose aim was to study the influence of finish rolling temperature on the microstructure and mechanical properties.

Different thermomechanical processes have been tested in order to optimise the material properties and the production process.

For all the tested steels, wire rods whose microstructure showed ultrafine ferrite grains ranging from 2-4 μm were produced.

The trend of 18CrMo4 steel average grain size is to decrease with the finishing rolling temperature and with increasing the rolling speed (6-20m/s).

Regarding 30MnB4 and 18MnB2 same results as before can be assessed. In particular ferrite grain size is fine for all the hot rolling temperatures and decreases with the hot rolling temperature.

For 50SiMoVNb8 steels both hardness and average grain size have not a clear trend, however the difference for the hot rolling speed 12-20 m/s is not meaningful.

Parametric investigation of relationship between microstructural features and cold formability in the new UFG long steels

The aim of Task 3.3 was to investigate the relationships between steel microstructure and plastic deformation behavior of the material. The main feature to be considered is ferrite grain size, in particular the study focused on the comparison between steel with conventional and ultrafine microstructure. Among the steel grades which are the subject of the project, medium-carbon steel for fastener has been selected (30MnB4).

The results of the mechanical tests allowed to build the ductility curves (strain to failure vs. triaxiality) related to the different microstructures (conventional vs. UFG) to be used to simulate cold forming taking into account the material damage.

By using the identified damage model, it was possible to evaluate the plastic damage accumulation during the head screw forming and in the compression tapered specimen.

It can be noted that the conventional 30MnB4 steel accumulates more plastic damage respect to UFG 30MnB4 steel.

It is also noted the compression tests, that have been used for building the ductility curves, are more severe respect to the forming process, leading to a higher damage in the critical points.

This means that any small deviation in geometry or any small local defect in the material may generate a crack initiation more likely in the conventional steel respect to the UFG steel. This is confirmed by the compression test results. In fact UFG steel didn't show any defect in any condition, while the conventional steel exhibited a surface crack in the barrelled region in one of the tests. The screw forming process is less critical, also confirmed by the fact that the conventional 30MnB4 steel is usually formed without criticalities. Also in this case it has to be noted that the UFG steel should have an higher safety margin respect to the conventional one.

Industrial production of UFG steel

Industrial production of long UFG steel was carried out at ORI MARTIN industrial plants. The chosen chemical composition was 30MnB4.

The material was hot rolled to wire-rods of 8 and 14mm diameter as agreed with Agrati for the next production of prototype screws (WP5). The steel was hot rolled according to the process indications suggested from the results after hot rolling in TUBAF pilot mill.

The indication come out from the previous experimentation was to lower the temperature at the finishing mill entry in order both to obtain a small prior austenite grain size and to do finishing rolling in a DIFT range. It could be done tuning the cooling devices before finishing mill in order to get at the entrance the requested temperature.

Results showed that the average grain size of final product industrially produced was 7 μm .

The conventional material grain size produced by ORI Martin is around 12 μm . It means that only decreasing the entrance temperature at finishing mill helps to almost halve the final grain size, even if it is not enough to arrive at ultrafine range ($< 4\mu\text{m}$). To furtherly decrease the grain size it is necessary to act on the deformation at finishing mill and to modify the cooling pattern.

2.4 WORK PACKAGE 4:

EVALUATION OF UFG STEELS THROUGH MICROSTRUCTURAL AND MECHANICAL CHARACTERIZATION

In this WP the steels produced according the new hot rolling practices defined in WP2 and applied in WP3 (UFG steels), from pilot mill and industrial plant, have been characterized in terms of mechanical and microstructural properties as well as, when it is required by the application, the response to fatigue and machining. The characterization has been carried out in comparison with the current material used for the same application. For each subject (static mechanical properties, response to fatigue, response to machining) the results are reported separately for those steel grades applications for which the respective properties (tensile, fatigue, machinability) are relevant.

Task 4.1 - Static mechanical properties

Fasteners (carbon range 0.15-0.30 %)

As reported in the previous section devoted to WP3, two different wire rod diameters were selected to be hot rolled on Ori Martin wire rod mill, in the process conditions which were identified to obtain an ultrafine microstructure (temperature at finishing block entry as low as 780 °C). Such diameters are 8 mm and 14 mm, aimed at manufacturing two selected components – M8 and M14 screws respectively – through cold forging at Agrati plant. The steel grade was 30MnB4. The evaluation of the tensile properties has been performed according to the procedures usually adopted to assess the product quality, on test specimens having the full cross-sectional area of the wire rod. A gage length equal to five times the diameter has been used for the measurement of elongation.

The results related to the coils wire rod of diameter 14 mm produced according to the special operating practices (UFG) are listed in Table 60, while the tensile properties typical of the reference standard product are reported in Table 61.

Position H = Head, T = Tail	Tensile Strength MPa	Elongation % (*)	Reduction of Area %
H	619	28.6	62
T	628	28.6	63
H	613	29.3	63
T	615	30.0	63
H	616	nd	64
T	610	28.6	62
H	619	27.1	62
T	614	29.3	63
H	615	28.6	62
T	613	27.1	64
H	611	nd	64
T	621	29.3	62
H	611	30.0	63
T	610	nd	64
H	617	nd	61
T	609	30.0	63
Average	615	28.9	63
Std deviation	5	1.0	1

(*) Gage length: 70 mm. nd: not determined.

Table 60: Tensile properties of the wire rod diameter 14 mm (UFG).

	Tensile Strength MPa	Elongation %	Reduction of Area %
Average	622	na	54
Std deviation	15		1

Table 61: Tensile properties of the wire rod diameter 14 mm (STD).

The results related to the coils wire rod of diameter 8 mm produced according to the special operating practices (UFG) are listed in Table 62, while the tensile properties typical of the reference standard product are reported in Table 63.

	Tensile Strength MPa	Elongation %	Reduction of Area %
Average	610	na	65
Std deviation	5		1

Table 62: Tensile properties of the wire rod diameter 8 mm (UFG).

	Tensile Strength MPa	Elongation %	Reduction of Area %
Average	621	na	62
Std deviation	14		1

Table 63: Tensile properties of the wire rod diameter 8 mm (STD).

The differences found in tensile properties between the steel hot rolled with low finishing temperature (UFG) and the reference product hot rolled with conventional cycle (STD) consist substantially in a slightly decreased tensile strength, and an increased reduction of area. Such increase is more significant in the case of diameter 14 mm.

Some examples of the related wire rod microstructures are reported in Figure 151 (diameter 14 mm) and Figure 152 (diameter 8 mm). The microstructures consist in ferrite (65-75 %) and pearlite (25-35 %) and the values of mean ferritic grain size are around 7 μm in both cases. This is significantly finer than that of standard product, hot rolled with the conventional cycle at high finishing temperature (10-12 μm).

The limited improvement in tensile properties and the increase in ductility (reduction of area) can be explained both by the complete absence in the final microstructure, due to the lower finishing temperature and accordingly to a finer initial austenite grain size, of hard phases as bainite, which may be present in small amount in the standard product and by finer grain size.

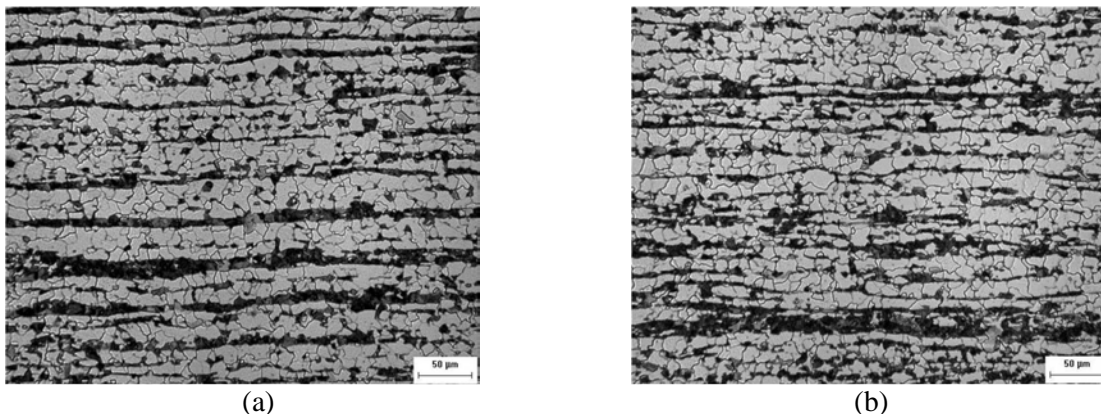


Figure 151: Microstructure of the wire rod diameter 14 mm (UFG). Ferrite + pearlite. (a) coil n. 4 (b) coil n. 8.

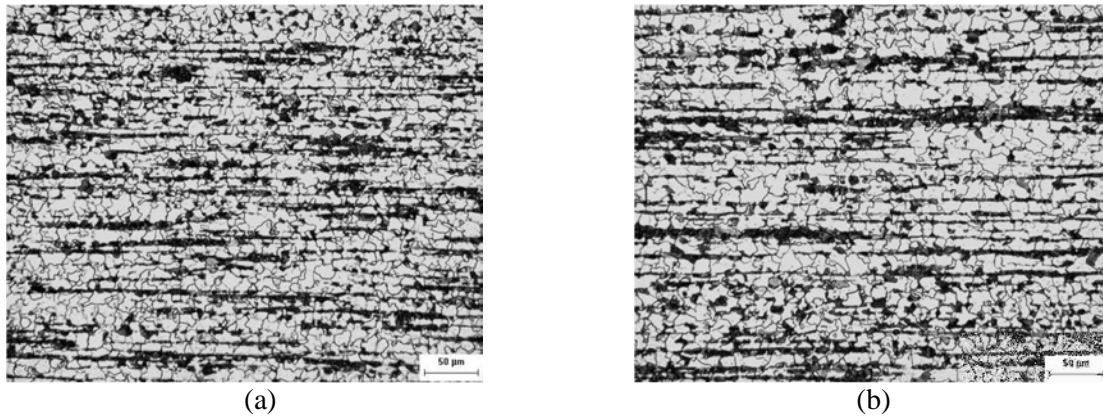


Figure 152: Microstructure of the wire rod diameter 8 mm (UFG). Ferrite + pearlite. (a) coil n. 13 (b) coil n. 14.

Automotive – powertrain (carbon range 0.15-0.20 %)

After producing UFG steels by pilot mill (WP3) as foreseen by the procedure reported in WP1 for fabrication of powertrain, some test samples of 18CrMo4 and 17CrV6 have been carburized following the process carried in FIAT with the fatigue test samples:

- Pre-heating at 880°C for 1 hour 20 minutes
- Carburizing at 920°C for 1 hour 20 minutes
- Diffusion at 860°C for 1 hour 20 minutes
- Quenching with hot oil at 80°C
- Washing in water at 60°C
- Stress relief at 160°C for 2 hours

The carburizing process has been performed with the samples for torsion and Charpy tests, in order to know the behaviour of the surface of the samples.

The hardness profile for the two industrial heats of carburizing steel grades with standard and ultrafine grain size has been compared (Figures 153 and 154).

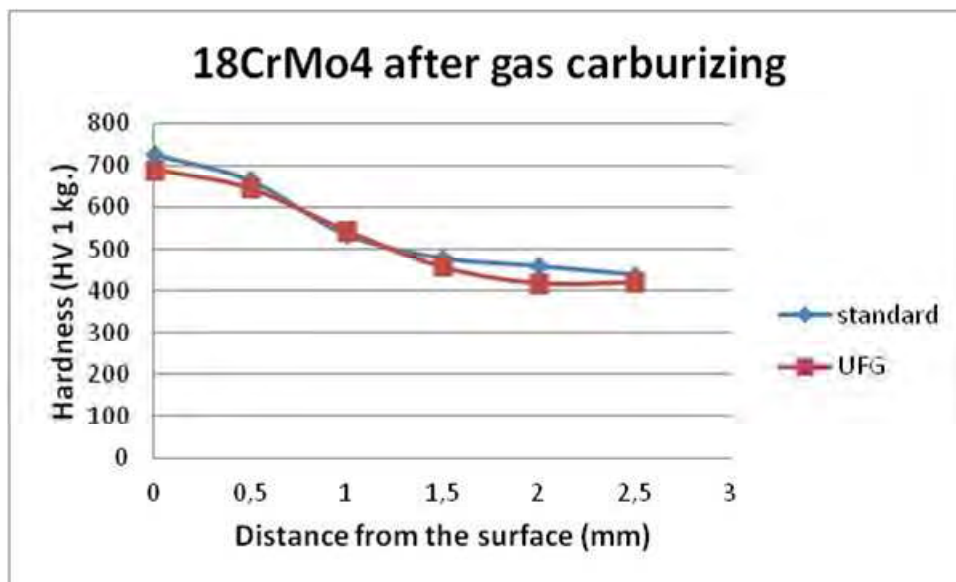


Figure 153: Hardness profile of the samples of 18CrMo4 with standard grain size and ultra-fine grain size.

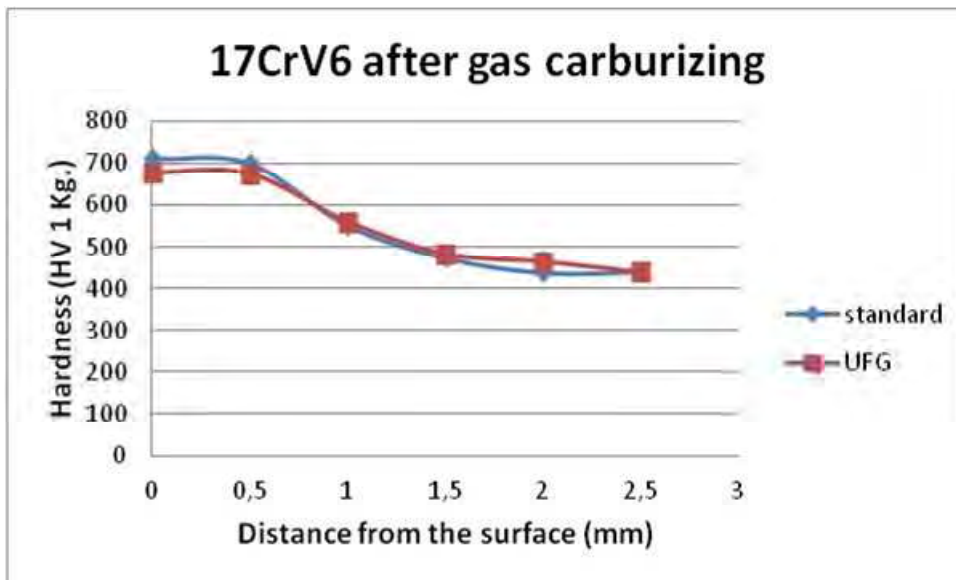


Figure 154: Hardness profile of the samples of 17CrV6 with standard grain size and UFG size.

It can be assumed that the hardness profile is the same with standard grain size and with ultrafine grain size and no significant difference is found. The microstructure in the carburized layer and in the core of the samples has been also compared (Figures 155 and 156).

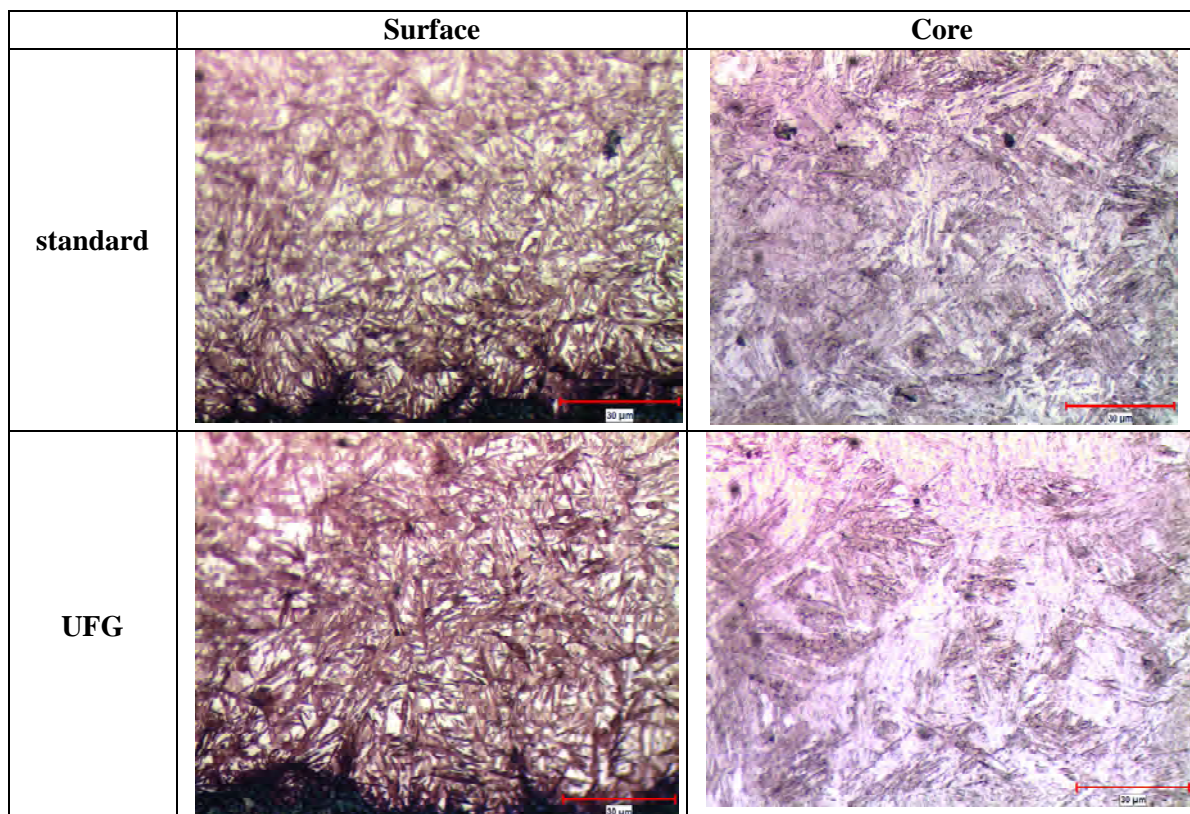


Figure 155: Microstructures obtained for 17CrV6 standard and with UFG.

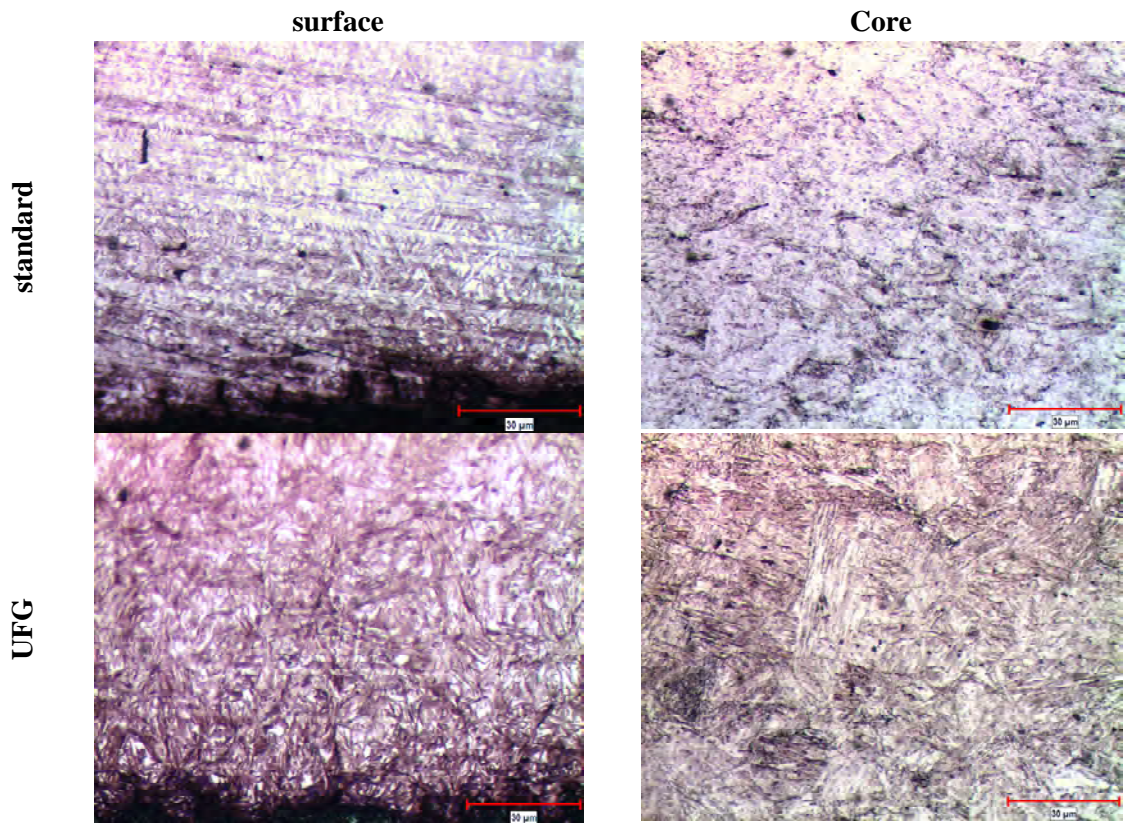


Figure 156: Microstructures obtained for 18CrMo4 standard and with UFG.

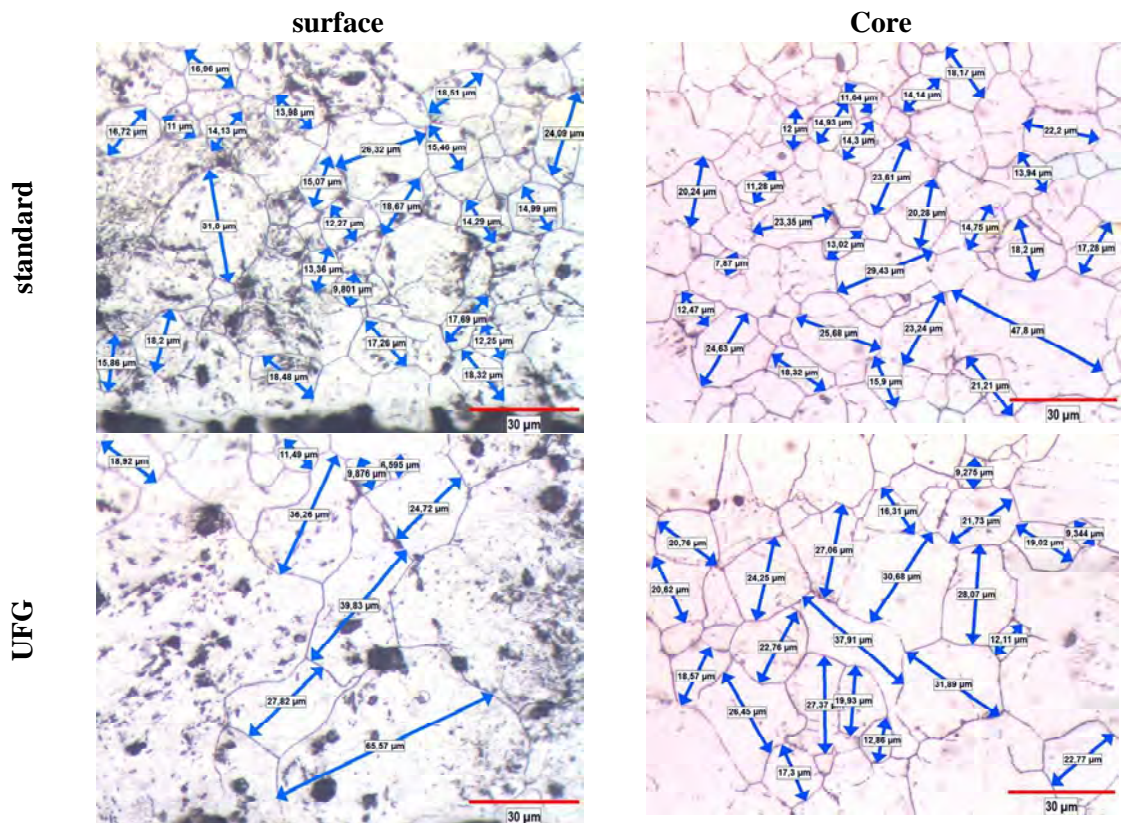


Figure 157: Prior austenite grain size for 17CrV6 standard and with UFG.

For the two steel grades, 17CrV6 and 18CrMo4, the microstructure in the surface is martensite with some retained austenite and in the core is bainite.

On the other hand, the prior austenite grain size has been also measured as it is shown in the Figures 157 and 158. An evaluation of the sizes of the different austenite grain sizes has been performed (Figures 159 and 60).

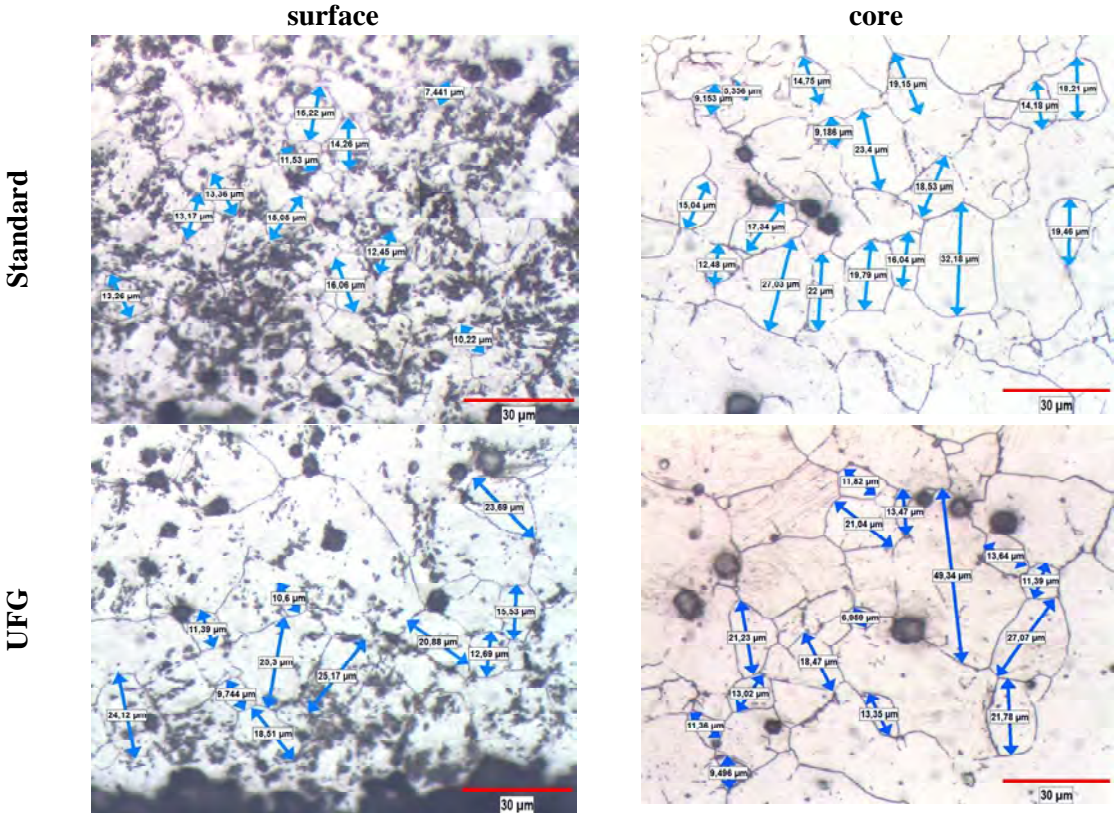


Figure 158: Prior austenite grain size for 18CrMo4 standard and with UFG.

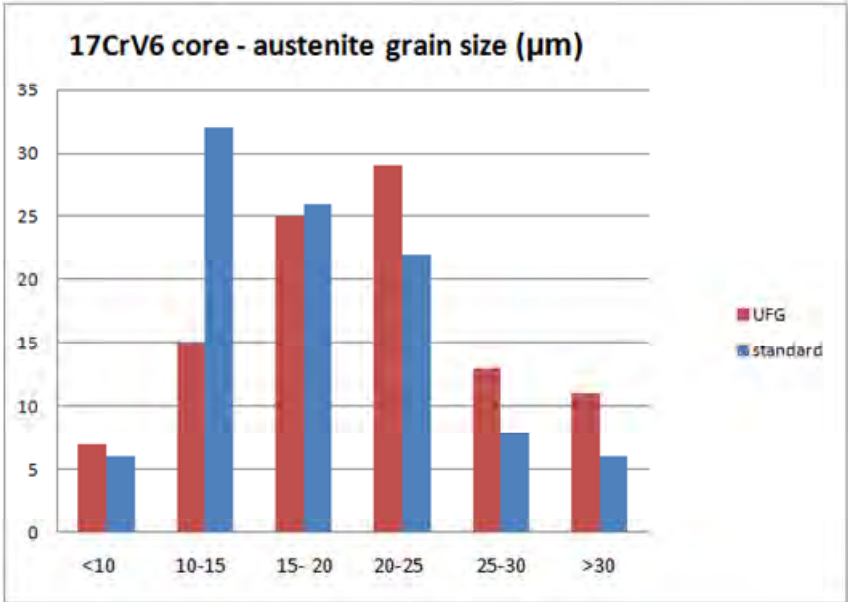


Figure 159: Percentage of the different austenite grains of 17CrV6 in the core.

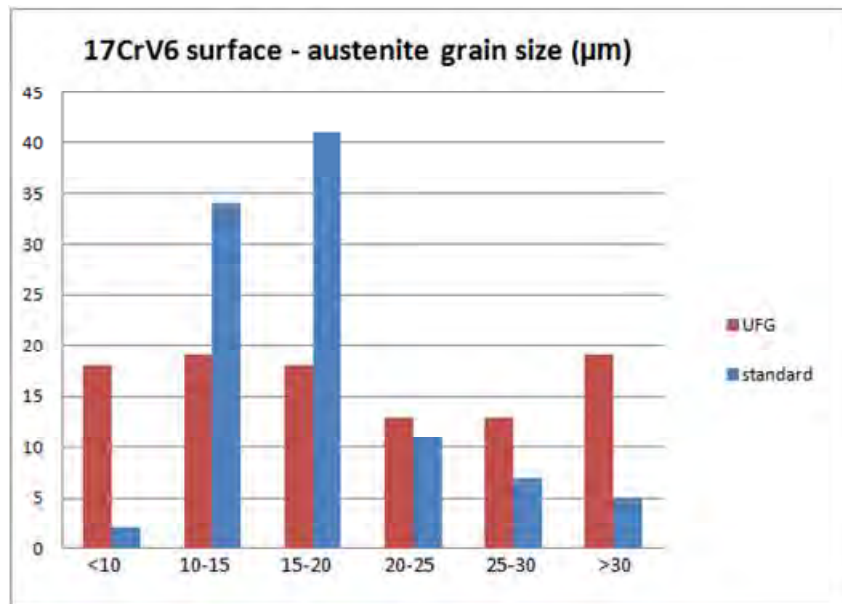


Figure 160: Percentage of the different austenite grains of 17CrV6 in the surface.

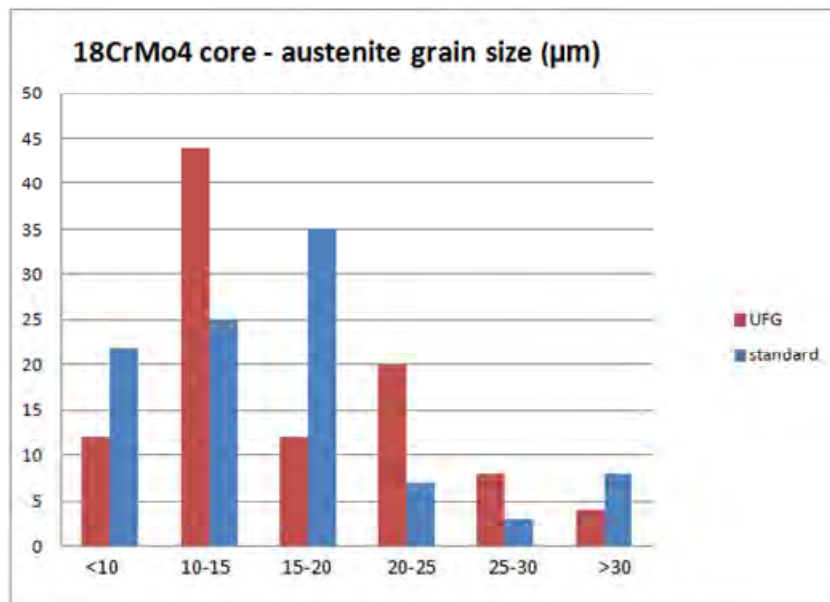


Figure 161: Percentage of the different austenite grains of 18CrMo4 in the core.

In the core, the most of austenite grains of 17CrV6 standard are between 10 and 20 µm and for the 17CrV6 UFG they are between 15 and 25 µm. In the surface, the most of the austenite grains of 17CrV6 standard are between 10 and 20 µm and no clear tendency is found for the 17CrV6 UFG.

In the core, the most of austenite grains of 18CrMo4 standard are finer than 20 µm and for the 18CrMo4 UFG they are between 10 and 15 µm. In the surface, the most of the austenite grains of 18CrMo4 standard are finer than 15 µm and for the 18CrMo4 UFG finer than 20 µm (Figures 116 and 162).

Afterwards, the comparison of the ductile-to-brittle Transition Temperature of the two carburizing steel grades with standard and ultrafine grain size has been performed (Figures 163 and 164).

It can be observed that the values of impact energy are higher for the samples with ultra fine grain size than for the samples with standard grain size.

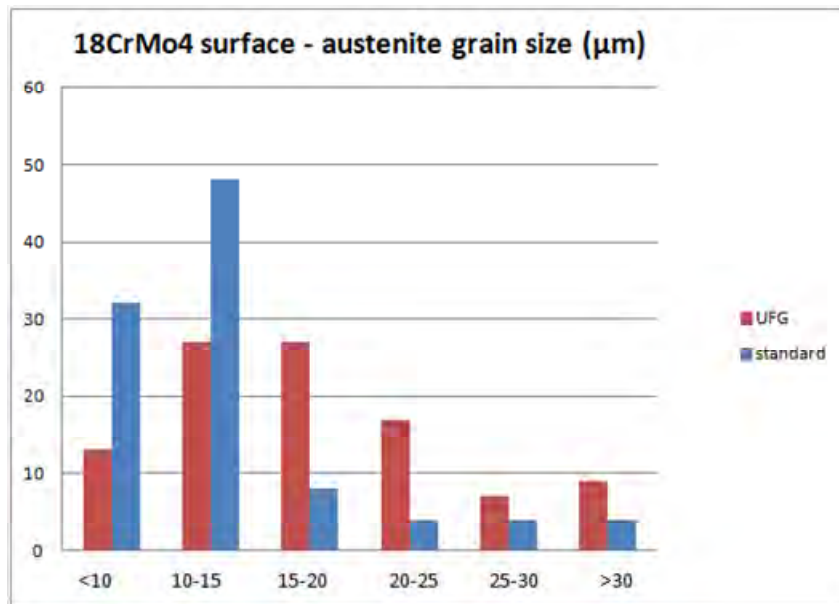


Figure 162: Percentage of the different austenite grains of 18CrMo4 in the surface.

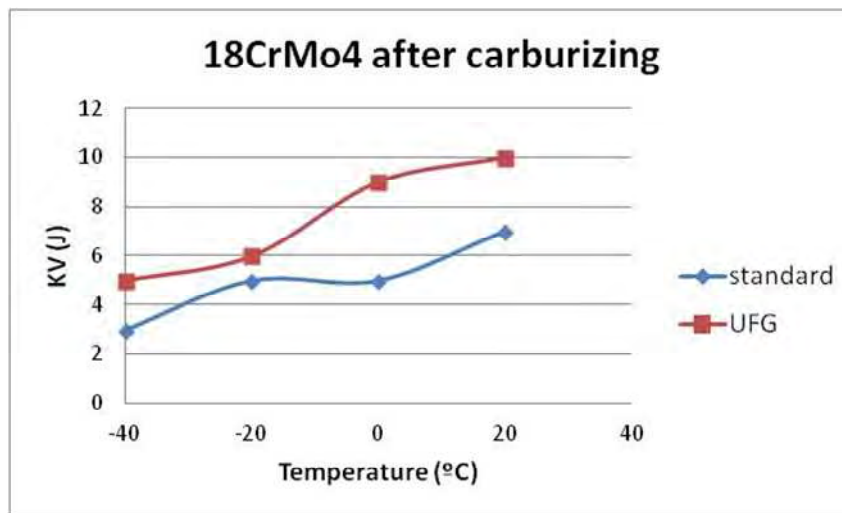


Figure 163: Ductile-to-Brittle Transition Temperature by Charpy V-notch impact tests of the samples of 18CrMo4 with standard grain size and ultra-fine grain size.

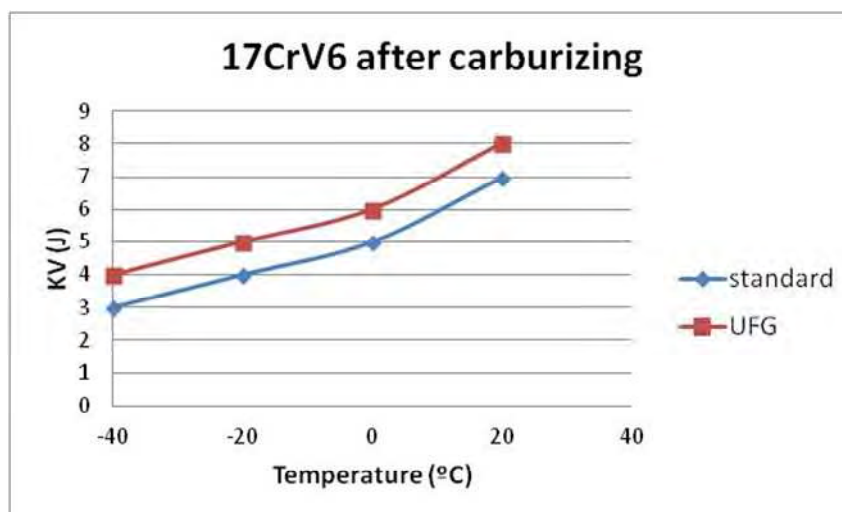


Figure 164: Ductile-to-Brittle Transition Temperature by Charpy V-notch impact tests of the samples of 17CrV6 with standard grain size and ultra-fine grain size.

Tensile tests

Some tensile test samples of 18CrMo4 have been heat treated: hardening at 840°C for 1 hour and stress relief at 180°C for 2 hours 30 minutes.

The results of the tensile tests are shown in the Figure 165 and in the Table 64. The mechanical properties have been similar for the steels with standard and with ultra fine grain size, although the tensile and yield strength have been slightly higher for the standard steel.

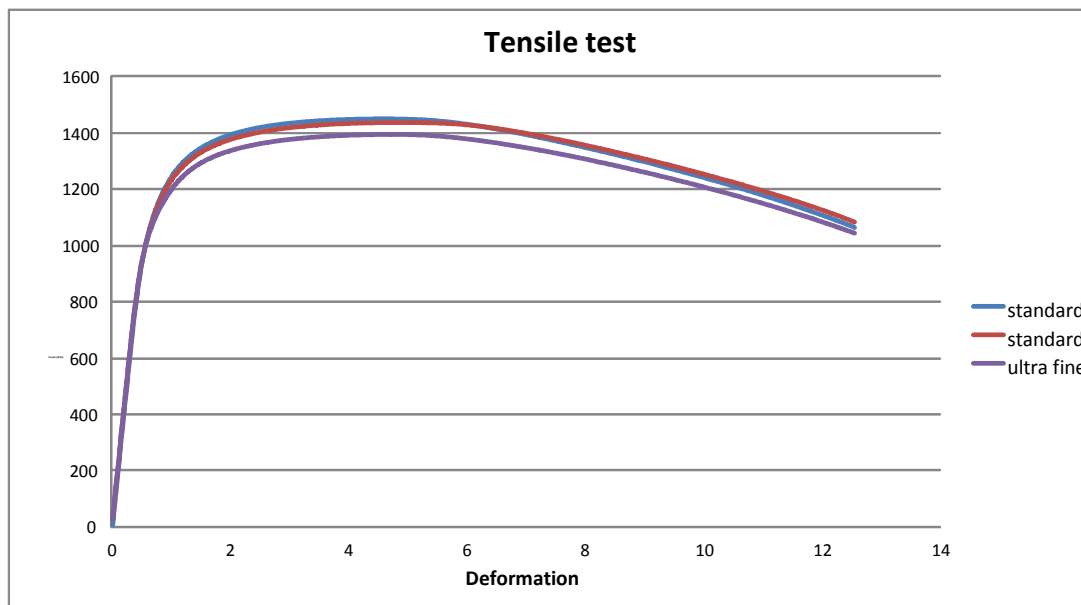


Figure 165: Results of tensile tests of 18CrMo4 standard and with ultra fine grain.

	Rm (MPa)	Re (MPa)	A(%)	Z(%)
Standard 1	1451	1146	53	12
Standard 2	1437	1127	48	13
Ultra-fine	1397	1102	55	10

Table 64: Results of the tensile tests.

Torsion tests

On the other hand, some torsion tests have been carburized before being tested; the maximum load is 100KN and the maximum torque has been 1100Nm. The results of torsion tests are shown in Table 65.

		Breakage angle (°)	Breakage torque (Nxmm)
18CrMo4	Standard grain size	75,54	232.595
	Ultra-fine grain size	114	>440.121
17CrV6	Standard grain size	75	237.005
	Ultra-fine grain size	67,61	230.882
		57,1	220068

Table 65: Results of torsion tests.

The torsion tests don't show a clear difference between the 18CrMo4 with standard and with ultra fine grain size. Some test samples after being broken by torsion tests are shown in the Figure 166.

Some of the fracture surfaces have been analysed by SFEG (Figure 167). The beginning of the fracture has been intergranular in the surface, although the propagation has been through the grains.



Figure 166: Torsion test samples.

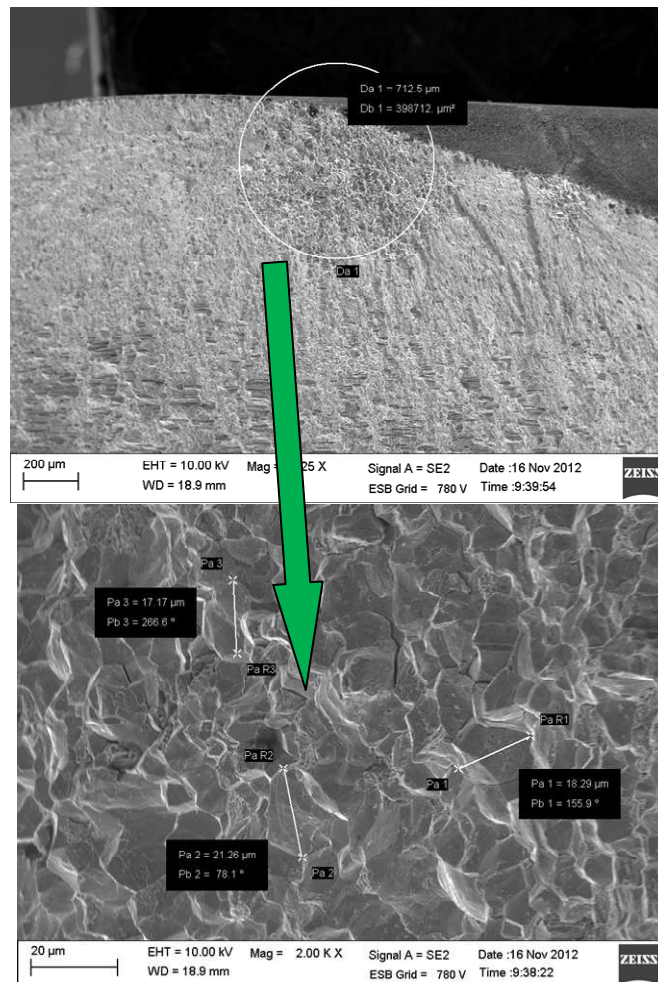


Figure 167: Fracture of 18CrMo4 standard.

50SiVMoNb8 - Fracture Mechanics Parameters

For both, the STDG and the UFG 50SiVMo8Nb materials, the toughness in model was measured. Prismatic samples were machined from the original heat treated rods supplied by CRF. The sample geometry used was similar to the 5 mm wide sub-size charpy samples (ASTM A370). Total dimensions were 5×10×50 mm with a 2 mm deep notch in the middle.

Once the samples were manufactured, a fatigue crack was grown at the notch tip using a three point bending setup. The distance between rods in the setup used was 40 mm. For this grow, a cyclic load that

ranges between +100 N and +1 kN ($R = 0.1$) was applied. The fatigue test was stopped periodically for estimating the length of the crack growth. This measurement was carried out using optical microscopy, as seen in Figure 168 (Left).

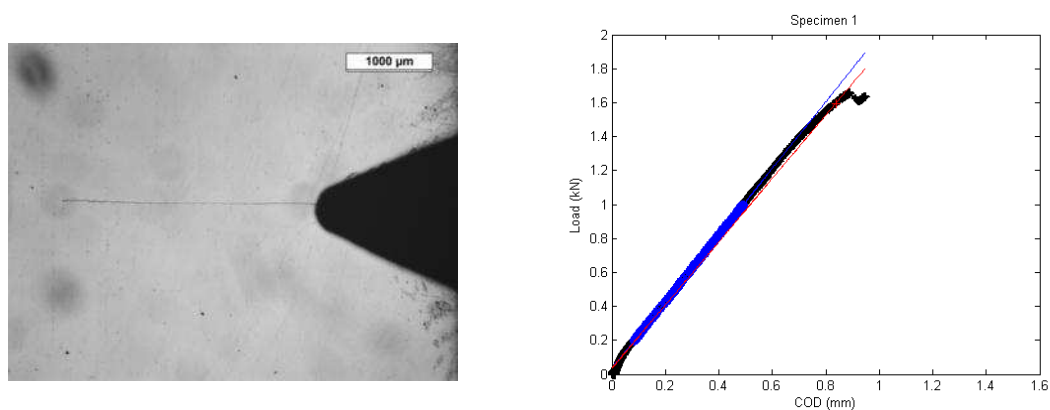


Figure 168: (Left) Optical micrograph used to estimate the fatigue growth pre-crack length. (Right) Load-Crack opening record used to estimate K_{IC} .

Once the crack reached a length between 2.5 and 3.5 mm, specimens were loaded up to break. During these fracture tests an extensometric clip was fixed to the samples for measuring how the crack opens. During tests, the applied load and the opening of the crack was recorded simultaneously. Figure 35 (Right) shows an example of a recorded test, where the fracture load determined by the standard ASTM E399-09 could be observed as a red cross [9].

The same standard as before was used to determine the real size of fatigue grown pre-cracks. All fracture surfaces observed for both materials were 100% brittle.

After analyzing the results of the three specimens tested for each material the average values obtained for K_{IC} were 38.0 and 35.3 $\text{MPa}\sqrt{\text{m}}$, for the STDG and the UFG, respectively. The standard deviation for each case was 0.84 and 0.64 $\text{MPa}\sqrt{\text{m}}$ for sample with standard and ultrafine grain size, respectively.

Task 4.2 – Response to fatigue

Automotive – powertrain (carbon range 0.15-0.20 %)

18CrMo4 - Metallographic analysis before gas carburizing

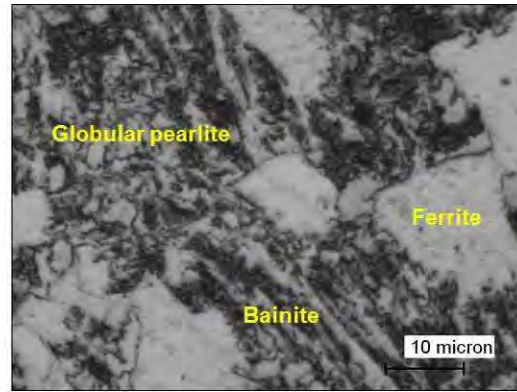
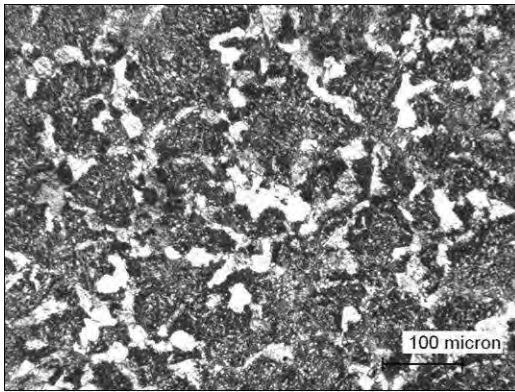
A preliminary metallographic analysis has been carried out on 18CrMo4 STDG steel supplied by GERDAU. Three metallographic samples have been cut from a bar. Two samples prepared on the transversal section were used for the metallographic analysis and grain size measurements, one samples prepared on the longitudinal section was used for inclusion analysis. The mean hardness value is 232 HV_{10} . The microstructure, close to the bar surface, is constituted by equiaxial ferrite grain (215HV_1) and bainite (350HV_1).

The bar core shows a microstructure (Figure 169) constituted by equiaxial ferrite grain + bainite + globular pearlite. The Vickers hardness measurement has given the same results for bar core and surface: 215HV_1 (ferrite) and 350HV_1 (bainite).

The inclusion analysis (Figure 170) has been evaluated following the UNI 3244 standard. The analysis has been carried out following the “Maximum grade method - M”. The grade of non-metallic inclusion has been evaluated according to Jern Kontoret scale (still used in FIAT) and according to Stahl Eisen Prufblatt scale. According to internal FIAT STD oxide and Mn sulphure inclusions are below the maximum admitted value (Scale J.K. 3).

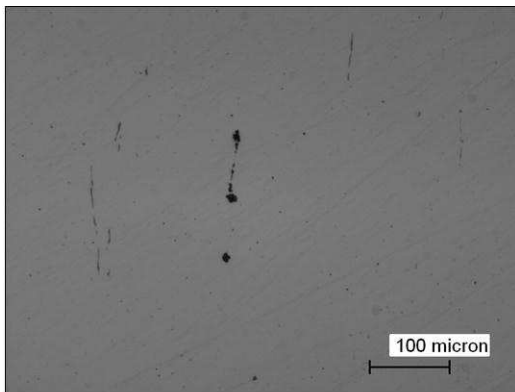
The same analyses have been done on 18CrMo4 UFG steel supplied by TU-Freiberg. The mean hardness value is 237 HV_{10} . The core bar microstructure (Figure 171) is constituted by equiaxial ferrite grain (231HV_1) and lower bainite (given by a higher cooling rate - 439HV_1) + globular pearlite.

The inclusion analysis (Figure 172) shows that oxide and Mn sulphure inclusions are below the maximum admitted value (Scale J.K. 3) and slightly lower than the value found in 18CrMo4 STDG bar.

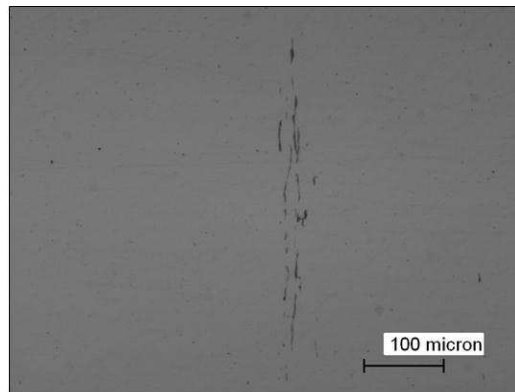


M10/088/1 - Microstructure
Equiaxial ferrite grain (light phase) and bainite + globular pearlite (dark phase).

Figure 169: Bar core microstructure of 18CrMo4 STDG steel.

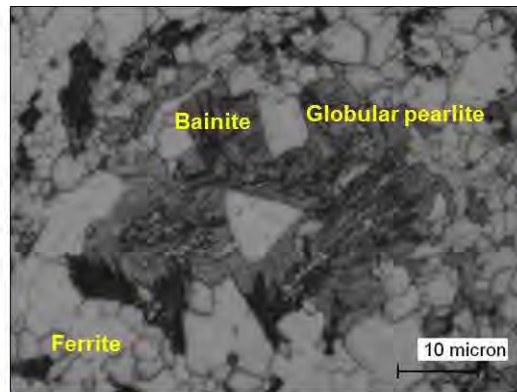
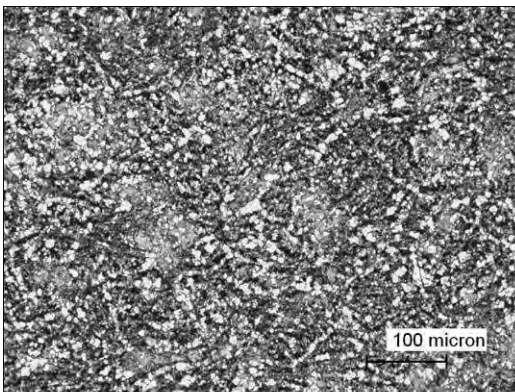


M10/088/2 - Maximum oxide size
Scale J.K.: D (1) heavy
Scale S.E.P.: OG (9,2)



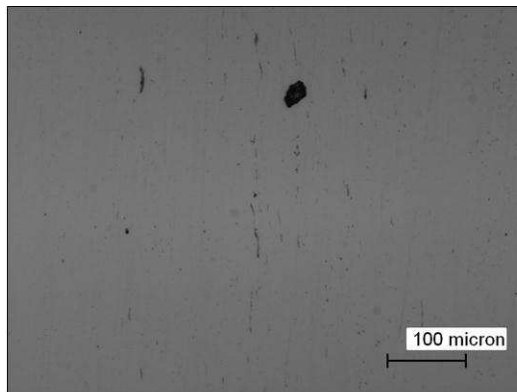
M10/088/2 - Maximum Mn sulphur size
Scale J.K.: A (3) heavy
Scale S.E.P.: SS (1,5)

Figure 170: Inclusion analysis - UNI 3244 of 18CrMo4 STDG steel.

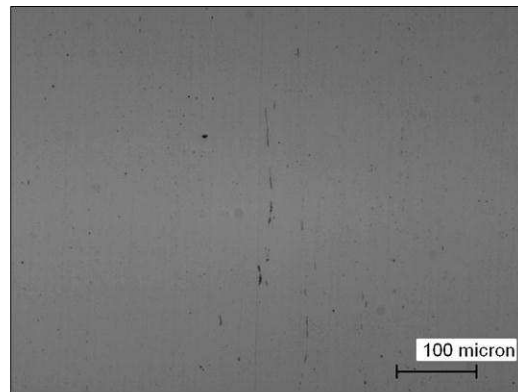


M11/023/1 - Microstructure
Equiaxial ferrite grain (light phase) and lower bainite (high cooling rate) + globular pearlite (dark-grey phase).

Figure 171: Bar core microstructure of 18CrMo4 UFG steel.



M11/023/2 - Maximum oxide size
Scale J.K.: D (1) heavy
Scale S.E.P.: OG (8.3)



M11/023/2 - Maximum Mn sulphur size
Scale J.K.: A (2) thin
Scale S.E.P.: SS (0.2)

Figure 172: Inclusion analysis of 18CrMo4 UFG steel - UNI 3244.

18CrMo4 - Rotate bending fatigue specimen production

Two lots of rotate bending fatigue specimen have been produced starting from 18CrMo4 STDG supplied by GERDAU and 18CrMo4 UFG supplied by TU-Freiberg. The central part of the specimen is grinded to achieve the required roughness value ($R_a=0.4\mu\text{m}$). The roughness measured on the surface is around $R_a=0.2\mu\text{m}$. After carburizing the metallurgical requirements are the following:

- Core hardness: 36 HRC to 45 HRC
- Surface hardness: 700HV_{10} min
- Effective case depth: 0.6 to 0.8 mm at 550HV_1

Heat treatment has been carried out by a FIAT supplier using a gas carburizing furnace, the treatment parameters are the following:

- gas carburizing with ENDOGAS + 3% Methane: pre-heating at 880°C for 1h20min, carburizing at 920°C for 1h20min, diffusion at 860°C for 1h20min, quenching at 80°C with hot oil, washing: water 60°C
- stress relief: 160°C for 2h

18CrMo4 - Metallographic analysis after gas carburizing

Metallurgical analysis has been carried out on 18CrMo4 STDG and UFG steel after gas carburizing. Two samples for each steel were used for the metallographic analysis and grain size measurements. The first one was cut transversally in the centre section of the specimen ($\Phi=5,5\text{mm}$), the second one across the cylindrical end ($\Phi=9,8\text{mm}$).

With reference to STDG steel the microstructure, close to the surface, (Figure 173) is constituted by martensite and some retained austenite grain (white phase). The mean hardness value is 725HV_{10} . The core microstructure is constituted by bainitic grain phase whose hardness average is 466HV_1 .

The metallographic structure of UFG steel after carburizing is quite similar. Close to the surface, (Figure 174) is constituted by martensite and some retained austenite grain (white phase).

The mean hardness value is 738HV_{10} . The core microstructure is constituted by bainitic grain phase whose hardness average is 453HV_1 .

The effective case depth has been measured at 550HV_1 on the hardness profile achieved on the transversal section in the specimen centre. The achieved values are the following: STDG specimen 0,81mm, UFG specimen 0,74mm.

The grain size has been evaluated following the Khon method: specimens has been heated at 900°C in controlled atmosphere (temperature higher than the critical point A_{c3} and lower than carburizing temperature, 4 min pre-heating, 6 min 900°C) subsequently oxidized for 5 min and then water quenched. Oxidation layer has been removed by abrasive diamond paste and etched with Vilella's reagent (1g Picric acid, 5ml hydrochloric acid, 100ml ethanol).

The grain size measured on STDG steel after carburizing is 8-11 μm corresponding to Grade 10-11 ASTM. This was quite in contrast to the value achieved before carburizing (16 μm) so it was necessary to repeat the analysis in another part of the bar achieving the results of 11-8 μm (Figure 175).

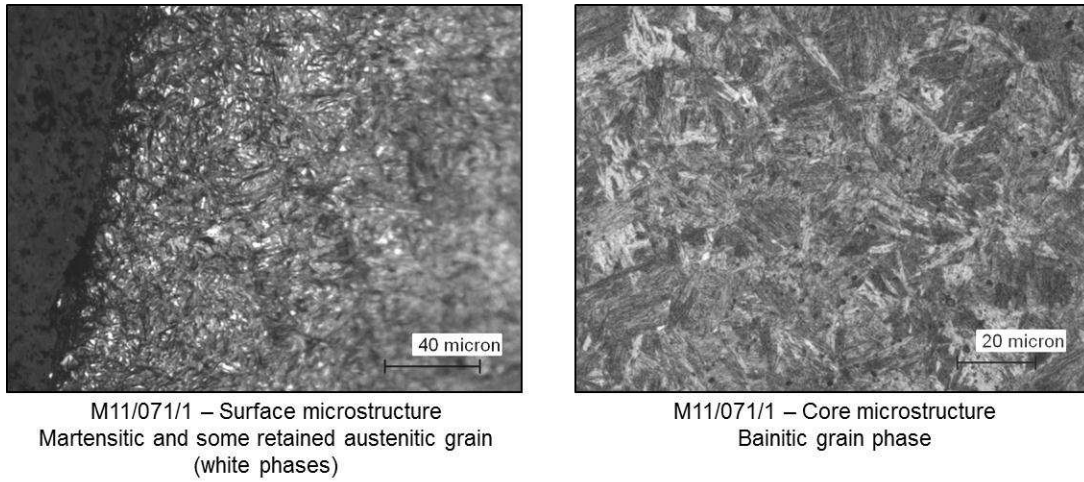


Figure 173: 18CrMo4 STDG carburizing layer – Specimen centre section.

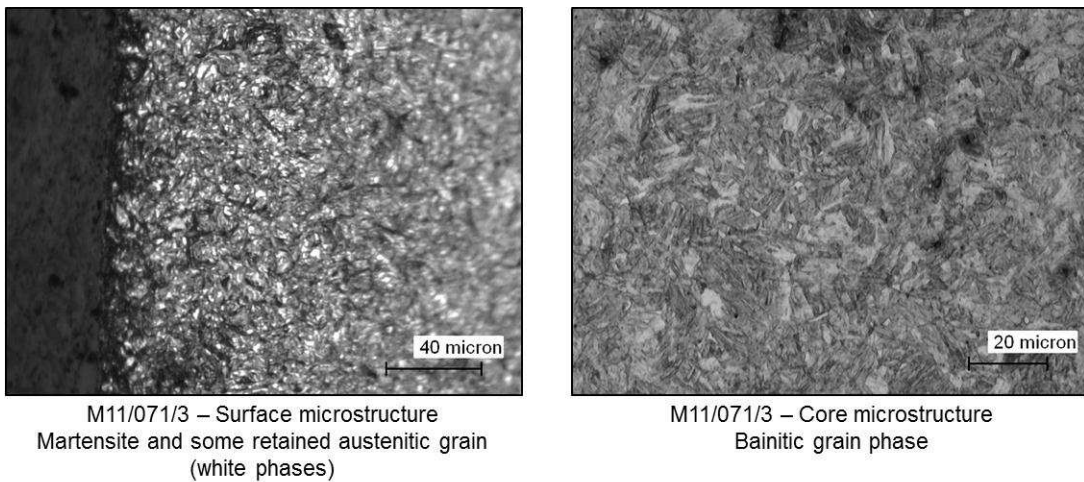


Figure 174: 18CrMo4 UFG carburizing layer – Specimen centre section.

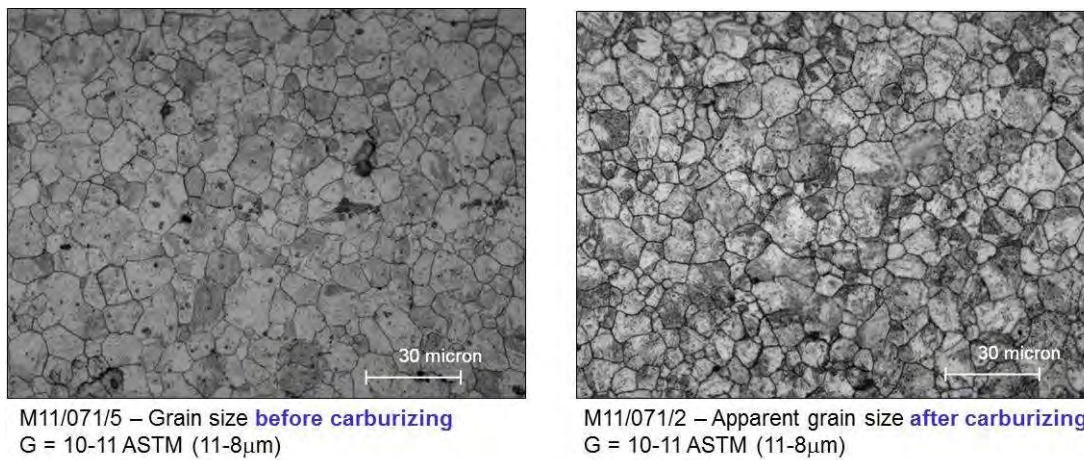
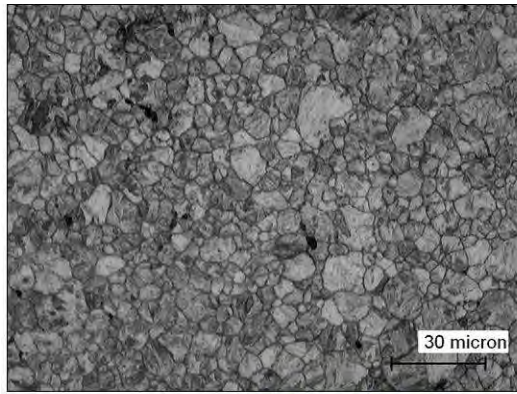


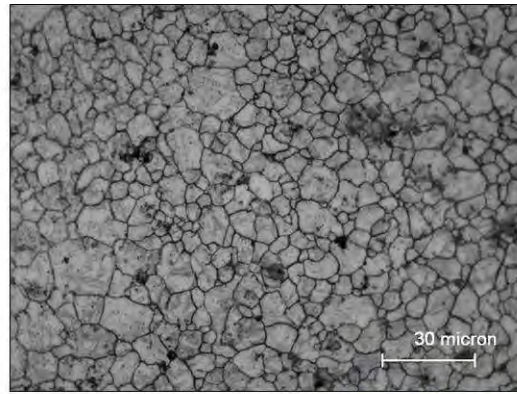
Figure 175: 18CrMo4 STDG Austenitic grain size - UNI EN ISO 643 (ASTM E112).

The grain size measured on UFG steel after carburizing is 6 μm corresponding to Grade 12 ASTM (Figure 176). In comparison to the analysis carried out before carburizing there is not any remarkable grain coarsening due the high carburizing temperature.



M11/023/3* – Grain size **before carburizing**
G = 13-12ASTM (6-4 μ m)

* Previous grain size analysis (heating 870° C).



M11/071/4 – Apparent grain size **after carburizing**
G = 11 ASTM (8 μ m)

Figure 176: 18CrMo4 UFG Austenitic grain size - UNI EN ISO 643 (ASTM E112).

18CrMo4 – Fatigue behaviour evaluation.

Carburized specimens have been ground on the cylindrical ends to recover the geometrical distortion due to the heat treatment. The hourglass section has been maintained “as carburized” in order to avoid any further operations that could alter the fatigue behaviour.

The equipment used for the fatigue test is a rotate bending machine (ITALSIGMA) able to apply a constant bending moment along the longitudinal axle of the specimen between the gripping devices (Figure 177). The maximum bending moment is 35Nm, the working speed can range between 300 and 4000 rpm, the loading is applied by adding certified mass on the loading device.

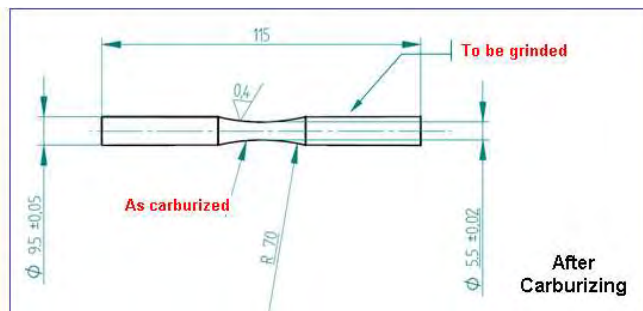


Figure 177: ITALSIGMA rotate bending fatigue machine.

For 18CrMo4 TDG, the fatigue strength at 5E6 cycles has been evaluated by stair-case method (Figure 178), the achieved values at 10%, 50% and 90% of survival probability are: 861MPa, 823MPa and 785MPa respectively.

The Woehler diagram is reported in Figure 179 (blue lines). The finite life part of the curve has been drawn, using also recovered samples from a lower load test after achievement of 5E6 cycles without failure. The S-N curve, elaborated with the StatFat software, is comprehensive of the fatigue strength at 50% of survival probability and the scatter bands at 10% and 90% of survival probability, which correspond to the estimated fatigue strength of 823MPa, 867MPa and 781MPa, respectively.

Level	Stress Sa [MPa]	SEQUENCE NUMBER OF SPECIMEN																				Numbers of tests		Ni	i	ixNi	i ²	i ² xNi
		1	2	3	4	5	6	7	8	9	10	11	12	13	14	15	16	17	18	19	20	x	o					
																						0	0	0	0	0	0	
																							0	0	0	0	0	0
																							0	0	0	0	0	0
4	860										X											1	0	0	0	0	0	
3	840	X		X				X		O		X										4	1	0	4	16	0	
2	820		O		X		O		O			X										2	3	3	2	6	4	12
1	800					O							X			X						2	1	1	1	1	1	1
0	780													O								0	1	0	0	0	0	0
																						0	0	0	0	0	0	0
N° of cycles x 10 ⁶		0.404	5.000	1.520	0.638	10.680	5.290	1.445	10.506	5.355	0.207	1.298	1.763	1.400	5.400	0.156					Σri = Σli =	9	6					
																						ri	li					
																						N=	A=	B=				
																						Ni=ri per Σri < Σli (caso1)						
																						Ni=li per Σri > Σli (caso2)						

d = 20 MPa

CASO 1 $m=x+d.(A/N-0.5)$

CASO 2 $m=x+d.(A/N+0.5)$

m = 823,3 MPa

s = 29,7 MPa

Salt. (10%) $m+1.28 s$ 861,4 MPa

Salt. (50%) m 823,3 MPa

Salt. (90%) $m-1.28 s$ 785,3 MPa

Standard deviation = $1.62 * d * \left(\frac{N.B - A}{N} + 0.029 \right)$

Standard deviation valid

X Failure

O Run-out

Figure 178: 18CrMo4 STDG fatigue strength – Stair Case method.

Similarly, the fatigue strength at 5E6 cycles of 18CrMo4 UFG evaluated by the same method, at 10%, 50% and 90% of survival probability are: 916MPa, 837MPa and 757MPa.

The Woehler diagram is reported in Figure 179 (pink lines). By the S-N curve, elaborated with the StatFat software, the estimated fatigue strength at 50%, 10% and 90% are 837MPa, 919MPa and 762MPa, respectively.

The smaller grain size of UFG steel (6μm) in comparison to STDG steel (8-11μm) achieved after carburizing treatment has not lead to a significant improvement on the fatigue properties. At 50% of survival probability UFG steel has a fatigue limit just 14MPa higher than STDG steel, moreover UFG steel is characterized by a higher scatter band probably due to an higher density of inclusion or segregation as specimen was machined by using the centre on the bar.

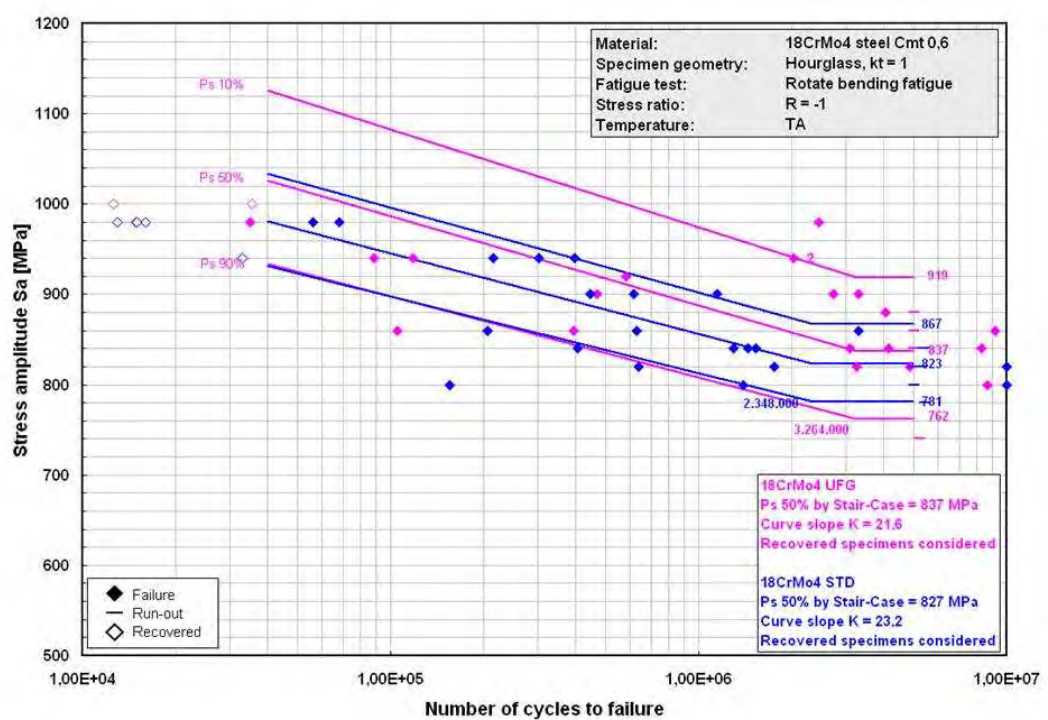
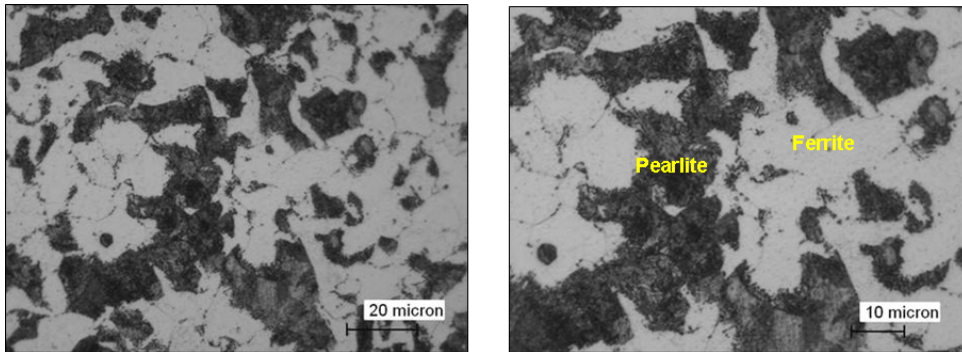


Figure 179: 18CrMo4 UFG and 18CrMo4 STDG S-N curves.

17CrV6 - Metallographic analysis before gas carburizing

A preliminary metallographic analysis has been carried out on 17CrV6 STDG steel supplied by GERDAU. Three metallographic samples have been cut from a bar.

Two samples prepared on the transversal section were used for the metallographic analysis and grain size measurements, one samples prepared on the longitudinal section was used for inclusion analysis. The microstructure (Figure 180) is constituted by ferrite grain and fine pearlite.



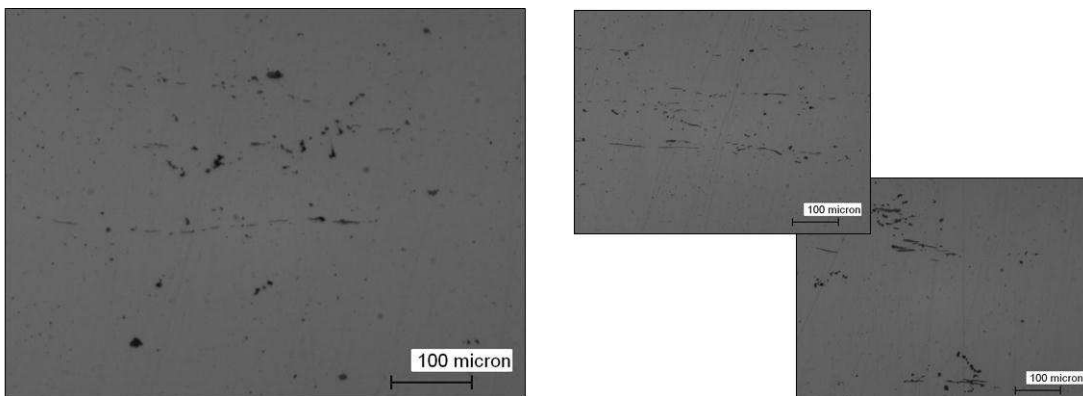
M11/110/12 - Microstructure

Ferrite grain (light phase) and fine pearlite (dark-grey phase)

Figure 180: 17CrV6 STDG bar surface microstructure.

The inclusion analysis is reported in Figure 181.

The same analysis has been done on 17CrV6 UFG steel supplied by TU-Freiberg. The core bar microstructure (Figure 182) is constituted by ferrite grain and fine pearlite.



M11/110/4 - Maximum oxide size

Scale J.K.: D (2) thin

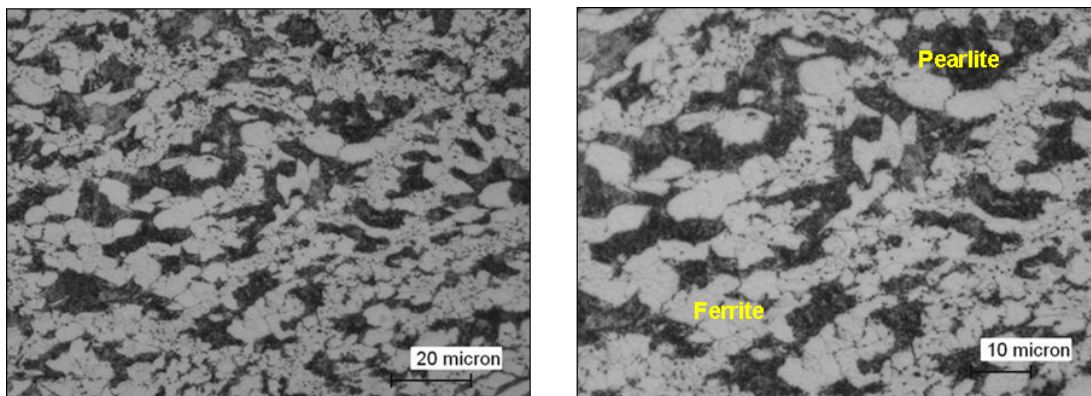
Scale S.E.P.: OG (8.3)

M11/110/4 - Maximum Mn sulphur size

Scale J.K.: A (2) heavy – A (3) thin

Scale S.E.P.: SS (1.5) - SS (0.5)

Figure 181 17CrV6 STDG inclusion analysis - UNI 3244.



M11/110/11 - Microstructure

Ferrite grain (light phase) and fine pearlite (dark-grey phase)

Figure 182: 17CrV6 UFG bar core microstructure.

The inclusion analysis (Figure 183) shows that oxide and Mn sulphure inclusions are below the maximum admitted value (Scale J.K. 3).

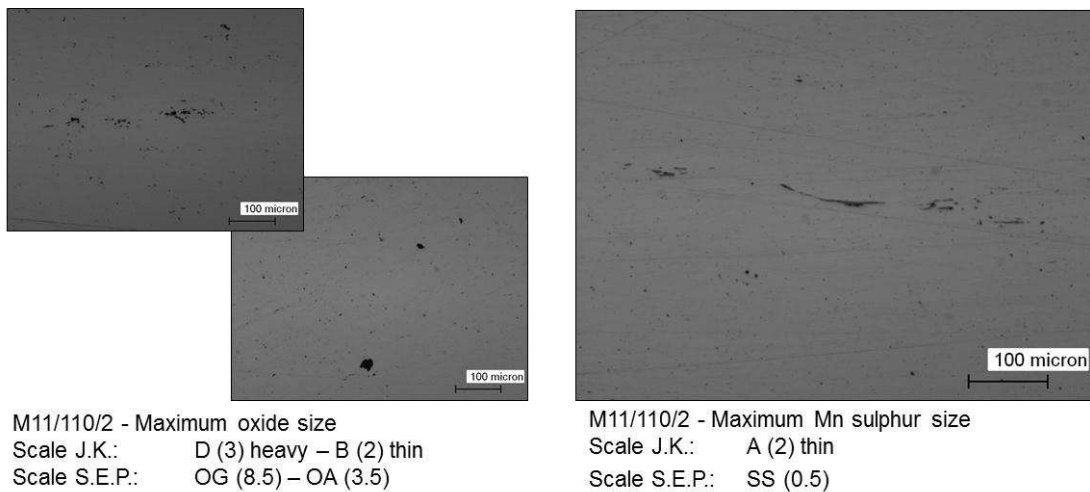


Figure 183: 17CrV6 UFG inclusion analysis - UNI 3244.

17CrV6 - Rotate bending fatigue specimen production

Two lots of rotate bending fatigue specimens have been produced starting from 17CrV6 STDG supplied by GERDAU and 17CrV6 UFG supplied by TU-Freiberg. The central part of the specimen is grinded to achieve the required roughness value ($R_a=0.4\mu\text{m}$). The roughness measured on the surface is below $R_a=0.2\mu\text{m}$.

Heat treatment has been carried out by a FIAT supplier using a gas carburizing furnace with the same treatment parameters used for 18CrMo4, consequently the same metallurgical characteristics of the 18CrMo4 are required.

17CrV6 - Metallographic analysis after gas carburizing

Metallurgical analysis has been carried out on 17CrV6 STDG and UFG steel after gas carburizing. Two samples for each steel were used for the metallographic analysis and grain size measurements. The first one was cut transversally in the centre section of the specimen ($\Phi=5.5\text{mm}$) the second one across the cylindrical end ($\Phi=9.8\text{mm}$).

With reference to STDG steel the microstructure, close to the surface, (Figure 184) is constituted by acicular martensite and some retained austenite (white phase). The mean hardness value is 769HV_{10} . The core microstructure is constituted by bainitic grain phase whose hardness average is 482HV_1 .

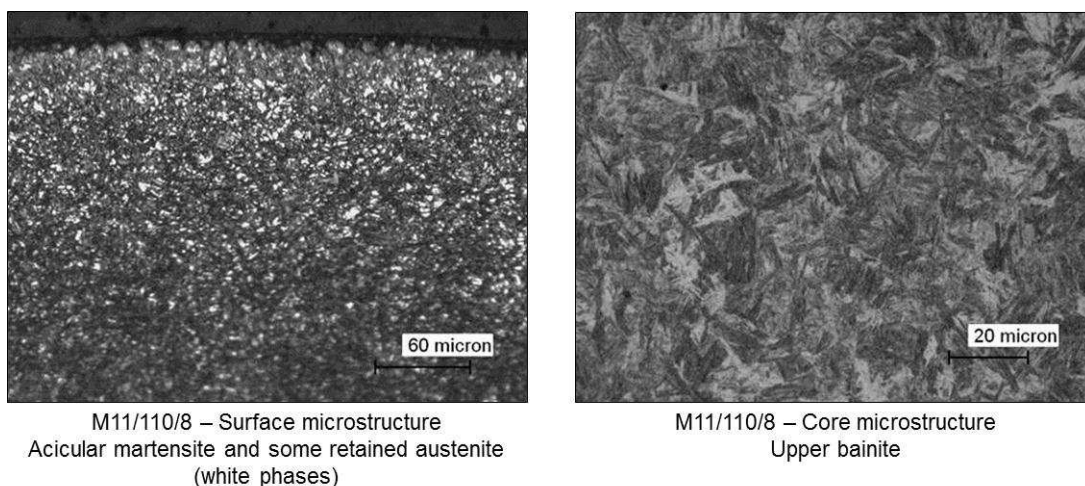


Figure 184: 17CrV6 STDG carburizing layer – Specimen center section.

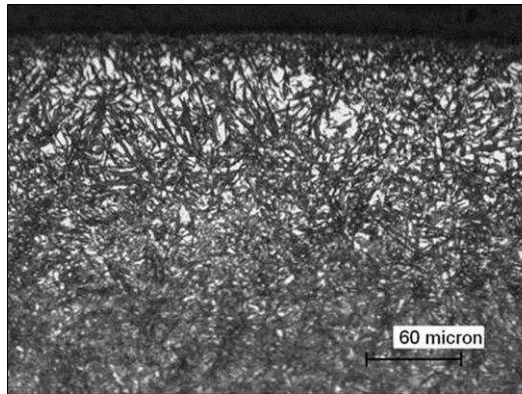
The metallographic structure of UFG steel after carburizing is quite similar. Close to the surface, (Figure 185) is constituted by martensite and some retained austenite (white phase). The mean hardness

value is 772HV₁₀. The core microstructure is constituted by bainitic grain phase whose hardness average is 466HV₁.

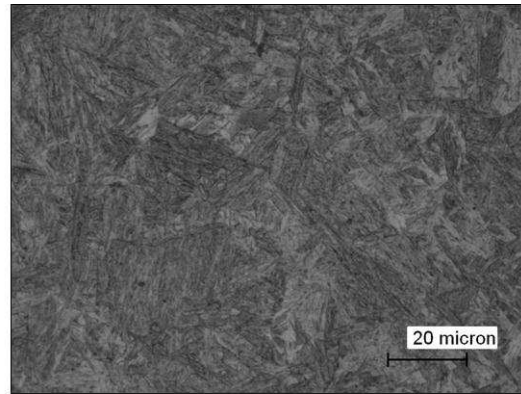
The effective case depth has been measured at 550HV₁ on the hardness profile achieved on the transversal section in the specimen centre. The achieved values are the following: STDG specimen 0,75mm, UFG specimen 0.73 mm.

The grain size measured on STDG steel after carburizing is 16µm corresponding to Grade 9 ASTM. The same value achieved before carburizing (Figure 186).

The grain size measured on UFG steel before carburizing is 4µm corresponding to Grade 13 ASTM (Figure 187). In comparison to the analysis carried out after carburizing there is a remarkable grain coarsening due the high carburizing temperature. The achieved grain size is 16µm (9 ASTM) the same value obtained on STDG steel.

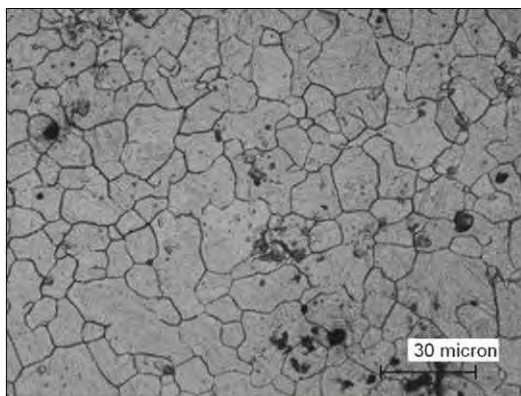


M11/110/6 – Surface microstructure
Acicular martensite and some retained austenite
(white phases)

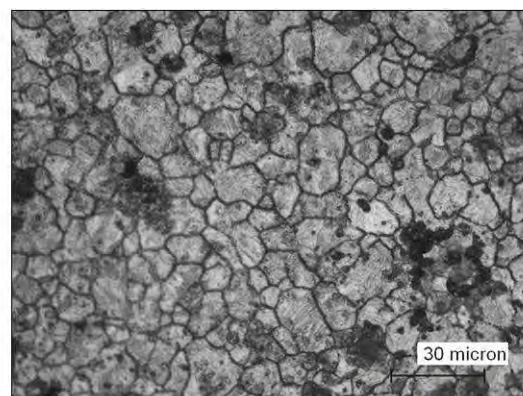


M11/110/6 – Core microstructure
Upper bainite

Figure 185: 17CrV6 UFG carburizing layer – Specimen center section.

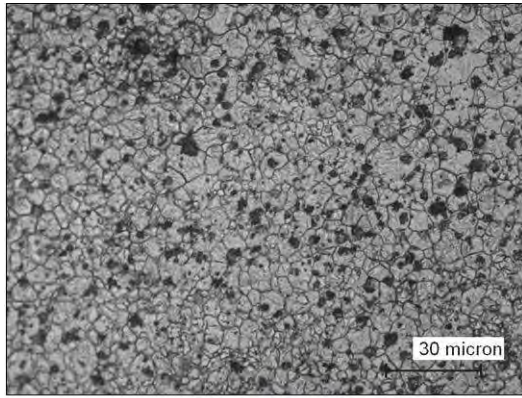


M11/110/3 – Grain size **before carburizing**
G = 9 ASTM (16µm)

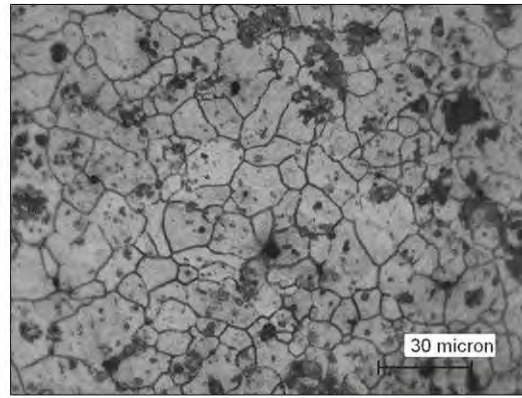


M11/110/10 – Apparent grain size **after carburizing**
G = 9 ASTM (16µm)

Figure 186: 17CrV6 STDG Austenitic grain size - UNI EN ISO 643 (ASTM E112).



M11/110/1 – Grain size **before carburizing**
G = 13 ASTM (4 μ m)



M11/110/9 – Apparent grain size **after carburizing**
G = 9 ASTM (16 μ m)

Figure 187: 17CrV6 UFG Austenitic grain size - UNI EN ISO 643 (ASTM E112).

17CrV6 – Fatigue behaviour evaluation.

Carburized specimens have been ground on the cylindrical ends to recover the geometrical distortion due to the heat treatment. The hourglass section has been maintained “as carburized” in order to avoid any further operations that could alter the fatigue behaviour. The fatigue tests were carried out by the same rotate bending machine used for 18CrMo4 steels.

The fatigue strength at 5E6 cycles of 17CrV6 STDG by stair-case method at 10%, 50% and 90% of survival probability are: 795MPa, 770MPa and 745MPa. The Woehler diagram is reported in Figure 188. The finite life part of the curve has been drawn, using also recovered samples from a lower load test after achievement of 5E6 cycles without failure. The estimated fatigue strength at 50%, 10% and 90% are 770MPa, 802MPa and 739MPa, respectively.

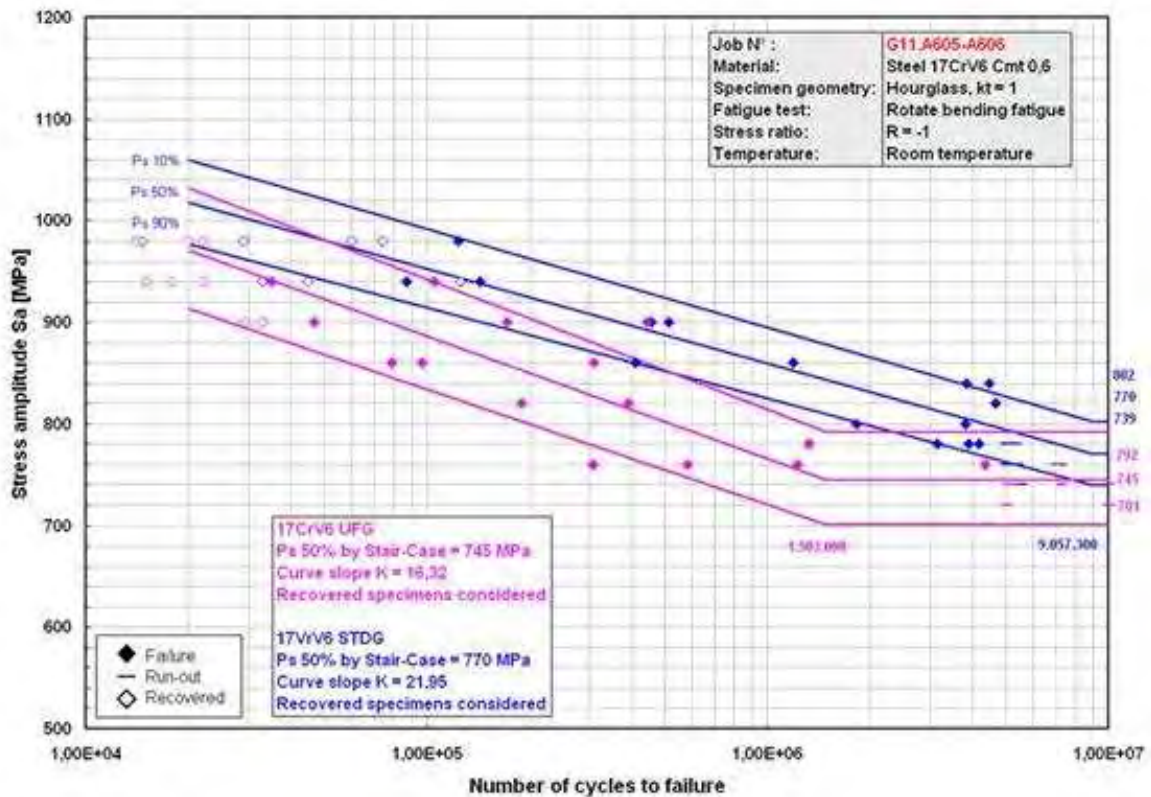


Figure 188: 17CrV6 STDG and UFG S-N curve comparison.

The fatigue strength at 5E6 cycles of 17CrV6 UFG, evaluated by stair-case method at 10%, 50% and 90% of survival probability are: 764MPa, 745MPa and 726MPa. As for STDG characterization the

finite life part of the curve has been drawn, using new and recovered samples after run-out achieving. The estimated fatigue strength by S-N curve at 50%, 10% and 90% of survival probability are 745MPa, 792MPa and 701MPa, respectively.

UFG steel has a fatigue limit lower than STDG steel, all the expected advantages related to the grain refinement have been loosened during carburizing. Moreover UFG steel is characterized by a higher scatter band. This could be due to a higher density of inclusion or segregation as UFG specimens were machined by using the centre of the bar.

Automotive – spring (carbon range 0.40-0.60 %)

The fatigue characterization was planned by using STDG and UFG bars heat treated by using the “Cold Route” process in ARA. The “Cold route” based on induction hardening is able to preserve a finer grain structure as the heating time in the austenitization temperature is very short. Bars with 15mm diameter of 50SiVMo8Nb, with different grain size, were supplied to ARA. STDG steel came from GERDAU, UFG steel came from Freiberg University after grain refinement.

50SiVMo8Nb - Metallographic analysis

A preliminary metallographic analysis has been carried out on 50SiVMo8Nb STDG steel supplied by GERDAU. Two samples prepared on the transversal section were used for the metallographic analysis and grain size measurements. The surface of the bars (Figure 189) is characterized by a complete decarburization layer that has not any detrimental effect on the following specimen production steps. The core microstructure of the bar is principally constituted of ferrite and globular pearlite. The average hardness is 350HV_{0.5}.

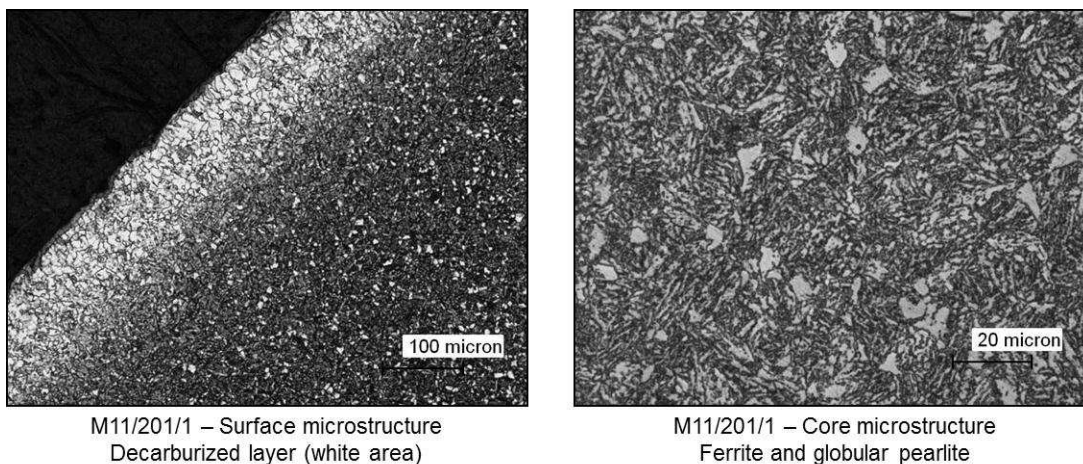


Figure 189: 50SiVMo8Nb STDG bars - Surface and core microstructure.

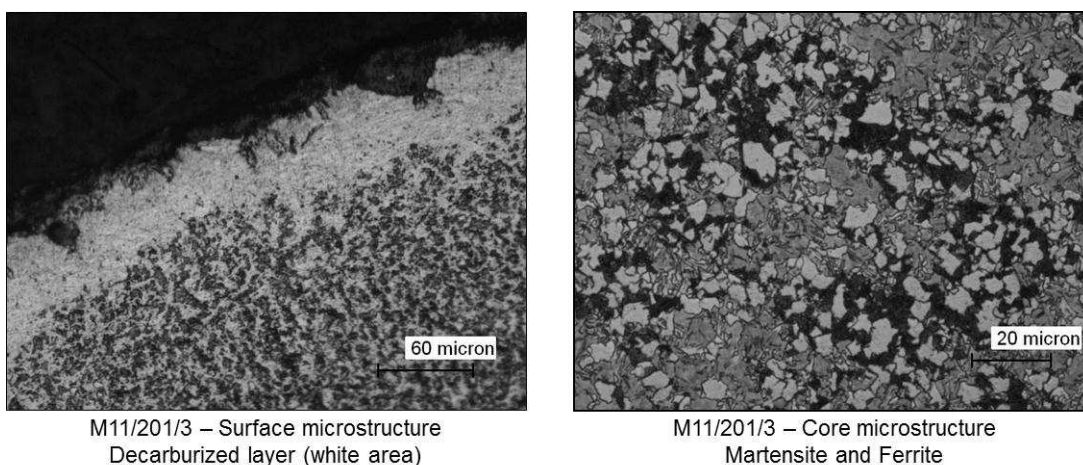


Figure 190: 50SiVMo8Nb UFG bars - Surface and core microstructure.

The same analysis has been done on 50SiVMo8Nb UFG steel supplied by TU-Freiberg. Two samples prepared on the transversal section were used for the metallographic analysis and grain size measurements. As for STDG steel a decarburized layer was found on the bar surface (Figure 190).

The core microstructure seems to be constituted by martensite and ferrite. The average hardness is 523H_{V0.5}.

A metallographic analysis has been carried out on 50SiVMo8Nb STDG and 50SiVMo8Nb UFG steels heat treated by ARA (Figures 191 and 193 respectively). Two samples prepared on the transversal section were used for the metallographic analysis and grain size measurements. In Figure 191 the surface of the bars of STDG steel is characterized by a complete decarburization layer, close to the surface and at the core the microstructure is constitute by martensite. The average hardness is 647HV_{0.5}. The grain size measured on STDG steel before induction hardening is 6µm corresponding to Grade 12 ASTM (Figure 192). The heat treatment has not lead to a significant grain coarsening, in fact the apparent grain size after induction hardening is 8µm (11 ASTM).

In Figure 193 a metallographic analysis of UFG steel is reported. The microstructure is constituted by tempered martensite. The average hardness is 649H_{V0.5}.

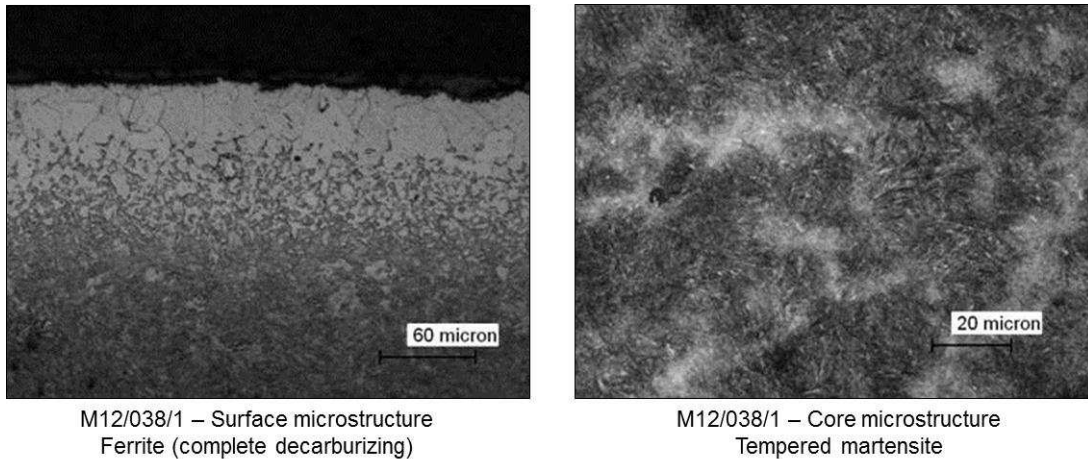


Figure 191: 50SiVMo8Nb STDG bars after induction hardening. Surface and core microstructure.

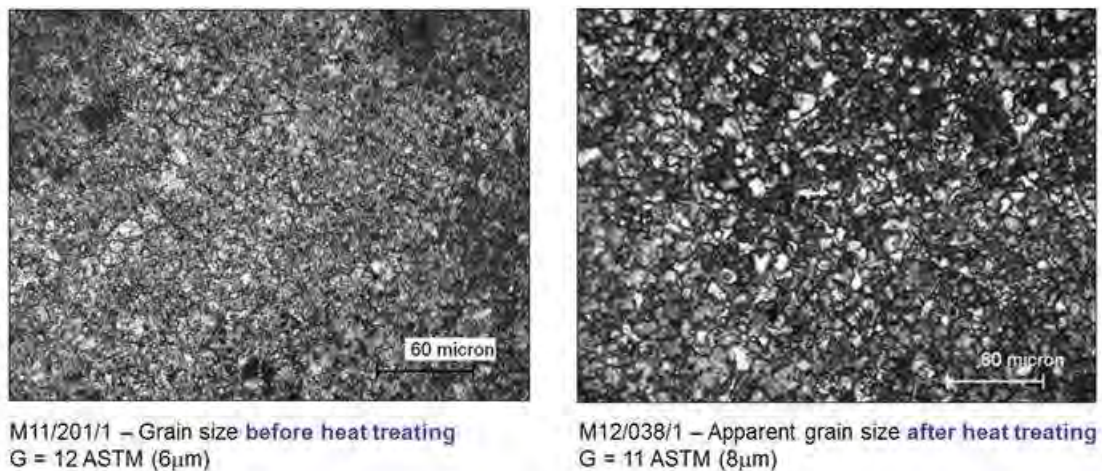


Figure 192: 50SiVMo8Nb STDG Austenitic grain size - UNI EN ISO 643 (ASTM E112).

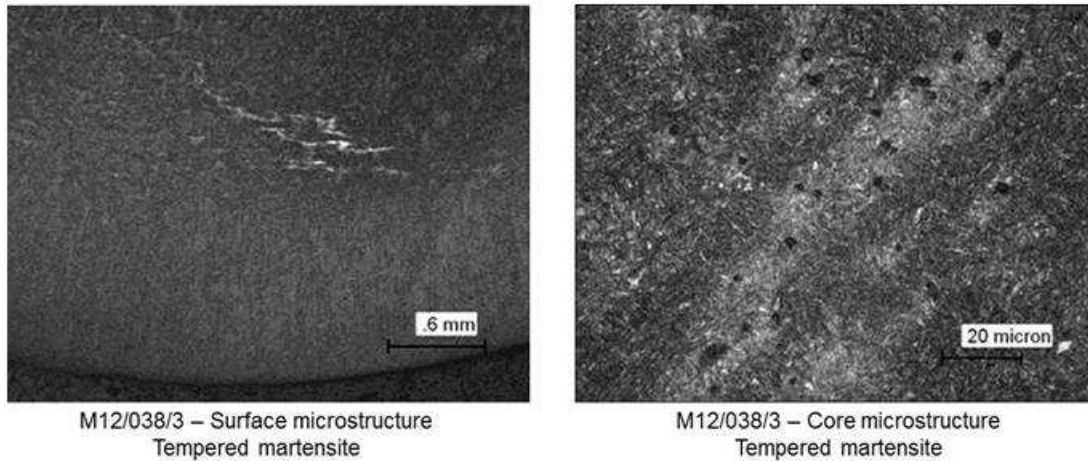


Figure 193: 50SiVMo8Nb UFG bars after induction hardening - Surface and core microstructure.

The grain size measured on UFG steel before induction hardening is $6\mu\text{m}$ corresponding to Grade 12 ASTM (Figure 194). Not any improvement has been achieved by the rolling process produced by TUBAF in comparison to standard rolling process applied by GERDAU. The further heat treatment has not lead to a significant grain coarsening, in fact the apparent grain size after induction hardening is $8\mu\text{m}$ (11 ASTM).

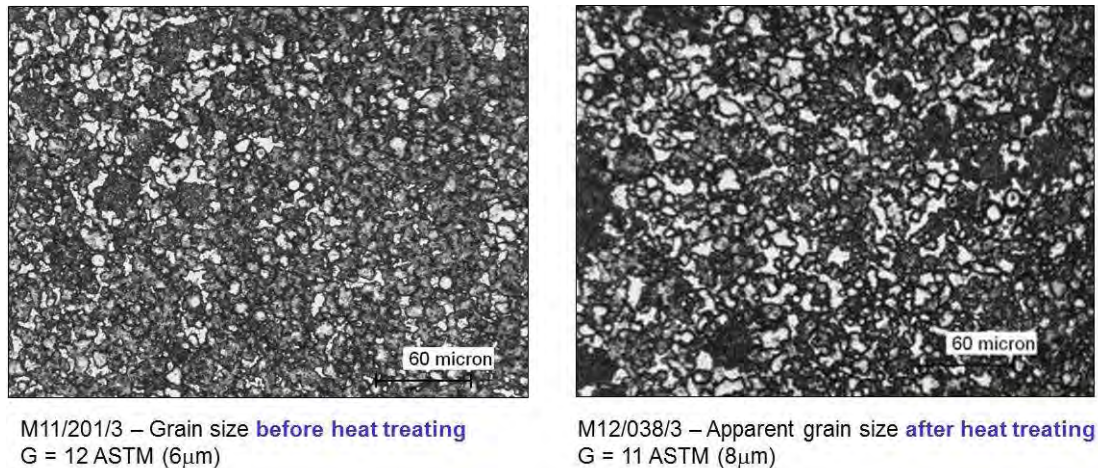


Figure 194: 50SiVMo8Nb UFG Austenitic grain size - UNI EN ISO 643 (ASTM E112).

50SiVMo8Nb - Rotate bending fatigue specimen production

Rotate bending fatigue specimens have been produced starting from 50SiVMo8Nb steel supplied by GERDAU and by TUBAF and heat treated by ARA.

The machining steps are the followings:

- Roughing turning with WC coated insert
- Finishing turning with SUMITOMO ceramic insert
- Several step of abrasive paper: 320, 400, 600, 1000, 1200, 2000 necessary to achieve smooth specimens to better evaluate the fatigue behaviour difference between STDG e UFG avoiding effects related to the surface morphology. With this procedure the roughness was reduced around $0.15\mu\text{m}$

50SiVMo8Nb – Fatigue behaviour evaluation.

The fatigue tests were carried out by the same rotate bending machine used for carburizing steels. The fatigue strength at $5E6$ cycles of 50SiVMo8Nb STDG at 10%, 50% and 90% of survival probability are: 1110MPa, 1090MPa and 1070MPa. The Woehler diagram is reported in Figure 195. The finite life part of the curve has been drawn, without using recovered samples. The S-N curve, gives the estimated fatigue strength at 1090MPa (50%), 1153MPa (10%) and 1031MPa (90%).

A first batch of specimen was cut by using the entire 1 m bar length. The fatigue strength at 5E6 cycles of 50SiVMo8Nb UFG evaluated by stair-case method at 10%, 50% and 90% of survival probability were: 1057MPa, 1045MPa and 1032MPa. The estimated fatigue strength at 50%, 10% and 90% of survival probability were 1045MPa, 1240MPa and 881MPa, respectively.

Since the scatter band of this curve was very high it was decided to prepare another batch of specimens cut just from the middle length of 1 m bars, in order to avoid the starting and final part of the bar that could be not uniformly heated during the induction hardening phase. The fatigue strength at 5E6 cycles of the second batch of 50SiVMo8Nb UFG specimens by stair-case method, at 10%, 50% and 90% of survival probability are: 1131MPa, 1095MPa and 1059MPa. The Woehler diagram is reported in Figure 195. The finite life part of the curve has been drawn, without using recovered samples. As for STDG characterization the finite life part of the curve has been drawn, without using recovered samples. The estimated fatigue strength at 50%, 10% and 90% of survival probability are 1095MPa, 1144MPa and 1048MPa, respectively.

UFG steel has the same fatigue limit than STDG steel. The Woehler curves are characterized by the same scatter band and the same slope. All the expected advantages related to the grain refinement could not be evaluated since before induction hardening STDG and UFG steels had the same grain size. The positive aspect is that induction hardening seems to have not a detrimental effect on grain size coarsening, so potentially could be used to treat this kind of steel.

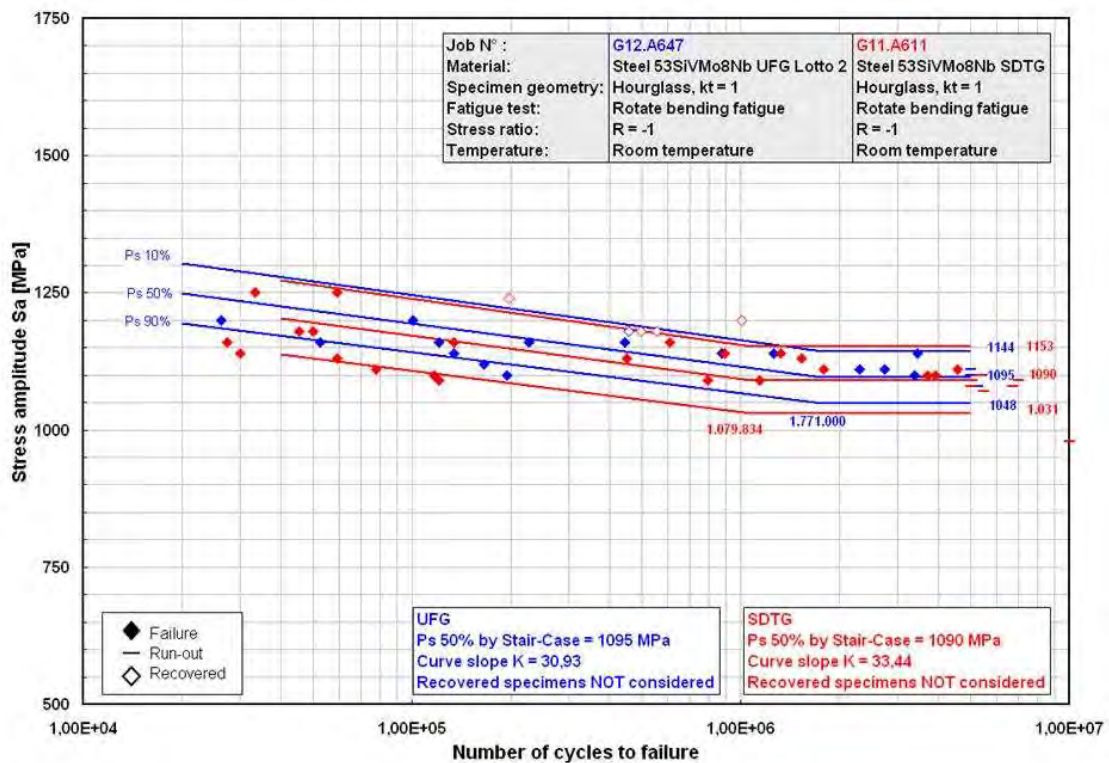


Figure 195: 50SiVMo8Nb STDG and UFG S-N curve comparison.

Task 4.3 – Response to machining

Automotive – powertrain (carbon range 0.15-0.20 %)

The machinability tests carried out have been turning tests (s/norm ISO-3685) in a lathe CNC DANUMERIC NI 1200 from the laboratory of GERDAU I+D and the test procedure has been the following one:

- External turning of 18CrMo4 bars of length <500 mm because of slenderness problems
- Diameter of 50 mm. for standard grain size and 35 mm. for ultra-fine grain size.
- Dry machining
- After machining 500 mm. the flank wear of cutting tool is measured
- Cutting depth: $a_p=1\text{mm}$
- Feed: $f=0.2\text{ mm/rev}$

The cutting tool used for the turning test has been coated carbide (GC4015) and the test speed has been 450 m/min. Before starting the turning tests an analysis of microstructure and hardness of the samples has been carried out (Figures 196 and 197).

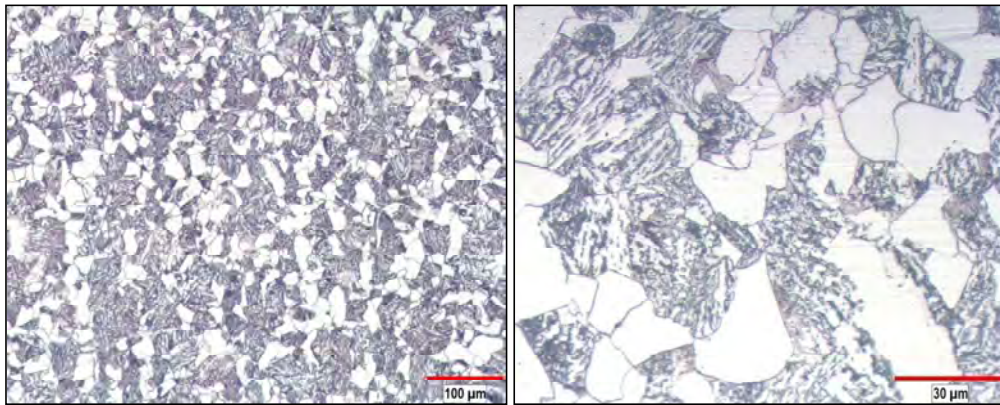


Figure 196: Standard material: ferrite + pearlite with some traces of bainite, 262 – 265 HV.

The wear evolution curves are shown in the Figure 198.

The bars with ultra-fine grain size show higher tool wear than the bars with standard grain size, which was expected because of their higher hardness.

The type of chip obtained in the two cases has been the same (Figure 199).

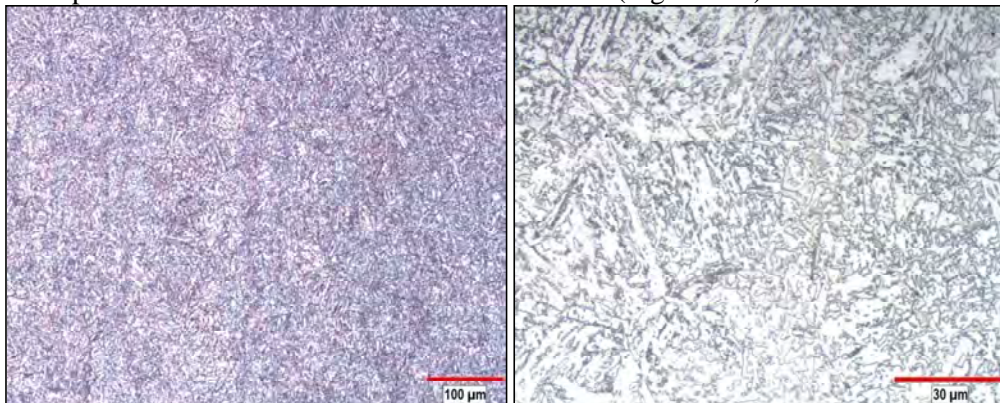


Figure 197: Ultra fine grain size: ≈100% bainite with some traces of martensite and ferrite, 230 – 232 HV.

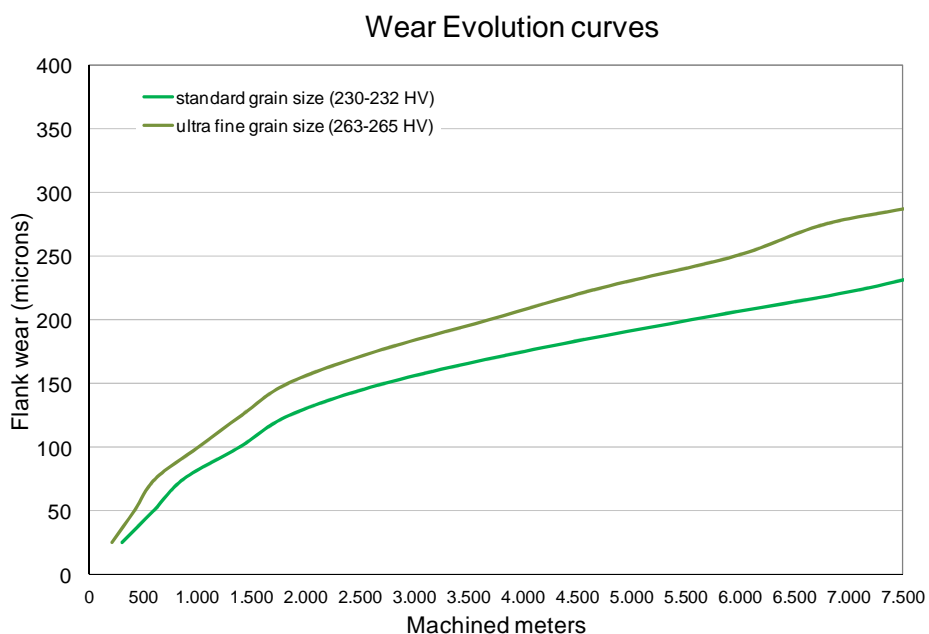


Figure 198: Wear evolution curve for standard and ultra fine grain size.



Figure 199: Type of chip obtained in the machining tests for the 18CrMo4 with standard and with ultra fine grain size.

Conclusions

Fasteners (carbon range 0.15-0.30 %)

The differences found in tensile properties between the steel hot rolled with low finishing temperature (UFG) and the reference product hot rolled with conventional cycle (STD) consist in a slight decrease of tensile strength and an increase of reduction of area, which is a measure of ductility. The microstructure of UFG material consist in ferrite and pearlite and the average ferrite grain size ($7\ \mu\text{m}$) is significantly finer than that of standard product ($12\ \mu\text{m}$).

The increase in ductility (reduction of area) can be explained both by grain refinement and by the complete absence in the final microstructure of hard phases as bainite. This is probably due to the initial austenite grain size, which is finer than in the conventional product, where a certain amount of hard phases may be present.

Automotive – powertrain (carbon range 0.15-0.20 %)

After the carburizing treatment, the hardness profiles have been practically the same for the samples of standard grain size and of ultra fine grain size, and no clear difference has been found between the austenitic grain size of the standard samples and of the UFG samples.

No significant differences have been found in the tensile properties of 18CrMo4 after hardening and stress relief for the steel with standard grain size and with ultra-fine grain size. The values of impact energy, determined by Charpy test, are higher for the samples with ultra fine grain size than for the samples with standard grain size. The torsion tests don't show a clear difference between the 18CrMo4 with standard and with ultra fine grain size.

In terms of response to fatigue, the smaller grain size of UFG steel in comparison to STDG steel achieved after carburizing treatment has not lead to a significant improvement on the fatigue properties of steels 18CrMo4 and 17CrV6. Moreover, UFG steel is characterized by a higher scatter band probably due to an higher density of inclusion or segregation as specimen was machined by using the centre on the bar.

The machining tests performed with the UFG 18CrMo4 and the STD 18CrMo4, in as-rolled conditions, show a higher flank wear in the case of UFG steel, presumably due to its higher hardness.

Automotive – spring (carbon range 0.40-0.60 %)

UFG steel has the same fatigue limit than STDG steel. The Woehler curves are characterized by the same scatter band and the same slope. All the expected advantages related to the grain refinement could not be evaluated since before induction hardening STDG and UFG steels had the same grain size. The positive aspect is that induction hardening seems to have not a detrimental effect on grain size coarsening, so potentially could be used to treat this kind of steel.

2.5 WORK PACKAGE 5:

MECHANICAL COMPONENTS REALIZATION AND FULL-SCALE ASSESSMENT

The objectives of this Work Package are the realization of selected components with the newly developed UFG steel long wire rods, the process and component qualification according to Internal Quality procedures and the identification of merits and criticalities.

Task 5.1 – Cold heading application of new UFG long steels and component qualification

As previously explained, two components (fasteners) have been selected in order to be manufactured from the wire rod produced by Ori Martin with the newly developed hot rolling practices for UFG steel production. As reported in WP4, the main differences between such wire rod and that hot rolled in standard conditions (STD) consist of a finer grain size, around 7 μm instead of 12 μm , and a better ductility (Reduction of Area). The two components selected are the M14 and M8 screws which are part of the group of components selected at the beginning (WP1). Their main characteristics and the current manufacturing processes adopted in Agrati are summarised as follows.

Bi-hexagon socket head cap screw with flange M14x1.5x92, property class 10.9 (Figure 200a), production process:

- Annealing.
- Cold drawing to diameter 13.60 mm.
- Cold forging and thread rolling.
- Quenching and tempering.
- Thread calibration.
- Coating.

Hexalobular flange screw M8x1.25x43, property class 10.9 (Figure 200b), production process:

- Cold drawing to diameter 7.70 mm.
- Cold forging and thread rolling.
- Quenching and tempering.
- Coating.

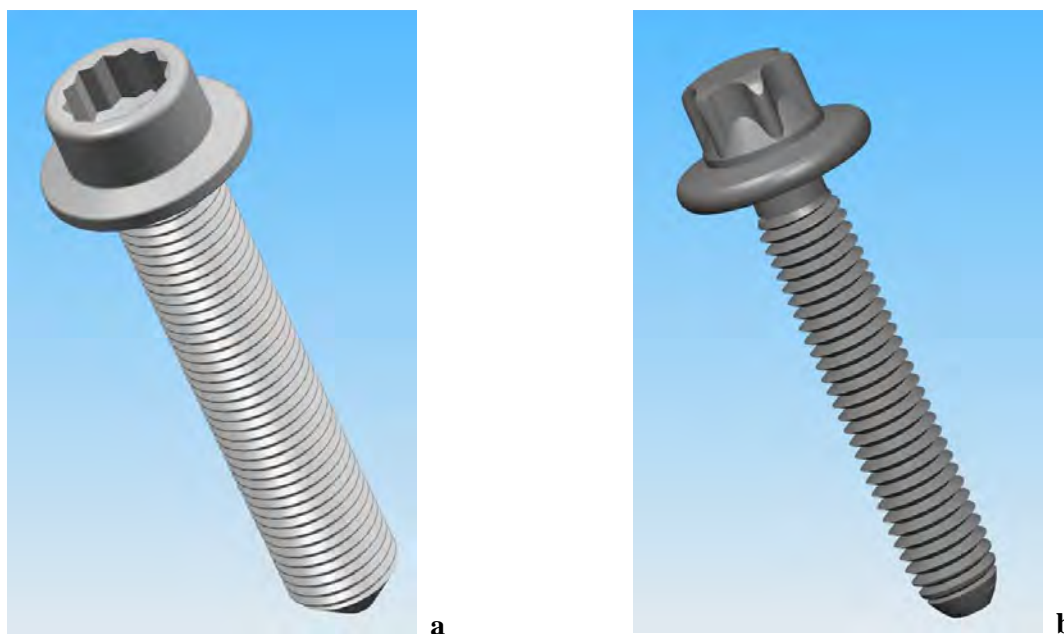


Figure 200: Components selected: M14 screw (a), M8 screw (b).

In order to manufacture a large number of components, which could be considered significant to put in evidence, besides the possible differences in forming operations, even the differences in scrap amount (due to *forging bursts*), 8 coils of 14 mm wire rod and 6 coils of 8 mm wire rod have been processed, respectively. The M14 screws, whose manufacturing process in Agrati includes annealing, have been produced according to two alternative process routes, i.e. with and without annealing. The M8 screws have been produced only without annealing, as the process production does not include it.

The results of the industrial trials in terms of total scrap amount after cold forging for M14 screw are reported in Table 66. Two different lots, manufactured from wire rod hot rolled with low finishing temperature (UFG), annealed and not annealed, are compared with a reference lot (standard wire rod, STD).

Component / wire rod	Process condition	Total pieces number	Total scrapped Pieces	Scrap %
M14 / UFG	not annealed	31775	331	1.04
M14 / UFG	annealed	51194	391	0.76
M14 / STD	annealed	59960	79	0.13

Table 66: Results of the industrial trials for M14 screw.

The results of the industrial trials in terms of total scrap amount after cold forging for M8 screw are reported in Table 67. A lot manufactured from wire rod hot rolled with low finishing temperature (UFG), not annealed, is compared with a reference lot (standard wire rod, STD).

Component / wire rod	Process condition	Total pieces number	Total scrapped Pieces	Scrap %
M8 / UFG	not annealed	362972	385	0.11
M8 / STD	not annealed	134000	64	0.05

Table 67: Results of the industrial trials for M8 screw.

These results can be summarised as follows. Firstly, for both screw sizes, the scrap amounts obtained by processing UFG materials, compared on equal terms (annealed in the case M14, not annealed in the case M8) have been larger than with STD material. Secondly, for M14 size, when the process route without annealing has been tried, the scrap amount has clearly increased.

Unexpectedly, such evidences would suggest that the use of UFG wire rod, despite the finer grain size and the better ductility, was not beneficial in term of scrap percentage, which on the contrary increased. However, it has to be noted that the data of scrap amount, determined during the forging operations at Agrati, merely refer to the total scrap, as no selection of the defect type has been done.

Actually, it has been found that for a significant number of pieces the real cause of rejection was not due to *forging bursts*, but to surface defects which were pre-existing on the wire rod.

This is quite clear from the example of Figure 201, showing some defective M14 screws: on the same side of the defect on the flange (the zone where the *forging burst* is expected to appear) another defect is visible on the screw head. Such situation is clearly related to a surface defect which was present on the wire rod. Furthermore, the typical appearance of a *forging burst* is a crack oriented approximately at 45°, while the cracks originated by surface defects are oriented longitudinally to rolling direction (Figure 202).



Figure 201: M14 screws rejected for defects originated by pre-existing surface defects.

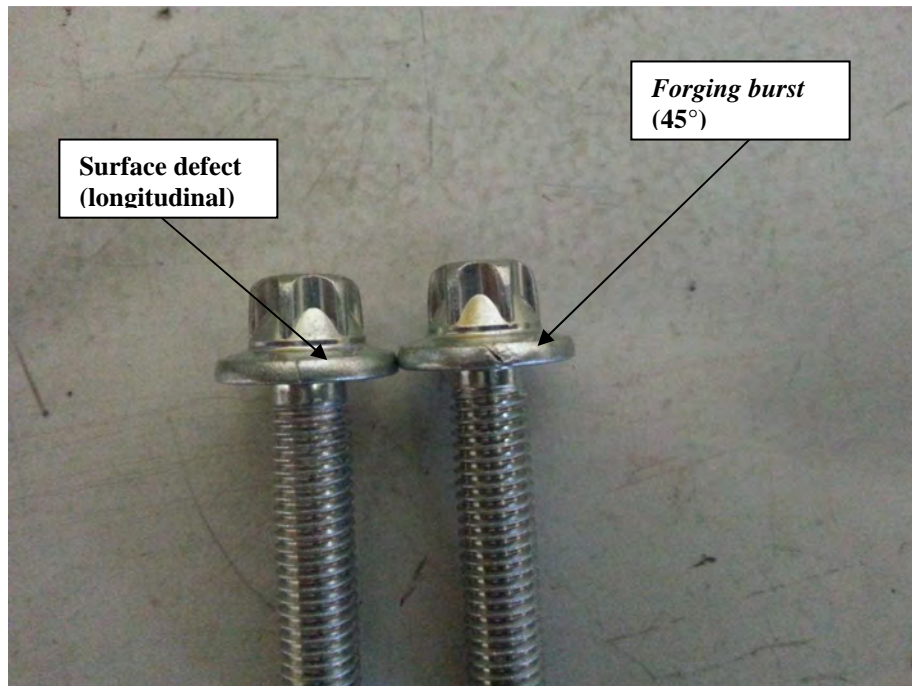


Figure 202: Surface defect and *forging burst* on M8 screws.

In any case, even taking into account these considerations about the origin of the defects, from the results of the cold forming trials without annealing it is not possible to observe any clear improvement coming from the use of UFG wire rod. A possible reason for that is that the entities of grain refinement and of the consequent improvement in ductility are too small to affect significantly the behaviour during the cold forming process.

The results of the product qualification, performed by Agrati in terms of hardness and mechanical properties of the components manufactured from UFG wire rod, are reported in Table 68. All the values fall in the accepted ranges.

Component	UTS (MPa)		Accepted range	HV30		Accepted range
	min	max		min	max	
M14 annealed	1105	1175	1040-1220	356	372	320-380
M14 not annealed	1107	1165		356	379	
M8 (not annealed)	1041	1170		341	356	

Table 68: Results of product qualification (Agrati).

Task 5.2 – Fabrication and qualification of prototype automotive components in UFG steels

Automotive – powertrain (carbon range 0.15-0.20 %)

Metallurgical and fatigue test performed on 18CrMo4 and 17CrV6 UFG steels have stated that the grain refinement is completely lost during carburizing. The long permanence at the austenitization temperature produce a phase transformation, so after carburizing UFG and STD steels have comparable grain size. The fatigue resistance properties are therefore very similar. As consequence, the possibility to produce the gear shaft selected by CRF as demonstrator prototype in carburizing UFG steel was definitively abandoned.

The effort was therefore focused on the quench and tempering steel family, in particular spring steels, as they need a shorter heating time to achieve the required hardness.

Automotive – spring (carbon range 0.40-0.60 %)

Spring manufacturing

ALLEVARD REJNA AUTOSUSPENSION-ARA showed its interest to the grain refinement as considered a way to achieve better performances without cost increasing for the limited addition of expensive elements in the chemical steel composition. Two different manufacturing ways to produce suspension spring are at present used in ARA: “Hot Route” and “Cold Route”.

In the “Hot Route” the rod coming from the steel maker with a ferritic-pearlitic structure and a grain size of 7-9ASTM is heated by conventional or induction furnace up to austenitization temperature (the heating time is short in comparison to carburizing process), the coil forming is performed at high temperature, than follow the quenching in oil and conventional tempering. At the end of the process the apparent grain size is in the range of 7-9 ASTM without particular coarsening.

In the “Cold Route” the rod coming from the steel maker is hardened and tempered by induction (the soaking time at high temperature is shorter than in “Hot Route”), the spring forming is performed at low temperature. At the end of the process the grain size is not changed in comparison to the grain size of the starting rod. “Cold Route” process is convenient for UFG steel as characterized by shorter heating time therefore useful to avoid grain size increasing.

Preliminary results achieved on STDG spring steel treated by “Cold Route” have shown a very low propensity to grain coarsening during induction hardening so it has been decide to proceed to the real spring manufacturing.

Springs manufacturing by using the “Cold Route” need a coil of wire rod of almost 200kg. This coil cannot be produced in TUBAF so it has been decided to compare STDG and UFG springs by using the “Hot Route” process. The “Hot Route” process needs just peeled bars of a length of 2m to produce real automotive springs. This length can be produced by TUBAF with UFG Steel.

Springs metallurgical analysis

A metallographic analysis has been carried out on 50SiVMo8Nb STDG spring steel heat treated by ARA (Figure 203). Two samples prepared on the transversal section were used for the metallographic analysis and grain size measurements. Close to the surface and at the core the microstructure is constituted by tempered martensite. The average hardness is 661HV_{0.5}.

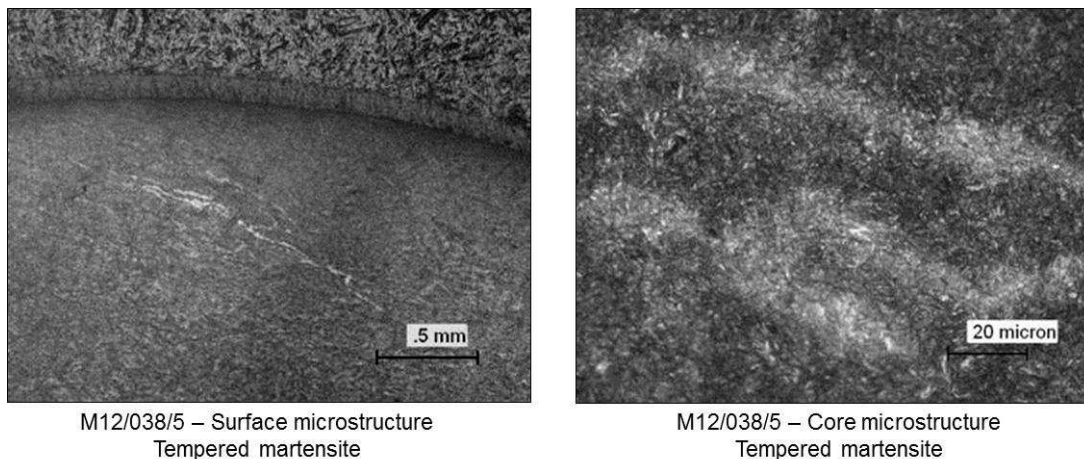
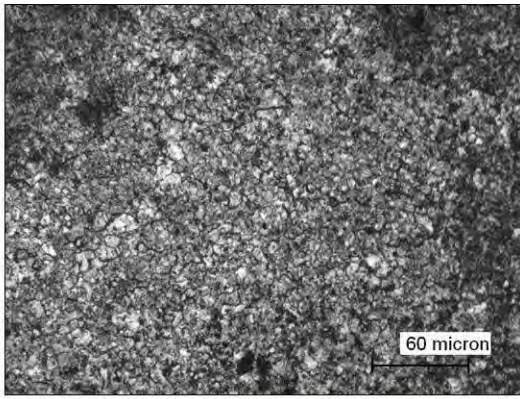
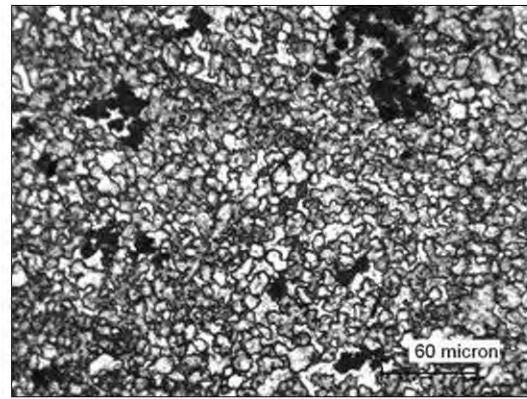


Figure 203: 53SiVMo8Nb STDG steel spring after conventional heat treatment.

The grain size has been evaluated following the Khon method. The grain size measured on STDG steel before conventional hardening was 6µm corresponding to Grade 12 ASTM (Figure 204). The heat treatment has not lead to a significant grain coarsening, in fact the apparent grain size after induction hardening is 8µm (11 ASTM).



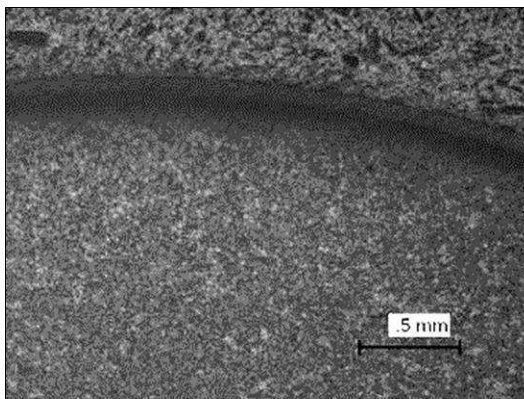
M11/201/1 – Grain size **before heat treatment**
G = 12 ASTM (6 μ m)



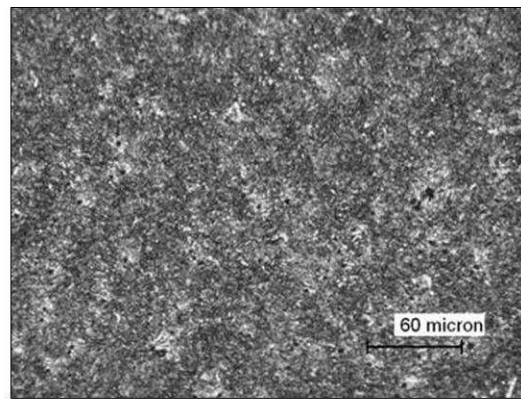
M12/038/5 – Apparent grain size **after heat treatment**
G = 11 ASTM (8 μ m)

Figure 204: 53SiVMo8Nb STDG Austenitic grain size - UNI EN ISO 643 (ASTM E112).

A metallographic analysis has been carried out on 53SiVMo8Nb UFG spring steel heat treated by ARA (Figure 205). Two samples prepared on the transversal section were used for the metallographic analysis and grain size measurements. The microstructure is constituted by tempered martensite. The average hardness is 671HV_{0.5}.

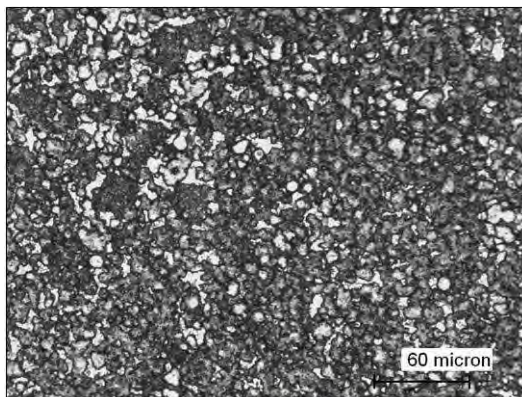


M12/038/7 – Surface microstructure
Tempered martensite

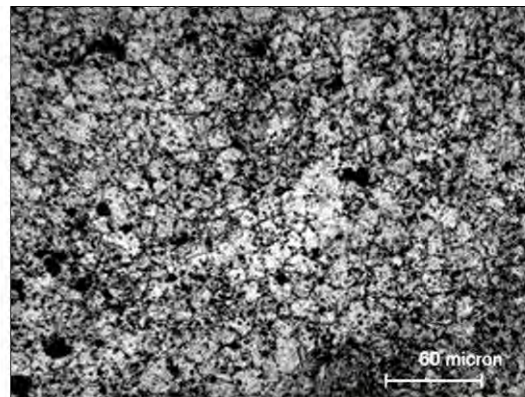


M12/038/7 – Core microstructure
Tempered martensite

Figure 205: 53SiVMo8Nb UFG steel spring after conventional heat treatment.



M11/201/3 – Grain size **before heat treatment**
G = 12 ASTM (6 μ m)



M12/038/7 – Apparent grain size **after heat treatment**
G = 10 ASTM (11 μ m)

Figure 206: 53SiVMo8Nb UFG Austenitic grain size - UNI EN ISO 643 (ASTM E112).

The grain size measured on UFG steel before conventional hardening was 6 μ m corresponding to Grade 12 ASTM (Figure 206). No improvement has been achieved by the rolling process produced by TUBAF in comparison to standard rolling process applied by GERDAU. The further heat treatment has not lead to a significant grain coarsening, in fact the apparent grain size after quenching and tempering was 11 μ m (10 ASTM).

Fatigue test on real spring

By using two batches of hot coiled coil “school” springs (Figure 207) manufactured at the same time in the same process conditions ARA has compared, by following its internal standard testing procedures, the fatigue durability of the steel grade 53SiVMb8Nb produced with current Gerdau hot rolling mill condition versus UFG Freiberg laboratory rolling mill condition.

The used school spring has the following geometry:

- Cylindrical shape
- Mean diameter of the springs = 130mm
- Free Length of the spring = ~ 385mm
- Number of coils = ~ 5.1turns

The test consists of stressing cyclically the spring until failure between 1350MPa (max stress level) and 820MPa (minimum stress level). The spring compression is achieved by using a servo hydraulic actuator able to impose a stroke between 117mm and 312mm.

To evaluate the spring life it is necessary to repeat the test several time in order to achieved statistically valid results. The fatigue tests results on STDG steel spring are summarized in Table 69.



Figure 207: ARA “school” spring.

CS N°	Number of cycles	Int	Side	Ext	Origin of the failure
1	98 061	X	X		1,7 coils from upper end coil - Fatigue failure starting from the surface. Torsion failure ; No marks (picture 1)
2	332 921		X		1,5 coils from upper end coil - Fatigue failure starting from the surface on inclusion. Torsion failure ; No marks (picture 2)
3	1 000 000				Not failed.
4	141 958		X	X	2,2 coils from upper end coil - Fatigue failure starting from the surface. Torsion failure ; No marks (picture 3)
5	187 060			X	2,6 coils from lower end coil - Fatigue failure starting from the surface on inclusion. Torsion failure ; No marks (picture 4)
6	252 212		X		1,2 coils from lower end coil - Fatigue failure starting from the surface. Torsion failure ; No marks (picture 5)
7	226 059	X	X		1,6 coils from upper end coil - Fatigue failure starting from the surface. Torsion failure ; No marks (picture 6)
8	173 211	X	X		1 coils from upper end coil - Fatigue failure starting from the surface. Torsion failure ; No marks (picture 7)
9	252 102		X	X	1,2 coils from upper end coil - Fatigue failure starting from the surface on inclusion. Torsion failure ; No marks (picture 8)

Table 69: 53SiVMo8Nb STDG spring – Fatigue results.

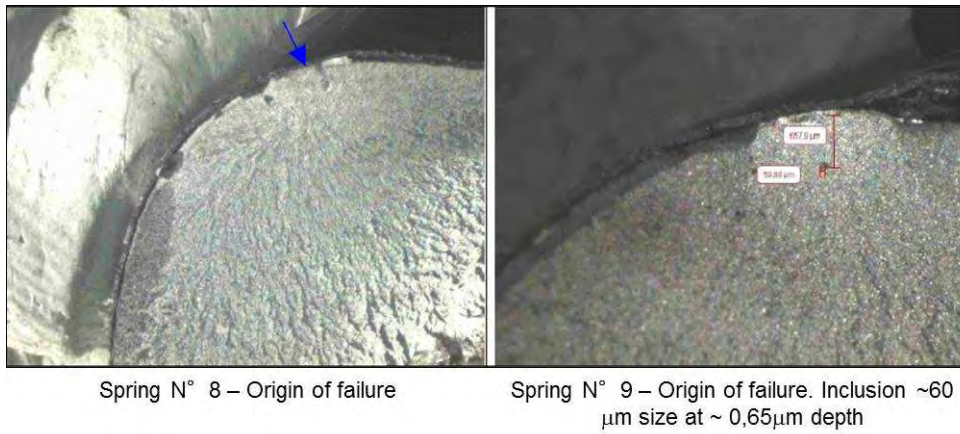


Figure 208: 53SiVMo8Nb STDG spring – Surface fracture analysis.

The fatigue life considering all the tested spring at 50% of survival probability is 296.000 cycles. Excluding the coil spring N°3, that could be considered outside the average, the fatigue life at 50% of survival probability is 208.000 cycles.

The fatigue tests results on UFG steel spring are summarized in Table 70.

CS N°	Number of cycles	Int	Side	Ext	Origin of the failure
1	143 719		X	X	1 coil from upper end coil - Fatigue failure starting from the surface on inclusion. Torsion failure ; No marks (picture 1).
2	83 718		X	X	1 coil from upper end coil - Fatigue failure starting from the surface on inclusion. Torsion failure ; No marks (picture 2).
3	103 691		X		1,2 coil from upper end coil - Fatigue failure starting from the surface on inclusion. Torsion/Flexion failure ; No marks (picture 3).
4	66 705		X		2 coil from lower end coil - Fatigue failure starting from the surface on inclusion. Torsion/Flexion failure ; No marks (picture 4).
5	7 041		X		1,2 coil from upper end coil - Fatigue failure starting from the surface. Torsion/Flexion failure ; defect (picture 5).
6	143 677				Not failed
7	30 043			X	1,7 coil from upper end coil - Fatigue failure starting from the surface. Torsion/Flexion failure ; defect (picture 6).
8	132 758			X	1,2 coil from upper end coil - Fatigue failure starting from the surface on inclusion. Torsion failure ; No marks (picture 7).
9	79 811			X	1,4 coil from upper end coil - Fatigue failure starting from the surface on inclusion. Torsion failure ; No marks (picture 8).
10	109 505			X	2,2 coil from upper end coil - Fatigue failure starting from the surface on inclusion. Torsion failure ; No marks (picture 9).

Table 70: 53SiVMo8Nb UFG spring – Fatigue results.

A metallurgical examination was done on coil spring N°1 (highest results), N°5 (lowest results) and on spring N°7. For the entire batch the metallographic structure was tempered martensite and no decarburization was observed on the surface of all the springs. The hardness was within the required range.

A surface morphological analysis was carried out on the fractured springs highlighting several defects. Some examples are shown in Figures 208÷210.

In Figure 209 defects on the surface fracture of spring N°1 and N°2 are shown. On spring N°1 crack initiation was due to an inclusion of 45μm size at 0.5mm depth, on spring N°2 crack started from an inclusion of 60μm size at 1mm depth.

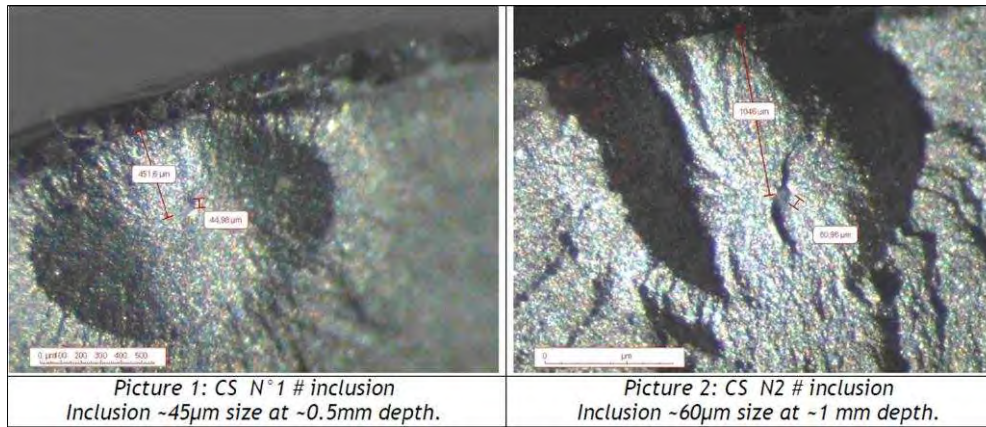


Figure 209: 53SiVMo8Nb UFG spring – Surface fracture analysis.

Dissimilar defects were found on spring N°5 and N°7. On spring N°5 the defect was an overlap positioned at 94μm from the surface. On spring N°7 the defect was a fold at 237μm depth. Some other defects, fold types, were observed in some other spring cuts.

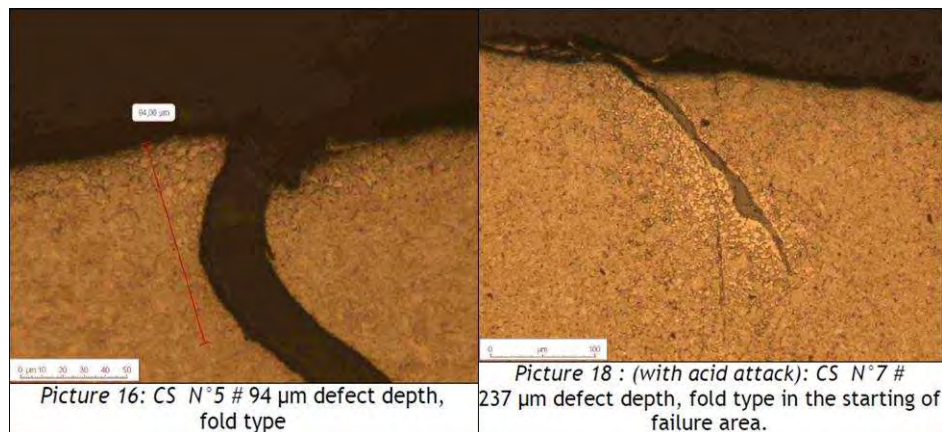


Figure 210: 53SiVMo8Nb UFG spring – Surface fracture analysis.

The fatigue life at 50% of survival probability, considering all the tested springs, is 90.000 cycles. Excluding the springs N°5 and N°7, whose life was reduced by the presence of important defects, the fatigue life at 50% of survival probability is 108.000 cycles. Practically ½ of the fatigue life of STDG steel spring.

Task 5.3 – Quantitative identification of criticalities and merits

Fasteners (carbon range 0.15-0.30 %)

The expected advantages in using UFG wire rod for the manufacturing of screw components were identified in a reduced amount of the scrap after cold forging due to *forging bursts* and in the possible suppression of the annealing of hot rolled wire rod before cold forging.

The cold forging trials performed at Agrati, reported in Task 5.1 were related to M14 and M8 screws. In both cases, UFG wire rod (ferrite grain size 7 μm) and STD wire rod (ferrite grain size 12 μm) were compared. In the specific case of M14 screw, whose process route includes annealing of wire rod, a lot was also produced without annealing.

The results of the cold forming trials did not show evident improvements ascribable to the use of UFG wire rod in terms of scrap amount. Moreover, when investigated (M14 screw) the suppression of annealing of wire rod produced a net increase of scrap amount.

The possible reason identified for that behaviour is that the experimented grain refinement (up to 7 μm) and the consequent increase in ductility are not enough to produce a significant improvement during the cold forming process.

However, it has to be noted that the data of scrap amount, determined during the forging operations at Agrati, merely refer to the total scrap, as no selection of the defect type has been done.

Actually, it has been found that for a significant number of pieces the real cause of rejection was not due to *forging bursts*, but to surface defects which were pre-existing on the wire rod.

In addition it must be noted that the parametric investigation of relationship between microstructural features and cold formability in Task 3.3, which put in evidence significant improvement in the forming behaviour of UFG steel, refers to the steel produced in TUBAF, whose grain size was 3-4 μm .

On the other hand, no important criticalities have been identified in the component quality, as the results of the product qualification show that the mechanical properties of the finished parts fall completely in the accepted ranges.

Automotive – spring (carbon range 0.40-0.60 %)

The expected advantages in using UFG wire rod for the manufacturing of spring components were identified in an improvement of fatigue resistance. Actually the results reported in the previous section (Task 5.2) showed that the fatigue life of UFG steel springs was shorter than that of STDG steel springs (approximately 50%).

This result can be explained by the fact that the austenite grain size of STDG steel, after induction treatment, was finer than that of UFG steel. This means that the microstructure after the treatment is not affected by the previous hot rolled microstructure, so the use of UFG steel in this case doesn't bring any advantage.

2.6 WORK PACKAGE 6:

GUIDELINES FOR UFG STEEL LONG PRODUCTS APPLICATION TO AUTOMOTIVE SECTOR

In this WP all experimental evidences have been synthesized and interpreted in order to draw guidelines for UFG steels (and related mechanical components) applications in the automotive fields. Guidelines for UFG steel long products application to mechanical and automotive sectors have been given.

Guidelines for UFG steel long production

Main parameters that control the formation of ultrafine ferrite are the following:

- **C content** : DIFT occurs at $C < 0.35\%$. For higher C contents the critical strain becomes too high to be applied in a industrial mill. However heavy γ deformation allows to obtain fine ferrite grains even at medium C content (0.3-0.5%).
- **Mn content**: a Low Mn content ($< 1\%$) is favourable for DIFT occurrence.
- **Small Prior Austenite grain size**: it is the most important parameter that can be tuned in an industrial plant. Small prior austenite grain size is always beneficial for both DIFT and Heavy γ deformation mechanisms and should be held lower than $20\ \mu\text{m}$ (better around $10\ \mu\text{m}$) in order to achieve fine ferrite grains and high ferrite volume fraction.
- **Deformation**: High strain level in the last rolling pass (possibly higher than $\epsilon=0.35$) or equivalent accumulated deformation at this stage are required to obtain UFG ferrite.
- **Strain rate**: The effect of strain rate for both mechanisms is not clear for the investigated range ($1-30\ \text{s}^{-1}$) that is not comparable with the one used in industrial mill.

An example of the possible conditions for a thermomechanical cycle aimed to produce UFG steel is:

- Low C content ($< 0.35\%$)
- Low Mn content ($< 1\%$)
- Small PAGS ($< 20\ \mu\text{m}$)
- Low T_{def} in last pass ($< A_{r3} + 25^\circ\text{C}$)
- Last pass strain or accumulated strain at last pass greater than 0.35.

In particular, according to the industrial experience carried out in this project by ORI MARTIN on the steel grade 30MnB4 for fastener application, a possible hot rolling route satisfying most of the conditions reported above can be the following:

- To keep the billet reheating temperature as low as possible (e.g. $1100-1150^\circ\text{C}$) compatibly with the other process requirements);
- Control the finishing mill entry temperature in order to keep it within $A_{r3}+40^\circ\text{C}$ ($770-790^\circ\text{C}$);
- To supply high strain values in the finishing passes.

Guidelines for UFG steel long products application

Automotive – powertrain (carbon range 0.15-0.20 %)

The prototype component selected for this steel grade (gear shaft) requires to be case hardened (carburized) in order to achieve the required surface hardness.

Metallurgical and fatigue test performed on 18CrMo4 and 17CrV6 UFG steels assessed that the grain refinement is completely lost during carburizing because the long permanence at the

austenitization temperature produces phase transformation, so UFG and STD steels have final comparable grain size. The fatigue resistance properties are therefore very similar. As consequence, the possibility to produce the gear shaft as demonstrator prototype in carburizing UFG steel, doesn't bring any advantage.

Automotive – spring (carbon range 0.40-0.60 %)

The expected advantages in using UFG wire rod for the manufacturing of spring components were identified in an improvement of fatigue resistance. Actually the results showed that the fatigue life of UFG steel springs was shorter than that of STDG steel springs (approximately 50%).

This result can be explained by the fact that the austenite grain size of conventional steel, after induction treatment, was finer than that of UFG steel. This means that the microstructure after the treatment is not affected by the hot rolled microstructure, so the use of UFG steel in this case doesn't bring any advantage.

Fasteners

The expected advantages of UFG steel in this range of applications consist in the chance to reduce or eliminate the annealing and to reduce the scraps caused by forging bursts in screw heads occurring during cold forming process.

With respect to the conventional process route for fastener fabrication, the only change that has been investigated is the suppression of the annealing step. Such change allowed to obtain components with good final properties but produced an increase of the scrap amount after cold forming in comparison with the process including the annealing.

The results of the cold forming trials did not show evident improvements ascribable to the use of UFG wire rod in terms of scrap amount. The possible reason identified for that behaviour is that the experimented grain refinement of steels industrially produced by ORI MARTIN was about 7 μm while the conventional steel show about 12 μm and the consequent change of ductility is not enough to produce a significant effect during the cold forming process.

It must be noted that the parametric investigation of relationship between microstructural features and cold formability in Task 3.3, which put in evidence significant improvement in the forming behaviour of UFG steel, refers to the steel produced in pilot mill in TUBAF whose grain size was 3-4 μm . It means that a further refinement of grain size should have produced a more evident effect in scrap reduction during the cold forming process.

Moreover, from the results of Task 3.3 it can be noted the compression tests, that have been used for building the ductility curves to be put in the model, are more severe respect to the industrial fastener forming process, leading to an higher damage in the critical points.

This means that any small deviation in geometry or any small local defect in the material may generate a crack initiation more likely in the conventional steel compared to the UFG steel.

For this reason if it were necessary to increase the complexity of the design of a screw introducing a more severe forming pattern, the use of UFG steel could be helpful and should have an higher safety margin respect to the conventional one.

3. CONCLUSIONS

In order to meet the increasing needs from economic and social developments in future, the research on new generation steels with higher strength and longer duration has become a worldwide issue.

It is well known that there exist various mechanisms to strengthen the steels, but grain refinement is the only method to improve both strength and toughness simultaneously.

A ferrite grain size in the range of 1–4 μm and a steel microstructure characterised by a mixture of ferrite-pearlite and/or martensite, bainite, retained austenite microstructure, can give a very good combination of mechanical (strength, ductility, toughness, fatigue) and technological properties (machinability, cold/warm metal forming, etc.) for final application to automotive components.

Applications of ultrafine grained steels for long products was considered in this project in the field of power train components (e.g. gears), suspension arms (e.g. springs), structural parts (e.g. safety component threaded screw for car steering system) for automotive applications, all of them obtained by the application of cold/warm forming procedures.

The general aim of LUNA project was to define the guidelines for the production and best utilisation of ultrafine grained (UFG) carbon steel long products for mechanical applications, using existing productive plants, through the exploitation of advanced thermomechanical processes and the identification of merits, in terms of microstructural and mechanical properties of UFG long steels in as-rolled conditions and after cold/warm forming.

Identification of the mechanisms to be exploited for producing UFG long product

On the basis of the results reported in the previous sections, both DIFT and Heavy γ deformation mechanisms can be exploited to obtain UFG long product steels.

Very promising results in terms of grain size has been achieved both exploiting DIFT mechanism (occurring at deformation temperature between $\text{Ar}_3 + 15^\circ\text{C}$ and $\text{Ar}_3 + 40^\circ\text{C}$) and Heavy γ deformation (deformation temperature at around $\text{Ar}_3 + 70^\circ\text{C}$).

DIFT mechanism has higher refining power compared with Heavy γ deformation mechanism, however it is not possible to fully exploit it using present industrial configurations because of high deformation level required at low temperature. So, for industrial steel production, the final microstructure will be a mix DIFT ferrite and Heavy γ deformation ferrite. For this reason it is necessary to optimize the thermomechanical cycle in order to maximize DIFT.

Main parameters that control the formation of ultrafine ferrite are the following:

- C content: DIFT occurs at $\text{C} < 0.35\%$. For higher C contents the critical strain becomes too high to be applied in a industrial mill.
- Mn content: a Low Mn content ($< 1\%$) is favourable for DIFT occurrence.
- Small Prior Austenite grain size: it is the most important parameter that can be tuned in an industrial plant. Small prior austenite grain size is always beneficial for both DIFT and Heavy γ deformation mechanisms and should be held lower than 20 μm (better around 10 μm) in order to achieve fine ferrite grains and high ferrite volume fraction.
- Deformation: High strain level in the last rolling pass (possibly higher than $\epsilon = 0.35$ or at this stage the total accumulated deformation should be more than this value) are required to obtain UFG ferrite.

Industrial production of UFG steel

Applying the conditions reported above, industrial production of long UFG steel was carried out at ORI MARTIN industrial plants. The chosen chemical composition was 30MNB4 and was hot rolled to wire-rods of 8 and 14mm diameter for the production of prototype screws.

The only change possible on the industrial plant was to lower the temperature at the entrance of finishing mill in order both to obtain a small prior austenite grain size and to do finishing rolling in a DIFT temperature range. It was done tuning the cooling devices before finishing mill in order to get at the entrance the requested temperature.

Results showed that the average grain size of UFG industrial product was 7 μm , while the conventional material grain size produced by ORI MARTIN is around 12 μm . It means that only decreasing the

entrance temperature at finishing mill helps to almost halve the final grain size, even if it is not enough to arrive at ultrafine range ($< 4\mu\text{m}$). To furtherly decrease the grain size it is necessary to act on the passes deformation at finishing mill and to better modify the cooling pattern.

Guidelines for application of UFG steels

The selected components for powertrain application (gear shaft and spring) after their fabrication require a further heat treatment that destroy the memory of the previous microstructure, as consequence, the possibility to produce the gear shaft or the spring in UFG steel doesn't bring any advantage.

However, the results obtained for fasteners did not show evident improvements ascribable to the use of UFG wire rod in terms of scrap amount. The possible reason identified for that behaviour is that the experimented grain refinement of steels industrially produced by ORI MARTIN was about $7\mu\text{m}$ while the conventional steel show about $12\mu\text{m}$ and the consequent change of ductility was not enough to produce a significant effect during the cold forming process.

However, it has to be noted that the data of scrap amount, determined during the forging operations at Agrati, merely refer to the total scrap, as no selection of the defect type has been done.

Actually, it has been found that for a significant number of pieces the real cause of rejection was not due to *forging bursts*, but to surface defects which were pre-existing on the wire rod.

No criticalities have been identified in the component quality, as the results of the product qualification show that the mechanical properties of the finished parts fall completely in the accepted ranges.

In addition, the investigation of relationship between microstructural features and cold formability carried out using the steel produced on pilot mill with grain size around $3\mu\text{m}$, put in evidence significant improvement in the forming behaviour of UFG steel. It means that a further refinement of grain size should have produced a more evident effect in scrap reduction during the cold forming process. Moreover, results showed that any small deviation in geometry or any small local defect in the material may generate a crack initiation more likely in the conventional steel compared to the UFG steel, and, if it were necessary to increase the complexity of the design of a screw introducing a more severe forming pattern, the use of UFG steel could be helpful and should have an higher safety margin respect to the conventional one.

Final conclusions

The use of UFG steel showed to be potentially able to allow the improvement of cold forming for fastener production. This evidence showed up when the UFG steel from pilot mill (grain size around $3\mu\text{m}$) and conventional steel (grain size around $12\mu\text{m}$) were compared, while the difference was not so evident between the industrially produced UFG (grain size around $7\mu\text{m}$) and conventional steel because it was not possible to produce industrially a finer grain size.

To furtherly decrease the grain size it is necessary to better tune the operating practices for hot rolling in terms of deformation passes at finishing mill and cooling pattern.

4. EXPLOITATION AND IMPACT OF THE RESEARCH RESULTS

This project allowed to assess the guidelines for the industrial production of UFG wire rod steels for fastener application. In particular it is shown that the used industrial thermomechanical cycle was not enough to obtain a grain size in UFG range (1-4 μm). It means that to industrially produce this UFG steel it is necessary to further modify the hot rolling practices.

About the fabrication of components using UFG steels, it was put in evidence a significant improvement in the forming behaviour of UFG steel compared to the conventional one.

It means that any small deviation in geometry or any small local defect in the material during component fabrication may generate a crack initiation more likely in the conventional steel than in UFG steel, and, if it were necessary to increase the complexity of the design of a screw introducing a more severe forming pattern, the use of UFG steel could be helpful to reduce the scrap.

By this project both the basic knowledge about the identification of the mechanisms to be exploited for producing UFG long product and the advantages of producing final components using UFG steel have been assessed. The results obtained in this project will be presented in international conferences and published in scientific journals.

5. REFERENCES

- [1] I. Salvatori et al., “*Ultrafine grained steel by innovative deformation cycles*”, ECSC Contract PR 288, Final Report publ. European Commission, EUR 22007, Luxembourg, 2006.
- [2] H. Hata et al., *Kobelco Technology Rev.* 25 (2002) p.25
- [3] C. Guarnaschelli et al., *Proc. Super High Strength Steels*, Peschiera del Garda, Italy, 2010.
- [4] Choi JK, Seo DH, Lee JS, Umk K & Choo WY (2003) *ISIJ International* 43: 746-754.
- [5] H. Dong and X. Sun, *Current Opinion in Solid State and Materials Science*, (2006).
- [6] Boratto, F. et al. in *THERMEC '88. Proceedings*. Iron and Steel Steel Institute of Japan, Tokyo, 1988, p. 383-390.
- [7] Coppola, T, Demofonti, G (2008). Advanced methods for the strain limit assessment in pipeline applications subjected to extreme loading, 2nd ISOPE Strain Based Design Symposium, SBD 2008, Paper N. ISOPE-2008-TPC-704 Vancouver, Canada, July 6-11.
- [8] T. Coppola, L. Cortese, P. Folgarait. The Effect of Stress Invariants on Ductile Fracture Limit in Steels, *Engineering Fracture Mechanics* 76 (2009) 1288–1302.
- [9] American Society for Testing and Materials “Standard Test Method for Linear-Elastic Plane-Strain Fracture Toughness K_{Ic} of Metallic Materials”. Vol. 03.01. Norm E399-09 (ASTM International) 2009.

LIST OF FIGURES

- Figure 1:** Initial microstructure of samples selected for fasteners applications.
- Figure 2:** Microstructure of a sample of 17CrV6 with isothermal annealing.
- Figure 3:** Influence of the different microalloying elements on the recrystallization-stop temperature.
- Figure 4:** Microstructures of laboratory heats.
- Figure 5:** The ferritic-pearlitic microstructure of steel 50SiMoVNb8 (etched in Nital for 5-10 s).
- Figure 6:** Overall views of the three screws selected.
- Figure 7:** Example of forging burst.
- Figure 8:** 1st gear shaft. C514 gear.
- Figure 9:** TEKFOR and FPT manufacturing cycle.
- Figure 10:** Suspension spring.
- Figure 11:** HOT ROUTE for helicoidally spring manufacturing.
- Figure 12:** COLD ROUTE for helicoidally spring manufacturing.
- Figure 13:** 18CrMo4 gear steel flow.
- Figure 15:** Spring steel flow for preliminary tests.
- Figure 16:** Spring steel flow for test on real component.
- Figure 17:** Spring steel flow for test on real component.
- Figure 18:** Schematic illustration of temperature dependencies of the critical strain for DIFT and DRX [4].
- Figure 19:** Thermomechanical cycles for determination of DIFT parameters.
- Figure 20:** Thermomechanical treatments carried out by dilatometer for prior austenite grain size determination.
- Figure 21:** Microstructure of 30MnB4 sample after the thermomechanical cycle without deformation with different austenitization temperatures.
- Figure 22:** Macrostructures of deformed samples.
- Figure 23:** Microstructure in zone “A” for samples with PAGS=10 μ m.
- Figure 24:** Determination of friction coefficient.
- Figure 25:** Equivalent strain distribution in compression tests.
- Figure 26:** True strain distribution vs. thickness.
- Figure 27:** Microstructure for samples 30MnB4 (Steel B).
- Figure 28a:** Ferrite volume fraction versus strain for Steel 30MnB4.
- Figure 28b:** Grain size versus strain for Steel 30MnB4.
- Figure 29:** Microstructure for samples 18MnB2 (Steel A).
- Figure 30a:** Ferrite volume fraction versus strain for Steel A (18MnB2).
- Figure 30b:** Grain size versus strain for Steel A (18MnB2).
- Figure 31:** Microstructure for samples 18MnB7 (2624).
- Figure 32a:** Ferrite volume fraction versus strain Steel 2624.
- Figure 32b:** Grain size versus strain Steel 2624.
- Figure 33 :** Microstructure for samples 18Mn7 (2623).
- Figure 34a:** Ferrite volume fraction versus strain for Steel 2623.
- Figure 34b:** Grain size versus strain for Steel 2623.
- Figure 35:** Microstructure for samples 30MnB7 (2625).
- Figure 36:** Effect of C and Mn content on ϵ_c .
- Figure 37:** Microstructure for 18MnB2 samples PAGS= 10 μ m (Steel A).
- Figure 38:** Microstructure for samples 18MnB2 PAGS= 50 μ m(Steel A).
- Figure 39:** Microstructure for samples 30MnB4 PAGS= 10 μ m(Steel B).

Figure 40: Microstructure for samples 30MnB4 PAGS= 50 μm (Steel B).

Figure 41: Ferrite volume fraction and grain size versus strain rate for samples 18MnB2.

Figure 42: Ferrite volume fraction and grain size versus strain rate for samples 30MnB4.

Figure 43: Microstructure of samples (left) #16 and (right) #17 of 18CrMo4 Experimental (etched in 2% Nital for 5-10 s).

Figure 44: Thermomechanical cycles corresponding to samples (left) #16 and (right) #17 of 18CrMo4 Experimental.

Figure 45: Thermo-mechanical cycle corresponding to the best result obtained with the 18CrMo4 Experimental (sample #10).

Figure 46: Thermo-mechanical cycles corresponding to samples (top) #23 and (bottom) #24 of 18CrMo4 Industrial.

Figure 47: Microstructure of samples (left) #23 and (right) #24 of 18CrMo4 Industrial (etched in 2% Nital for 5-10 s).

Figure 48: Thermo-mechanical cycles corresponding to samples (left) #16 to (right) #18 of 50SiMoVNb8.

Figure 49: Microstructure of samples (left) #16 and (right) #17 of 50SiMoVNb8 (etched in 2% Nital for 5-10 s).

Figure 50: Thermo-mechanical cycle corresponding to the best result obtained with the 50SiMoVNb8 (sample #14).

Figure 51: Scheme of mechanisms occurring during rolling [5].

Figure 52: CCT diagram of VM2623 (18Mn7 steel).

Figure 53: CCT diagram of VM2624 (18MnB7steel).

Figure 54: CCT diagram of VM2625 (30MnB7steel).

Figure 55: CCT diagram of A steel (18MnB2 steel).

Figure 56: CCT diagram of B steel (30MnB4 steel).

Figure 57: Prior austenite grain boundaries (PAGS) as revealed by quenching non-deformed samples. $\langle d \rangle$ is the mean value of PAGS.

Figure 58: Microstructure for 18MnB2 samples deformed at $T=867^\circ\text{C}$ (Ar_3+70) (Steel A).

Figure 59: Microstructure for 30MnB4 samples deformed at $T=820^\circ\text{C}$ (Ar_3+70) (Steel B).

Figure 60: Microstructures obtained at the different cooling rates of the CCT curve.

Figure 61: CCT curve of the industrial heat of 17CrV6 (36624).

Figure 62: Microstructures obtained at the different cooling rates for the Experimental heat of 17CrV6.

Figure 63: CCT diagram of the experimental heat of 17CrV6.

Figure 64: Microstructures obtained at the different cooling rates for the 17CrVNb6.

Figure 65: CCT diagram of the experimental heat of 17CrVNb6.

Figure 66: Geometry of the sample after the compression test.

Figure 67: Prior austenite grain size after soaking during 2 minutes at 1200°C .

Figure 68: First thermomechanical cycle performed in the GLEEBLE machine.

Figure 69: Microstructures obtained of the first thermomechanical cycle.

Figure 70: Second thermomechanical cycle performed in the GLEEBLE machine.

Figure 71: Microstructures obtained after the second thermomechanical cycle.

Figure 72: Third thermomechanical cycle performed in the GLEEBLE machine.

Figure 73: Fourth thermomechanical cycle performed in the GLEEBLE machine.

Figure 74: Microstructures obtained for the thermomechanical cycle number III.

Figure 75: Microstructures obtained for the thermomechanical cycle number IV.

Figure 76: 7th thermomechanical cycle performed in GLEEBLE machine.

Figure 77: Microstructures obtained for the thermomechanical cycle number VII.

Figure 78: The 8th thermomechanical cycle.

Figure 79: Microstructures of grain size, hardness and microstructure obtained with the 8th thermomechanical cycle.

Figure 80: The 9th thermomechanical cycle.

Figure 81: Microstructure obtained after the 9th thermomechanical cycle.

Figure 82: The 10th thermomechanical cycle.

Figure 83: Microstructures obtained after the 10th thermomechanical cycle.

Figure 84: The 11th thermomechanical cycle.

Figure 85: Microstructures obtained after the 11th thermomechanical cycle.

Figure 86: Percentage of ferrite grain sizes for heat 719 (17CrV6) after the 11th thermomechanical cycle.

Figure 87: Percentage of ferrite grain sizes for heat 721 (17CrVNb6) after the 11th thermomechanical cycle and a deformation grade of 0.2.

Figure 88: Percentage of ferrite grain sizes for heat 721 (17CrVNb6) after the 11th thermomechanical cycle and a deformation grade of 0.4.

Figure 89: Percentage of ferrite grain sizes for heat 36624 (17CrV6) after the 11th thermomechanical cycle.

Figure 90: Percentage of ferrite grain sizes for heat 50654 (18CrMo4) after the 11th thermomechanical cycle.

Figure 91: Austenite grain size obtained by chemical analysis after heating at 1200°C for 5 minutes.

Figure 92: Austenite grain size obtained by thermal etching in Gleeble machine after heating at 1200°C for 5 minutes and the first deformation at 1150°C.

Figure 93: Austenite grain size obtained by thermal etching in Gleeble machine after heating at 1200°C and the two deformation at 1150°C and 800°C.

Figure 94: The 12th thermomechanical cycle.

Figure 95: Microstructures obtained after the 12th thermomechanical cycle.

Figure 96: Ferrite grain size for the three tested heats.

Figure 97: Percentage of ferrite grain sizes for heat 36624 (17CrV6) after the 12th thermomechanical cycle.

Figure 98: Percentage of ferrite grain sizes for heat 50654 (18CrMo4) after the 12th thermomechanical cycle.

Figure 99: Percentage of ferrite grain sizes for heat 719 (17CrV6) after the 12th thermomechanical cycle.

Figure 100: (a) Schematic drawing of the rotation assembly of the MaxStrain System and (b) MaxStrain system.

Figure 101: Microstructural evolution of 18MnB2 after each hot rolling pass.

Figure 102: Microstructural evolution of 30MnB4 after the simulated hot rolling passes.

Figure 103: (a) Two-high rolling mill, (b) measurement of the start and (c) finish rolling temperature.

Figure 104: Grain size distribution after rolling for steel 18CrMo4 a) finish rolling temperature 740°C, air cooling, b) finish rolling temperature 840°C, air cooling.

Figure 105: Micrographs of the structure in air cooled after the rolling specimens. Finish rolling temperature a) 840°C, b) 805°C, c) 748°C and d) 740°C.

Figure 106: Grain size distribution chart for the metallographic samples extracted from steel 18CrMo4 after rolling: a) finish rolling temperature 740°C, water cooling and b) finish rolling temperature 840°C, water cooling.

Figure 107: Micrographs of the structure in water cooled after the rolling specimens. Finish rolling temperature a) 840°C, b) 805°C, c) 737°C and d) 730°C.

Figure 108: Average grain size (a) and hardness (b) of the steel 18CrMo4 in dependence on the finish rolling temperature after the air and water cooling.

Figure 109: Continuous rolling mill.

Figure 110: Microstructure of air cooled specimens of steel 18CrMo4 versus finish rolling temperature and rolling speed.

Figure 111: Microstructure of water cooled specimens of steel 18CrMo4 versus finish rolling temperature and rolling speed.

Figure 112: Microstructure of air cooled specimens of steel 50SiMoVNb8 versus finish rolling temperature and rolling speed.

Figure 113: Microstructure of water quenched specimens of steel 50SiMoVNb8 versus finish rolling temperature and rolling speed.

Figure 114: Average grain size and hardness of air and water quenched specimens of steel 50SiMoVNb8.

Figure 115: Microstructure of air cooled specimens of steel 18MnB2 versus finish rolling temperature

Figure 116: Microstructure of water cooled specimens of steel 18MnB2 versus finish rolling temperature.

Figure 117: Microstructure of air cooled specimens of steel 30MnB4 versus finish rolling temperature.

Figure 118: Microstructure of water cooled specimens of steel 30MnB4 in dependence of finish rolling temperature.

Figure 119: Flow chart of the investigation of relationship between microstructural features and cold formability.

Figure 120: Extended stress-strain curve for 33MnB5.

Figure 121: Screw dimensions.

Figure 122: Screw head cold forming steps.

Figure 123: Equivalent plastic strain field at the end of step 2.

Figure 124: Equivalent plastic strain field at the end of step 3.

Figure 125: Equivalent plastic strain field at the end of step 4.

Figure 126: Strain evolution in the upsetting test.

Figure 127: Flanged (a) and tapered bulged (b) specimens.

Figure 128: Strain evolution for different upsetting specimens.

Figure 129: Strain evolution at the flange tip in screw head forming.

Figure 130: Stress parameters T and X evolution at flange tip during head forming.

Figure 131: Example of ductile fracture locus.

Figure 132: Strain path comparison for screw head forming and tapered specimen.

Figure 133: Tensile test specimen.

Figure 134: Tensile Round notched specimen RNB10.

Figure 135: Tensile Round notched specimen RNB2.

Figure 136: Torsion test specimen.

Figure 137: Compression tapered specimen.

Figure 138: Extended true stress-true strain curve.

Figure 139: Visual cracks for different compression conditions and materials.

Figure 140: Visual cracks for TAP 1 standard sample.

Figure 141: Fracture locus for steel LN and ST.

Figure 142: Damage evolution for steel LN and ST during compression test.

Figure 143: Damage evolution for steel LN and ST during head screw forming.

Figure 144: ORI Martin Industrial Plant.

Figure 145: (a) Temperature evolution for each fabricated billet of 8mm diameter (T1 green line, T2 blue line, T3 red line), (b) example of temperature evolution of a single billet (T1 light blue line, T2 blue line, T3 red line).

Figure 146: (a) Temperature evolution for each fabricated billet of 14mm diameter (T1 green line, T2 blue line, T3 red line), (b) example of temperature evolution of a single billet (T1 green line, T2 blue line, T3 red line).

Figure 147: Prior austenite grain size of quenched samples before entering in the finishing line (BGV).

Figure 148: Microstructure of quenched samples after the finishing line (BGV) and before entering the Stelmor line.

Figure 149: Microstructure of wire rods final product of 14 mm diameter (different coils sampling).

$D_{\text{ferr}}=7.2\mu\text{m}$, $FV_{\text{ferr}}=63\%$, $FV_{\text{pearlite}}=37\%$.

Figure 150: Microstructure of wire rods final product of 8 mm diameter (different coils sampling).

$D_{\text{ferr}}=7.0\mu\text{m}$, $FV_{\text{ferr}}=79\%$, $FV_{\text{pearlite}}=21\%$.

Figure 151: Microstructure of the wire rod diameter 14 mm (UFG). Ferrite + pearlite. (a) coil n. 4 (b) coil n. 8.

Figure 152: Microstructure of the wire rod diameter 8 mm (UFG). Ferrite + pearlite. (a) coil n. 13 (b) coil n. 14.

Figure 153: Hardness profile of the samples of 18CrMo4 with standard grain size and ultra-fine grain size.

Figure 154: Hardness profile of the samples of 17CrV6 with standard grain size and UFG size.

Figure 155: Microstructures obtained for 17CrV6 standard and with UFG.

Figure 156: Microstructures obtained for 18CrMo4 standard and with UFG.

Figure 157: Prior austenite grain size for 17CrV6 standard and with UFG.

Figure 158: Prior austenite grain size for 18CrMo4 standard and with UFG.

Figure 159: Percentage of the different austenite grains of 17CrV6 in the core.

Figure 160: Percentage of the different austenite grains of 17CrV6 in the surface.

Figure 161: Percentage of the different austenite grains of 18CrMo4 in the core.

Figure 162: Percentage of the different austenite grains of 18CrMo4 in the surface.

Figure 163: Ductile-to-Brittle Transition Temperature by Charpy V-notch impact tests of the samples of 18CrMo4 with standard grain size and ultra-fine grain size.

Figure 164: Ductile-to-Brittle Transition Temperature by Charpy V-notch impact tests of the samples of 17CrV6 with standard grain size and ultra-fine grain size.

Figure 165: Results of tensile tests of 18CrMo4 standard and with ultra fine grain.

Figure 166: Torsion test samples.

Figure 167: Fracture of 18CrMo4 standard.

Figure 168: (Left) Optical micrograph used to estimate the fatigue growth pre-crack length. (Right) Load-Crack opening record used to estimate K_{IC} .

Figure 169: Bar core microstructure.

Figure 170: Inclusion analysis - UNI 3244.

Figure 171: Bar core microstructure.

Figure 172: Inclusion analysis - UNI 3244.

Figure 173: 18CrMo4 STDG carburizing layer – Specimen centre section.

Figure 174: 18CrMo4 UFG carburizing layer – Specimen centre section.

Figure 175: 18CrMo4 STDG Austenitic grain size - UNI EN ISO 643 (ASTM E112).

Figure 176: 18CrMo4 UFG Austenitic grain size - UNI EN ISO 643 (ASTM E112).

Figure 177: ITALSIGMA rotate bending fatigue machine.

Figure 178: 18CrMo4 STDG fatigue strength – Stair Case method.

Figure 179: 18CrMo4 UFG S-N curve.

Figure 180: 17CrV6 STDG bar surface microstructure.

Figure 181: 17CrV6 STDG inclusion analysis - UNI 3244.

Figure 182: 17CrV6 UFG bar core microstructure.

Figure 183: 17CrV6 UFG inclusion analysis - UNI 3244.

Figure 184: 17CrV6 STDG carburizing layer – Specimen center section.

Figure 185: 17CrV6 UFG carburizing layer – Specimen center section.

Figure 186: 17CrV6 STDG Austenitic grain size - UNI EN ISO 643 (ASTM E112).

Figure 187: 17CrV6 UFG Austenitic grain size - UNI EN ISO 643 (ASTM E112).

Figure 188: 17CrV6 STDG and UFG S-N curve comparison.

Figure 189: 50SiVMo8Nb STDG bars - Surface and core microstructure.

Figure 190: 50SiVMo8Nb UFG bars - Surface and core microstructure.

Figure 191: 50SiVMo8Nb STDG bars after induction hardening. Surface and core microstructure.

Figure 192: 50SiVMo8Nb STDG Austenitic grain size - UNI EN ISO 643 (ASTM E112).

Figure 193: 50SiVMo8Nb UFG bars after induction hardening - Surface and core microstructure.

Figure 194: 50SiVMo8Nb UFG Austenitic grain size - UNI EN ISO 643 (ASTM E112).

Figure 195: 50SiVMo8Nb STDG and UFG S-N curve comparison.

Figure 196: Standard material: ferrite + pearlite with some traces of bainite, 262 – 265 HV.

Figure 197: Ultra fine grain size: \approx 100% bainite with some traces of martensite and ferrite, 230 – 232 HV.

Figure 198: Wear evolution curve for standard and ultra fine grain size.

Figure 199: Type of chip obtained in the machining tests for the 18CrMo4 with standard and with ultra fine grain size.

Figure 200: Components selected: M14 screw (a), M8 screw (b).

Figure 201: M14 screws rejected for defects originated by pre-existing surface defects.

Figure 202: Surface defect and *forging burst* on M8 screws.

Figure 203: 50SiVMo8Nb STDG steel spring after conventional heat treatment.

Figure 204: 50SiVMo8Nb STDG Austenitic grain size - UNI EN ISO 643 (ASTM E112).

Figure 205: 50SiVMo8Nb UFG steel spring after conventional heat treatment.

Figure 206: 50SiVMo8Nb UFG Austenitic grain size - UNI EN ISO 643 (ASTM E112).

Figure 207: ARA “school” spring.

Figure 208: 50SiVMo8Nb STDG spring – Surface fracture analysis.

Figure 209: 50SiVMo8Nb UFG spring – Surface fracture analysis.

Figure 210: 50SiVMo8Nb UFG spring – Surface fracture analysis.

LIST OF TABLES

- Table 1:** Chemical compositions of Ori Martin industrial heats (% mass, N and B in ppm).
- Table 2:** Chemical compositions of CSM laboratory heats (% mass, N and B in ppm).
- Table 3:** Rolling parameters for 50 mm diameter bars produced at Ori Martin.
- Table 4:** Phase transition critical points of steels for fasteners (°C).
- Table 5:** Chemical compositions of Gerdau industrial heats (% mass).
- Table 7:** Mechanical characteristics of 17CrV6 isothermally annealed.
- Table 8:** Chemical compositions of Gerdau Experimental heats (% mass).
- Table 9:** Critical points of experimental heats.
- Table 10:** Mechanical properties of 17CrV6 and 17CrVNb6.
- Table 11:** Chemical composition of Gerdau industrial heat (% mass).
- Table 12:** Critical points of industrial heat.
- Table 13:** Selected components (fasteners).
- Table 14:** Prior austenite grain sizes (μm) (PAGS) for all the steels at different soaking temperatures.
- Table 15:** Critical strain for medium-C steels.
- Table 16:** Critical strain for low C steels.
- Table 17:** Microstructural composition (phases, amount and size) and Vickers hardness (0.5 kg) of the DIFT cycles of 18CrMo4 Experimental.
- Table 18:** Microstructural composition (phases, amount and size) of the best result obtained with the 18CrMo4 Experimental.
- Table 19:** Microstructural composition (phases, amount and size) and Vickers hardness (0.5 kg) of the DIFT cycles of 18CrMo4 Industrial.
- Table 20:** Microstructural composition (phases, amount and size) and Vickers hardness (0.5 kg) of the DIFT cycles of 50SiMoVNb8.
- Table 21:** Microstructural composition (phases, amount and size) of the best result obtained with 50SiMoVNb8.
- Table 22:** Summary of results for steel A (18MnB2) ($A_{r3} + 70\text{ }^{\circ}\text{C} = 867\text{ }^{\circ}\text{C}$).
- Table 23:** Summary of results for steel B (30MnB4) ($A_{r3} + 70\text{ }^{\circ}\text{C} = 820\text{ }^{\circ}\text{C}$).
- Table 24:** Results of the dilatometry tests for the industrial heat of 17CrV6.
- Table 25:** Results of dilatometry tests of the Experimental heat of 17CrV6.
- Table 26:** Results of dilatometry tests of 17CrVNb6.
- Table 27:** Results obtained after the 1st thermomechanical cycle.
- Table 28:** Results obtained for the different samples after the thermomechanical cycles III and IV.
- Table 29:** Results obtained for the different samples after the thermomechanical cycle VII.
- Table 30:** Results of grain size, hardness and microstructure obtained with the 9th thermomechanical cycle.
- Table 31:** Results of grain size, hardness and microstructure obtained with the 10th thermomechanical cycle.
- Table 32:** Results of grain size, hardness and microstructure obtained with the 11th thermomechanical cycle.
- Table 33:** Maximum forces obtained at the different temperatures of the last deformation.
- Table 34:** Summary of results for the different experimental and industrial heats after the last thermomechanical cycle.
- Table 35:** Summary of the best results obtained in the different thermomechanical tests with an austenization temperature of 1200°C.
- Table 37:** Comparison of the best results after an austenization temperature of 1000° and 1200°C.
- Table 38:** Thermomechanical conditions simulated at Gleeble for steel 18MnB2.
- Table 39:** Thermomechanical conditions simulated at Gleeble for steel 30MnB4.

Table 40: Measured start and finish rolling temperatures (by pyrometer).

Table 41: Average grain size, microstructure and hardness of the steel 18CrMo4 versus finish rolling temperature after air cooling.

Table 42: Average grain size, microstructure and hardness of the steel 18CrMo4 in dependence on the finish rolling temperature after the water cooling.

Table 43: Rolling schedule of steels 18CrMo4 and 50SiMoVNb8.

Table 44: Calculated parameters of the rolling of steels 18CrMo4 and 50SiMoVNb8 versus rolling speed.

Table 45: Ferrite grain size, average grain size and hardness of air cooled specimens of steel 18CrMo4.

Table 46: Austenite grain size and hardness of water quenched specimens of steel 18CrMo4.

Table 47: Ferrite and average grain size and hardness of air cooled specimens of steel 50SiMoVNb8.

Table 48: Austenite grain size and hardness of water cooled specimens of steel 50SiMoVNb8.

Table 49: Ferrite, average grain size and hardness of air cooled specimens of steel 18MnB2.

Table 50: Austenite grain size and hardness of water cooled specimens of steel 30MnB4.

Table 51: Ferrite grain size, average grain size and hardness of air cooled specimens of steel 30MnB4.

Table 52: Austenite grain size and hardness of water quenched specimens of steel 30MnB4.

Table 53: Chemical composition of 33MnB5 from CSM database.

Table 54: Test type and related stress parameters.

Table 55: Tensile test results.

Table 56: Compression test results.

Table 57: Fracture strain summary for steel LN.

Table 58: Fracture strain summary for steel ST.

Table 59: Damage model parameters for steels LN and ST.

Table 60: Tensile properties of the wire rod diameter 14 mm (UFG).

Table 60: Tensile properties of the wire rod diameter 14 mm (UFG).

Table 62: Tensile properties of the wire rod diameter 8 mm (UFG).

Table 63: Tensile properties of the wire rod diameter 8 mm (STD).

Table 64: Results of the tensile tests.

Table 65: Results of torsion tests.

Table 66: Results of the industrial trials for M14 screw.

Table 67: Results of the industrial trials for M8 screw.

Table 68: Results of product qualification (Agrati).

Table 69: 53SiVMo8Nb STDG spring – Fatigue results.

Table 70: 53SiVMo8Nb UFG spring – Fatigue results.

LIST OF ACRONYMS AND ABBREVIATIONS

CCT = Continuous Cooling Transformation

DIFT = Deformation Induced Ferrite Transformation

DRX = Dynamic Recrystallization

FEM = Finite Element Modeling

PAGS = Prior austenite grain size

STD = Conventional

STDG = Conventional grain

UFG = Ultrafine grained

European Commission

EUR 26176 — Guidelines for long ultrafine grained steel production and application to the automotive sector (LUNA)

Luxembourg: Publications Office of the European Union

2013 — 173 pp. — 21 × 29.7 cm

ISBN 978-92-79-33089-6

doi:10.2777/42639

HOW TO OBTAIN EU PUBLICATIONS

Free publications:

- one copy:
via EU Bookshop (<http://bookshop.europa.eu>);
- more than one copy or posters/maps:
from the European Union's representations (http://ec.europa.eu/represent_en.htm);
from the delegations in non-EU countries (http://eeas.europa.eu/delegations/index_en.htm);
by contacting the Europe Direct service (http://europa.eu/eurodirect/index_en.htm) or
calling 00 800 6 7 8 9 10 11 (freephone number from anywhere in the EU) (*).

(*) The information given is free, as are most calls (though some operators, phone boxes or hotels may charge you).

Priced publications:

- via EU Bookshop (<http://bookshop.europa.eu>).

Priced subscriptions:

- via one of the sales agents of the Publications Office of the European Union
(http://publications.europa.eu/others/agents/index_en.htm).

The main objectives of this project were to supply the EU Steelmaking and Automotive Industry with guidelines for the production using existing productive plants and best utilisation of ultrafine grained carbon steel long products for mechanical applications.

A ferrite grain size in the range of $1\div 4\ \mu\text{m}$ and a steel microstructure characterised by a mixture of ferrite-pearlite and/or martensite, bainite, microstructure, can give a very good combination of mechanical (strength, ductility, toughness, fatigue) and technological properties (machinability, cold/warm metal forming, etc.) for final application to automotive components.

In particular the project objectives were:

- Definition of the most suitable thermomechanical process for long ultrafine grained (UFG) steel production;
- Identification of merits, in terms of microstructural and mechanical properties of UFG long steels in as-rolled conditions and after cold/warm forming;
- Production of components or component-like dummies in UFG long products and evaluation of their mechanical performances.

To give guidelines for automotive UFG long products applications.

On the basis of the results of the project DIFT and Heavy γ deformation mechanisms were identified as suitable to be exploited to industrially produce UFG long product steels and the main parameters that control the formation of ultrafine ferrite were assessed.

The use of UFG steel showed to allow the improvement of cold forming for fastener production, while no significant advantage was found for powertrain applications since, after their fabrication, they require a further heat treatment that modifies the previous UFG microstructure..

Studies and reports